). FHWA/RD-81/051

ANALYSES, EXPERIMENTAL STUDIES, AND EVALUATIONS OF CONTROL MEASURES FOR AIR FLOW AND AIR QUALITY ON AND NEAR HIGHWAYS

Vol. I. Experimental Studies, Analyses, and Model Development

March 1981

Final Report

Document is available to the public through the National Technical Information Service, Springfield, Virginia 22161

Prepared for
FEDERAL HIGHWAY ADMINISTRATION
Offices of Research & Development
Environmental Division
Washington, D.C. 20590

FOREWORD

This report presents the basic technology, experimental investigations, and concepts concerning air contaminant entrainment and dispersion near highways. A simulation model called ROADMAP was developed for evaluation of the dispersion of vehicle emissions from highways. This report will be of interest to researchers and advisors involved in air pollution and related environmental investigations.

Reports of this study, "Analyses, Experimental Studies, and Evaluation of Control Measures for Air Flows and Air Quality On and Near Highways," include:

FHWA/RD-81/051 Volume I, "Experimental Studies, Analyses, and Model Development"

FHWA/RD-81/052 Volume II, "User Guidelines and Application Notes for Estimating Air Quality for Alternative Roadway Configurations"

FHWA/RD-81/054 Volume III, "User's Manual for FHWA Data Base and Retrieval Programs" (Data Base on magnetic tapes)

FHWA/RD-81/053 An Executive Summary

Research in highway air pollution is included in the Federally Coordinated Program (FCP) of Highway Research and Development in Project 3F, "Pollution Reduction and Environmental Enhancement." Dr. H. A. Jongedyk is the FCP project manager.

One copy is being sent to each FHWA regional office. This report is also being given a limited initial distribution to pertinent offices and specialists. A limited number of additional copies are available for official use upon request.

Charles F. Scheffey
Director, Office of Research
Federal Highway Administration

NOTICE

Technical Report Documentation Page

1. Report No.	2. Government Accession No.	3. Recipient's Catalog No.
FHWA/RD-81/051		

4. Title and Subtitle
ANALYSES, EXPERIMENTAL STUDIES, AND EVALUATIONS OF CONTROL MEASURES FOR AIR FLOW AND AIR QUALITY ON AND NEAR HIGHWAYS; VOL. I — Experimental Studies, Analyses, and Model Development

5. Report Date
March 1981

6. Performing Organization Code

7. Author(s)
Walter F. Dabberdt, Eugene Shelar, David Marimont, and George Skinner

8. Performing Organization Report No.
Final Report
SRI Project 2761

9. Performing Organization Name and Address
SRI International
333 Ravenswood Avenue
Menlo Park, California 94025

10. Work Unit No. (TRAIS)
33F3082

11. Contract or Grant No.
DOT-FH-11-8125

12. Sponsoring Agency Name and Address
U.S. Department of Transportation
Federal Highway Administration
Offices of Research and Development
Environmental Division
Washington, D.C. 20590

13. Type of Report and Period Covered
Final Report (1973-1980)

14. Sponsoring Agency Code

15. Supplementary Notes
FHWA Contract Manager: Dr. Howard A. Jongedyk (HRS-42)

16. Abstract

Experimental and theoretical investigations have been made of meteorological and air quality conditions near a broad range of complex roadway configurations. These are described, and some new insights into the interrelationships among traffic, meteorology, and configuration are discussed. The development of a new and versatile dispersion model, called ROADMAP, is also described together with an evaluation of the model's performance relative to measured atmospheric and wind tunnel pollutant concentration data. (Volume II of this final report — FHWA/RD-81/052— is a set of guidelines for the understanding and estimation of air quality conditions for alternative roadway configurations.)

The atmospheric experiments were conducted at a grade-level, depressed, and elevated freeway sections; approximately 50 h of meteorological, traffic, air quality, and dual-tracer data were obtained at each site. The wind tunnel tests comprised measurements at nine distinctly different roadway configurations; helium was released at a controlled rate from the model vehicles and was sampled at 20 locations above, upwind, and downwind of the roadway. Wind speed and direction, traffic speed and direction, and ground roughness were varied among the 360 tests. Visual tracers and high-speed photography were also used in the wind tunnel.

The experimental data indicates a significant effect of waste heat on near-roadway dispersion. The combined effects of traffic movement and waste heat emissions cause increases in the turbulence intensity of up to 200% across the roadway. However, there is apparently little effect on turbulence caused by changes in traffic volume or speed (for the moderate-to-heavy traffic conditions present during the tests). An aerodynamic or shelter effect is postulated to exist and to be a significant influence for grade-level roads.

The semi-empirical roadway atmospheric dispersion model for air pollution (ROADMAP) simulates two-dimensional dispersion patterns for various roadway configurations: grade-level, vertical and slant-wall cut, fill, and viaduct sections.

The two-component formulation of the model treats the dispersion as the geometric sum of roadway-parallel and -perpendicular terms. The introduction of a height-offset parameter enables ROADMAP to simulate the effects of changes in the height of the plume centerline and the level of nearby terrain. Evaluation of ROADMAP with independent CO field data downwind of the grade-level road resulted in encouragingly high values of the linear correlation coefficient: 0.91 for neutral stability, 0.67 for stable atmospheric conditions, and 0.80 for unstable conditions. Values for the cut- and elevated-section tests in the wind tunnel ranged from 0.69 to 0.93.

17. Key Words	18. Distribution Statement
Air pollution, atmospheric experiments, modeling, wind tunnel experiments, traffic effects, dispersion	This document is available to the public through the National Technical Information Service, Springfield, Virginia 22161

19. Security Classif. (of this report)	20. Security Classif. (of this page)	21. No. of Pages	22. Price
Unclassified	Unclassified	269	

Form DOT F 1700.7 (8-72) Reproduction of completed page authorized

TABLE OF CONTENTS

TABLE OF CONTENTS (Continued)

LIST OF FIGURES

Errata Sheet

Text of report contains erroneous or superceded report numbers:

These are:

Report FHWA/RD-81/051 wrongly identified as Report FHWA/RD-78-179

Report FHWA/RD-81/052 wrongly identified as Report FHWA/RD-78-180

Report FHWA/RD-81/053 wrongly identified as Report FHWA/RD-78-181

Report FWWA/RD-81/054 wrongly identified as Report FHWA/RD-78-182

or Report FHWA/RD-78-128

LIST OF FIGURES (Continued)

LIST OF FIGURES (Continued)

LIST OF TABLES

LIST OF TABLES (Continued)

SYMBOLS

ppm	parts per million (volume, n.d.
l	characteristic length scale, m
z_o	aerodynamic roughness height, m
m	model
p	prototype
u_*	friction velocity, m s^{-1}
z	height, m
u,v	horizontal wind speed components, m s^{-1}
ur	horizontal wind component perpendicular to road, m s^{-1}
vr	horizontal wind component parallel to road, m s^{-1}
w	vertical wind component, m s^{-1}
q	"Studentized" range
t	Student's t score
k	constant, n.d.
c_p	specific heat at constant pressure, J $\cdot$ g^{-1} $\cdot$ $^oC^{-1}$
a	regression constant
b	regression coefficient, n.d.
r	linear correlation coefficient, n.d.
r^2	explained variance, n.d.
z'	height-offset parameter in ROADMAP, m
m	metre, m
ms	millisecond, s
i	measurement level (number) on tower, n.d.
v_{net}	sum of drag wind and roadway-parallel wind, m s^{-1}
e	experimental error
f	lateral dispersion parameter in ROADMAP
H_R	reference height, m
H_c	car height, m
D	zero-plane displacement, m
He	helium

Re	Reynolds number, n.d.
CO	carbon monoxide
Q	pollutant volumetric flux, $m^3\ s^{-1}$
Ri	gradient Richardson number, n.d.
W	the within-group variation
B	the between-group variation
F	Snedecor's ratio
K_m	eddy diffusivity for mass, $m^2\ s^{-1}$
H	sensible heat flux, $J \cdot m^{-2}\ s^{-1}$
J	Joules
K_H	eddy diffusivity for heat, $m^2\ s^{-1}$
K	eddy diffusivity, $m^2\ s^{-1}$
FS	factor score
EV	environmental variable
N	sample size, n.d.
U	vector wind speed, $m\ s^{-1}$
H	roadway height above grade level, m
AQS	air quality sampler
TTI	total turbulence intensity, $m\ s^{-1}$
NTTI	normalized total turbulence intensity, n.d.
OCC	vehicle occupancy, $s\ m^{-1}$
VOL	vehicle volume (number), n.d.
DRAG	vehicle-induced drag wind, $m\ s^{-1}$
X	datum
M	grand mean of all observations
W	roadway width, m
ν	kinematic viscosity, $m^2\ s^{-1}$
τ	shear stress, $g \cdot m^{-1}\ s^{-2}$
ρ	density, $g \cdot m^{-3}$
Φ^*	pollutant volumetric flux, $m^3\ s^{-1}$
Θ	azimuthal wind direction, deg
ϕ	elevation angle of wind, deg
σ_ϕ	standard deviation of elevation angle, deg
Γ	dry adiabatic lapse rate, $^oC \cdot m^{-1}$
σ_ω	standard deviation of vertical wind speed component, $m\ s^{-1}$

SYMBOLS (Continued)

μ	micrometre, m
ℓ	litre, m^3
ΔT	temperature difference, ^oC
σ_z	vertical dispersion coefficient, m
χ	gas concentration, $g \cdot m^{-3}$

METRIC CONVERSION FACTORS

Approximate Conversions to Metric Measures

Symbol	When You Know	Multiply by	To Find	Symbol
		LENGTH		
in	inches	*2.5	centimeters	cm
ft	feet	30	centimeters	cm
yd	yards	0.9	meters	m
mi	miles	1.6	kilometers	km
		AREA		
in^2	square inches	6.5	square centimeters	cm^2
ft^2	square feet	0.09	square meters	m^2
yd^2	square yards	0.8	square meters	m^2
mi^2	square miles	2.6	square kilometers	km^2
	acres	0.4	hectares	ha
		MASS (weight)		
oz	ounces	28	grams	g
lb	pounds	0.45	kilograms	kg
	short tons (2000 lb)	0.9	tonnes	t
		VOLUME		
tsp	teaspoons	5	milliliters	ml
Tbsp	tablespoons	15	milliliters	ml
fl oz	fluid ounces	30	milliliters	ml
c	cups	0.24	liters	l
pt	pints	0.47	liters	l
qt	quarts	0.95	liters	l
gal	gallons	3.8	liters	l
ft^3	cubic feet	0.03	cubic meters	m^3
yd^3	cubic yards	0.76	cubic meters	m^3
		TEMPERATURE (exact)		
°F	Fahrenheit temperature	5/9 (after subtracting 32)	Celsius temperature	°C

*1 in = 2.54 (exactly). For other exact conversions and more detailed tables, see NBS Misc. Publ. 286, Units of Weights and Measures, Price $2.25, SD Catalog No. C13.10:286.

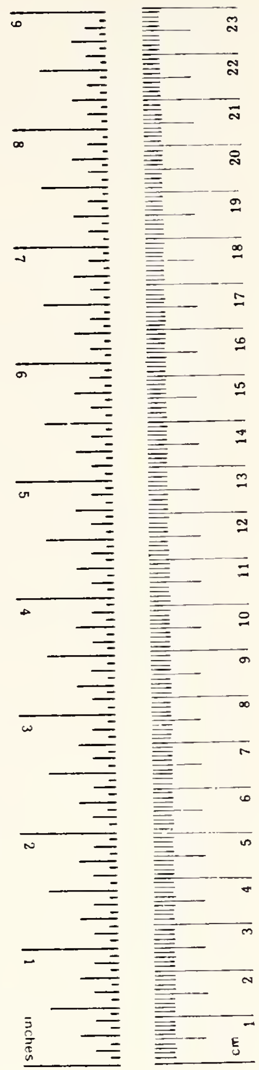

Approximate Conversions from Metric Measures

Symbol	When You Know	Multiply by	To Find	Symbol
		LENGTH		
mm	millimeters	0.04	inches	in
cm	centimeters	0.4	inches	in
m	meters	3.3	feet	ft
m	meters	1.1	yards	yd
km	kilometers	0.6	miles	mi
		AREA		
cm^2	square centimeters	0.16	square inches	in^2
m^2	square meters	1.2	square yards	yd^2
km^2	square kilometers	0.4	square miles	mi^2
ha	hectares (10,000 m^2)	2.5	acres	
		MASS (weight)		
g	grams	0.035	ounces	oz
kg	kilograms	2.2	pounds	lb
t	tonnes (1000 kg)	1.1	short tons	
		VOLUME		
ml	milliliters	0.03	fluid ounces	fl oz
l	liters	2.1	pints	pt
l	liters	1.06	quarts	qt
l	liters	0.26	gallons	gal
m^3	cubic meters	35	cubic feet	ft^3
m^3	cubic meters	1.3	cubic yards	yd^3
		TEMPERATURE (exact)		
°C	Celsius temperature	9/5 (then add 32)	Fahrenheit temperature	°F

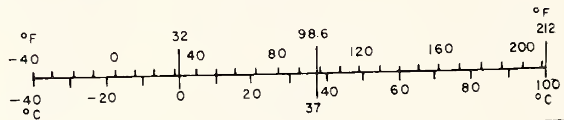

I INTRODUCTION

The basic objective of this study is the development of principles and guidelines for the description of dispersion and air quality conditions on and near roadways. Specifically, the research has been directed toward:

- Understanding how traffic, meteorology, and the geometry of the roadway and nearby buildings interact to influence the transport and diffusion of pollutants on the local or microscale (i.e., within the roadway right-of-way).
- Developing a simulation procedure for predicting ambient pollutant concentrations that result from roadway emissions.

This simulation procedure would give planners a technique with which to assess the probable atmospheric impacts within the corridor of proposed roadways; where adverse impacts are projected, the methodology could be used to evaluate alternative roadway designs.

Because of the aerodynamically complex nature of major roadways, particularly in urban areas, and the impact on atmospheric turbulence and pollutant dispersion, it was proposed that a theoretical/experimental/empirical approach would (1) provide a firm basis for understanding the problem and (2) offer the best chance of developing a generic methodology that would effectively describe the impacts of traffic, meteorology, and geometry.

The conceptual approach of the study is summarized in Figure 1. At the outset, previous work related to microscale pollution-dispersion from highways and the influences of roadway geometry, meteorology, surface roughness, and traffic and vehicle motion was reviewed. The earlier theoretical and experimental investigations at that time (1973) did not adequately treat the combined effects of these four factors; even the effects of individual factors had, for the most part, not been properly addressed on the microscale. As a consequence, we undertook several preliminary theoretical investigations and data analyses to develop a

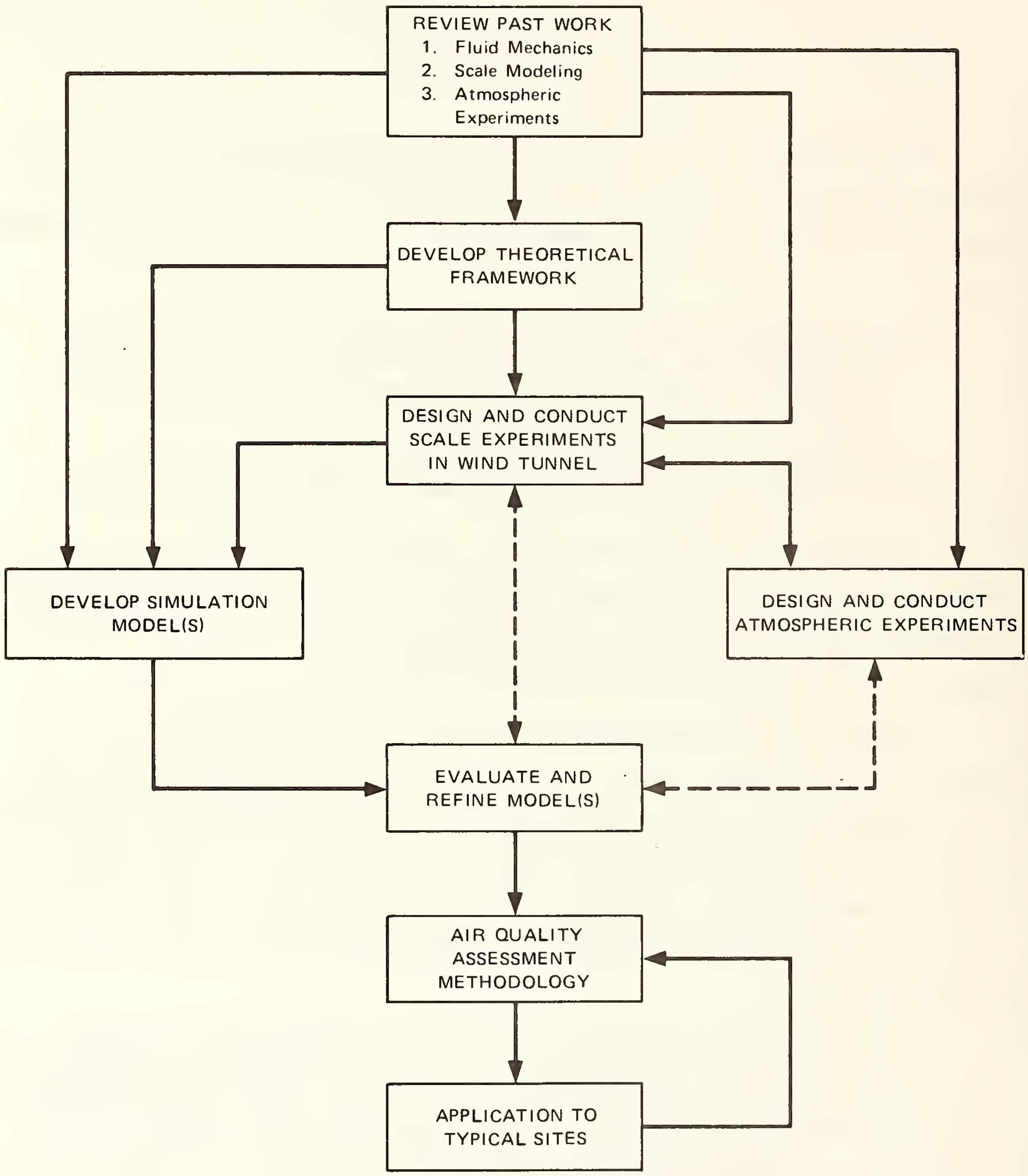

FIGURE 1 CONCEPTUAL FRAMEWORK FOR A PROGRAM TO DEVELOP A RATIONALE FOR THE ASSESSMENT OF THE IMPACT OF VEHICLE, METEOROLOGICAL, ROADWAY, AND ADJACENT BUILDING CHARACTERISTICS ON MICROSALE AIR QUALITY

framework for the subsequent atmospheric and wind tunnel tests that were to fill in many of the voids in the area of microscale dispersion processes and the nature of air quality conditions on and near roadways. These preliminary investigations (Dabberdt, 1974) included: analytical modeling of the principle features of wake-induced turbulence and drag flow, and the use of statistical methods to relate near-roadway pollutant concentrations (measured during several earlier studies in Los Angeles) to meteorological and site characteristics.

Using the results of these preliminary efforts, an extensive number of aerometric experiments was designed and conducted. In all, 16 different roadway configurations were investigated; these included various types of at-grade, elevated, and depressed sections with both rough and smooth adjacent terrain. Three tests were conducted at existing roadway locations, and the remaining 13 were conducted in the controlled environment of an environmental wind tunnel. These scale model tests had the advantage of flexibility in that wind, traffic, and geometric variables could be easily varied at will. On the other hand, the atmospheric tests permitted the analysis of impacts due to diabatic stability conditions and vehicular thermal emissions. The design and scope of the wind tunnel and atmospheric tests are thoroughly described in Chapter II. The air quality, meteorological, and traffic data collected in these tests are available to the public. The data have been archived on magnetic tape and a user's manual has been prepared. Inquiries regarding acquisition of the data should be made to: U.S. Department of Transportation, Federal Highway Administration, Office of Research, Environmental Control Group, Washington, D.C. 20590.

The experimental data were first analyzed to investigate the interrelationships among effects from traffic, meteorology, and ground roughness. This proceeded in two phases: first, the data from the atmospheric test at the grade-level roadway section were analyzed to understand dispersion effects due to variations in traffic and meteorology; these analysis are described in detail in Chapter III. Next, statistical analyses using factor analysis and multiple regression were made of the grade-level wind tunnel data to further identify individual and combined effects resulting from variations in wind, traffic, and ground roughness--Chapter IV.

In addition to providing new and useful insights into the dispersion process, these analyses also helped to identify the framework of a simulation model that could both accurately simulate air quality conditions downwind of a range of roadway configurations and be rapidly and easily applied by nonresearch users. An empirical model was subsequently developed (Chapter V) and has been called ROADMAP (Roadway Dispersion Model for Air Pollution). One feature of the model is that it seeks to characterize dispersion from a line source as the vector sum of two components: one from transport and diffusion along the horizontal wind component that is perpendicular to the line source, and the other along the wind component parallel to the roadway. A second feature of ROADMAP is that it implicitly describes aerodynamic and thermal vehicular effects on dispersion. The ROADMAP model was evaluated by comparison of model simulations with measurements from wind tunnel and atmospheric tests. The evaluations included grade-level roadway configurations, cut sections, and elevated sections; discussions of the form of the dispersion functions and the model's performance are provided in Chapter VI. The model also forms the basis for the evaluation methodology discussed in Volume II of this report. The evaluation methodology consists of a fully self-contained set of guidelines for estimating air quality for alternative roadway configurations. To promote the proper assessment of air quality, the guidelines consist of three levels of analysis: first, there is a discussion of theoretical and empirical considerations in quantifying the dispersion process (i.e., transport, diffusion, and terrain and traffic effects). Second, the assessment methodology gives an introduction to the basis and formulation of ROADMAP, followed by a series of worksheets, tables, and graphs to systematize the calculations. Third, the applications section addresses the use of ROADMAP and other considerations in evaluating thirty alternative roadway configurations and environments. A final section discusses the philosophy of the proper use and application of the guidelines as well as providing some insights into possibilities for air quality management and control.

The theoretical, analytical, and experimental aspects of the study are summarized in this volume of the final report (FHWA-RD-78-179). The user's guide and application notes are presented in Volume II (FHWA-RD-78-180), together with some considerations on the practicality and potential of several active and passive pollution control concepts. A user's manual for the experimental data collected in the field and wind tunnel tests is also available (FHWA-RD-78-182). A 16-mm color movie entitled "Highway Pollution Dispersion: Air Quality in the Right-of-Way" was also prepared during the research study and is available. This 20-min sound movie uses animation, sketches, and film sequences to present a comprehensive introduction to the causes and characteristics of microscale pollution dispersion near highways. The movie is directed toward a wide audience ranging from interested nonspecialists to highway engineers to researchers.

oo Coperating Organizations: SRI: Dr. Ronald Ruff, Dr. Randall Pozdena, Mr. Hisao Shigeishi, Mr. Albert Smith, Mr. Lu Salas, and Mr. Charles Flohr. Design and construction of the mechanical highway model and the wind tunnel dispersion tests were conducted at Calspan Corporation, Buffalo, New York, under subcontract to SRI: Dr. George Skinner, Dr. Gary Ludwig, and Dr. Al Ritter. Atmospheric tests and installation of traffic sensors: Mr. James Collins and District 04 of the California Department of Transportation and Mr. Earl Shirley, Transportation Research Laboratory. Meteorological Instrumentation: Mr. Lawrence Niemeyer and the Meteorology Laboratory of the U.S. Environmental Protection Agency, Research Triangle Park, North Carolina.

II EXPERIMENTAL STUDIES

The wind tunnel and atmospheric experiements were phased to incorporate the results and findings derived from the early tests into the design of the later tests. The wind tunnel tests were initiated first; the initial series of tests focused mainly on the identification of vehicle and traffic effects rather than on effects due to site configuration. With preliminary results on the sensitivity of dispersion patterns to traffic variations, the later tests incorporated a reduced number of traffic variations in order to focus more on the effects of meteorology and site configuration. Also, the initial wind tunnel tests provided data that were used to help design the sampling procedures for the grade-level atmospheric test series. Finally, the implications of the data from the first atmospheric test series and the wind tunnel series were considered in the design and operation of the subsequent atmospheric tests at depressed and elevated roadway sections.

A. Wind Tunnel Experiments

A. Introduction

The objective of the experimental wind-tunnel studies was to test basic highway models to obtain data that could be used to better understand microscale dispersion phenomena and subsequently to develop analytical techniques for predicting air quality on or near highways. The Calspan Atmospheric Simulation Facility (ASF) that was used in the experiments is shown in Figure 2. The principal component of the highway models was a moving roadway. The roadbed section was made very thin to permit it to be used for simulation of elevated highways.

The function of the model roadway is to distribute the vehicle exhausts in a manner analogous to the full-scale situation. The vehicles move at a velocity that bears the same relationship to the wind velocity as in full-scale, and the wakes of the vehicles initiate the exhaust

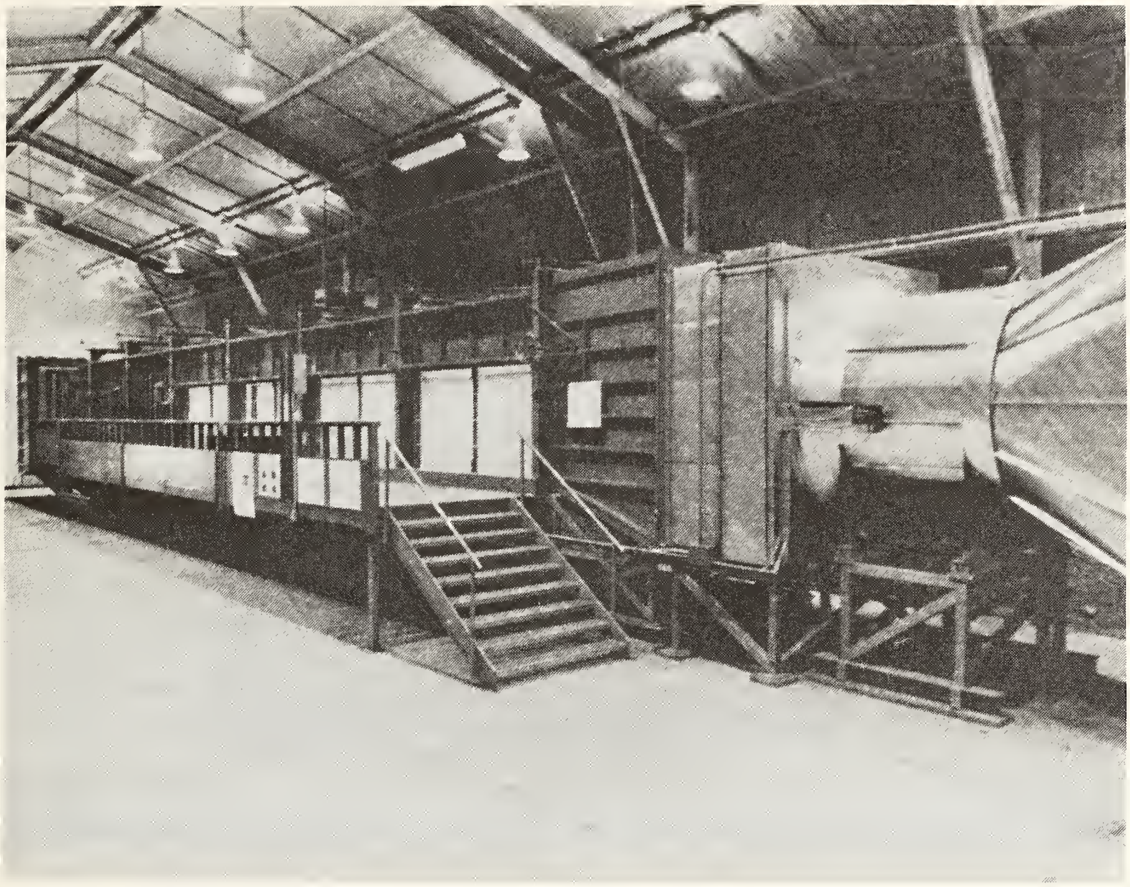

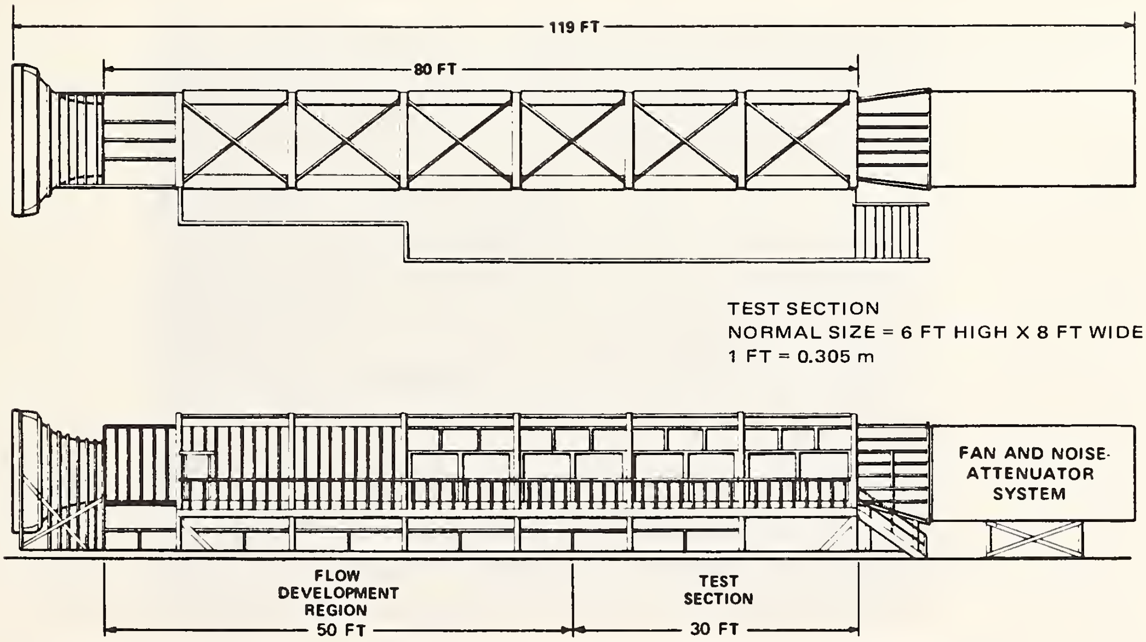

FIGURE 2 THE CALSPAN ATMOSPHERIC SIMULATION FACILITY (ASF)

dispersion in essentially the same way as do actual vehicle wakes. The subsequent dispersion by atmospheric boundary-layer turbulence is simulated by the flow generated in the ASF. The theory and the experimental results of this latter simulation have been discussed in a number of papers (McVehil, Ludwig, and Sundaram, 1967; Ludwig and Sundaram, 1969; Ludwig, Sundaram, and Skinner, 1971; Sundaram, Ludwig, and Skinner, 1972).

Pollutant levels in full scale were obtained by sampling helium (He) concentrations emitted from the model cars at 20 locations near the roadway. Helium was used in the model work because of the high sampling sensitivity that can be achieved.

2. The Model Roadway

The model roadway (Figures 3-5) had two moving belts to which model vehicles were attached. The belts could be driven in the same or in opposite directions by an electronic speed controller. The belts passed over elevated plenum chambers filled with He to supply simulated vehicle exhaust and were sealed by metal guides attached to the surfaces at the sides of the chambers. The complete unit was constructed to fit into the 2.24-m diameter turntable of the ASF.

Two scales of model vehicles were used in the tests. For mixed traffic, consisting of autos and trucks, a scale of 1 in 300 was used, with each belt carrying two lanes of traffic. An additional series of tests was run with only automobiles, a single lane to each belt, at 3.5 times the above scale (1:85). The 1:85 scale models are shown in Figures 3-5; Figure 6 shows the smaller vehicles (1:300). The models were attached to the belt at only the exhaust flow tube so that they were free to pass around the end pulleys without bending. The small-scale cars and trucks were mounted on belts with two different spacing configurations: high density, with an average spacing between vehicles of two car lengths; and a low-density spacing of four car lengths. Only a high-density (1.5 car-length spacing) configuration was used with the large-scale vehicles. The probability distribution of vehicles in each lane has been taken as a gamma semi-Poisson function (Buckley, 1969),

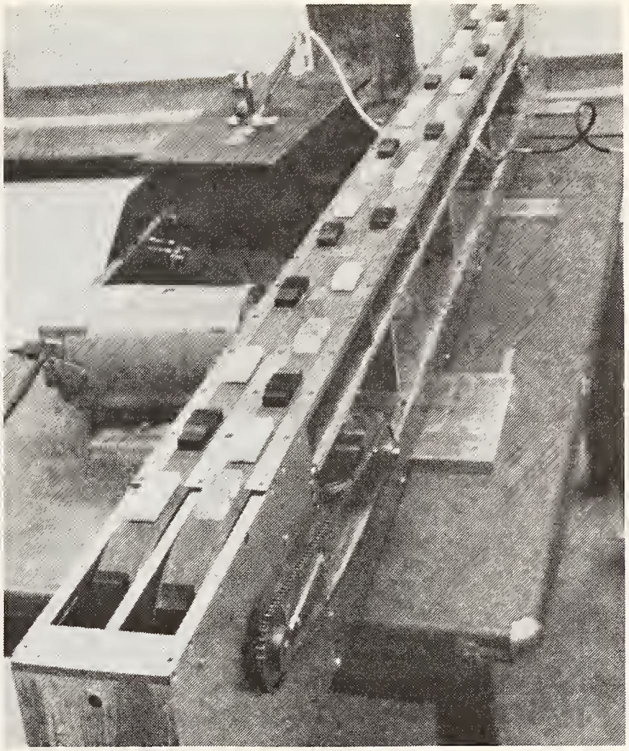

FIGURE 3 MOVING BELT/TRACER ROADWAY MODEL WITH HIGH DENSITY, LARGE-SCALE VEHICLES

FIGURE 4 INSTALLATION OF THE ROADWAY MODEL IN THE WIND TUNNEL TURNTABLE

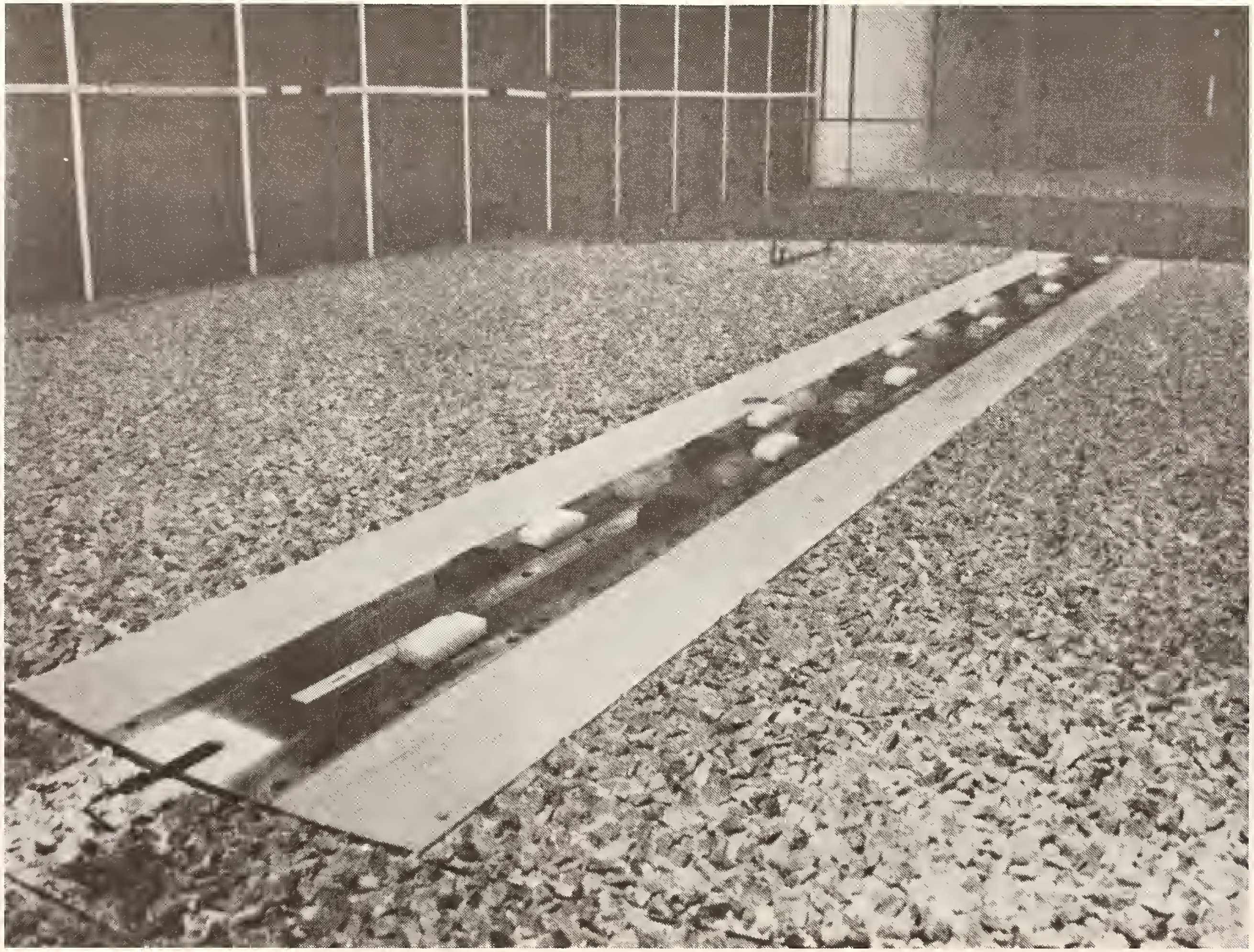

FIGURE 5 ROADWAY MODEL INSTALLED AT GRADE IN THE WIND TUNNEL WITH THE SAMPLING ARRAY IN THE BACKGROUND

FIGURE 6 CLOSE-UP PHOTO OF THE MODEL SHOWING LARGE AND SMALL ROUGHNESS GROUNDS AND THE GAS-SAMPLING PROBE ARRAY
(The Scale of the 0.60-in. Long Cars is 1:300)

where the particular sequence of spacings was chosen randomly. Table 1 lists the vehicle layout for each configuration.

3. Gas-Sampling System

Helium was used as the pollution simulant gas in the sampling system. An advantage of using He as the simulant is that the background concentration in normal air is low, generally about 5 ppm.

Briefly, the sampling system consisted of a ring of 24 chambers, which were initially pumped down to a hard vacuum, into which the samples were drawn through 3.7-m long capillaries (Figure 6). Three of these capillaries were taken to calibration gases. The other capillaries were taken to the mixtures drawn from the 20 sampling points on the model and one upstream reference to determine background level. Each capillary was connected to the top of a sample collection chamber through a solenoid

Table 1

DISTRIBUTION OF VEHICLES ON MOVING BELT SYSTEM

Vehicle No.	Spacing (Car Lengths)		
	Small-Scale Vehicles		Large-Scale Vehicles
	High-Density	Low-Density	High-Density
1	0.9	1.8	0.68
2	1.8	4.8	1.35
3	1.2	3.6	0.90
4	2.1	0.6	1.58
5	0.3	Truck	0.23
6	2.1	3.0	1.58
7	3.0	2.4	2.25
8	2.1	1.8	1.58
9	1.2	3.6	0.90
10	0.9	1.8	0.68
11	0.6	2.4	0.45
12	Truck	7.8	1.13
13	1.5	3.0	3.83
14	5.1	3.0	0.68
15	0.9	4.2	0.68
16	0.9	5.4	1.58
17	2.1	1.8	0.90
18	1.2	3.6	0.90
19	1.2	6.6	1.13
20	1.5	2.4	1.35
21	1.8	6.0	2.93
22	3.9	3.0	0.45
23	Truck	3.0	0.90
24	0.6	3.0	3.60
25	1.2	3.0	1.35
26	4.8	4.8	0.90
27	1.8	3.0	1.35
28	1.2	3.6	0.90
29	1.8	6.0	4.28
30	1.2	3.6	0.90
31	5.7	1.2	0.90
32	1.2	4.2	0.90
33	1.2	1.2	1.13
34	1.2	5.4	2.03
35	1.5	2.4	2.03

Table 1 (Continued)

Vehicle No.	High-Density	Low-Density	High-Density
36	2.7	6.6	0.90
37	2.7	3.6	1.13
38	1.2	1.2	2.25
39	1.5	2.4	2.70
40	3.0	3.6	
41	3.6	1.2	
42	3.0	4.2	
43	1.8	8.4	
44	2.4	4.2	
45	1.5	4.2	
46	2.4	1.8	
47	0.3	5.4	
48	1.5	9.6	
49	0.6	4.8	
50	1.8	4.2	
51	0.9	2.4	
52	1.8	7.2	
53	1.5	Truck	
54	3.3	4.8	
55	2.7	7.2	
56	2.4	1.8	
57	0.6	2.4	
58	3.6	6.0	
59	0.9		
60	2.4		
61	1.5		
62	3.3		
63	3.0		
64	0.6		
65	2.7		
66	1.5		
67	2.1		
68	1.5		
69	1.5		
70	0.6		
71	1.8		
72	2.1		
73	1.8		

Table 1 (Concluded)

Vehicle No.	High-Density	Low-Density	High-Density
74	Truck		
75	1.5		
76	3.3		
77	0.9		
78	2.1		
79	2.1		
80	3.9		
81	1.8		
82	5.4		
83	2.1		
84	0.9		
85	4.2		
86	2.4		
87	4.5		
88	0.9		
89	3.6		
90	2.7		
91	2.4		
92	2.4		
93	1.8		

Notes: (1) Staggered spacing sequence on adjacent lanes for small-scale vehicles.

(2) Spacing behind trucks $\cong$ 1 truck length for high-density belt and $\cong$ 2 lengths for low-density belt. Also, 1 truck length additional to spacing in front of trucks.

valve that was electrically driven so that all 24 solenoids could be opened or closed simultaneously. The bottom of each collection chamber was open to a vacuum plenum, which is held at roughly 10^{-5} torr* by a diffusion pump backed by a large mechanical pump. A single plate valve was used to seal off all 24 chambers from the vacuum plenum at the start of sample collection in the chambers.

The method of collecting the samples was as follows: the collection chambers were pumped down to a hard vacuum (10^{-5} torr) with the capillary end of the chambers closed by the solenoid valves. Then, with the conditions for a test established (model operating and capillaries exposed to the proper calibration gases and flows to be sampled), the capillaries were flushed for 15 s by opening the solenoid valves. This was sufficient time to draw legitimate samples into the full lengths of the capillaries. The solenoid valves were then closed and the chambers were pumped down to a hard vacuum. This took about 15 s. During this time the capillaries returned to atmospheric pressure but by then they contained legitimate samples. Once the hard vacuum was attained in the chambers, the large plate valve at the bottom of the chambers was closed to seal off all 24 chambers from the vacuum plenum. Finally, the solenoid valves were reopened for, generally, 90 s to allow samples to flow into the chambers. The solenoid valves were then closed to seal the collection chambers, which then contained the collected samples at a final pressure of 1 or 2 torr.

At the end of sampling, each chamber was analyzed for He concentration by connecting it, in turn, to the measuring system through an electrically-driven scanning valve. The measurement was made on a modified He leak detector in which the pressure was regulated by the fixed geometrical (area) relationship between an inlet pinhole at the scanning valve and the outlet restriction of a butterfly valve, which is part of the leak detector. Since each sample chamber was at the same pressure, the leak detector provided a direct reading of the concentration level. Calibration mixtures in the three calibration channels allowed direct standardization on each scan. The system was trimmed so that when all

*1 torr = 1 mm Hg.

channels were exposed to the same source the readouts lay within ±5% of the mean, down to concentrations of about 5 ppm He. A complete scan of the 24 channels takes about 10 min.

4. Scaling Criteria

In attempting small-scale modeling of flows in the atmospheric boundary layer, care must be taken to ensure that all important features of the full-scale situation are represented in the model. Broadly speaking, these include the ambient wind environment, including both the mean and turbulent characteristics, as well as the local terrain.

The most obvious requirement is that of geometric scaling between the full-scale and model flows, with regard to buildings and local topography. This also implies that the ratio of some characteristic geometric length, say ℓ, should be held to a length characteristic of the local ground roughness, say z_o, constant between full-scale and the model:

$$\frac{(\ell)}{(z_o)}_m = \frac{(\ell)}{(z_o)}_p \tag{1}$$

where subscripts m and p denote model and prototype (full-scale), respectively. Since z_o essentially determines the scale of the turbulent eddies near the ground, this ensures that the relative size of the structures and the eddies is maintained.

The majority of flows very near the ground are "aerodynamically rough;" i.e., no laminar sublayer exists, and the flow is fully turbulent. In such cases, molecular diffusion is negligible compared with that from turbulent transport. For this reason, holding the usual Reynolds' number constant based on free-stream conditions and a characteristic model length is generally not required. Experience has shown that the flow will be aerodynamically rough when a Reynolds' number based on surface conditions is sufficiently large; i.e.,

$$\frac{u_* z_o}{\nu} \simeq 3 \quad . \tag{2}$$

The reference height at which the wind velocity was specified is illustrated in Figure 7. The velocity profile in the ASF is logarithmic and the effective zero-velocity height is just below the tops of the roughness elements. The reference velocity was set at one car-height, H_c, above this level. In the ASF calibrations, height (z) has been measured from the base-board as shown in Figure 7. The reference height, H_R, thus becomes $H_c + D$, where D is the height of the effective zero-velocity. Two logarithmic velocity profiles corresponding to different surface roughness were used. These are shown in Figures 8 and 9, where the ratio of the velocity, $\bar{u}$, at any height (z − D) to the velocity above the boundary layer, u_∞, is given in the form

$$\frac{\bar{u}}{u_\infty} = \frac{u_*}{u_\infty} \; 5.75 \log_{10} \frac{z - D}{z_o} \qquad (3)$$

where

		Small Roughness	Large Roughness
$\frac{u_*}{u_\infty}$	=	0.045	0.052
z_o	=	0.0070 in. (0.018 cm)	0.048 in. (0.122 cm)
D	=	0.2 in. (0.508 cm)	1.5 in. (3.81 cm)

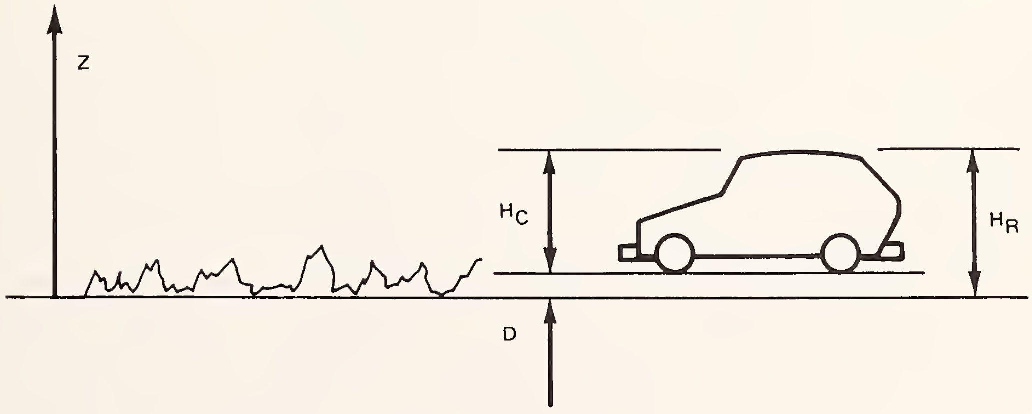

FIGURE 7 DEFINITION OF REFERENCE HEIGHT (H_R)

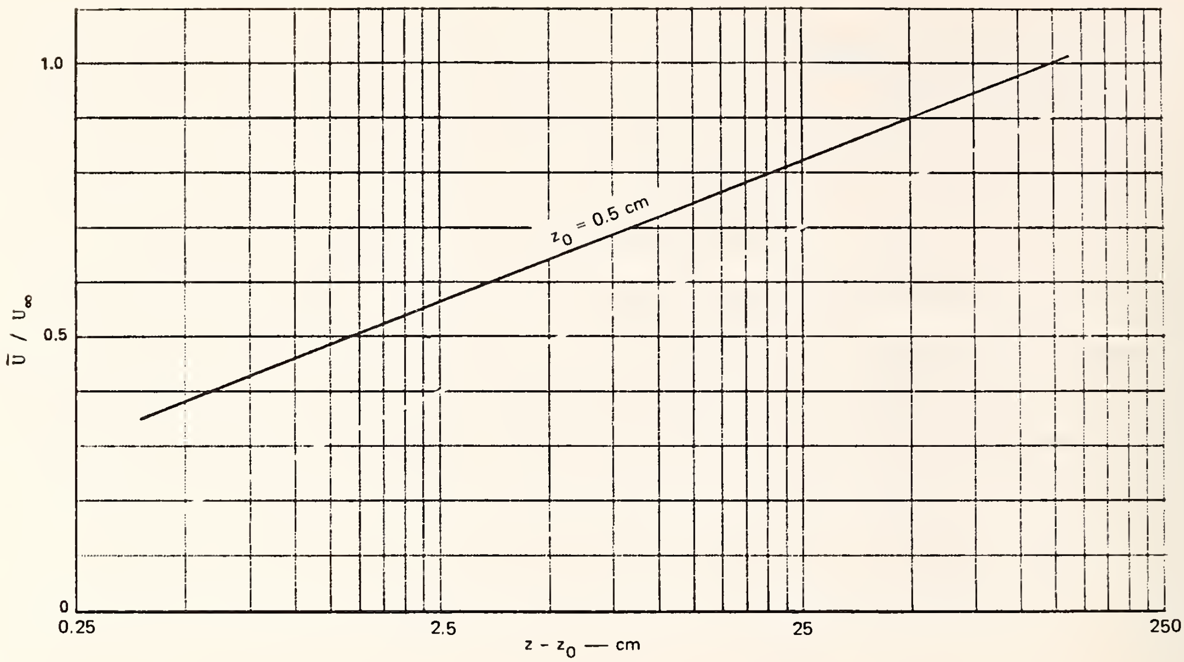

FIGURE 8 MEAN-VELOCITY PROFILE OVER SMALL-ROUGHNESS GROUND (GRAVEL; z_o = 0.5 cm)

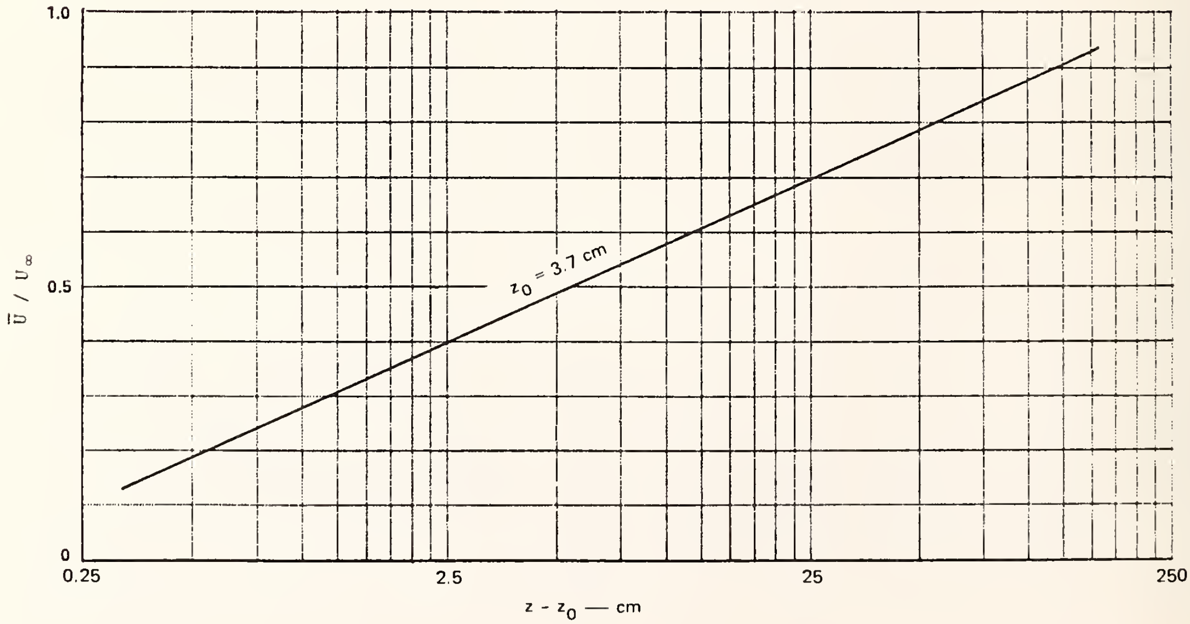

FIGURE 9 MEAN-VELOCITY PROFILE OVER LARGE-ROUGHNESS GROUND (BLOCKS; z_o = 3.7 cm)

and u_*, the friction velocity, is related to the shear stress at the ground, τ, by $u_* = \sqrt{\tau/\rho}$. Here ν is the kinematic viscosity and ρ the air density.

Of the two conditions, scaling for local conditions and ambient wind environment, it is more important to satisfy the latter condition. In addition to these criteria, it is also necessary to make certain that the turbulence spectra of the tunnel flow are suitably scaled reproductions of the atmospheric flow. When these conditions are met, the wind environment in the tunnel flow is a proper representation of the atmosphere, for neutrally stable conditions.

The problem of actually generating the required flow in a laboratory facility is one that has received a great deal of attention in recent years. The proper flow can be developed in a number of ways: these involve the use of various types of roughness elements, fences, spires, and jets transverse to the flow. For this program, a matched fence/rough-floor combination was used. With this technique, it was possible to generate the appropriate logarithmic mean velocity profile, as well as a turbulence spectrum representative of that in the neutral atmosphere.

The dispersal of emissions is influenced by three principal factors: (1) the wind environment, (2) the buoyancy of the emissions, and (3) the initial velocity with which the emissions leave the vehicles. The first of these factors includes the wind velocity profile, the turbulence structure, and the surrounding terrain or buildings; the modeling of these was discussed above. In addition, the relative velocity between the wind and the vehicles must be maintained in the model so that the model wind environment will be directionally similar to the full-scale prototype. The second fact, buoyancy, can be neglected in all cases tested since the distance to the farthest measuring point is too small for buoyancy forces of the dilute helium-in-nitrogen mixture to make any significant contribution. All cases tested involved a significant wind velocity so that turbulent mixing in the atmosphere dominated the processes before buoyancy could become important. (Note, however, that this condition may not hold for atmospheric conditions.) In modeling the roadway, where He was used as the carbon monoxide (CO) simulant, it was important that the exhaust not be subject to buoyancy effects. An analysis by Fay (1973) was used to estimate how much He could be used in each vehicle's exhaust (see Dabberdt et al., 1974). The actual amount used in this extended program was always less than 5% of what had been estimated as an upper limit; thus buoyancy did not affect the model results. The third factor, initial exhaust velocity, does not contribute significantly to the mixing process in the full-scale case. The only change made was to use less He while maintaining the plenum pressure (under the roadway) at 0.5 in. of water by adding more air. The total volumetric flow rate was reduced by this change; thus, the model exhaust contributed less volume to the wake than was originally estimated. Therefore, the effect of the model exhaust flow on the mixing in the wake of the vehicle remained small.

In summary, the scaling laws for the exhaust flows reduce, in this case, to a single equation relating concentration to scale size and scale velocity:

$$\frac{\chi_p}{\chi_m} = \frac{Q_p}{\rho_p \, \phi^*_m} \, \frac{\ell^2_m}{\ell^2_p} \, \frac{u_{am}}{u_{ap}} \qquad (4)$$

where

ℓ = characteristic length

u_a = average wind velocity at some reference height

χ = concentration of pollutant (CO in prototype; He in model)

Q = mass flux of pollutant (per car)*

ϕ^* = volumetric flux of pollutant (per car)*

ρ = density of pollutant gas when sampled (taken at 20°C)

$(\ )_m$ = model

$(\ )_p$ = prototype

---

*One truck was made equivalent to 1.9 cars.

The model scale is

$$\frac{\ell_m}{\ell_p} = \frac{1}{300} \tag{5}$$

and the velocity scale was chosen so that the highest permissible model-vehicle speed (i.e., the maximum speed at which the belt, carrying the model vehicles over the plenum, could be run) corresponded to the highest full-scale vehicle speed. Thus, 3 m/s in the model corresponded to 50 mph (22.4 m/s) in the prototype, so that

$$\frac{u_{am}}{u_{ap}} = 0.136 \ . \tag{6}$$

The factor involving Q_p, the mass flux of CO from the full-scale vehicle, and ϕ^*_m, the volumetric flux of He from the model vehicle, is discussed in Chapter V.

It is also very important that the mixing of the exhaust gases in the wake of the model vehicle duplicate the full-scale process. In the initial stages, before atmospheric turbulent diffusion takes over, the diffusion processes are dominated by the wakes of the vehicles. Since the model scale is very small and the tunnel and roadway velocities are small, it becomes important to inquire whether Reynolds' number effects will be important. The models were made with sharp edges to minimize these effects. The wake mixing is determined principally by the momentum fed into the wake turbulence by the vehicle drag force. For the small-scale model cars, the drag force is of the order of 7 dynes*, and it is not really practical to try either to measure this force or to measure the momentum defect in the wake. What one <u>can</u> do, however, is to address the mixing problem directly and use a flow-visualization technique to see whether the wake mixing is Reynolds'-number-dependent. Figures 10a and b are streak photographs of smoke tests in which titanium dioxide smoke is shown mixing with the vehicle wake at two velocities, approximately 2 m/s and 12 m/s. The small-scale car was mounted roughly 5 cm from the leading edge of a flat plate. The exhaust on the model auto covers a

*1 dyne = 10^{-7} joules/cm

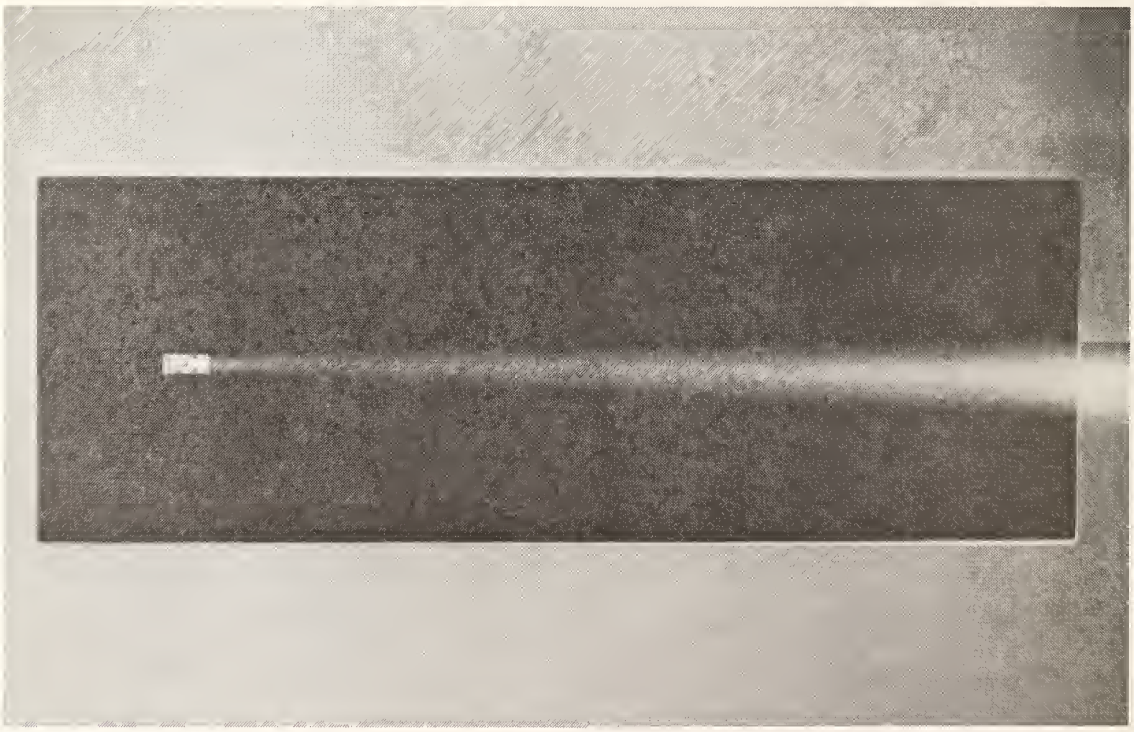

(b)

FIGURE 10 STREAK PHOTOGRAPH OF VEHICLE EXHAUST MIXING IN WAKE AT (a) HIGH VELOCITY AND (b) LOW VELOCITY relatively large fraction of the rear of the vehicle to assist the initial mixing. In the smoke test at 12 m/s, the thickness of the laminar boundary layer on the plate at the model auto is negligible, while at 2 m/s it is about 3 mm. Thus, in the low-speed case, the exhaust duct is actually immersed in the laminar boundary layer, making this a more severe test of exhaust mixing than on a moving belt in the ASF. Yet, clearly, the average extent of the mixing process shows little difference from the high-speed case even at a few car-lengths downstream. On this basis, then, we are confident that the model design produces a good approximation to the initial wake mixing of the exhaust in full scale.

It should be noted that above some critical exhaust-flow rate the exhaust pattern changes abruptly, with the wake "blooming" out at the rear of the vehicle. When the final flow rate was determined, a check was made to ensure that the exhaust rate was below the critical flow.

5. Model Configurations

Table 2 summarizes the conditions of the 18 series of wind tunnel test data for the small-scale vehicles; the 18 series consisted of a total of 357 tests. Each test consisted of tracer concentration measurements at 20 locations, averaged over the equivalent of a 1-h period in full scale. Initially, 49 tests were made with the large-scale (1:85) cars to check out the system. Subsequently, small-scale (1:300) vehicles were used in all other tests because of the larger test areas that could be simulated and to increase the magnitude of the surface roughness relative to the model. The first 7 small-scale test series (i.e., Q, R, S, T, U, V, and W) were designed to examine the effects on near-roadway dispersion caused by variations in traffic density, traffic speed and direction, and surface roughness in conjunction with joint variations in wind speed and direction. The subsequent set of 10 test series (C, D, E, F, G, H, I, J, K, and L) was designed to examine dispersion effects resulting from variations in the configuration of the roadway and nearby terrain; traffic density and direction were not varied during these tests, although traffic speed along with wind speed and direction were.

Table 2

SUMMARY OF WIND TUNNEL TEST FEATURES

Test Series	Roadway Configuration	Surface Roughness	Traffic Density	Traffic Flow	Traffic Speeds† (mph)	Wind Speeds† (mph)	Wind Directions	Number of Tests
P	At-grade*	Smooth	Hi-Hi	2-way	1.25 3.75 15.0 30.0 50.0	10.0 20.0	0, 15, 30, 60, 90°	49
Q	At-grade	Smooth	Hi-Hi	2-way	1.25 12.5 50.0	10.0 20.0	0, 15, 30, 60, 90°	30
R	At-grade	Smooth	Hi-Lo	2-way	12.5 50.0	20.0	0, 15, 30, 90°	18
S	At-grade	Smooth	Hi-Hi	1-way	12.5 50.0	10.0 20.0	0, 30, 90°	15
T	At-grade; narrow right-of-way	Rough	Hi-Hi	1-way	12.5 25.0 50.0	5.0 10.0 20.0	0, 30, 90°	15
U	At-grade; narrow R-O-W	Rough	Hi-Lo	1-way	25.0 50.0	5.0 10.0	0, 30, 90°	16
V	At-grade; narrow R-O-W	Rough	Hi-Lo	2-way	12.5 50.0	2.5 10.0	0, 15, 30, 90°	18
W	At-grade; narrow R-O-W	Rough	Hi-Hi	2-way	1.25 12.5 25.0 50.0	2.5 5.0 10.0	0, 15, 30, 60, 90°	32
C	At-grade; narrow R-O-W	Rough	Lo-Lo	2-way	1.25 12.5 25.0 50.0	2.5 5.0 10.0	0, 15, 30, 60, 90°	20
D	At-grade; wide R-O-W	Rough	Lo-Lo	2-way	1.25 12.5 25.0 50.0	2.5 5.0 10.0	0, 15, 30, 60, 90°	20
E	Cut section; vertical side walls	Smooth	Lo-Lo	2-way	1.25 12.5 25.0	10.0 20.0	0, 15, 30, 90°	16
F	Cut section; sloping side walls	Smooth	Lo-Lo	2-way	1.25 12.5 25.0	10.0 20.0	0, 15, 30, 90°	16
G	Elevated; fill section	Smooth	Lo-Lo	2-way	1.25 12.5 25.0	10.0 20.0	0, 15, 30, 90°	16
H	Elevated; via-duct section	Smooth	Lo-Lo	2-way	1.25 12.5 25.0	10.0 20.0	0, 15, 30, 90°	16
I	At-grade; narrow R-O-W	Smooth downwind; Rough upwind	Lo-Lo	2-way	1.25 12.5 25.0	10.0 20.0	0, 15, 30, 90°	16
J	At-grade; narrow R-O-W	Rough downwind; Smooth upwind	Lo-Lo	2-way	1.25 12.5 25.0	10.0 20.0	0, 15, 30, 90°	16
K	Side of hill	Smooth	Lo-Lo	2-way	1.25 12.5 25.0	10.0 20.0	0, 90, 270°	12
L	Vertical cut section with adjacent air-right structure	Smooth	Lo-Lo	2-way	1.25 12.5 25.0	10.0 20.0	0, 30, 150, 180°	16

*Large scale vehicles

†1 mph = 1.6 kmph

Figures 11 through 20 illustrate the roadway configuration, adjacent geometry, and sampling probe array for each of the 11 different model configurations. At the conclusion of the gas-sampling tests, flow visualization sequences were filmed with high-speed photography. Visible smoke was emitted through the exhausts of the model vehicles for various wind and traffic conditions and site configurations.

B. Comprehensive At-Grade Atmospheric Experiment

1. Introduction and Scope

The first atmospheric experiment was conducted in the San Francisco Bay Area on a stretch of U.S. Highway 101, midway between the Lawrence and San Tomas Expressways in Santa Clara, California (Figure 21). The road is a major intrastate freeway with three lanes of traffic in each direction.

The three basic objectives of this first atmospheric experiment were to:

- Investigate the impact of freeway traffic on the atmospheric wind and turbulence structure on and near the roadway.
- Determine the in-situ rate of emission from traffic flows of varying speed, density, and mix.
- Investigate freeway and nearby CO and hydrocarbon concentrations in relationship to traffic and meteorological conditions.

This particular site was chosen for several reasons related to the overall objective of trying to understand the effect of traffic flow on near-roadway pollutant dispersion. First, the site is relatively simple and homogeneous; within an 0.75-km radius of the sampling location, the land is flat, consisting mainly of level fields with a low growth of grasses. With only two exceptions, this land characteristic actually extends to more than a kilometer around the site. To the west-northwest is a subdivision of tract homes (see Figure 21), while about 350 m to the east a new overpass was partially constructed at the time. The two 7-m-high earth mounds were in place, but the access roads shown on the figure were not yet constructed. The test site was chosen to the west of the new overcrossing since east and northeast winds are least dominant.

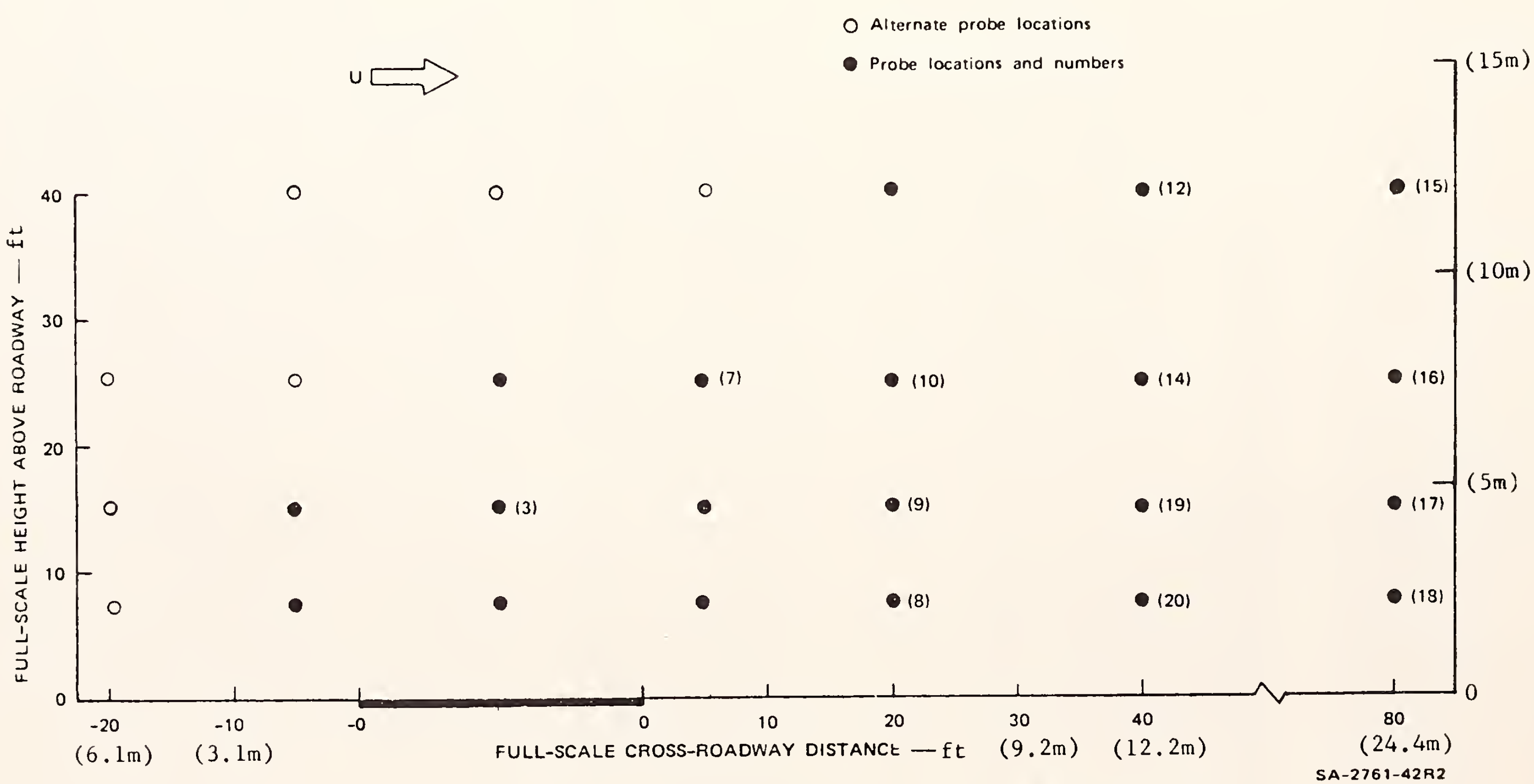

FIGURE 11 PROBE LOCATIONS FOR TEST SERIES Q, R, AND S; TERRAIN SMOOTH UPWIND AND DOWNWIND

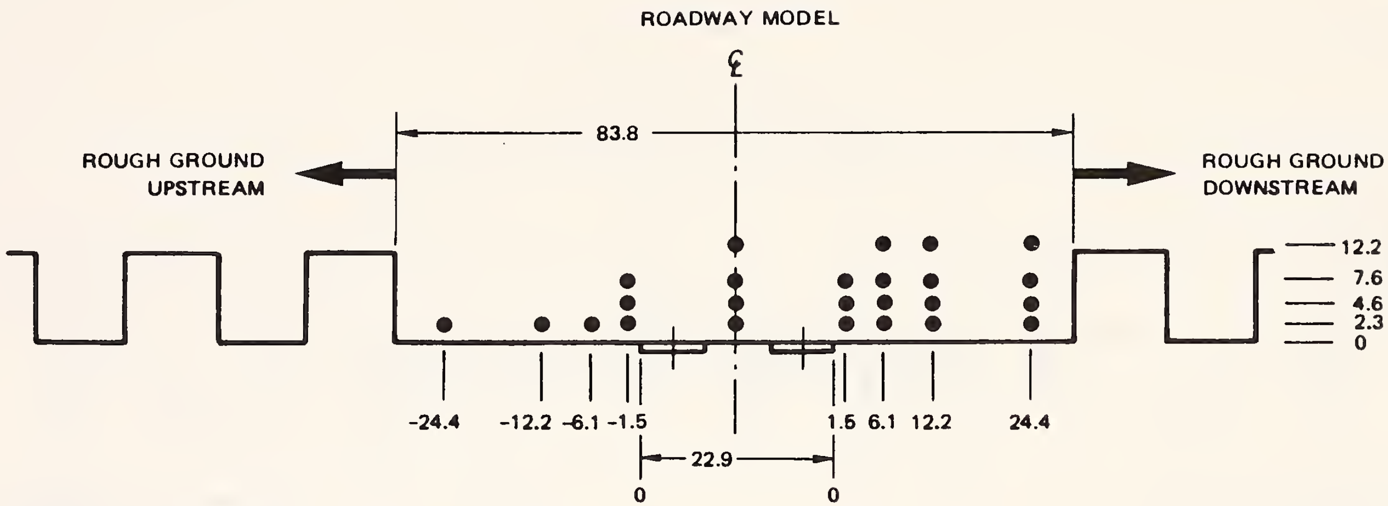

FIGURE 12 PROBE LOCATIONS AND TERRAIN GEOMETRY FOR TEST SERIES T, U, V, W, AND C

(All Distances Are In Metres)

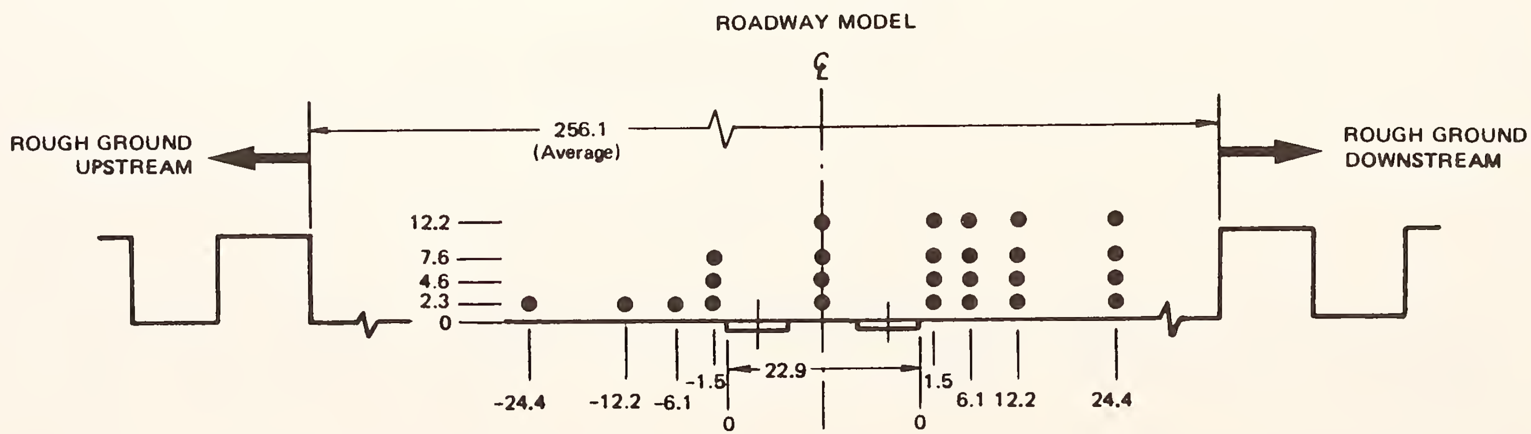

FIGURE 13 PROBE LOCATIONS AND TERRAIN GEOMETRY FOR TEST SERIES D

(All Distances Are In Metres)

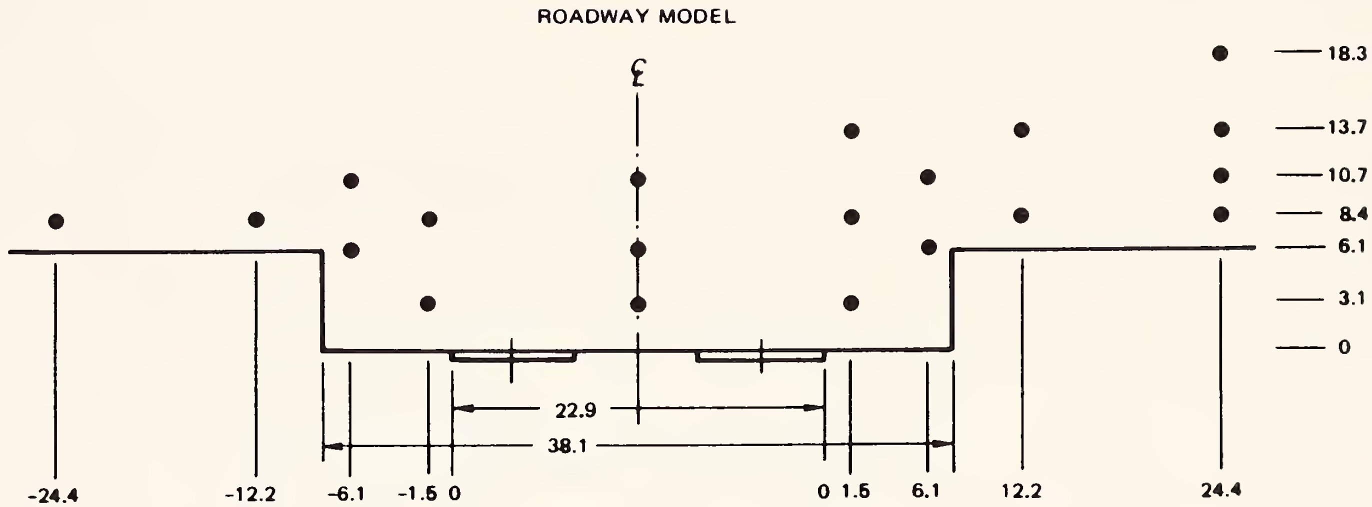

FIGURE 14 PROBE LOCATIONS AND TERRAIN GEOMETRY FOR TEST SERIES E AND L

(All Distances Are In Metres)

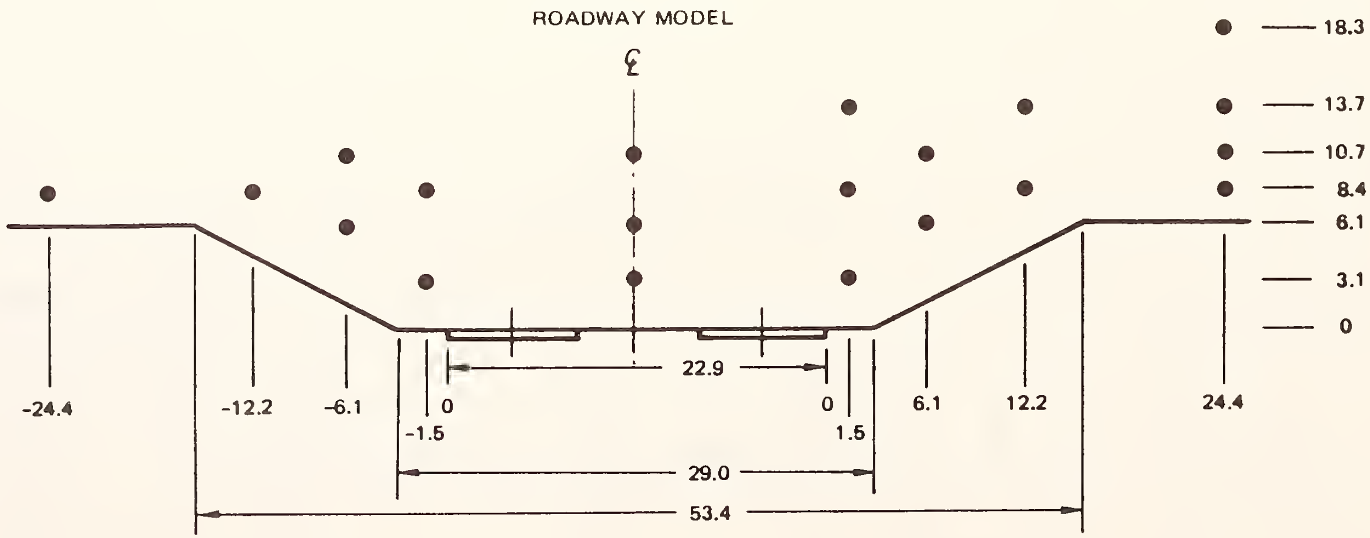

FIGURE 15 PROBE LOCATIONS AND TERRAIN GEOMETRY FOR TEST SERIES F

(All Distances Are In Metres)

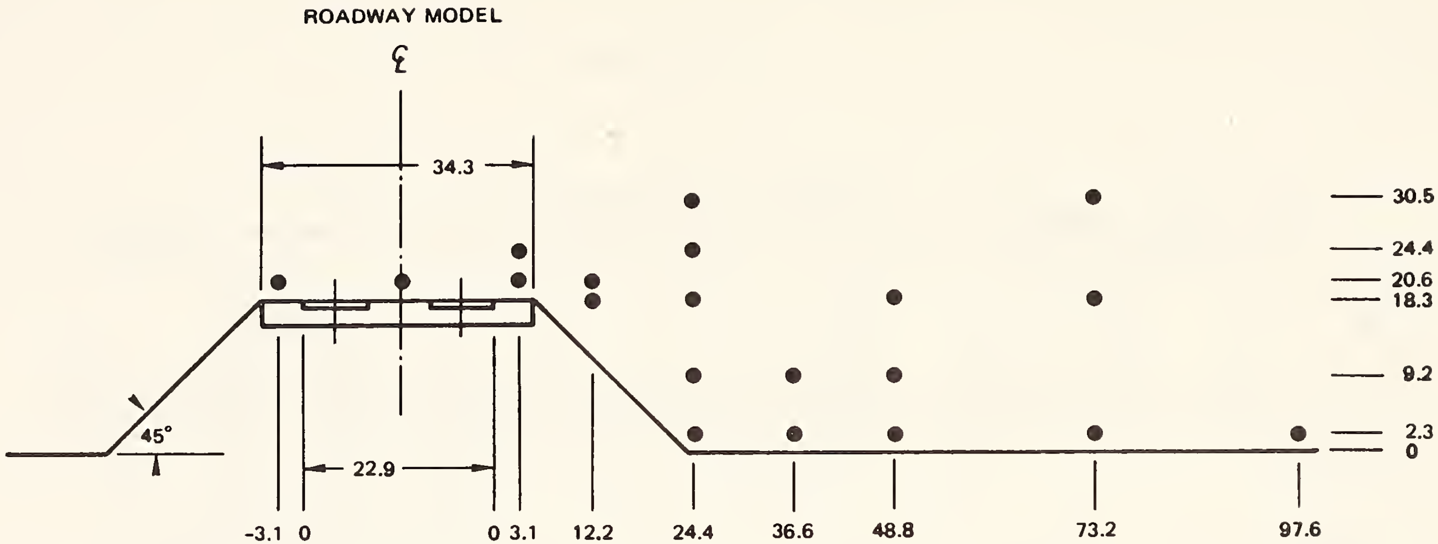

FIGURE 16 PROBE LOCATIONS AND TERRAIN GEOMETRY FOR TEST SERIES G

(All Distances Are In Metres)

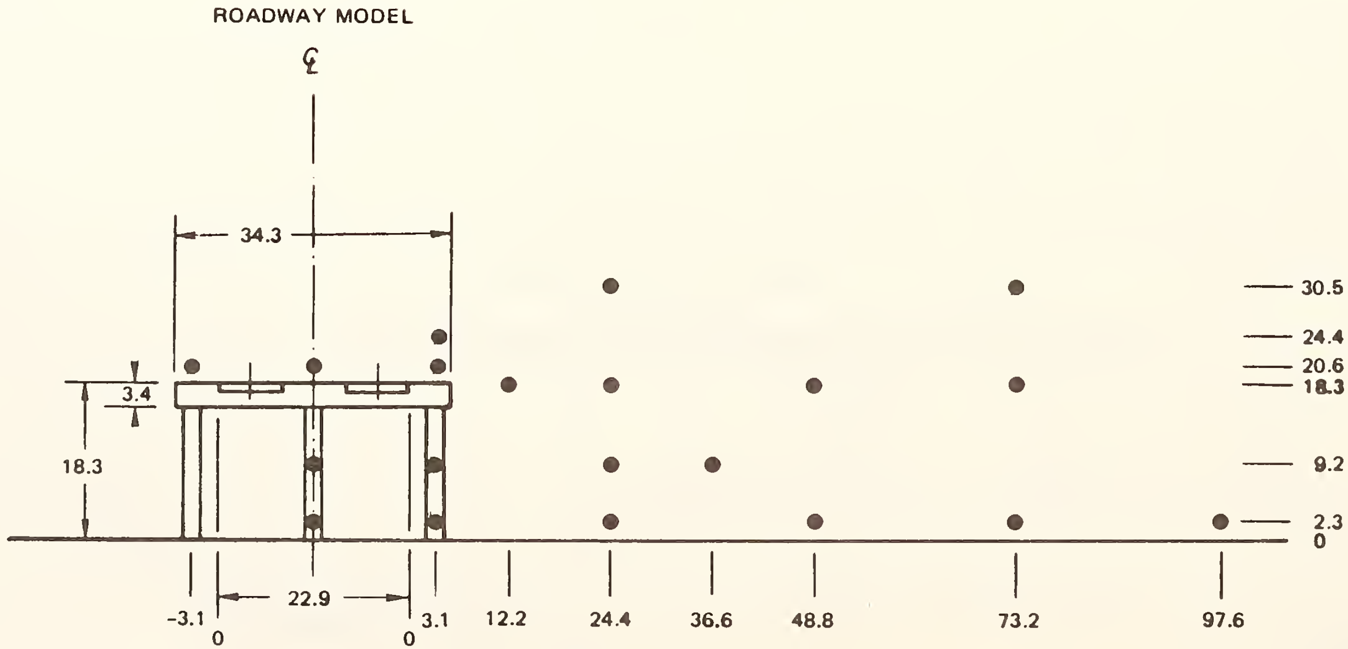

FIGURE 17 PROBE LOCATIONS AND TERRAIN GEOMETRY FOR TEST SERIES H

(All Distances Are In Metres)

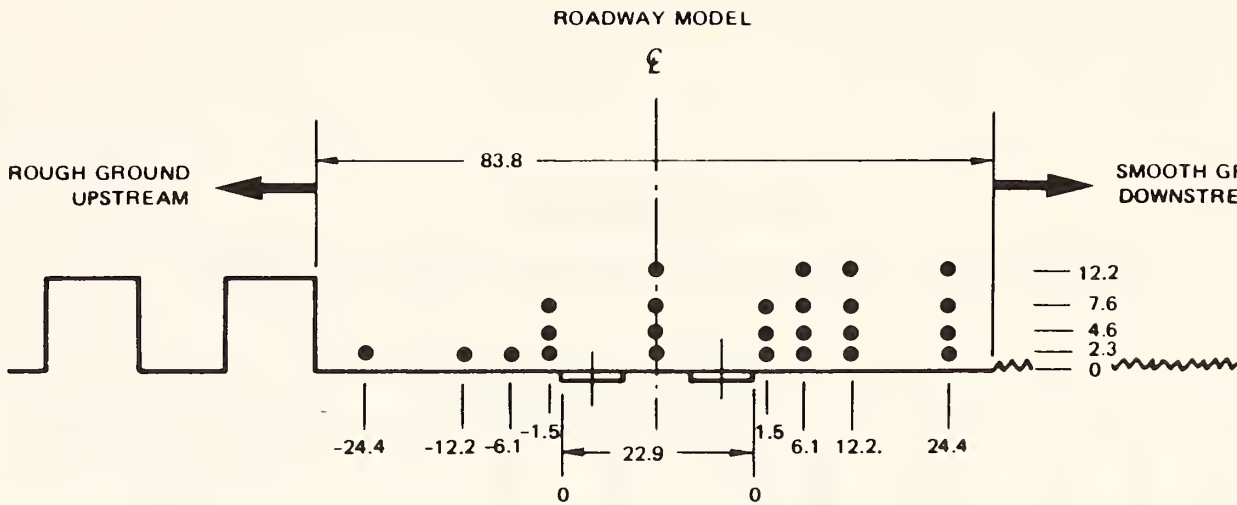

FIGURE 18 PROBE LOCATIONS AND TERRAIN GEOMETRY FOR TEST SERIES I

(All Distances Are In Metres)

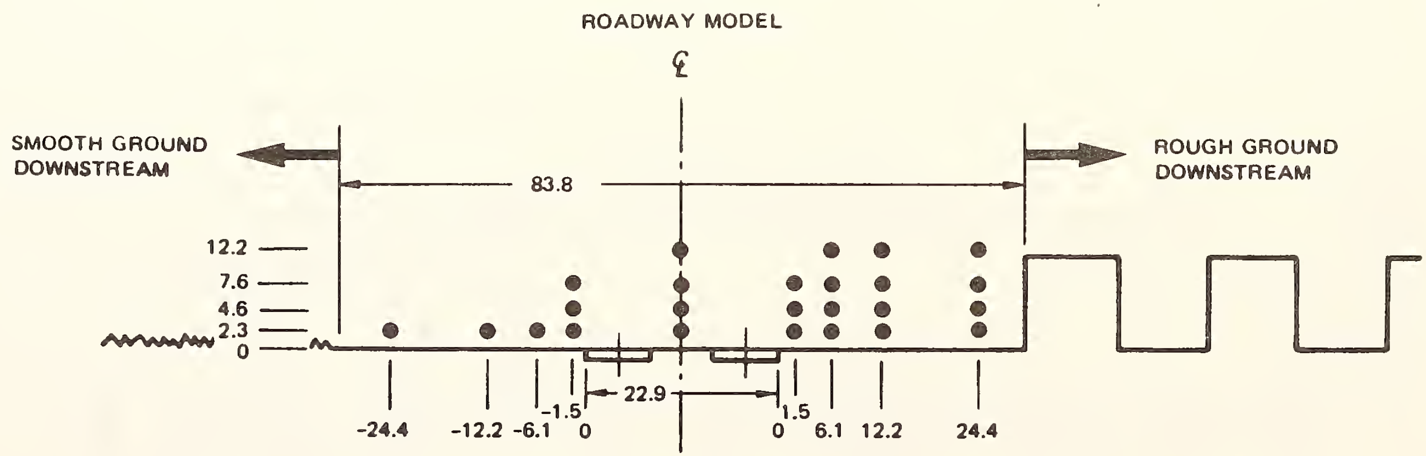

FIGURE 19 PROBE LOCATIONS AND TERRAIN GEOMETRY FOR TEST SERIES J

(All Distances Are In Metres)

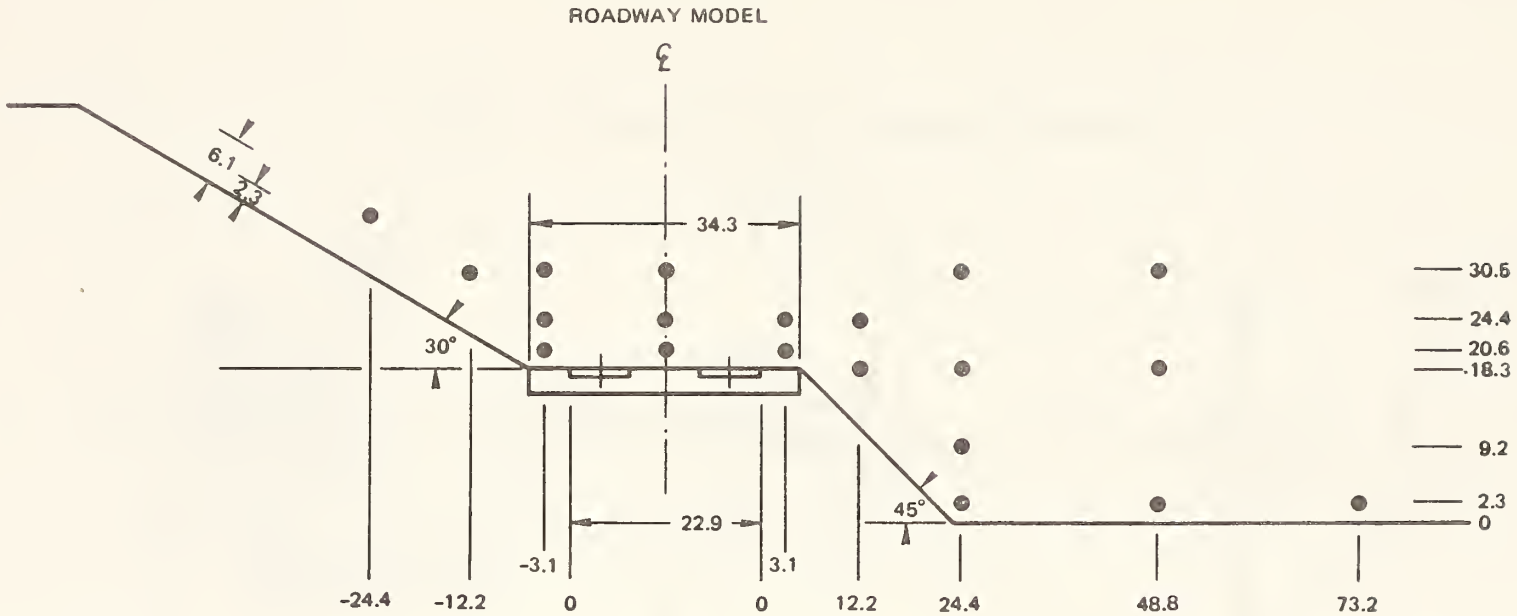

FIGURE 20 PROBE LOCATIONS AND TERRAIN GEOMETRY FOR TEST SERIES K

(All Distances Are In Metres)

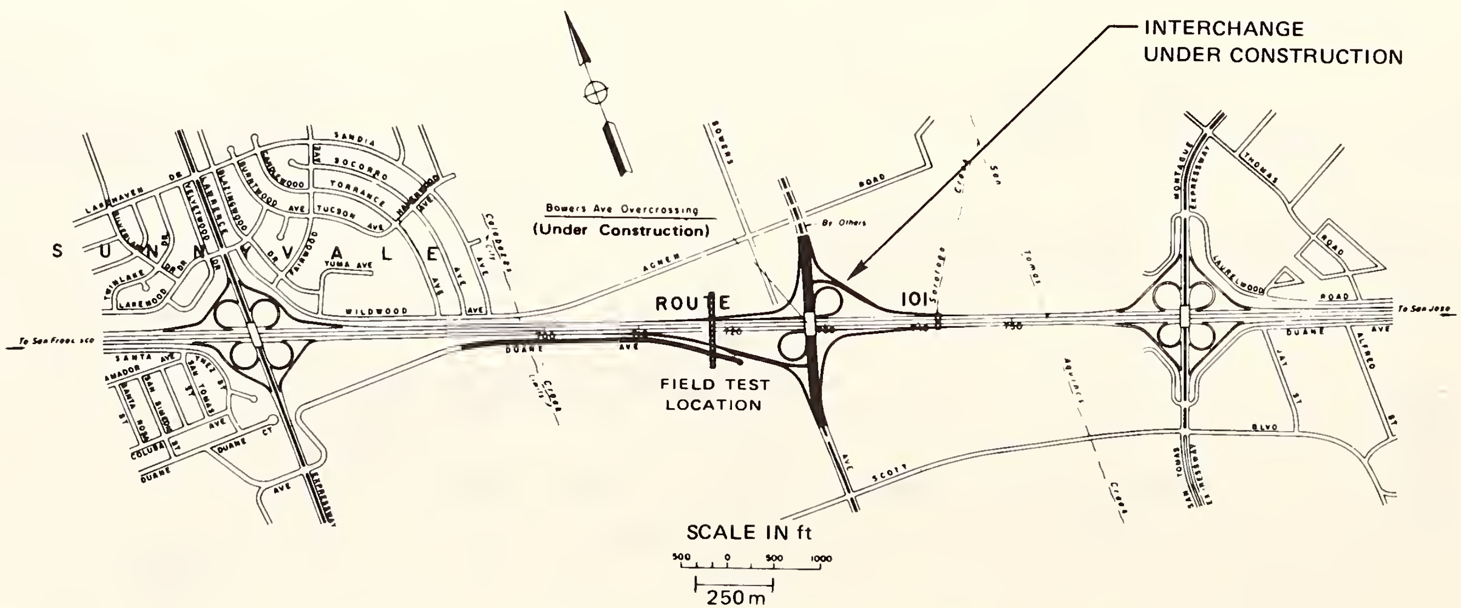

FIGURE 21 LOCATION OF HIGHWAY DISPERSION EXPERIMENT

The site had other advantages: traffic flow is heavy (around 100,000 ADT) and varies markedly throughout the day both in speed and volume by direction; also, the median strip is sufficiently wide to permit installation of a tower for meteorological and air sampling purposes. In fact, this is the only at-grade stretch of freeway in the south Bay Area that has all the features listed above.

To satisfy the experimental objectives, a comprehensive microsampling network was established to monitor wind, temperature, air quality, and traffic. Figures 22 and 23 illustrate the location and orientation of the meteorological instrumentation. All 50 meteorological data inputs were sampled, digitized, and recorded on magnetic tape every 2.5 s. Fifteen-minute summaries of both primary and derived parameters were prepared according to the format illustrated in Table 3. Comprehensive traffic information was recorded throughout the study, consisting of speed and axle number for each vehicle, segregated on a lane-by-lane basis. Fifteen-minute summaries were obtained as illustrated in Table 4(a); an explanatory key is given in Table 4(b). Two inert tracer gases were released from vehicles driven in the traffic stream; one tracer was released exclusively from the westbound lanes, the other from the eastbound. By controlling the release rate and location, measurements of tracer concentrations were used directly to quantify the pollutant dispersion processes from both traffic streams.

2. Instrumentation

a. Traffic Sensors

The traffic sensing system* contained three major components: traffic sensors, data processor and recorder (TDR), and a programmer. Two shielded cables were placed across each traffic lane at a separation of precisely 1.83 m [see Figure 24(a)]. The forward axle of a vehicle hitting the cable induced a signal of a few tenths of a volt; the time delay to the second cable was then detected and the near-instantaneous

---

*Transportation Data Corporation, P. O. Box 862, Arlington, Texas 76010.

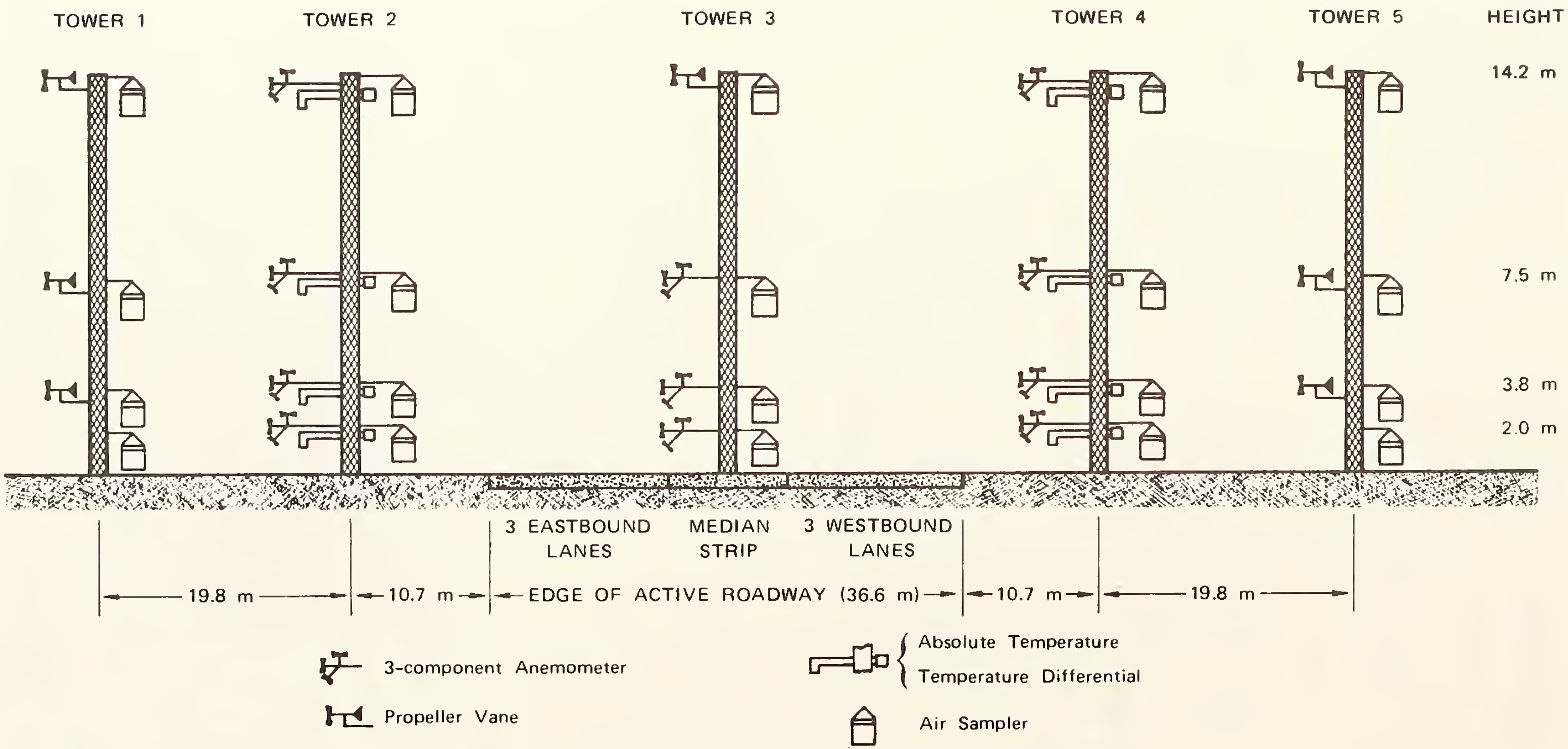

NOTE: Additional air samplers located at ground level (m) on both sides of road at 15.2-m intervals to 91, 5 m from roadway edges; see also Table 22.

FIGURE 22 AEROMETRIC INSTRUMENTATION LAYOUT AT GRADE-LEVEL TEST SITE

FIGURE 23 AEROMETRIC INSTRUMENTATION AND SRI MOBILE ENVIRONMENTAL MONITORING LABORATORY AT GRADE-LEVEL HIGHWAY TEST SITE

Table 3(a)

SAMPLE METEOROLOGICAL DATA SUMMARY

TIME PERIOD: 1345-1400 PST — DATE: 17 JAN 75

HEIGHT = 14.2 METERS	TOWER 1	TOWER 2	TOWER 3	TOWER 4	TOWER 5
WIND SPEED (M/S)	3.00	3.10	3.02	2.89	3.15
WIND DIR, TRUE	275.	320.	330.	320.	326.
SIGMA UR(M/S)	.71	.92	1.05	1.05	1.16
SIGMA VR(M/S)	.45	.61	.59	.59	.65
SIGMA U (M/S)	.36	.63	.63	.63	.69
SIGMA V (M/S)	.76	.92	1.05	1.03	1.16
SIGMA W (M/S)		.37		.36	
SIGMA THETA (DEG)	14.83	16.32	20.99	19.36	22.79
SIGMA PHI (DEG)		8.07		7.85	
TURB INT, HORIZ(M/S)	.84	1.11	1.05	1.20	1.33
TURB INT, TOTAL(M/S)		1.17		1.26	
TEMPERATURE (C)		15.22		15.14	
HEIGHT = 7.5 METERS					
WIND SPEED (M/S)	2.92	2.63	2.18	2.58	2.92
WIND DIR, TRUE	313.	323.	331.	320.	320.
SIGMA UR(M/S)	.99	1.06	1.09	1.06	1.14
SIGMA VR(M/S)	.57	.68	.71	.65	.61
SIGMA U (M/S)	.57	.59	.89	.74	.67
SIGMA V (M/S)	1.00	1.12	.94	1.00	1.13
SIGMA W (M/S)		.38	.16	.33	
SIGMA THETA (DEG)	20.00	22.23	26.64	22.78	23.50
SIGMA PHI (DEG)		7.72	6.94	8.57	
TURB INT, HORIZ(M/S)	1.14	1.26	1.30	1.24	1.29
TURB INT, TOTAL(M/S)		1.32	1.31	1.29	
TEMPERATURE (C)		15.64		15.36	
HEIGHT = 3.8 METERS					
WIND SPEED (M/S)	2.74	2.58	1.68	2.34	2.86
WIND DIR, TRUE	319.	318.	338.	317.	320.
SIGMA UR(M/S)	.79	.93	1.05	.99	1.14
SIGMA VR(M/S)	.62	.78	.99	.65	.68
SIGMA U (M/S)	.57	.66	1.01	.80	.72
SIGMA V (M/S)	.84	1.02	1.03	.87	1.14
SIGMA W (M/S)		.35	.45	.26	
SIGMA THETA (DEG)	19.01	22.01	40.73	23.32	25.47
SIGMA PHI (DEG)		7.57	18.11	8.88	
TURB INT, HORIZ(M/S)	1.00	1.21	1.45	1.18	1.33
TURB INT, TOTAL(M/S)		1.26	1.51	1.21	
TEMPERATURE (C)		16.15		15.56	
INSOLATION (LY/MIN)		0.000			
HEIGHT = 2 METERS					
WIND SPEED (M/S)		2.56	1.23	2.00	
WIND DIR,TRUE		311.	350.	318.	
SIGMA UR(M/S)		.76	.87	1.06	
SIGMA VR(M/S)		.72	.97	.69	
SIGMA U (M/S)		.64	.81	.87	
SIGMA V (M/S)		.83	1.02	.91	
SIGMA W (M/S)		.26	.48	.22	
SIGMA THETA (DEG)		19.95	44.59	35.94	
SIGMA PHI (DEG)		6.06	21.12	10.73	
TURB INT, HORIZ(M/S)		1.05	1.31	1.26	
TURB INT, TOTAL(M/S)		1.08	1.39	1.28	
TEMPERATURE (C)		16.46		15.80	
GRADIENT RI (2.0 - 3.8 M)		-34.85		-.16	
(3.8 - 7.5 M)		-27.29		-.40	
(7.5 - 14.2 M)		-.53		-.64	
BULK RI NUMBER		-48.93		-.71	

Table 3(b)

KEY TO METEOROLOGICAL DATA SUMMARY

SIGMA	= standard deviation
UR	= horizontal cross-roadway wind component
VR	= horizontal along-roadway wind component
U	= east-west wind component
V	= north-south wind component
W	= vertical wind component
SIGMA THETA	= standard deviation of horizontal wind-direction fluctuations
SIGMA PHI	= standard deviation of vertical wind direction fluctuations
TURB INT, HORIZ	= modified intensity of fluctuations of horizontal wind components
TURB INT, TOTAL	= modified intensity of fluctuations of horizontal and vertical wind components
INSOLATION	= flux density of downwelling solar radiation
GRADIENT RI	= gradient Richardson number
BULK RI	= bulk Richardson number

Table 4(a)

SAMPLE TRAFFIC SURVEY SUMMARY

```
TDC REPORT 50909-2-STAR      -1      PG  5      15-MINUTE SUMMARIES

          ALL RECORDED VEHICLES                        :  MULTI-AXLE VEHICLES
                                     5%-               :                 5%-
L    V    M   15%  MED  85%  95%   95% %/P %SP  MX MI:  V   M   85%   95% %/P
================================================================================
TIME 07:30  75/09/03

A   212 59.7 56.6 60.0 62.4 64.3  9.7 91  2.8 67 51:   5 58.6**************
B   292 56.9 54.1 56.7 59.7 62.3 10.2 90  2.1 73 47:   2 57.0**************
C   346 53.8 49.7 53.7 57.7 59.7 12.2 80  0.3 65 45:   8 52.8 57.6 14.0 75
D   391 51.9 42.3 48.5 55.8 97.1 74.4 60 11.1 97 17:  25 42.2 50.8 36.7 64
AB  504 58.1 54.7 57.9 61.5 63.7 11.1 86  2.6 73 47:   7 58.1 62.0 14.0 71
CD  737 52.8 45.3 51.5 57.6 96.3 56.1 61  5.9 97 17:  33 44.8 54.0 39.6 57
TIME 07:45, LS  16;A 79 @ 07:40;B106 @ 07:40;C123 @ 07:40;D135 @ 07:40

A   240 60.0 57.0 59.9 63.2 65.5 11.1 87  6.3 69 49:   5 60.6**************
B   302 57.1 53.8 57.0 60.2 63.3 11.0 89  2.3 71 35:   1 55.0**************
C   318 54.9 50.4 54.8 59.1 62.0 13.8 76  1.3 67 45:  10 52.6 56.5 10.8 90
D   405 51.3 40.9 49.4 56.4 97.0 76.9 55 10.3 97 17:  28 37.6 51.1 35.9 56
AB  542 58.4 54.6 58.4 61.9 64.6 12.1 82  4.1 71 35:   6 59.7**************
CD  723 52.9 45.0 52.3 58.8 96.2 60.7 59  6.2 97 17:  38 41.5 53.1 39.1 55
TIME 08:00, LS  16;A 89 @ 07:45;B116 @ 07:50;C121 @ 07:50;D141 @ 07:45

A   164 60.6 57.1 60.8 63.6 66.3 11.0 88  7.9 71 49:   7 59.3 62.9 14.5 85
B   243 57.7 53.9 57.9 61.7 63.7 12.7 81  2.1 67 45:   2 59.0**************
C   277 55.1 51.1 55.1 58.7 61.7 13.0 81  0.7 67 41:   9 52.6 55.7  8.5100
D   336 53.3 41.2 49.1 62.5 97.3 75.9 46 14.7 97 17:  23 45.9 53.1 25.9 73
AB  407 58.9 55.0 59.1 62.8 64.8 12.4 83  4.4 71 45:   9 59.2 62.6 14.5 88
CD  613 54.2 44.5 53.3 59.1 96.7 61.3 58  8.1 97 17:  32 47.8 54.6 21.3 62
TIME 08:15, LS  14;A 65 @ 08:00;B 87 @ 08:00;C 97 @ 08:05;D123 @ 08:00

A   128 60.8 57.3 60.8 63.7 67.4 12.4 84 10.9 73 51:   4 62.0**************
B   232 57.4 54.0 57.4 61.2 64.3 13.8 81  3.9 69 43:   1 57.0**************
C   276 53.7 49.5 54.4 57.9 60.1 14.0 78  0.4 67 23:  11 51.9 58.7 20.3 72
D   336 52.0 42.6 49.0 56.4 97.1 74.7 60 10.8 97 17:  16 38.1 49.1 34.7 56
AB  360 58.6 54.6 58.6 62.6 65.8 14.4 81  6.4 73 43:   5 61.0**************
CD  612 52.8 45.0 51.9 57.7 96.1 57.9 59  6.0 97 17:  27 43.7 53.9 42.4 48
TIME 08:30, LS  13;A 81 @ 08:15;B 88 @ 08:15;C 93 @ 08:20;D116 @ 08:20

A   133 60.2 57.3 60.1 63.2 65.3  9.5 91  6.0 69 53:   4 60.5**************
B   239 57.7 54.0 57.5 61.2 63.6 11.3 86  2.1 73 51:   0
C   263 54.8 51.0 54.6 59.2 61.6 13.2 79  0.0 65 45:   6 51.7**************
D   306 50.5 41.9 48.6 55.6 96.0 73.4 50  7.4 97 17:  15 48.2 52.7 39.6 46
AB  372 58.6 55.0 58.8 62.0 64.3 11.7 84  3.5 73 51:   4 60.5**************
CD  569 52.6 45.7 52.3 57.9 62.8 34.0 59  3.8 97 17:  21 43.5 53.4 38.7 47
TIME 08:45, LS  10;A 55 @ 08:40;B 85 @ 08:30;C 89 @ 08:40;D106 @ 08:35

A   111 61.6 58.3 61.4 65.1 67.0 10.3 91 16.2 71 55:   7 60.7 63.9  6.0100
B   206 58.0 54.2 57.8 61.8 64.3 12.1 83  4.4 71 51:   1 61.0**************
C   254 54.9 50.7 54.9 59.0 61.4 13.2 79  0.0 69 41:   5 55.0**************
D   289 48.8 42.1 47.9 54.9 61.2 35.0 59  4.1 97 17:  18 45.3 49.8 30.4 77
AB  317 59.3 55.0 59.2 63.5 65.9 13.1 79  8.5 71 51:   8 60.8 63.6  6.8100
CD  543 51.7 44.8 52.3 57.8 61.4 22.2 57  2.5 97 17:  23 47.6 55.6 29.6 60
TIME 09:00, LS  17;A 42 @ 08:45;B 83 @ 08:45;C 94 @ 08:45;D105 @ 08:50
```

Table 4(b)

KEY TO TRAFFIC SURVEY SUMMARY*

SITE AND OPERATOR IDENTIFIERS:

LOCATION:	101 EASTBOUND 1-24-75 STANFORD RESEARCH INSTITUTE W. DABBERDT
TYPE OF REPORT:	15-MINUTE STATISTICAL SUMMARY
SAMPLE PERIOD:	START: FRI 75/24/01 04:55 STOP: FRI 75/24/01 13:15
ROADWAY TYPE:	FREEWAY 3 LANES, EACH DIRECTION - SURFACE CLEAN 20 TO 30 FT MEDIAN DIVIDED, BARRIER LESS THAN FOUR FT.
ROADWAY CONDITION:	SURFACE VERY GOOD, 12 FT. LN. WIDTH LANE MARKINGS RAISED
LANE IDENT.:	A - EAST BOUND LANE 3 B - EAST BOUND LANE 2 C - EAST BOUND LANE 1 (CURB) D -
WEATHER:	CLEAR AND DRY - 60 DEG F - AT START OF RUN
SPEED LIMIT:	55 MPH
SYSTEM OPERATOR:	WFD OF RESEARCH DEPT.
DATA RECORDER:	SERIAL NUMBER 00*09
DATA PROCESSED BY:	TDC PROGRAM A1 ON 27-JAN-75 - REPORT FORMAT A1.0

V=VOLUME   M=MEAN SPEED   %=PERCENTILE   MED=MEDIAN

5%-95%=SPEED SPREAD IN MPH 5 TO 95 PERCENTILE   %/P=%VEHICLES IN 10 MPH PACE

%SP=% VEHICLES EXCEEDING 10 MPH ABOVE POSTED LIMIT

MX=MAXIMUM SPEED IN PERIOD IN MPH   MI=MINIMUM SPEED IN PERIOD IN MPH

TIME=BEGINNING AND ENDING TIME (IN 24-HOUR CLOCK)

LS=LANE STRADDLERS IN ALL LANES   A 66 @ 07:35;=PEAK 5-MINUTE VOLUME THIS PERIOD IS 66 VEHICLES---IN LANE A BETWEEN 7:35 & 7:40.

*1 ft = 0.305 m

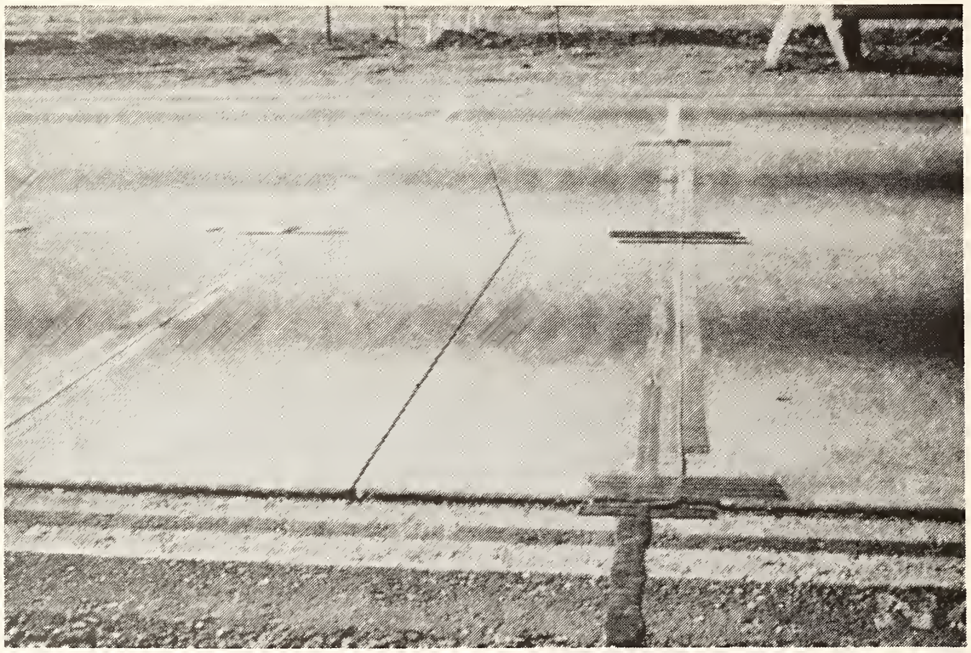

SA-2761-47a

FIGURE 24a TRAFFIC SENSOR CABLES ON THE EASTBOUND LANES OF U.S. HIGHWAY 101

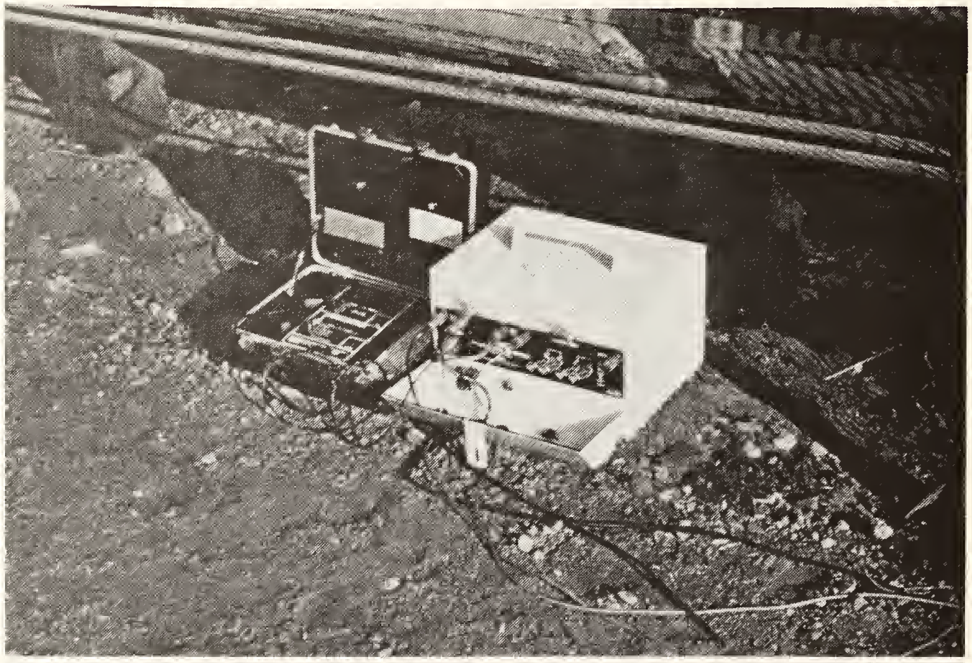

SA-2761-47b

FIGURE 24b TRAFFIC DATA RECORDER AND PROGRAMMER vehicle speed was determined. Subsequent axles hitting the cable within a distance of 8.2 m were assigned to the same vehicle, and the speed and axle-number data per vehicle were recorded on a cassette recorder within the TDR. The programmer was used to start and stop the TDR, and also to input site-characteristic and lane identifier data on the tape [see Figure 24(b)].*

b. Meteorological Sensors

(1) Wind Measuring Systems

Wind and turbulence measurements were obtained from five instrumented towers. Propeller vanes were located at three heights on two of the towers and UVW anemometers were placed at four heights on the remaining three towers (except on the median tower where a propeller vane was located at a height of 14.2 m). The locations of these instruments are shown in Figure 22.

The UVW anemometers (Model 27002) were manufactured by R. M. Young Company† and are shown in Figure 25. This instrument has a threshold sensitivity of 0.1 to 0.2 m/s and a distance constant of 0.94 m. It consists of three orthogonally-oriented, low-inertia propellers to measure the three wind components.

The propeller vanes (Model 35003) were also manufactured by R. M. Young Company. The propellers on this instrument, like those on the three-component sensors, have a low starting speed, about 0.2 m/s, and a distance constant of 1.2 m.

---

*Physical and logistical support in the installation of the cable sensors and construction of barriers to shield the towers was provided by the California Department of Transportation, District 04, San Francisco.

†R. M. Young Company, 2801 Aero-Park Drive, Traverse City, Michigan 49684.

FIGURE 25 15-m METEOROLOGICAL TOWER WITH UVW ANEMOMETERS, PLATINUM-RESISTANCE TEMPERATURE SENSERS, AND AIR QUALITY SAMPLER

(2) Temperature Profile System

Temperature profile measurements were obtained from the two towers adjacent to the roadway. Both towers measured ambient temperature near the base (2.0 m) and the temperature differential at three heights (3.8 m, 7.5 m, and 14.2 m).

The sensor (Figure 25) used had platinum wire resistance elements[*] that were mounted in 0.125-in. (3.1-mm) stainless steel tubes. These tubes were housed in radiation shields[†] of silvered, double-walled glass cylinders similar to Dewar flasks and were ventilated at a rate of 5 m/s. The time constant of the aspirated, steel-housed sensor was about 40 s. Temperature differences of as little as 0.01°C between sensors could be detected.

(3) Insolation

The solar insolation was continuously measured by an Eppley Laboratory, Black and White Pyrometer (Model 8-48).[‡] The pyrometer uses a differential thermopile enclosed in a glass casing to measure incident solar radiation. The instrument has built-in temperature compensation. The glass dome covering the receiver is made of precision ground optical glass that admits radiation in the wavelength interval from about 0.28μ to 2.8μ. The instrument was located on the roof of the mobile laboratory (Figure 14) away from any obstructions.

c. Air Quality Samplers (AQS)

Environmental Measurements Incorporated (EMI)[§] sequential multiple-bag samplers were used during the field test. The samplers were programmed to obtain 4-ℓ hourly air samples at each of 35 locations (Figures 22

---

[*] Rosemount Engineering Model 104MK-57-BB-CC, Minneapolis, Minnesota

[†] R. M. Young Model 43404.

[‡] Eppley Laboratory, Newport, Rhode Island.

[§] Environmental Measurements, Inc., 1166 Independence Way, Mt. View, CA 94040.

and 23); 20 samplers were located at the ground surface and out to 100 m from the roadway edge, while 15 were placed on the towers. The samplers obtain an integrated air sample by utilizing a 150-ms ON cycle every second. The sample bags are made of clear Tedlar and can hold about 5 ℓ of air. Figure 26 shows the programmable sampler with Tedlar bags.

FIGURE 26 SEQUENTIAL MULTIPLE-BAG SAMPLER (top raised for photograph)

d. Tracer Gas Release Vans

Two vans (Figures 27a and 27b) were equipped to release both of the two tracer gases. They were driven continuously in the traffic stream for the entire run series, always in the middle lane at the general traffic speed, but not exceeding 55 mph (90 km hr^{-1}). Figure 28 is a diagram of the release system in the vans. The systems for both SF_6 and F13B1 were identical. The gas cylinders were weighed before and after each 8-h run. The drivers released SF_6 in the west direction and F13B1

FIGURE 27a CONTROL VAN IN TRAFFIC STREAM

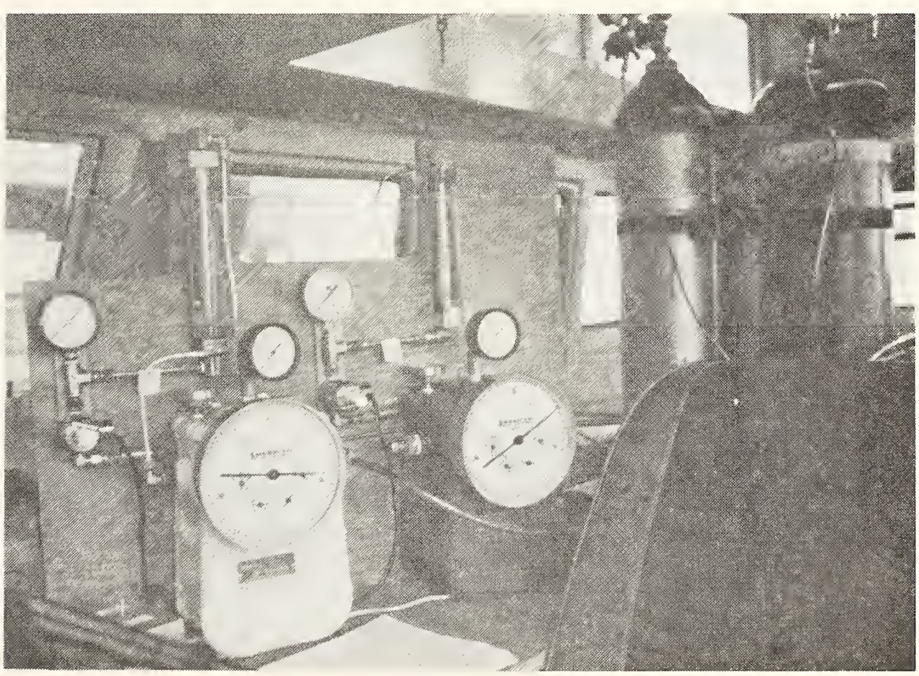

FIGURE 27b VAN INTERIOR, SHOWING DUAL GAS RELEASE AND MONITORING SYSTEM

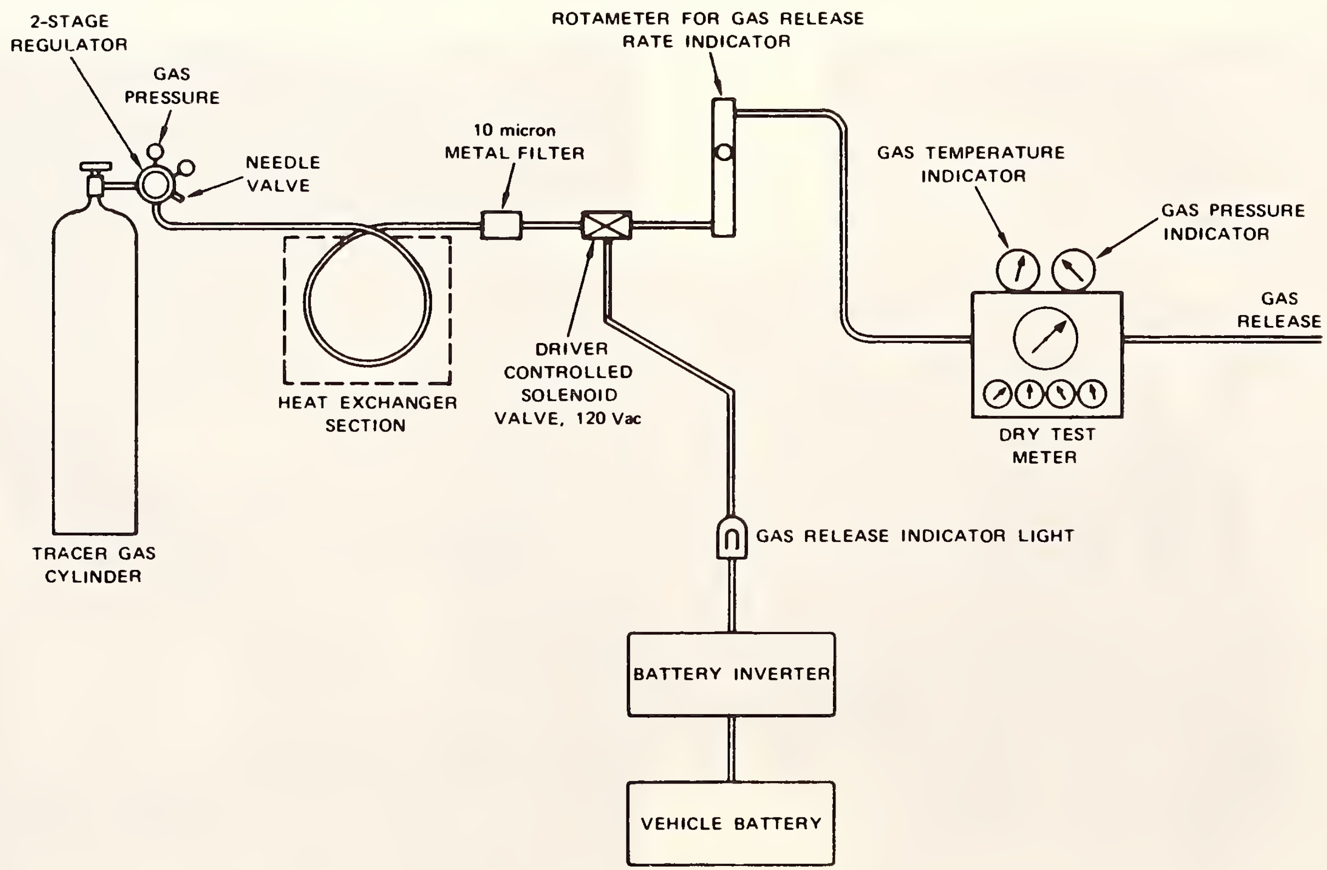

FIGURE 28 TRACER GAS RELEASE SYSTEM

(Same for SF_6 and F13B1)

in the east direction. At the start of each release the driver recorded the time, gas cylinder pressure, flow rate, dry test meter volume, and the pressure and temperature of the gas.

With this information, the amount of tracer released could then be obtained by two methods:

- Determining the total weight loss of the cylinder with the precision scale (2-oz resolution).
- Measuring the total volume flow during each test with the dry test meter, and converting to weight using measured temperature and pressure.

e. Analytical Detectors

(1) Sulfur Hexafluoride (SF_6 and Fluorotribromomethane (F13B1)

(a) GC System

The tracer gas (SF_6 and F13B1) samples were analyzed by means of a dual gas chromatograph (GC) coupled to a two-channel electronic peak integrator. The system is a Perkin-Elmer* Model 3920 GC equipped with two variable pulse electron capture (EC) detectors. Each EC detector has its own electrometer GC column and injection system. In essence, this unit is operated as two identical, yet independent, GCs in parallel within one column oven. Each detector output signal is connected to one channel of the dual channel recorder and dual channel electronic peak integrator.

(b) Exponential Dilution System

An exponential Dilution System (EDS) was specially designed, fabricated, and used to obtain dynamic calibration standards starting from the initial calibration gas concentration (approximately 1 ppm SF_6 and 10 ppm F13B1) down to the lower limit of GC detectability.

---

*Perkin-Elmer, Norwalk, Connecticut 06856.

Surface adsorption of tracer gases initially was found to be a problem when the unit was run at room temperature, and was minimized by operating the entire unit at a temperature of 40°C or higher, using electrical heating tapes.

The EDS unit is composed of two concentric tubes, with the inner tube directly connected to the inlet of the diluent gas (nitrogen or air). Holes drilled on the surface of the inner tube near the inlet connect it to the outer shell. A critical orifice is installed at the inlet and is designed to control the flow at 0.5 ℓ min^{-1}. The critical flow orifice creates a jet or gas at sonic velocity as the diluent gas enters the EDS.

To start the operation, the EDS unit is filled with the known standard and evacuated. The fill-evacuate cycle is repeated twice and the EDS is then brought to atmospheric pressure with the standard. The diluent gas flow is then started. Because of the incoming sonic velocity of the diluent gas, the entire gas column in the inner tube in rapidly pushed forward. The internal gas circulation pattern is highly turbulent with velocities that exceed 300 m/s. Complete and rapid mixing is obtained and exponential dilution laws apply.

(c) Verification of Concentration of Calibration Gas Mixture

The gas mixture used for the GC calibrations as ordered from the supplier was supposed to contain 1 ppm (by weight) of SF_6 and 10 ppm of F13B1. Independent determinations of the tracer gas concentrations in this cyliner were obtained by SRI personnel by preparing diluted samples of pure SF_6 and F13B1, and comparing the resulting absolute concentrations of the samples with those for the calibration gas as measured by the GC. This procedure was repeated eight times for both SF_6 and F13B1 (Table 5). The final values used for the calibration gas concentrations are 0.71 ppm for SF_6 and 8.35 ppm for F13B1.

Table 5

RESULTS OF ANALYSES CONDUCTED TO VERIFY CONCENTRATION OF CALIBRATION GAS

Sample Number	Derived Concentration of Calibration Gas (ppm)	
	SF_6	F13B1
1	0.79	10.2
2	0.78	8.5
3	0.63	7.6
4	0.69	7.5
5	0.76	9.9
6	0.74	8.5
7	0.60	7.3
8	0.65	7.3
Average SF_6 = 0.71 ppm F13B1 = 8.35 ppm		

(d) Calibration of the GC System

Both channels of the GC system were routinely calibrated for both SF_6 and F13B1 during each analysis run, using the calibration gas mixture in conjunction with the SRI-designed EDS unit. The resulting calibrations and associated data are presented in Figure 29. These data were used to convert the raw output (counts) from the GC system to absolute tracer concentrations.

(2) Carbon Monoxide (CO) and Hydrocarbons (HC)

The Beckman* Model B6800 Air Quality Chromatograph was used to measure the concentration of CO, methane (CH_4), and HC in the bag samples. The atmospheric sample is drawn into the analyzer by an internal suction pump. Within the instrument, components are separated by column

*Beckman Instruments, Inc., Fullerton, CA 92634.

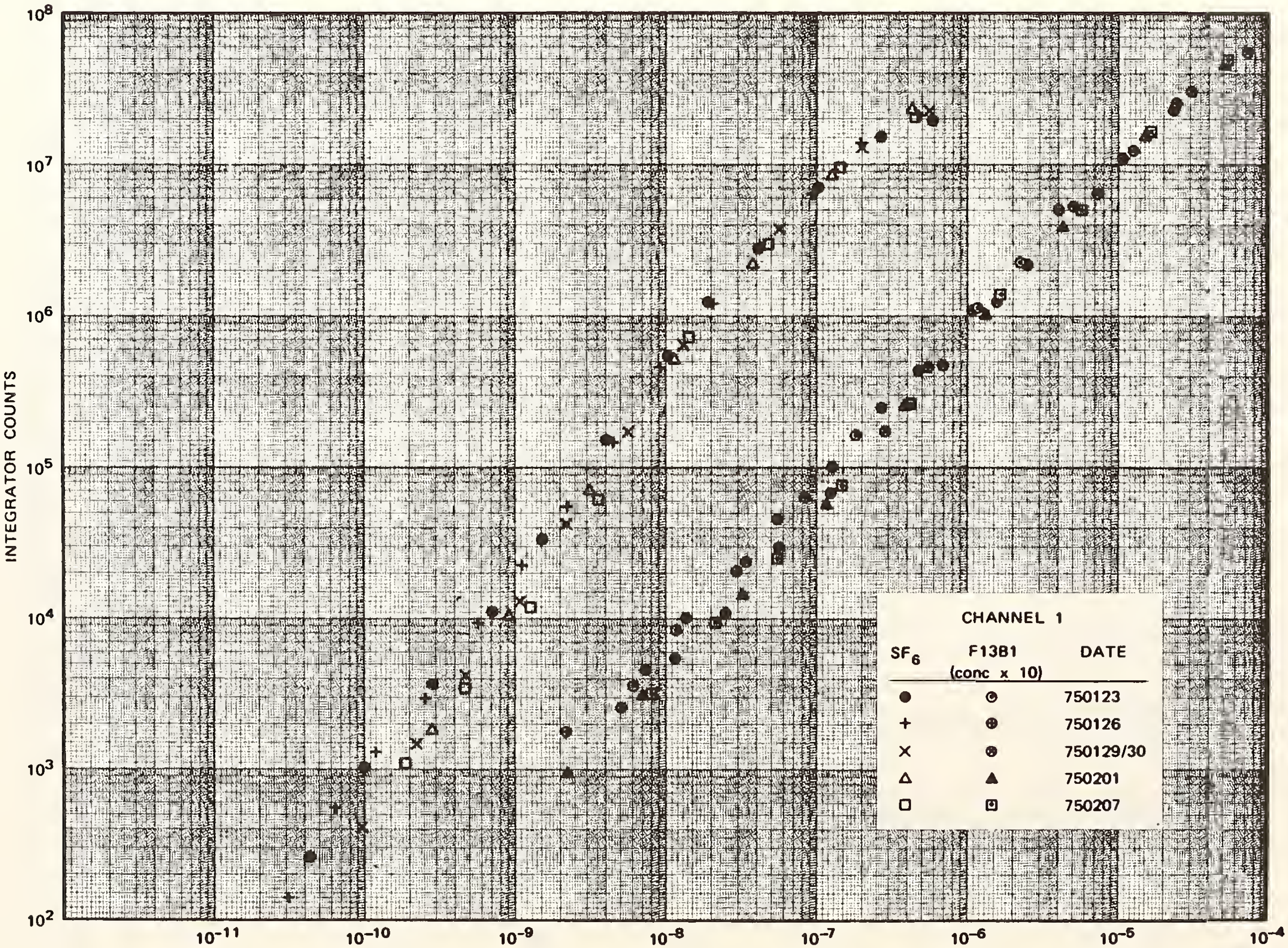

SA-2761-60

CONCENTRATION, vol/vol

FIGURE 29a GC CALIBRATION CURVE FOR SF_6 AND F13B1 (CHANNEL 1)

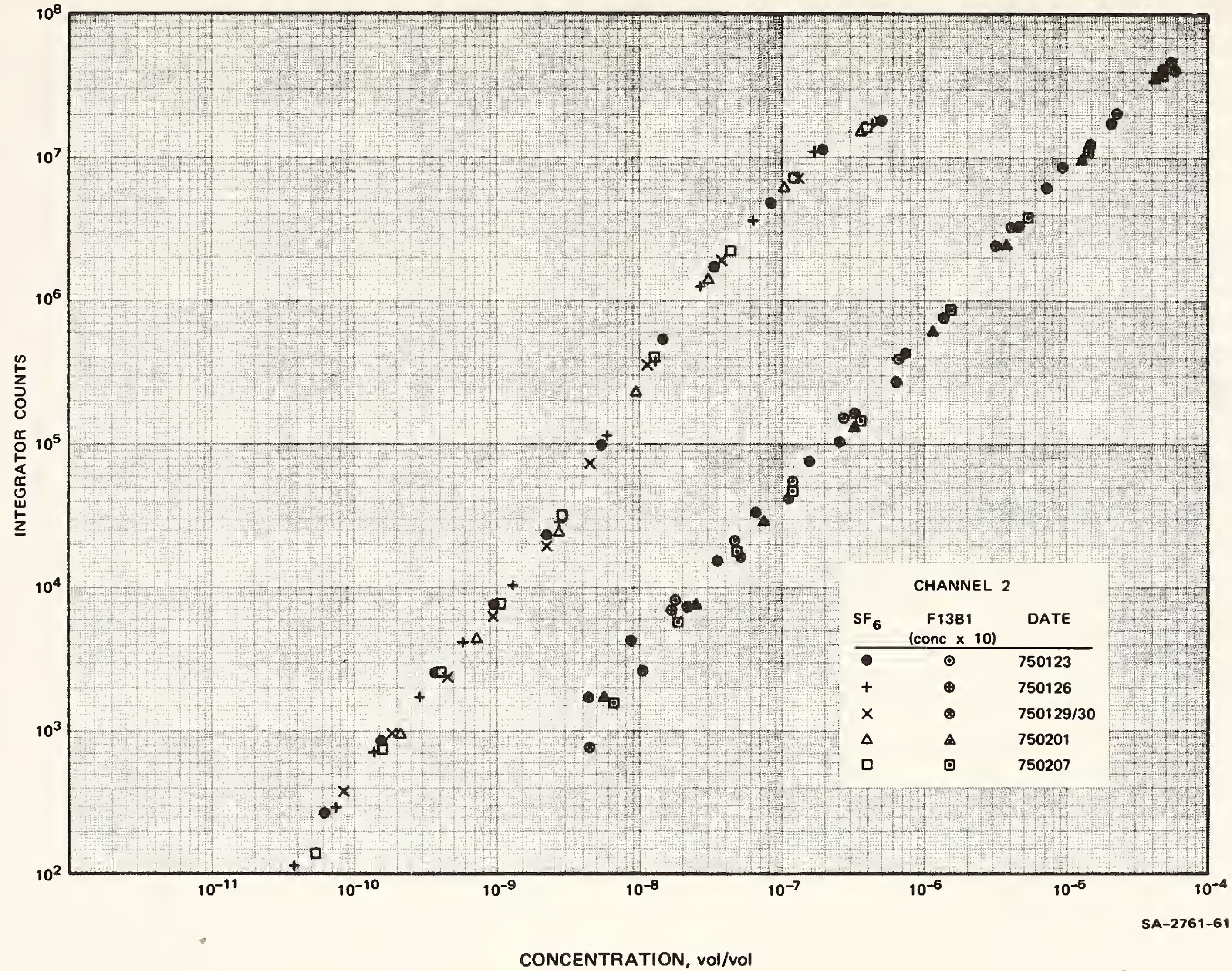

FIGURE 29b GC CALIBRATION CURVE FOR SF_6 AND F13B1 (CHANNEL 2)

chromatography. The column effluent is routed to a flame-ionization detector (FID). Electronic circuitry then measures the detector signal and provides output to a strip-chart recorder.

Before each test series the system was calibrated with a known source of CO. In addition, at several intervals during the analysis, this known source was injected into the system to check for drift.

This standard was checked with the standard used by the Bay Area Pollution Control District (BAAPCD); the results are shown in Table 6.

Table 6

STANDARDS COMPARISON WITH BAY AREA
AIR POLLUTION CONTROL DISTRICT
(BAAPCD)

	CO Values (ppm)		
SRI	0.15	22.8	54.0
BAAPCD	0.50	23.0	49.5

On the basis of the close agreement found in the range of CO concentrations monitored, there was no need to depart from the certified value of the SRI calibration gas.

3. Experimental Procedure

Six eight-hourly test runs were made between January 17 and February 5, 1975; the actual date, time, and duration of each test are given in Table 7. Before each series of test runs, the sample bags were thoroughly cleaned and each AQS was serviced. After bag installation, the AQSs were programmed for the proper cycle sequence, then set out in the appropriate array. An hour before the run, the tracer gas cylinders were weighed and the vans made ready. Thirty minutes before the run, the two traffic data processors and recorders were deployed and programmed.

Table 7

SCHEDULE OF HIGHWAY TRACER TESTS

Date (1975)	Hours (PST)	Number of 1-h Tests*
17 January	1200-2000	8
21 January	0500-1300	8
24 January	0500-1300	8
28 January	0500-1300	8
30 January	1200-2000	8
5 February	1200-2000	8
	Total	48

*Three hours had invalid tracer data:

12-1300, 17 January
05-0600, 21 January
05-0600, 24 January

About 15 min before the run, the meteorological data recording was activated and the tracer release vans started their runs.

The two vans were driven continuously in the traffic stream; the vehicles always drove in the center lane at the general traffic speed, but not exceeding 55 mph. SF_6 was released in the west direction and the F13B1 in the east direction. Both gases were released at a measured and uniform rate, between points approximately 400 m to either side of the sampling array. At the end of the eight-hour series, the tracer gas cylinders were weighed again and the sample bags collected. To ensure correct identification of the bags, labels were affixed directly to each bag. The bags were then assembled and arranged for analyses. The TDRs were collected, and meteorological data collection terminated. The next 20 hours were spent analyzing the contents of the bags.

Tables 8 through 11 summarize the hourly meteorological, traffic, and emissions data. Table 8 is a key to the symbols and units that are used in the three subsequent data tabulations. For orientation, the actual geographic bearing of the roadway is 110.6/290.6° at the experimental site (see Figure 21); accordingly, the traffic moving towards San Francisco is designated westbound and towards San Jose, eastbound.

Table 8

KEY TO SYMBOLS AND UNITS USED IN METEOROLOGICAL, TRAFFIC, AND EMISSIONS DATA SUMMARIES

WSBAR	≡ average wind speed ($m\ s^{-1}$)
WDBAR	≡ average wind direction (deg true)
SIGMAW	≡ standard deviation of vertical component of the wind ($m\ s^{-1}$)
V1E	≡ traffic volume (v), lane one (1), eastbound (E)
SPD	≡ traffic speed (mph)
V2W	≡ traffic volume (V), lane two (2), westbound (W)
HQSF	≡ hourly SF_6 emissions ($g\ m^{-1}\ s^{-1}$)
HQFR	≡ hourly F13B1 emissions ($g\ m^{-1}\ s^{-1}$)
HQCOE	≡ hourly eastbound CO emissions ($g\ m^{-1}\ s^{-1}$)
HQCOW	≡ hourly westbound CO emissions ($g\ m^{-1}\ s^{-1}$)
HQHE	≡ waste heat emissions, eastbound (10^4 cal $mi^{-1}\ h^{-1}$)
HQHW	≡ waste heat emissions, westbound (10^4 cal $mi^{-1}\ h^{-1}$)

C. Cut-Section Atmospheric Experiment

The second atmospheric experiment was conducted between July 2 and 22, 1975, at a cut-section segment of Interstate-280 in San Jose. The cut section is 8.2 m deep and about 58 m wide; the sides are vertical concrete retaining walls that extend the full depth of the cut on the south side and about 5 m upwards on the north side. Traffic is distributed among five eastbound lanes and six westbound lanes. On the neighboring terrain are primarily one- and two-story suburban residences. The scope of the experiment was virtually identical to the 101-study except that the complex nature of the site precluded the installation of

Table 9

METEOROLOGICAL DATA FOR AT-GRADE ROADWAY DISPERSION STUDY

	DATE	TIME	WSBAR	WDBAR	SIGMAW
BAYSHORE	17 JAN 75	1300-1400	2.85	305.	.33
BAYSHORE	17 JAN 75	1400-1500	3.49	317.	.22
BAYSHORE	17 JAN 75	1500-1600	2.84	312.	.18
BAYSHORE	17 JAN 75	1600-1700	2.48	341.	.13
BAYSHORE	17 JAN 75	1700-1800	2.70	324.	.15
BAYSHORE	17 JAN 75	1800-1900	.38	350.	.11
BAYSHORE	17 JAN 75	1900-2000	.20	28.	.13
BAYSHORE	21 JAN 75	514- 600	1.00	158.	.04
BAYSHORE	21 JAN 75	600- 700	.94	120.	.19
BAYSHORE	21 JAN 75	700- 800	.63	157.	.18
BAYSHORE	21 JAN 75	800- 900	.24	86.	.26
BAYSHORE	21 JAN 75	900-1000	.98	32.	.15
BAYSHORE	21 JAN 75	1000-1100	1.00	87.	.20
BAYSHORE	21 JAN 75	1100-1200	.79	87.	.26
BAYSHORE	21 JAN 75	1200-1300	1.96	300.	.32
BAYSHORE	24 JAN 75	503- 600	1.59	100.	.08
BAYSHORE	24 JAN 75	600- 700	1.16	155.	.08
BAYSHORE	24 JAN 75	700- 800	1.14	148.	.06
BAYSHORE	24 JAN 75	800- 900	.39	158.	.21
BAYSHORE	24 JAN 75	900-1000	.71	72.	.15
BAYSHORE	24 JAN 75	1000-1100	.55	93.	.31
BAYSHORE	24 JAN 75	1100-1200	1.25	347.	.23
BAYSHORE	24 JAN 75	1200-1300	1.71	335.	.25
BAYSHORE	28 JAN 75	500- 600	2.40	136.	.14
BAYSHORE	28 JAN 75	600- 700	2.51	143.	.18
BAYSHORE	28 JAN 75	700- 800	2.72	157.	.21
BAYSHORE	28 JAN 75	800- 900	2.79	166.	.25
BAYSHORE	28 JAN 75	900-1000	2.41	162.	.28
BAYSHORE	28 JAN 75	1000-1100	1.53	143.	.31
BAYSHORE	28 JAN 75	1100-1200	.69	189.	.34
BAYSHORE	28 JAN 75	1200-1300	.48	16.	.34
BAYSHORE	30 JAN 75	1200-1300	.85	99.	.29
BAYSHORE	30 JAN 75	1300-1400	.70	61.	.33
BAYSHORE	30 JAN 75	1400-1500	1.67	340.	.28
BAYSHORE	30 JAN 75	1500-1600	2.45	341.	.19
BAYSHORE	30 JAN 75	1600-1700	2.15	357.	.13
BAYSHORE	30 JAN 75	1700-1800	1.91	347.	.05
BAYSHORE	30 JAN 75	1800-1900	1.85	331.	.04
BAYSHORE	30 JAN 75	1900-2000	.25	204.	.07
BAYSHORE	5 FEB 75	1200-1300	2.45	157.	.26
BAYSHORE	5 FEB 75	1300-1400	3.28	174.	.26
BAYSHORE	5 FEB 75	1400-1500	2.92	178.	.27
BAYSHORE	5 FEB 75	1500-1600	4.20	183.	.28
BAYSHORE	5 FEB 75	1600-1700	3.12	183.	.27
BAYSHORE	5 FEB 75	1700-1800	1.50	180.	.16
BAYSHORE	5 FEB 75	1800-1900	.68	166.	.09
BAYSHORE	5 FEB 75	1900-2000	.26	66.	.17

Table 10

TRAFFIC DATA FOR AT-GRADE ROADWAY DISPERSION STUDY

DATE	TIME	V1E	SPD	V2E	SPD	V3E	SPD	V1W	SPD	V2W	SPD	V3W	SPD
17JAN75	1300	741.	63.	1063.	58.	722.	53.	714.	59.	926.	54.	711.	51.
17JAN75	1400	856.	61.	1125.	58.	724.	53.	867.	59.	1073.	54.	863.	50.
17JAN75	1500	1562.	46.	1468.	44.	846.	42.	1243.	58.	1233.	53.	1002.	51.
17JAN75	1600	1424.	21.	1161.	21.	893.	21.	1075.	59.	1187.	54.	857.	51.
17JAN75	1700	1452.	21.	1369.	21.	958.	20.	1070.	58.	1161.	54.	834.	51.
17JAN75	1800	1002.	59.	1099.	55.	697.	51.	638.	59.	865.	55.	658.	53.
17JAN75	1900	595.	62.	788.	58.	526.	55.	428.	60.	623.	55.	530.	53.
21JAN75	600	240.	63.	508.	58.	357.	55.	1696.	53.	1564.	50.	1387.	48.
21JAN75	700	995.	62.	1131.	56.	704.	52.	1881.	36.	1757.	34.	1561.	33.
21JAN75	800	900.	63.	917.	57.	491.	54.	1413.	52.	1357.	49.	1060.	46.
21JAN75	900	533.	63.	857.	57.	469.	54.	713.	59.	994.	55.	734.	51.
21JAN75	1000	525.	63.	875.	57.	475.	54.	606.	60.	944.	56.	726.	52.
21JAN75	1100	558.	64.	908.	57.	517.	54.	639.	61.	987.	55.	756.	52.
21JAN75	1200	540.	64.	872.	58.	441.	55.	571.	60.	920.	55.	774.	51.
24JAN75	600	252.	64.	578.	56.	265.	55.	1626.	53.	1539.	50.	1319.	46.
24JAN75	700	1082.	61.	1152.	56.	539.	54.	1887.	37.	1789.	35.	1679.	33.
24JAN75	800	845.	63.	1037.	57.	502.	54.	1391.	53.	1679.	49.	1060.	47.
24JAN75	900	540.	63.	874.	57.	436.	54.	888.	60.	1307.	55.	741.	53.
24JAN75	1000	525.	63.	875.	57.	475.	54.	752.	59.	938.	55.	759.	51.
24JAN75	1100	558.	64.	908.	57.	517.	54.	697.	60.	1022.	55.	802.	51.
24JAN75	1200	540.	64.	872.	58.	441.	54.	657.	59.	978.	55.	792.	52.
28JAN75	500	24.	61.	142.	55.	90.	58.	211.	61.	397.	56.	357.	54.
28JAN75	600	313.	63.	602.	56.	288.	54.	1686.	54.	1602.	51.	1332.	48.
28JAN75	700	1127.	60.	942.	55.	524.	53.	1831.	31.	1722.	30.	1565.	27.
28JAN75	800	900.	61.	917.	55.	495.	54.	1384.	55.	1384.	52.	1026.	49.
28JAN75	900	553.	63.	861.	56.	464.	54.	754.	59.	1048.	55.	722.	51.
28JAN75	1000	525.	64.	875.	57.	475.	55.	565.	59.	917.	55.	702.	52.
28JAN75	1100	558.	64.	908.	57.	517.	54.	575.	61.	887.	55.	707.	52.
28JAN75	1200	541.	64.	857.	58.	437.	55.	559.	60.	894.	55.	676.	53.
30JAN75	1200	529.	63.	785.	53.	720.	53.	624.	60.	944.	55.	699.	51.
30JAN75	1300	636.	62.	750.	53.	722.	53.	586.	59.	950.	55.	726.	52.
30JAN75	1400	696.	62.	765.	51.	736.	53.	836.	59.	1094.	55.	799.	51.
30JAN75	1500	1459.	46.	1084.	41.	846.	42.	1161.	58.	1278.	54.	989.	50.
30JAN75	1600	1582.	25.	1038.	24.	893.	21.	1012.	58.	1179.	54.	942.	50.
30JAN75	1700	1527.	22.	1028.	21.	958.	20.	1062.	58.	1157.	54.	861.	51.
30JAN75	1800	1140.	58.	859.	49.	703.	51.	507.	59.	822.	56.	580.	53.
30JAN75	1900	442.	62.	575.	53.	526.	55.	310.	59.	577.	55.	463.	53.
5FEB75	1200	720.	63.	775.	58.	720.	54.	558.	60.	818.	55.	578.	52.
5FEB75	1300	741.	61.	840.	58.	722.	53.	635.	60.	837.	55.	636.	52.
5FEB75	1400	856.	62.	874.	58.	724.	53.	783.	59.	962.	55.	663.	53.
5FEB75	1500	1462.	48.	1210.	44.	846.	41.	1089.	58.	1121.	54.	823.	51.
5FEB75	1600	1424.	21.	1430.	21.	893.	21.	953.	58.	1074.	54.	743.	51.
5FEB75	1700	1452.	21.	1520.	21.	958.	20.	970.	58.	1019.	55.	681.	52.
5FEB75	1800	994.	60.	988.	55.	703.	51.	493.	58.	653.	56.	455.	53.
5FEB75	1900	595.	63.	613.	57.	526.	55.	264.	58.	484.	56.	352.	53.

Table 11

EMISSIONS DATA FOR AT-GRADE ROADWAY DISPERSION STUDY

DATE	TIME	HQSF	HQFR	HQCOE	HQCOW	HQHE	HQHW
17JAN75	1300	.166E-04	.133E-03	.791E-02	.736E-02	.398E+06	.360E+06
17JAN75	1400	.321E-04	.264E-03	.847E-02	.878E-02	.425E+06	.428E+06
17JAN75	1500	.336E-04	.326E-03	.122E-01	.109E-01	.538E+06	.530E+06
17JAN75	1600	.223E-04	.395E-03	.234E-01	.977E-02	.463E+06	.481E+06
17JAN75	1700	.262E-04	.418E-03	.255E-01	.960E-02	.503E+06	.468E+06
17JAN75	1800	.280E-04	.259E-03	.876E-02	.677E-02	.432E+06	.334E+06
17JAN75	1900	.297E-04	.238E-03	.598E-02	.495E-02	.302E+06	.245E+06
21JAN75	600	.127E-03	.428E-04	.346E-02	.146E-01	.174E+06	.684E+06
21JAN75	700	.951E-04	.532E-04	.886E-02	.184E-01	.444E+06	.691E+06
21JAN75	800	.146E-03	.576E-04	.723E-02	.120E-01	.368E+06	.558E+06
21JAN75	900	.106E-03	.201E-03	.582E-02	.764E-02	.295E+06	.376E+06
21JAN75	1000	.102E-03	.251E-03	.587E-02	.713E-02	.297E+06	.353E+06
21JAN75	1100	.105E-03	.268E-03	.621E-02	.746E-02	.315E+06	.369E+06
21JAN75	1200	.104E-03	.292E-03	.580E-02	.709E-02	.295E+06	.349E+06
24JAN75	600	.113E-03	.117E-03	.343E-02	.140E-01	.173E+06	.656E+06
24JAN75	700	.532E-04	.237E-03	.868E-02	.190E-01	.435E+06	.712E+06
24JAN75	800	.160E-03	.308E-03	.747E-02	.129E-01	.380E+06	.607E+06
24JAN75	900	.122E-03	.254E-03	.579E-02	.920E-02	.294E+06	.455E+06
24JAN75	1000	.102E-03	.288E-03	.587E-02	.767E-02	.297E+06	.377E+06
24JAN75	1100	.110E-03	.303E-03	.621E-02	.790E-02	.315E+06	.389E+06
24JAN75	1200	.124E-03	.311E-03	.580E-02	.760E-02	.295E+06	.374E+06
28JAN75	500	.114E-03	.292E-03	.802E-03	.302E-02	.400E+05	.151E+06
28JAN75	600	.112E-03	.302E-03	.377E-02	.145E-01	.189E+06	.682E+06
28JAN75	700	.102E-03	.219E-03	.812E-02	.204E-01	.406E+06	.681E+06
28JAN75	800	.129E-03	.320E-03	.724E-02	.119E-01	.363E+06	.568E+06
28JAN75	900	.110E-03	.244E-03	.588E-02	.790E-02	.296E+06	.387E+06
28JAN75	1000	.994E-04	.275E-03	.587E-02	.684E-02	.298E+06	.337E+06
28JAN75	1100	.101E-03	.288E-03	.621E-02	.679E-02	.315E+06	.335E+06
28JAN75	1200	.105E-03	.266E-03	.575E-02	.667E-02	.292E+06	.329E+06
30JAN75	1200	.115E-03	.277E-03	.637E-02	.710E-02	.315E+06	.349E+06
30JAN75	1300	.984E-04	.300E-03	.660E-02	.708E-02	.326E+06	.349E+06
30JAN75	1400	.105E-03	.276E-03	.688E-02	.855E-02	.339E+06	.421E+06
30JAN75	1500	.103E-03	.388E-03	.109E-01	.107E-01	.463E+06	.521E+06
30JAN75	1600	.912E-04	.378E-03	.210E-01	.981E-02	.467E+06	.479E+06
30JAN75	1700	.708E-04	.408E-03	.233E-01	.965E-02	.467E+06	.473E+06
30JAN75	1800	.856E-04	.300E-03	.846E-02	.598E-02	.409E+06	.295E+06
30JAN75	1900	.111E-03	.300E-03	.483E-02	.423E-02	.239E+06	.208E+06
5FEB75	1200	.920E-04	.319E-03	.694E-02	.612E-02	.352E+06	.303E+06
5FEB75	1300	.123E-03	.336E-03	.721E-02	.660E-02	.363E+06	.326E+06
5FEB75	1400	.125E-03	.318E-03	.769E-02	.754E-02	.388E+06	.373E+06
5FEB75	1500	.114E-03	.401E-03	.112E-01	.950E-02	.490E+06	.464E+06
5FEB75	1600	.103E-03	.424E-03	.252E-01	.868E-02	.498E+06	.426E+06
5FEB75	1700	.105E-03	.406E-03	.265E-01	.836E-02	.523E+06	.411E+06
5FEB75	1800	.978E-04	.300E-03	.841E-02	.501E-02	.416E+06	.247E+06
5FEB75	1900	.112E-03	.331E-03	.543E-02	.345E-02	.275E+06	.169E+06

a dense meteorological sampling network. Instead, a single 15-m tower was mounted on an adjacent overpass to provide representative ambient wind and temperature data at five levels and air quality data at two levels. Figure 30 provides photographs of the roadway configuration and the aerometric tower. Figures 31a and 31b are plan and cross-sectional views of the site, and illustrate the position of the 35 sampling locations. As in the 101-study, SF_6 and F13B1 tracers were released exclusively in the westbound and eastbound directions, respectively. Again, traffic sensors were installed to obtain coincident speed and volume data.

Table 12 summarizes the testing schedule, while Tables 13 through 15 tabulate the hourly meteorological, traffic, and emissions data, respectively. As before, the key to symbols and units is given in Table 8.

Table 12

SCHEDULE OF HIGHWAY TRACER TESTS AT CUT SECTION ON I-280, SAN JOSE

Date (1975)	Hours (PDT)	Number of 1-h Tests
2 July	1300-2000	7
8 July	1200-2000	8
10 July	1200-2000	8
14 July	0500-1300	8
16 July	0500-1300	8
18 July	0500-0800	3
22 July	0500-1300	8

D. Elevated-Section Atmospheric Experiment

The third atmospheric experiment was conducted between August 12 and September 3, 1975, at a viaduct section of I-280 in San Jose (about two miles east-northeast of the cut-section site). The section consists

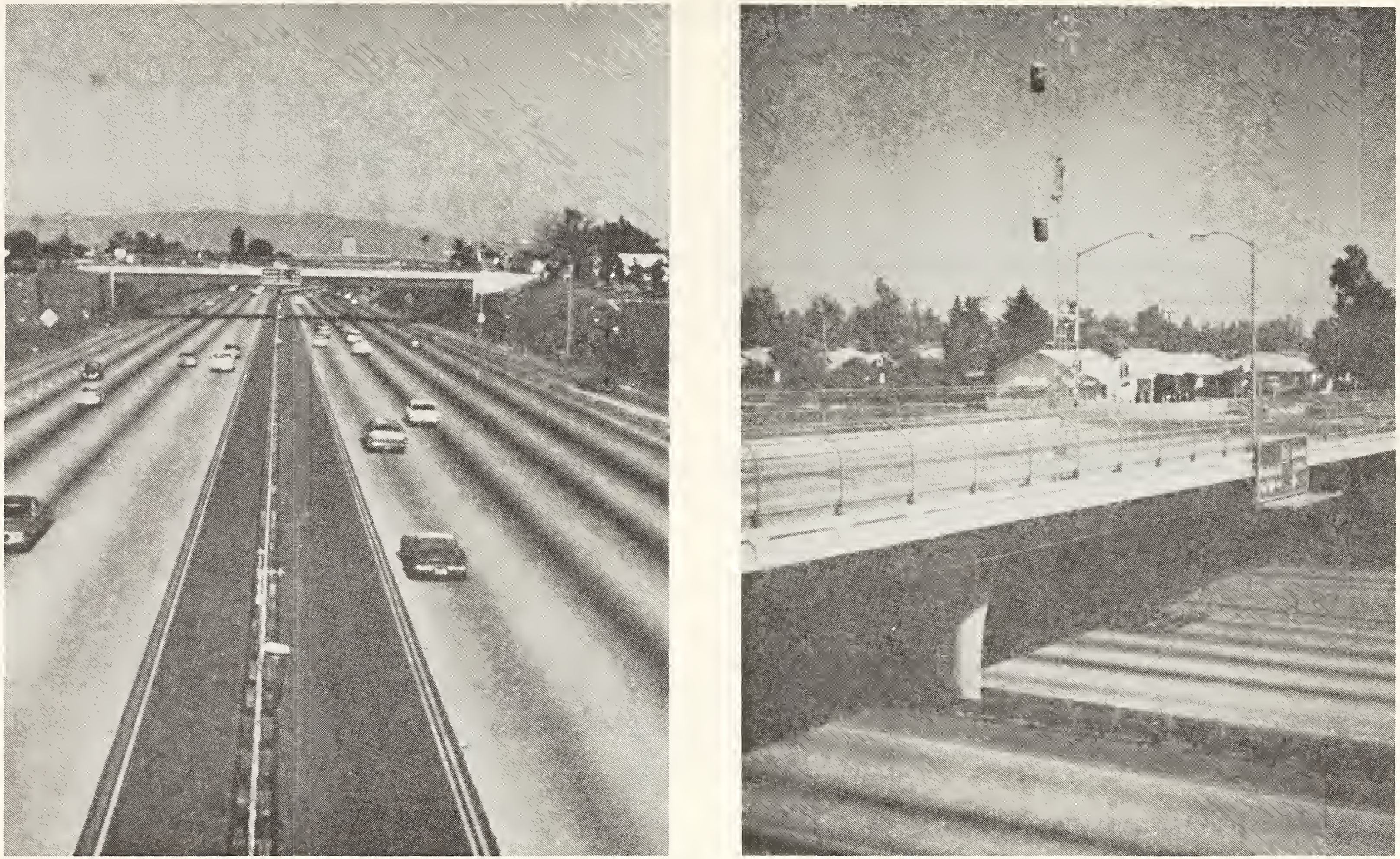

FIGURE 30 CUT-SECTION TEST SITE ON I-280 IN SAN JOSE

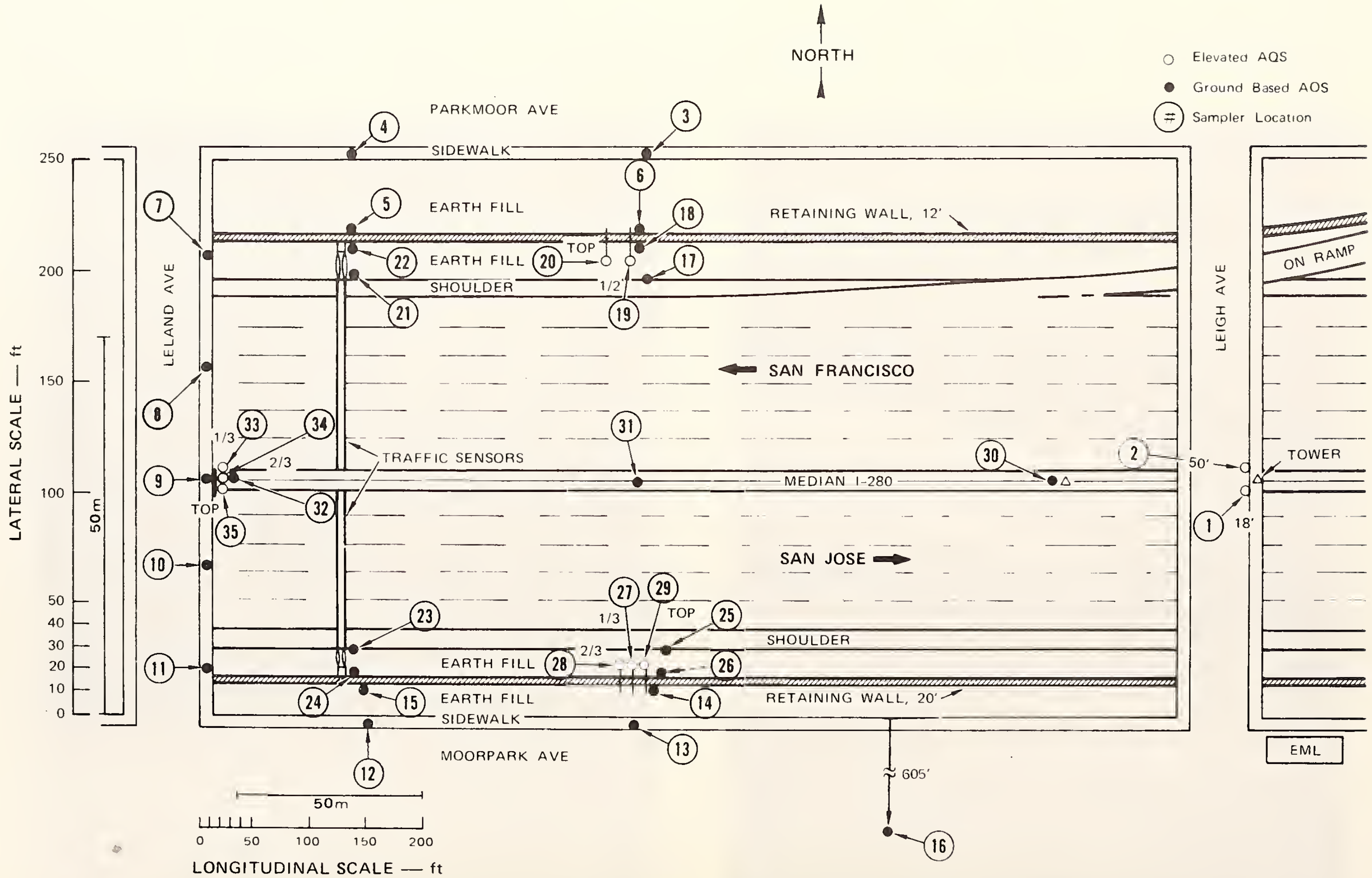

FIGURE 31a PLAN VIEW OF INSTRUMENTATION AT CUT-SECTION ROADWAY SITE

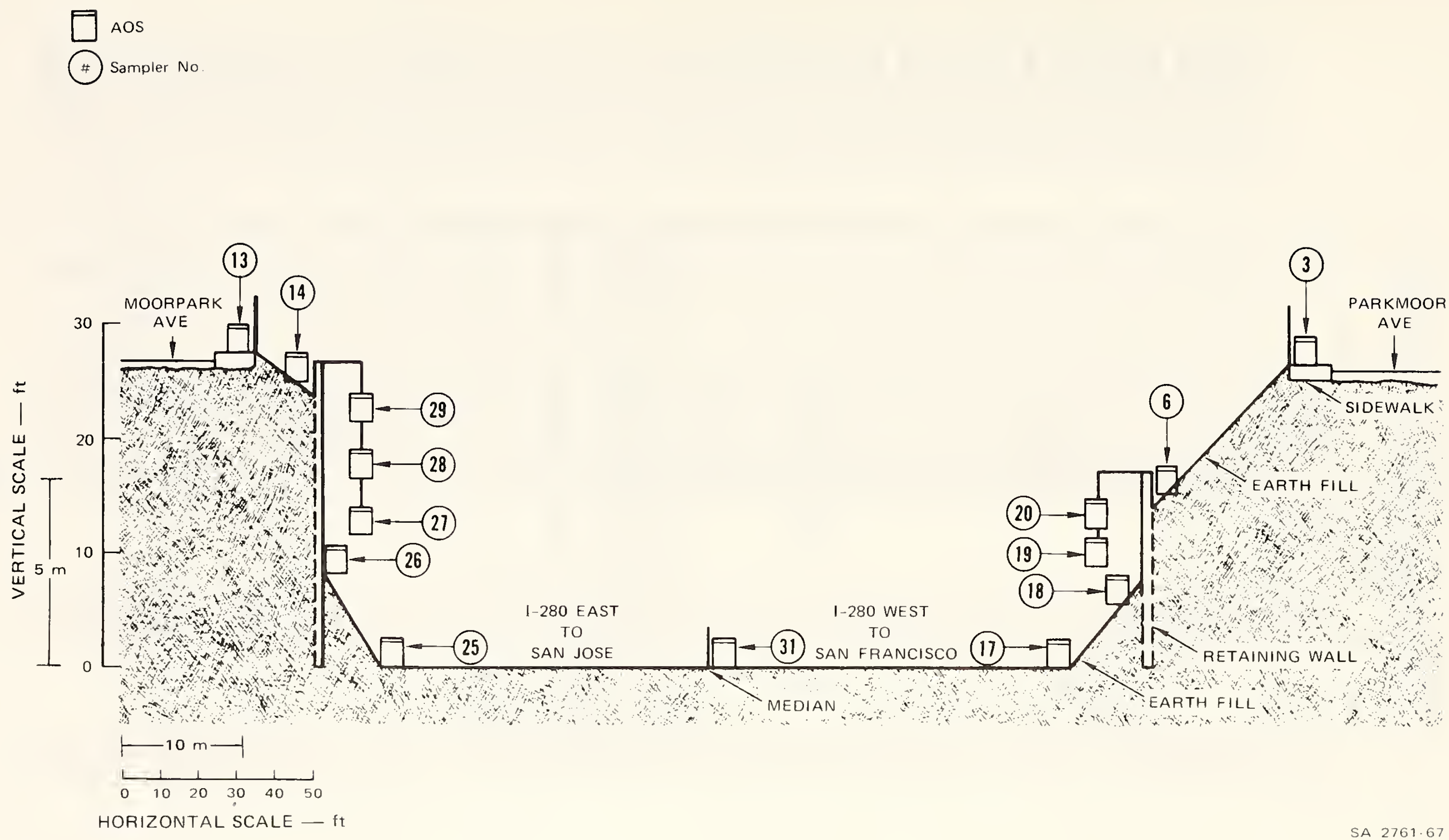

FIGURE 31b CROSS-SECTIONAL VIEW OF AIR QUALITY SAMPLES AT CUT-SECTION ROADWAY SITE

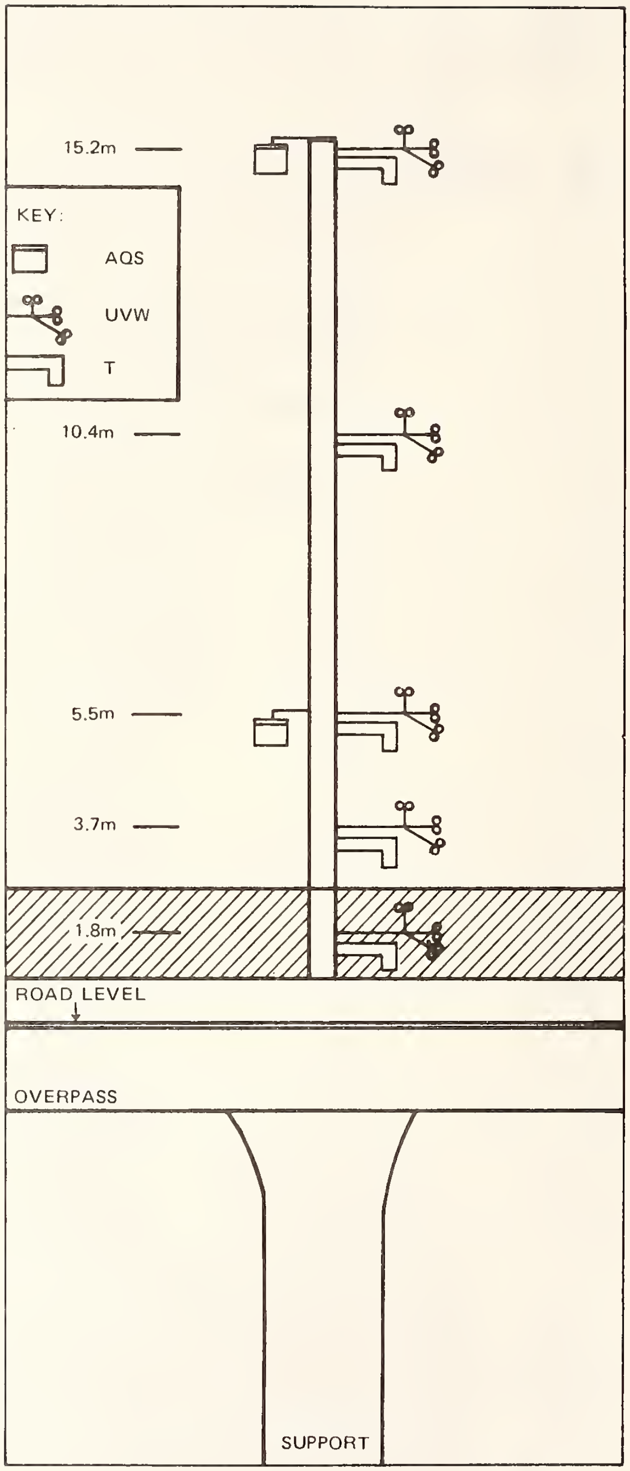

FIGURE 31c INSTRUMENTATION ON THE AEROMETRIC SAMPLING TOWER AT THE CUT-SECTION SITE

Table 13

METEOROLOGICAL DATA (10.4-m LEVEL)
FOR CUT-SECTION ROADWAY DISPERSION STUDY

	DATE	TIME	WSBAR	WDBAR	SIGMAW
HWY280-LE	2 JUL 75	1305-1400	3.08	324.	.55
HWY280-LE	2 JUL 75	1400-1500	3.33	334.	.55
HWY280-LE	2 JUL 75	1500-1600	3.85	344.	.63
HWY280-LE	2 JUL 75	1600-1700	4.16	352.	.64
HWY280-LE	2 JUL 75	1700-1800	4.15	358.	.66
HWY280-LE	2 JUL 75	1800-1900	4.11	355.	.60
HWY280-LE	2 JUL 75	1900-2000	3.33	1.	.52
HWY280-LE	8 JUL 75	1200-1300	1.65	329.	.54
HWY280-LE	8 JUL 75	1300-1400	2.07	328.	.58
HWY280-LE	8 JUL 75	1400-1500	2.92	331.	.58
HWY280-LE	8 JUL 75	1500-1559	3.19	317.	.55
HWY280-LE	8 JUL 75	1600-1700	3.38	309.	.57
HWY280-LE	8 JUL 75	1700-1800	3.36	318.	.55
HWY280-LE	8 JUL 75	1800-1900	3.38	323.	.52
HWY280-LE	8 JUL 75	1900-2000	3.02	328.	.55
HWY280-LE	10 JUL 75	1200-1300	1.62	337.	.59
HWY280-LE	10 JUL 75	1300-1400	2.29	319.	.52
HWY280-LE	10 JUL 75	1400-1500	2.45	324.	.57
HWY280-LE	10 JUL 75	1500-1600	2.18	328.	.69
HWY280-LE	10 JUL 75	1600-1700	2.05	315.	.31
HWY280-LE	10 JUL 75	1700-1800	2.30	318.	.41
HWY280-LE	10 JUL 75	1800-1900	2.89	323.	.36
HWY280-LE	10 JUL 75	1900-2000	3.08	320.	.59
HWY280-LE	14 JUL 75	500- 600	3.65	136.	.67
HWY280-LE	14 JUL 75	600- 700	3.25	137.	.60
HWY280-LE	14 JUL 75	700- 800	2.51	139.	.65
HWY280-LE	14 JUL 75	800- 900	1.90	136.	.62
HWY280-LE	14 JUL 75	900-1000	2.09	121.	.60
HWY280-LE	14 JUL 75	1000-1100	1.31	128.	.41
HWY280-LE	14 JUL 75	1100-1200	2.11	128.	.61
HWY280-LE	14 JUL 75	1200-1300	1.73	112.	.56
HWY280-LE	16 JUL 75	458- 500	1.35	317.	.37
HWY280-LE	16 JUL 75	500- 600	1.21	336.	.37
HWY280-LE	16 JUL 75	600- 700	1.06	6.	.49
HWY280-LE	16 JUL 75	700- 800	1.02	354.	.63
HWY280-LE	16 JUL 75	800- 841	.61	322.	.64
HWY280-LE	16 JUL 75	901-1000	.71	4.	.54
HWY280-LE	16 JUL 75	1000-1100	.53	18.	.65
HWY280-LE	16 JUL 75	1100-1200	1.08	342.	.71
HWY280-LE	16 JUL 75	1200-1300	1.51	331.	.59
HWY280-LE	18 JUL 75	500- 600	.94	341.	.19
HWY280-LE	22 JUL 75	500- 600	.39	304.	.11
HWY280-LE	22 JUL 75	600- 700	.65	200.	.18
HWY280-LE	22 JUL 75	700- 800	.77	222.	.43
HWY280-LE	22 JUL 75	800- 900	.40	163.	.50
HWY280-LE	22 JUL 75	900- 945	.38	239.	.24
HWY280-LE	22 JUL 75	1108-1200	1.27	342.	.01
HWY280-LE	22 JUL 75	1200-1300	1.26	337.	.25
HWY280-LE	22 JUL 75	1300-1357	1.89	336.	.63

Table 14

TRAFFIC DATA FOR CUT-SECTION ROADWAY DISPERSION STUDY

DATE	TIME	V1E	SPD	V2E	SPD	V3E	SPD	V4E	SPD	V1W	SPD	V2W	SPD	V3W	SPD	V4W	SPD
2JUL75	1300	266.	61.	577.	60.	1129.	58.	547.	58.	304.	61.	633.	58.	1783.	54.	584.	54.
2JUL75	1400	298.	61.	598.	60.	1185.	58.	603.	58.	359.	61.	597.	58.	1328.	54.	639.	54.
2JUL75	1500	480.	61.	758.	60.	1445.	57.	641.	57.	436.	62.	695.	59.	1343.	54.	709.	54.
2JUL75	1600	614.	61.	829.	58.	1507.	56.	646.	56.	642.	61.	847.	58.	1735.	53.	968.	53.
2JUL75	1700	746.	61.	1091.	59.	1780.	56.	761.	56.	783.	60.	977.	58.	2193.	54.	1103.	54.
2JUL75	1800	431.	61.	825.	59.	1408.	57.	598.	57.	410.	63.	670.	59.	1496.	56.	669.	56.
2JUL75	1900	268.	61.	660.	59.	1078.	58.	507.	58.	243.	63.	519.	59.	1192.	57.	487.	57.
8JUL75	1200	209.	61.	539.	60.	1028.	58.	482.	58.	36.	63.	633.	58.	1319.	54.	664.	54.
8JUL75	1300	221.	61.	544.	60.	1015.	58.	505.	58.	84.	64.	616.	58.	1727.	54.	638.	54.
8JUL75	1400	209.	61.	609.	60.	1021.	58.	506.	58.	63.	63.	474.	58.	1062.	54.	444.	54.
8JUL75	1500	382.	61.	738.	60.	1234.	58.	545.	58.	209.	61.	682.	58.	1324.	54.	618.	54.
8JUL75	1600	565.	61.	851.	59.	1464.	56.	594.	56.	184.	61.	963.	57.	1976.	53.	1103.	53.
8JUL75	1700	429.	61.	688.	59.	1209.	58.	481.	58.	48.	61.	869.	57.	1947.	53.	971.	53.
8JUL75	1800	313.	61.	686.	60.	1171.	58.	447.	58.	171.	61.	616.	59.	1367.	56.	646.	56.
8JUL75	1900	195.	61.	536.	60.	925.	58.	414.	58.	183.	61.	528.	58.	1218.	55.	497.	55.
10JUL75	1200	247.	60.	592.	60.	1019.	58.	473.	58.	163.	63.	628.	59.	1305.	54.	626.	54.
10JUL75	1300	208.	61.	589.	60.	1056.	58.	537.	58.	152.	62.	545.	58.	1539.	54.	552.	54.
10JUL75	1400	279.	61.	636.	60.	1099.	58.	475.	58.	295.	61.	686.	58.	1540.	54.	606.	54.
10JUL75	1500	498.	61.	794.	59.	1411.	58.	583.	58.	411.	61.	727.	59.	1400.	55.	749.	55.
10JUL75	1600	741.	61.	896.	58.	1577.	56.	712.	56.	364.	61.	811.	58.	1669.	54.	841.	54.
10JUL75	1700	689.	61.	885.	57.	1501.	58.	649.	58.	515.	60.	893.	57.	1992.	54.	981.	54.
10JUL75	1800	453.	61.	755.	60.	1301.	58.	556.	58.	356.	61.	649.	59.	1437.	56.	706.	56.
10JUL75	1900	230.	61.	580.	60.	1000.	58.	440.	58.	190.	61.	436.	58.	996.	56.	393.	56.
14JUL75	500	11.	61.	64.	60.	177.	58.	113.	58.	66.	63.	197.	59.	313.	57.	88.	57.
14JUL75	600	101.	61.	309.	61.	540.	58.	376.	58.	538.	63.	844.	58.	971.	55.	348.	55.
14JUL75	700	698.	61.	896.	60.	1282.	58.	836.	58.	918.	62.	853.	59.	1454.	55.	711.	55.
14JUL75	800	422.	61.	763,	60.	1228.	58.	720.	58.	578.	62.	695.	59.	1112.	55.	680.	55.
14JUL75	900	201.	61.	529.	60.	873.	58.	459.	58.	294.	62.	538.	59.	986.	55.	536.	55.
14JUL75	1000	198.	61.	518.	60.	983.	58.	509.	58.	279.	62.	476.	59.	1062.	55.	543.	55.
14JUL75	1100	217.	59.	571.	60.	991.	58.	496.	58.	346.	63.	571.	59.	1214.	55.	664.	55.
14JUL75	1200	228.	61.	599.	60.	1054.	58.	506.	58.	286.	63.	516.	59.	1076.	55.	641.	55.
16JUL75	500	11.	61.	64.	60.	177.	58.	113.	58.	66.	63.	197.	59.	313.	57.	88.	57.
16JUL75	600	101.	61.	309.	61.	540.	58.	376.	58.	538.	63.	844.	58.	971.	55.	348.	55.
16JUL75	700	698.	61.	896.	60.	1282.	58.	836.	58.	918.	62.	853.	59.	1454.	55.	711.	55.
16JUL75	800	422.	61.	763.	60.	1228.	58.	720.	58.	578.	62.	695.	59.	1112.	55.	680.	55.
16JUL75	900	201.	61.	529.	60.	873.	58.	459.	58.	294.	62.	538.	59.	986.	55.	536.	55.
16JUL75	1000	198.	61.	518.	60.	983.	58.	509.	58.	279.	62.	476.	59.	1062.	55.	543.	55.
16JUL75	1100	217.	59.	571.	60.	991.	58.	496.	58.	346.	63.	571.	59.	1214.	55.	664.	55.
16JUL75	1200	228.	61.	599.	60.	1054.	58.	506.	58.	286.	63.	516.	59.	1076.	55.	641.	55.
18JUL75	500	12.	62.	66.	59.	177.	58.	113.	58.	36.	65.	187.	58.	297.	54.	81.	54.
18JUL75	600	106.	62.	303.	59.	540.	58.	376.	58.	269.	65.	570.	59.	655.	55.	247.	55.
18JUL75	700	523.	62.	824.	59.	1233.	58.	820.	58.	358.	63.	676.	58.	1160.	54.	384.	54.
22JUL75	500	11.	61.	73.	60.	177.	58.	113.	58.	48.	65.	195.	58.	310.	53.	93.	53.
22JUL75	600	102.	61.	321.	60.	521.	58.	363.	58.	511.	64.	679.	58.	786.	54.	326.	54.
22JUL75	700	601.	61.	944.	60.	1282.	58.	836.	58.	743.	62.	927.	58.	1585.	54.	615.	54.
22JUL75	800	411.	61.	835.	60.	1228.	58.	758.	58.	482.	63.	754.	58.	1174.	54.	600.	54.
22JUL75	900	185.	61.	539.	60.	837.	58.	493.	58.	256.	63.	574.	59.	1047.	54.	497.	54.
22JUL75	1000	168.	61.	547.	60.	831.	58.	480.	58.	250.	63.	549.	59.	1236.	54.	535.	54.
22JUL75	1100	203.	61.	537.	60.	894.	58.	472.	58.	275.	62.	580.	59.	1228.	54.	649.	54.
22JUL75	1200	212.	61.	538.	60.	911.	58.	450.	58.	290.	63.	603.	58.	1248.	54.	647.	54.

Table 15

EMISSIONS DATA FOR CUT-SECTION ROADWAY DISPERSION STUDY

DATE	TIME	HQSF	HQFR	HQCOE	HQCOW	HQHE	HQHW
2JUL75	1300	.318E-04	.108E-03	.789E-02	.103E-01	.401E+06	.512E+06
2JUL75	1400	.752E-04	.407E-03	.841E-02	.915E-02	.427E+06	.454E+06
2JUL75	1500	.109E-03	.354E-03	.104E-01	.997E-02	.528E+06	.497E+06
2JUL75	1600	.103E-03	.293E-03	.113E-01	.131E-01	.567E+06	.647E+06
2JUL75	1700	.918E-04	.281E-03	.137E-01	.158E-01	.693E+06	.785E+06
2JUL75	1800	.800E-04	.250E-03	.102E-01	.102E-01	.517E+06	.513E+06
2JUL75	1900	.101E-03	.356E-03	.787E-02	.764E-02	.400E+06	.387E+06
8JUL75	1200	.873E-04	.288E-03	.707E-02	.831E-02	.359E+06	.409E+06
8JUL75	1300	.956E-04	.289E-03	.716E-02	.960E-02	.364E+06	.473E+06
8JUL75	1400	.851E-04	.284E-03	.734E-02	.640E-02	.373E+06	.316E+06
8JUL75	1500	.101E-03	.271E-03	.908E-02	.887E-02	.462E+06	.439E+06
8JUL75	1600	.891E-04	.252E-03	.109E-01	.132E-01	.549E+06	.646E+06
8JUL75	1700	.929E-04	.283E-03	.879E-02	.120E-01	.447E+06	.585E+06
8JUL75	1800	.881E-04	.277E-03	.820E-02	.877E-02	.417E+06	.440E+06
8JUL75	1900	.881E-04	.269E-03	.648E-02	.760E-02	.330E+06	.377E+06
10JUL75	1200	.100E-03	.279E-03	.730E-02	.852E-02	.371E+06	.423E+06
10JUL75	1300	.107E-03	.305E-03	.749E-02	.873E-02	.380E+06	.431E+06
10JUL75	1400	.117E-03	.334E-03	.780E-02	.979E-02	.397E+06	.485E+06
10JUL75	1500	.115E-03	.312E-03	.103E-01	.103E-01	.523E+06	.514E+06
10JUL75	1600	.105E-03	.308E-03	.123E-01	.116E-01	.619E+06	.576E+06
10JUL75	1700	.105E-03	.313E-03	.117E-01	.137E-01	.591E+06	.678E+06
10JUL75	1800	.106E-03	.303E-03	.960E-02	.986E-02	.489E+06	.496E+06
10JUL75	1900	.119E-03	.312E-03	.705E-02	.631E-02	.358E+06	.317E+06
14JUL75	500	.877E-04	.264E-03	.121E-02	.208E-02	.611E+05	.105E+06
14JUL75	600	.101E-03	.344E-03	.415E-02	.846E-02	.212E+06	.426E+06
14JUL75	700	.223E-03	.276E-03	.116E-01	.123E-01	.593E+06	.620E+06
14JUL75	800	.105E-03	.296E-03	.981E-02	.960E-02	.499E+06	.482E+06
14JUL75	900	.982E-04	.364E-03	.646E-02	.737E-02	.328E+06	.369E+06
14JUL75	1000	.995E-04	.318E-03	.692E-02	.739E-02	.351E+06	.369E+06
14JUL75	1100	.101E-03	.340E-03	.712E-02	.875E-02	.362E+06	.438E+06
14JUL75	1200	.102E-03	.251E-03	.748E-02	.789E-02	.380E+06	.394E+06
16JUL75	500	.104E-03	.285E-03	.114E-02	.208E-02	.579E+05	.105E+06
16JUL75	600	.124E-03	.314E-03	.415E-02	.846E-02	.212E+06	.426E+06
16JUL75	700	.118E-03	.301E-03	.116E-01	.123E-01	.593E+06	.620E+06
16JUL75	800	.115E-03	.301E-03	.981E-02	.960E-02	.499E+06	.482E+06
16JUL75	900	.126E-03	.335E-03	.646E-02	.737E-02	.328E+06	.369E+06
16JUL75	1000	.120E-03	.281E-03	.692E-02	.739E-02	.351E+06	.369E+06
16JUL75	1100	.116E-03	.323E-03	.712E-02	.875E-02	.362E+06	.438E+06
16JUL75	1200	.942E-04	.207E-03	.748E-02	.789E-02	.380E+06	.394E+06
18JUL75	500	.927E-04	.297E-03	.115E-02	.188E-02	.583E+05	.934E+05
18JUL75	600	.108E-03	.309E-03	.415E-02	.545E-02	.211E+06	.275E+06
18JUL75	700	.923E-04	.307E-03	.106E-01	.807E-02	.542E+06	.402E+06
22JUL75	500	.899E-04	.284E-03	.117E-02	.202E-02	.594E+05	.997E+05
22JUL75	600	.892E-04	.305E-03	.409E-02	.721E-02	.208E+06	.363E+06
22JUL75	700	.919E-04	.300E-03	.115E-01	.121E-01	.585E+06	.605E+06
22JUL75	800	.956E-04	.310E-03	.101E-01	.943E-02	.515E+06	.471E+06
22JUL75	900	.968E-04	.276E-03	.643E-02	.744E-02	.327E+06	.371E+06
22JUL75	1000	.104E-03	.324E-03	.635E-02	.805E-02	.323E+06	.400E+06
22JUL75	1100	.101E-03	.284E-03	.660E-02	.856E-02	.335E+06	.425E+06
22JUL75	1200	.970E-04	.322E-03	.661E-02	.873E-02	.336E+06	.433E+06

of two 7-m high viaducts, each about 24 m wide. A 15-m gap separated the two viaducts. The top of the viaduct is just above the roof level of the two-story houses that are located on both sides of the roadway. Six lanes of traffic flow eastbound (actually 057.5°) and five westbound (including a double on-ramp). The scope of the experiment was identical to the I-280 cut-section study. A single 18-m tower located between the two viaduct sections was used to obtain wind, temperature, and air quality data at five levels. Figure 32 provides photographs of the roadway configuration and location of the aerometric tower. Figures 33a and 33b are plan and cross-sectional views of the site, and illustrate the position of the 34 sampling locations.

Table 16 summarizes the testing schedule, while Tables 17-19 tabulate the hourly meteorological, traffic, and emissions data, respectively. As before, the key to symbols and units is given in Table 8.

Table 16

SCHEDULE OF HIGHWAY TRACER TESTS AT
VIADUCT SECTION ON I-280, SAN JOSE

Date (1975)	Hours (PDT)	Number of 1-h Tests
12 August	1200-2000	8
14 August	1200-2000	8
19 August	1200-2000	8
21 August	0500-1300	8
26 August	0500-1300	8
3 September	0500-1300	8

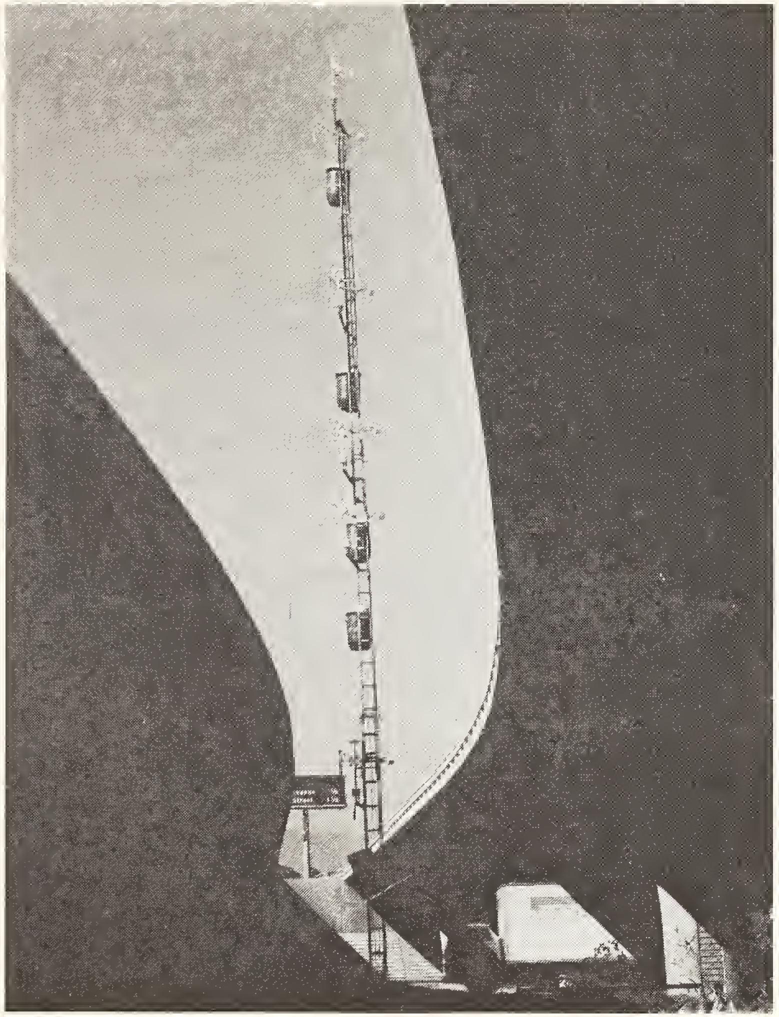

FIGURE 32 VIADUCT SECTION TEST-SITE ON I-280 IN SAN JOSE

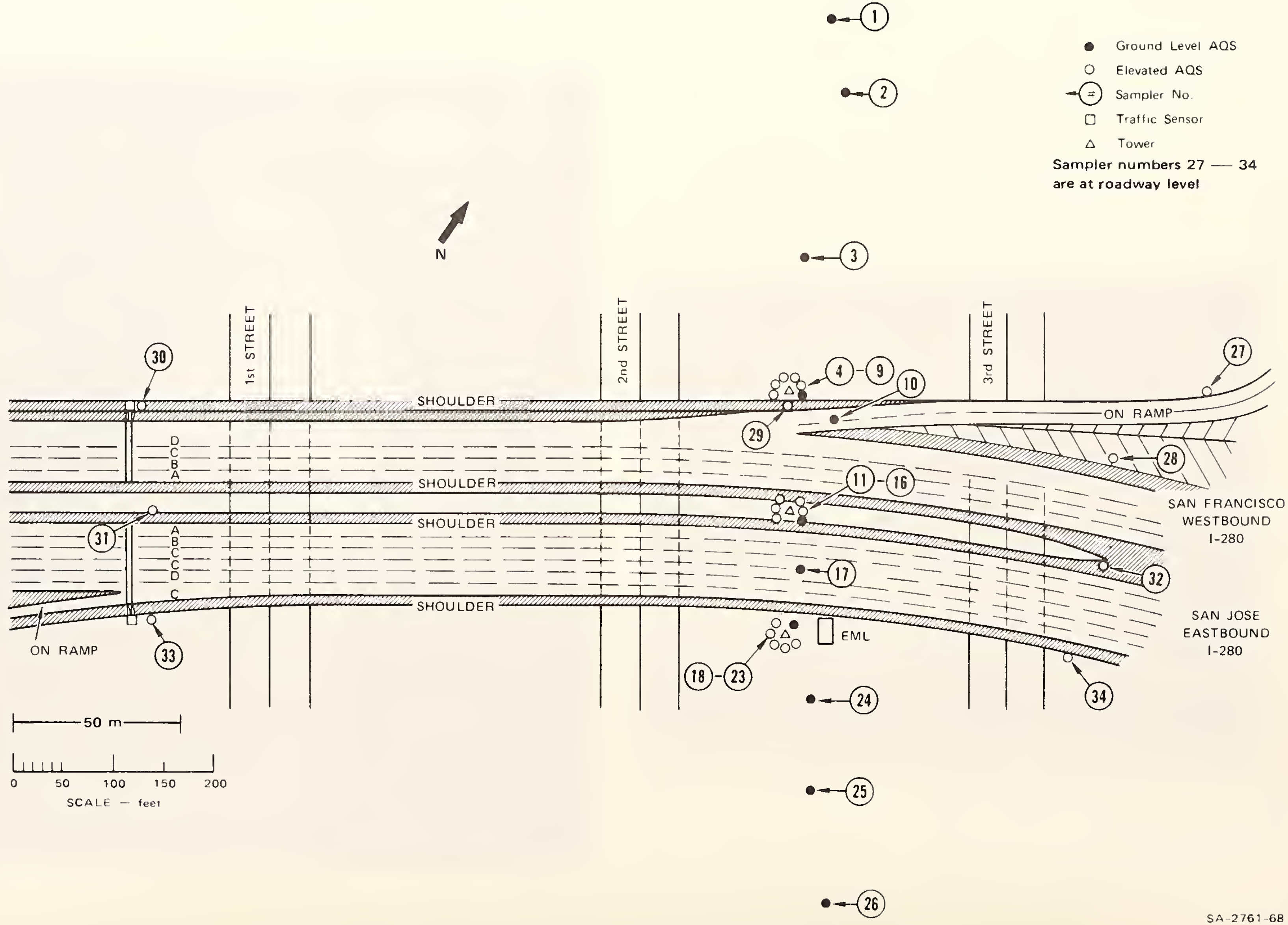

FIGURE 33a PLAN VIEW OF INTRUMENTATION AT VIADUCT-SECTION ROADWAY SITE

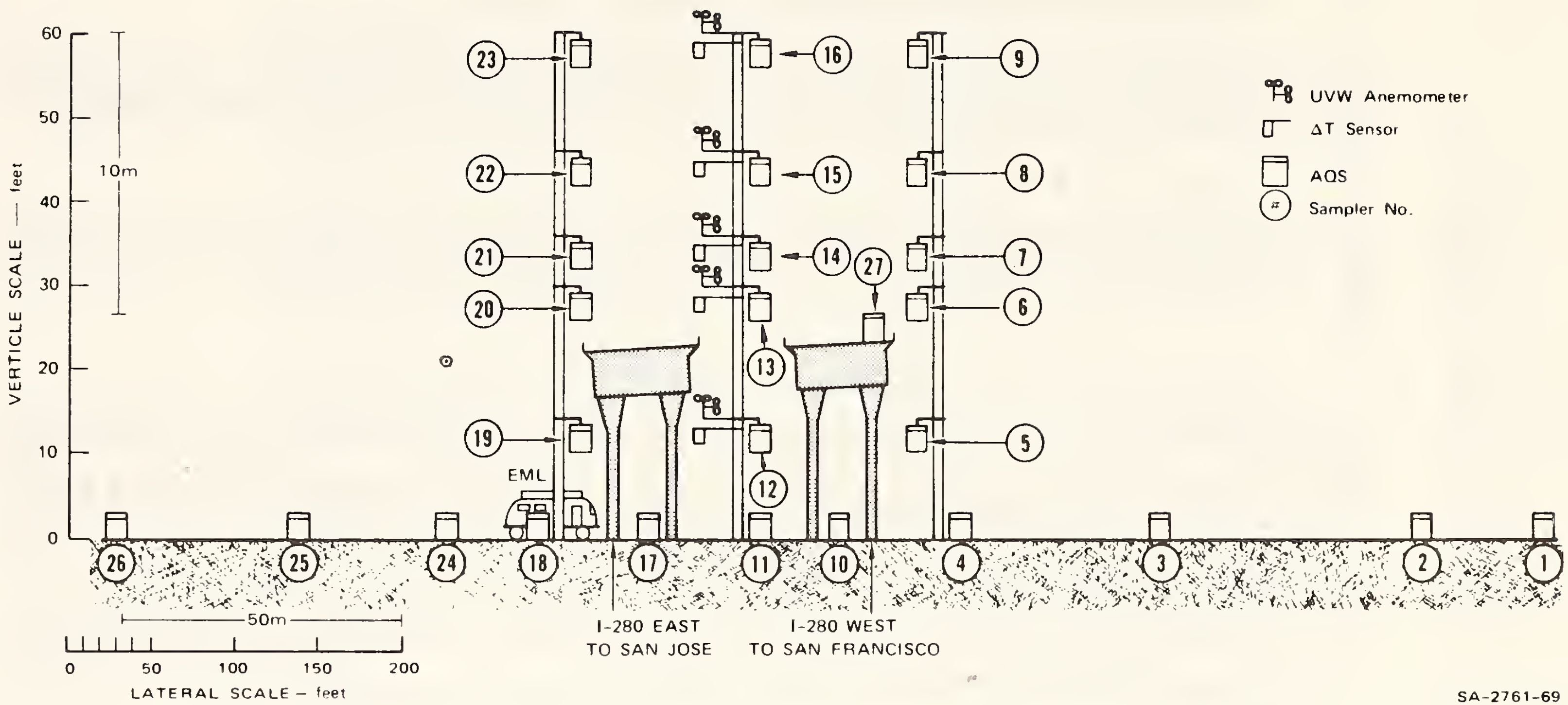

FIGURE 33b CROSS-SECTIONAL VIEW OF AEROMETRIC INSTRUMENTATION AT VIADUCT-SECTION ROADWAY SITE

Table 17

METEOROLOGICAL DATA (11.0-m level)
FOR VIADUCT-SECTION ROADWAY DISPERSION STUDY

IDENT	DATE	TIME (PST)	WSBAR (10.97 M)	WDBAR (10.97 M)	SIGMAW (10.97 M)
WY280-SEC	12 AUG 75	1224-1300	.24	175.	.54
WY280-SEC	12 AUG 75	1300-1400	1.16	329.	.55
WY280-SEC	12 AUG 75	1400-1500	1.69	335.	.63
WY280-SEC	12 AUG 75	1500-1600	2.29	338.	.71
WY280-SEC	12 AUG 75	1600-1700	2.36	346.	.66
WY280-SEC	12 AUG 75	1700-1800	2.05	335.	.62
WY280-SEC	12 AUG 75	1800-1900	1.65	343.	.55
WY280-SEC	12 AUG 75	1900-2000	1.66	340.	.53
WY280-SEC	14 AUG 75	1200-1300	1.70	216.	.56
WY280-SEC	14 AUG 75	1300-1400	.70	282.	.54
WY280-SEC	14 AUG 75	1400-1500	1.85	343.	.63
WY280-SEC	14 AUG 75	1500-1600	2.22	339.	.66
WY280-SEC	14 AUG 75	1600-1700	2.05	345.	.68
WY280-SEC	14 AUG 75	1700-1800	1.90	338.	.68
WY280-SEC	14 AUG 75	1800-1900	1.66	338.	.58
WY280-SEC	14 AUG 75	1900-2000	1.45	353.	.50
WY280-SEC	19 AUG 75	1200-1300	1.30	227.	.53
WY280-SEC	19 AUG 75	1300-1400	.53	270.	.64
WY280-SEC	19 AUG 75	1400-1500	1.75	353.	.56
WY280-SEC	19 AUG 75	1500-1600	1.75	353.	.59
WY280-SEC	19 AUG 75	1600-1700	1.64	1.	.62
WY280-SEC	19 AUG 75	1700-1800	1.95	355.	.63
WY280-SEC	19 AUG 75	1800-1900	1.82	343.	.59
WY280-SEC	19 AUG 75	1900-2000	1.83	338.	.57
WY280-SEC	21 AUG 75	518- 600	3.46	21.	.34
WY280-SEC	21 AUG 75	600- 700	3.22	27.	.34
WY280-SEC	21 AUG 75	700- 800	2.65	23.	.48
WY280-SEC	21 AUG 75	800- 900	2.71	38.	.74
WY280-SEC	21 AUG 75	900-1000	1.86	147.	.50
WY280-SEC	21 AUG 75	1000-1100	1.94	152.	.56
WY280-SEC	21 AUG 75	1100-1200	1.99	172.	.56
WY280-SEC	21 AUG 75	1200-1300	1.16	192.	.52
WY280-SEC	26 AUG 75	500- 600	2.52	132.	.56
WY280-SEC	26 AUG 75	600- 700	1.99	148.	.49
WY280-SEC	26 AUG 75	700- 800	1.75	167.	.50
WY280-SEC	26 AUG 75	800- 900	1.92	156.	.45
WY280-SEC	26 AUG 75	900-1000	1.57	177.	.45
WY280-SEC	26 AUG 75	1000-1100	1.26	170.	.62
WY280-SEC	26 AUG 75	1100-1159	1.16	196.	.56
WY280-SEC	26 AUG 75	1200-1300	.86	191.	.55
WY280-SEC	3 SEP 75	515- 600	.17	196.	.17
WY280-SEC	3 SEP 75	600- 700	.58	189.	.27
WY280-SEC	3 SEP 75	700- 800	1.98	222.	.43
WY280-SEC	3 SEP 75	819- 859	1.30	228.	.36
WY280-SEC	3 SEP 75	900- 959	.70	231.	.43
WY280-SEC	3 SEP 75	1000-1100	.10	343.	.52
WY280-SEC	3 SEP 75	1100-1200	.96	18.	.54
WY280-SEC	3 SEP 75	1200-1300	1.34	7.	.54

Table 18

TRAFFIC DATA FOR VIADUCT-SECTION ROADWAY DISPERSION STUDY

DATE	TIME	V1E	SPD	V2E	SPD	V3E	SPD	V4E	SPD	V1W	SPD	V2W	SPD	V3W	SPD	V4W	SPD
12AUG75	1300	210.	61.	453.	59.	1490.	51.	518.	51.	215.	61.	568.	58.	770.	55.	1069.	50.
12AUG75	1400	228.	61.	496.	59.	1510.	52.	524.	52.	261.	61.	643.	58.	816.	54.	1064.	50.
12AUG75	1500	368.	60.	605.	58.	1720.	50.	607.	50.	366.	60.	795.	58.	966.	55.	1298.	48.
12AUG75	1600	677.	59.	792.	58.	2220.	51.	656.	51.	469.	60.	949.	58.	1201.	54.	1532.	48.
12AUG75	1700	658.	59.	815.	58.	2280.	51.	610.	51.	473.	61.	923.	58.	1112.	54.	1497.	47.
12AUG75	1800	342.	61.	603.	60.	1720.	53.	470.	53.	304.	62.	751.	58.	789.	56.	1065.	50.
12AUG75	1900	245.	61.	495.	59.	1405.	51.	410.	51.	242.	62.	518.	59.	671.	56.	868.	51.
14AUG75	1200	207.	62.	453.	60.	1395.	52.	552.	52.	199.	62.	644.	58.	797.	55.	1124.	50.
14AUG75	1300	192.	61.	485.	59.	1429.	51.	526.	51.	215.	62.	613.	58.	803.	55.	1101.	49.
14AUG75	1400	257.	61.	502.	58.	1514.	51.	524.	51.	235.	62.	677.	58.	831.	54.	1170.	49.
14AUG75	1500	390.	60.	626.	58.	1722.	51.	573.	51.	375.	62.	772.	58.	985.	54.	1233.	49.
14AUG75	1600	642.	59.	809.	58.	2221.	51.	663.	51.	480.	62.	954.	58.	1154.	54.	1654.	47.
14AUG75	1700	602.	60.	783.	58.	2288.	52.	634.	52.	475.	62.	988.	58.	1175.	54.	1524.	48.
14AUG75	1800	466.	59.	633.	58.	1714.	53.	476.	53.	335.	62.	756.	58.	813.	55.	1037.	50.
14AUG75	1900	283.	61.	538.	59.	1426.	52.	360.	52.	230.	62.	565.	58.	681.	55.	872.	50.
19AUG75	1200	238.	62.	503.	59.	1541.	42.	559.	42.	203.	65.	529.	58.	795.	55.	1100.	50.
19AUG75	1300	199.	61.	462.	58.	1540.	50.	542.	50.	214.	64.	611.	58.	795.	55.	1080.	50.
19AUG75	1400	195.	60.	472.	58.	1509.	50.	552.	50.	228.	63.	679.	58.	805.	55.	1115.	50.
19AUG75	1500	396.	60.	637.	57.	1756.	49.	548.	49.	377.	62.	785.	57.	960.	55.	1260.	49.
19AUG75	1600	690.	59.	791.	57.	2235.	48.	697.	48.	489.	61.	996.	56.	1170.	53.	1590.	47.
19AUG75	1700	677.	58.	797.	58.	2343.	48.	667.	48.	492.	61.	940.	57.	1150.	54.	1520.	48.
19AUG75	1800	365.	61.	623.	60.	1664.	49.	476.	49.	354.	62.	715.	57.	815.	55.	1060.	50.
19AUG75	1900	226.	60.	480.	60.	1434.	49.	473.	49.	245.	63.	609.	58.	680.	55.	880.	50.
21AUG75	500	4.	63.	36.	59.	193.	38.	69.	38.	40.	60.	160.	57.	184.	57.	291.	51.
21AUG75	600	77.	63.	137.	60.	495.	38.	300.	38.	365.	62.	637.	58.	601.	58.	922.	50.
21AUG75	700	395.	61.	427.	60.	1011.	42.	897.	42.	645.	60.	917.	58.	935.	58.	1332.	50.
21AUG75	800	295.	61.	279.	58.	1149.	42.	532.	42.	369.	60.	721.	58.	777.	57.	1178.	50.
21AUG75	900	369.	59.	17.	56.	891.	40.	368.	40.	166.	61.	520.	58.	650.	57.	952.	53.
21AUG75	1000	526.	58.	75.	57.	945.	35.	331.	35.	175.	60.	528.	58.	693.	56.	1044.	53.
21AUG75	1100	173.	59.	148.	61.	1647.	41.	597.	41.	229.	60.	570.	58.	768.	56.	1172.	51.
21AUG75	1200	45.	60.	177.	61.	1836.	41.	660.	41.	227.	61.	622.	58.	768.	56.	1176.	51.
26AUG75	500	9.	63.	69.	59.	277.	44.	68.	44.	44.	61.	143.	58.	196.	62.	659.	50.
26AUG75	600	76.	64.	251.	61.	788.	48.	308.	48.	382.	61.	634.	59.	651.	56.	1790.	50.
26AUG75	700	412.	61.	587.	60.	1550.	45.	900.	45.	654.	61.	962.	58.	963.	56.	2369.	50.
26AUG75	800	268.	61.	523.	61.	1586.	45.	556.	45.	360.	61.	752.	58.	821.	56.	2025.	50.
26AUG75	900	210.	61.	512.	61.	1560.	45.	301.	45.	138.	62.	391.	58.	637.	56.	1685.	50.
26AUG75	1000	203.	61.	459.	62.	1667.	45.	312.	45.	162.	61.	473.	58.	716.	55.	1440.	53.
26AUG75	1100	213.	62.	439.	63.	1683.	47.	455.	47.	214.	61.	571.	58.	727.	55.	1638.	54.
26AUG75	1200	187.	60.	480.	63.	1627.	44.	485.	44.	195.	61.	579.	58.	807.	55.	1674.	53.
3SEP75	500	5.	59.	39.	59.	269.	48.	66.	48.	39.	58.	121.	57.	167.	55.	243.	53.
3SEP75	600	17.	68.	290.	61.	179.	50.	304.	50.	407.	61.	643.	58.	632.	56.	829.	53.
3SEP75	700	79.	64.	641.	62.	39.	48.	1120.	48.	796.	60.	1070.	58.	1180.	55.	1381.	52.
3SEP75	800	36.	65.	598.	63.	237.	49.	1026.	49.	536.	61.	920.	58.	1070.	55.	1267.	51.
3SEP75	900	6.	65.	473.	63.	1181.	50.	630.	50.	247.	60.	605.	57.	764.	54.	959.	51.
3SEP75	1000	4.	65.	476.	63.	1370.	50.	728.	50.	225.	61.	618.	58.	750.	54.	979.	50.
3SEP75	1100	17.	63.	530.	62.	1499.	50.	833.	50.	216.	61.	659.	58.	827.	55.	1138.	49.
3SEP75	1200	56.	63.	565.	62.	1529.	50.	881.	50.	254.	60.	590.	57.	834.	55.	1302.	48.

Table 19

EMISSIONS DATA FOR VIADUCT-SECTION
ROADWAY DISPERSION STUDY

DATE	TIME	HQSF	HQFR	HQCOE	HQCOW	HQHE	HQHW
12AUG75	1300	.106E-03	.344E-03	.837E-02	.821E-02	.422E+06	.401E+06
12AUG75	1400	.135E-03	.370E-03	.864E-02	.872E-02	.437E+06	.425E+06
12AUG75	1500	.120E-03	.365E-03	.103E-01	.107E-01	.516E+06	.520E+06
12AUG75	1600	.127E-03	.425E-03	.136E-01	.130E-01	.682E+06	.630E+06
12AUG75	1700	.101E-03	.270E-03	.137E-01	.125E-01	.685E+06	.607E+06
12AUG75	1800	.115E-03	.317E-03	.982E-02	.911E-02	.501E+06	.448E+06
12AUG75	1900	.181E-03	.347E-03	.800E-02	.720E-02	.405E+06	.357E+06
14AUG75	1200	.166E-03	.352E-03	.816E-02	.866E-02	.414E+06	.422E+06
14AUG75	1300	.171E-03	.387E-03	.824E-02	.856E-02	.416E+06	.417E+06
14AUG75	1400	.195E-03	.362E-03	.876E-02	.912E-02	.438E+06	.443E+06
14AUG75	1500	.208E-03	.398E-03	.104E-01	.105E-01	.519E+06	.514E+06
14AUG75	1600	.179E-03	.376E-03	.136E-01	.133E-01	.680E+06	.643E+06
14AUG75	1700	.198E-03	.352E-03	.135E-01	.130E-01	.677E+06	.633E+06
14AUG75	1800	.184E-03	.432E-03	.103E-01	.921E-02	.517E+06	.452E+06
14AUG75	1900	.202E-03	.400E-03	.816E-02	.735E-02	.414E+06	.360E+06
19AUG75	1200	.194E-03	.442E-03	.897E-02	.823E-02	.442E+06	.402E+06
19AUG75	1300	.226E-03	.606E-03	.859E-02	.846E-02	.428E+06	.413E+06
19AUG75	1400	.260E-03	.672E-03	.854E-02	.885E-02	.426E+06	.433E+06
19AUG75	1500	.176E-03	.462E-03	.105E-01	.106E-01	.519E+06	.517E+06
19AUG75	1600	.122E-03	.313E-03	.138E-01	.133E-01	.686E+06	.639E+06
19AUG75	1700	.225E-03	.593E-03	.140E-01	.128E-01	.699E+06	.623E+06
19AUG75	1800	.154E-03	.363E-03	.980E-02	.922E-02	.497E+06	.452E+06
19AUG75	1900	.153E-03	.293E-03	.818E-02	.756E-02	.414E+06	.371E+06
21AUG75	500	.246E-03	.559E-03	.963E-03	.211E-02	.465E+05	.104E+06
21AUG75	600	.216E-03	.533E-03	.324E-02	.791E-02	.154E+06	.391E+06
21AUG75	700	.195E-03	.461E-03	.866E-02	.120E-01	.418E+06	.592E+06
21AUG75	800	.246E-03	.582E-03	.713E-02	.954E-02	.346E+06	.468E+06
21AUG75	900	.240E-03	.496E-03	.524E-02	.717E-02	.250E+06	.355E+06
21AUG75	1000	.168E-03	.441E-03	.600E-02	.764E-02	.287E+06	.377E+06
21AUG75	1100	.238E-03	.553E-03	.811E-02	.858E-02	.400E+06	.421E+06
21AUG75	1200	.208E-03	.468E-03	.860E-02	.875E-02	.424E+06	.430E+06
26AUG75	500	.201E-03	.501E-03	.132E-02	.326E-02	.663E+05	.159E+06
26AUG75	600	.182E-03	.492E-03	.446E-02	.108E-01	.226E+06	.528E+06
26AUG75	700	.182E-03	.566E-03	.108E-01	.155E-01	.537E+06	.757E+06
26AUG75	800	.224E-03	.548E-03	.919E-02	.124E-01	.465E+06	.603E+06
26AUG75	900	.128E-03	.352E-03	.809E-02	.893E-02	.414E+06	.431E+06
26AUG75	1000	.168E-03	.392E-03	.827E-02	.874E-02	.425E+06	.429E+06
26AUG75	1100	.180E-03	.424E-03	.874E-02	.987E-02	.452E+06	.488E+06
26AUG75	1200	.199E-03	.559E-03	.870E-02	.102E-01	.447E+06	.500E+06
3SEP75	500	.180E-03	.234E-03	.119E-02	.179E-02	.596E+05	.876E+05
3SEP75	600	.234E-03	.241E-03	.247E-02	.786E-02	.124E+06	.392E+06
3SEP75	700	.196E-03	.247E-03	.588E-02	.139E-01	.286E+06	.686E+06
3SEP75	800	.245E-03	.360E-03	.594E-02	.119E-01	.294E+06	.586E+06
3SEP75	900	.195E-03	.189E-03	.717E-02	.806E-02	.368E+06	.395E+06
3SEP75	1000	.209E-03	.247E-03	.807E-02	.806E-02	.414E+06	.393E+06
3SEP75	1100	.179E-03	.180E-03	.902E-02	.889E-02	.458E+06	.433E+06
3SEP75	1200	.169E-03	.183E-03	.949E-02	.933E-02	.482E+06	.449E+06

III ANALYSIS OF TRAFFIC AND AEROMETRIC DATA FROM GRADE-LEVEL ATMOSPHERIC EXPERIMENT

A. Introduction

The objectives behind the broad scope of tests described in Chapter II were to provide an experimental data base that would be more comprehensive than previous individual experiments and that would provide basic measurements of transport and diffusion that could be used to assess various principles of fluid mechanics and evaluate and improve mathematical dispersion models. The atmospheric and wind tunnel studies conducted here were designed to complement each other and to expand the data bases available from earlier, less comprehensive experimental programs. In this regard, the current study represents a significant advance in the base of knowledge concerning wind flow, dispersion, and air quality in the near field of a broad variety of roadway configurations. Whereas the various atmospheric tests provided data on actual ambient conditions and the effects of meteorological and traffic vagaries and variations, the wind tunnel experiments provided the opportunity to assess conditions across a broader range of traffic and roadway conditions, and to do so by a series of discrete and systematic variations in roadway type, traffic speed, wind speed, wind direction, and ground roughness.

In particular, the at-grade atmospheric tests were designed to be especially detailed and comprehensive; the number and types of measurements made was significantly greater than in any earlier or subsequent highway dispersion study. The objective was to obtain a data base that would provide an improved understanding of atmospheric physical processes and form the basis for improved models of entrainment and dispersion. Because of the detail provided by the at-grade atmospheric test and the broad scope encompassed by the other atmospheric and wind tunnel tests, the following approach was taken in the analysis of the various data and the development of a practical simulation model:

- Detailed analyses were made of the at-grade atmospheric test data to better understand the relationships among meteorological and traffic parameters, and the subsequent dispersion of traffic emissions.

- Factor analysis and multiple regression analysis of the wind tunnel data were used to further quantify relationships between traffic and environmental variables and air quality for various roadway configurations.
- The new ROADMAP simulation model was proposed and subsequently applied to and evaluated with data from the various wind tunnel and atmospheric tests.

The first of these three steps is discussed in this chapter, while the second and third are the subject of Chapter IV and Chapters V and VI, respectively.

Three specific, fundamental objectives of the at-grade atmospheric tests were to:

- Investigate the impact of freeway traffic on near-roadway atmospheric dispersion.
- Determine in-situ emission rates from freeway traffic.
- Investigate pollutant concentrations near the roadway in relationship to traffic and meteorological conditions.

The first and second of these objectives are addressed in this section, while the third is the subject of Section VI.

B. Analysis of Near-Roadway Dispersion

Vehicle influences on near-roadway dispersion can theoretically arise from one of three physical processes:

- Buoyant mixing from atmospheric instabilities created by vehicle thermal exhaust.
- Mechanical mixing from wake turbulence.
- Transport from induced drag flow.

The grade-level atmospheric dispersion experiment was designed to provide data that could be analyzed to evaluate these processes as they occur under actual highway conditions.

The following discussions focus on the various analyses that were conducted in attempting to understand the nature and significance of these processes. These analyses were conducted prior to the application of existing dispersion models, and provided insights that were subsequently used in the development of a new semi-empirical Gaussian-type model. Similarly, data from the wind tunnel experiments were also analyzed, first, to understand the causal effects of traffic, meteorology, and site configuration on dispersion, and, second, in the development and evaluation of the ROADMAP model.

1. Temperature Structure

To examine the first effect, we have analyzed variations in the cross-roadway temperature gradient as they relate to wind direction and wind speed, ambient turbulence intensity, vehicle volume and speed, and height above ground. The cross-roadway temperature gradient (ΔT_{horiz}) is obtained by taking the temperature difference at each level between the north (#4) and south (#2) towers, after first normalizing by the 14.2-m values (thus assuming $\Delta T_{horiz} = 0$ at the level--in fact, this difference was only of the order of a few hundredths of a degree). Thus

$$\Delta T \text{ (ref.)} \equiv T_4 \text{ (14.2 m)} - T_2 \text{ (14.2 m)} \qquad (7)$$

and

$$\Delta T_{horiz} \text{ (i)} = T_4 \text{ (i)} - T_2 \text{ (i)} + \Delta T \text{ (ref.)} \qquad (8)$$

where i is the level (2.0, 3.8, or 7.5 m) and the subscripts refer to tower location. Figure 34 (a-c) shows 15-minute averages of ΔT_{horiz} as a function of the cross-roadway wind speed (u_{road}) for each of the three levels. For these figures, averages of u_{road} were obtained as follows: first, the average ambient wind direction ($\overline{\theta}$) was obtained as the vector* average of the 14.2-m winds on each of the five towers. Then, the 3.8-m wind speed was taken from the most upwind tower (#1 or #5), and the cross-roadway component was computed using $\overline{\theta}$. In the data plots, different

---

*The vector average wind direction is calculated by first obtaining instantaneous values of u and v, then calculating the period-average component winds ($\overline{u}$ and $\overline{v}$) and using these to calculate $\overline{\theta}$.

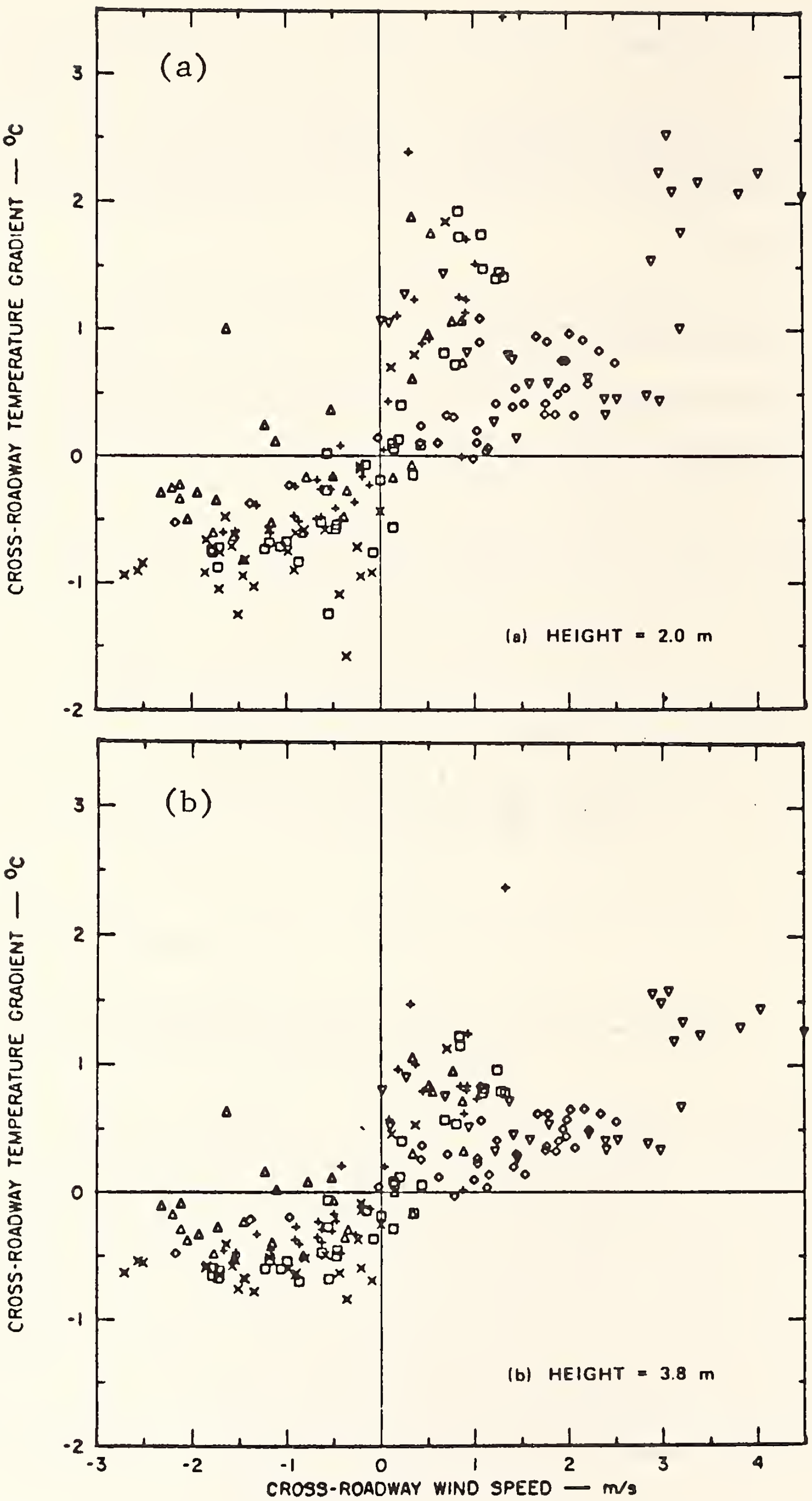

FIGURE 34 15-MIN VALUES OF CROSS-ROAD TEMPERATURE GRADIENT vs CROSS-ROAD WIND SPEED COMPONENT, AT THREE HEIGHTS ABOVE THE ROAD SURFACE

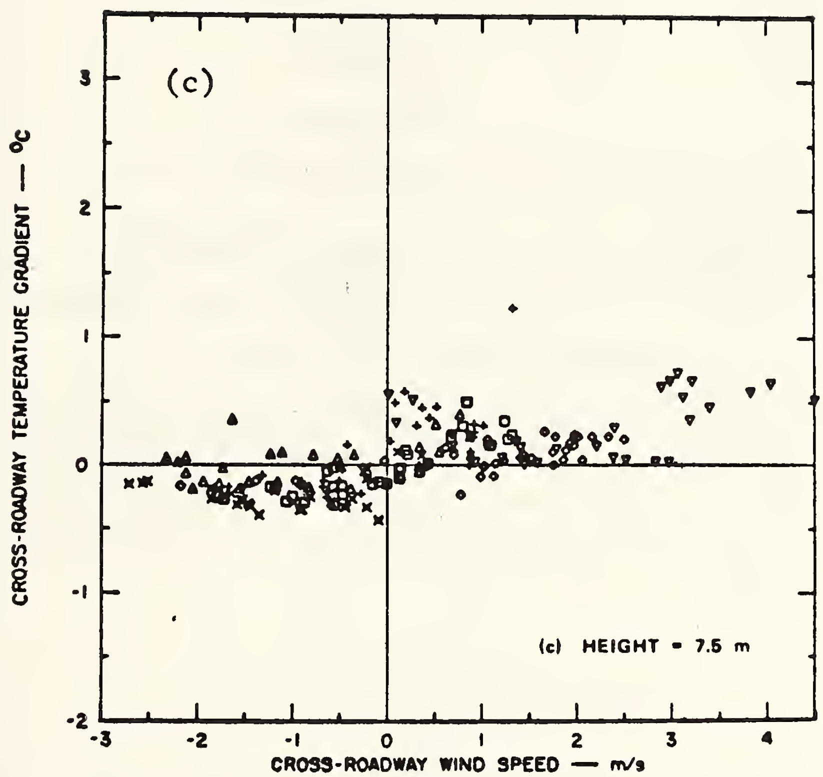

FIGURE 34 15-MIN VALUES OF CROSS-ROAD TEMPERATURE GRADIENT vs CROSS-ROAD WIND SPEED COMPONENT, AT THREE HEIGHTS ABOVE THE ROAD SURFACE (Concluded) symbols have been used to identify data from each of the six days. The key is:

Symbol	Date
×	17 January
+	21 January
□	24 January
◇	28 January
Δ	30 January
∇	5 February

The cross-roadway temperature gradient was quite large: at 2 m, maximum values from -1.5 to 2.5°C were obtained across the 57-m tower separation of the two towers at the roadway edges; at 3.8 m, the difference ranged from -0.75°C to 1.5°C; while at 7.5 m, it was still moderately large (from -0.4 to 0.75°C). The difference was small for low wind speeds and increased with higher cross-road wind speeds. Figure 35 (a-c) shows ΔT_{horiz} as a function of the cross-roadway wind angle (θ_{road}), where

$$\theta_{road} = 110.6° - \overline{\theta} \quad . \tag{9}$$

Here 110.6° is the orientation of the road (i.e., "eastbound"). The figures show that with a positive (0° to 180°) cross-roadway wind angle, the maximum ΔT_{horiz} values occur with winds nearly perpendicular to the road. For negative angles (180° to 250° and 0° to -110°), the maximum values of ΔT_{horiz} seem to occur around 40°.

The cross-roadway temperature structure is of itself only an indirect indicator of potential mixing near the roadway; however, further examination of its cause may have significance for another reason. Such examination may reveal whether cross-road temperature gradients are a result of waste heat emissions of the vehicles, differences in the thermal chracteristics of the roadway and adjacent soil, or mixing of the

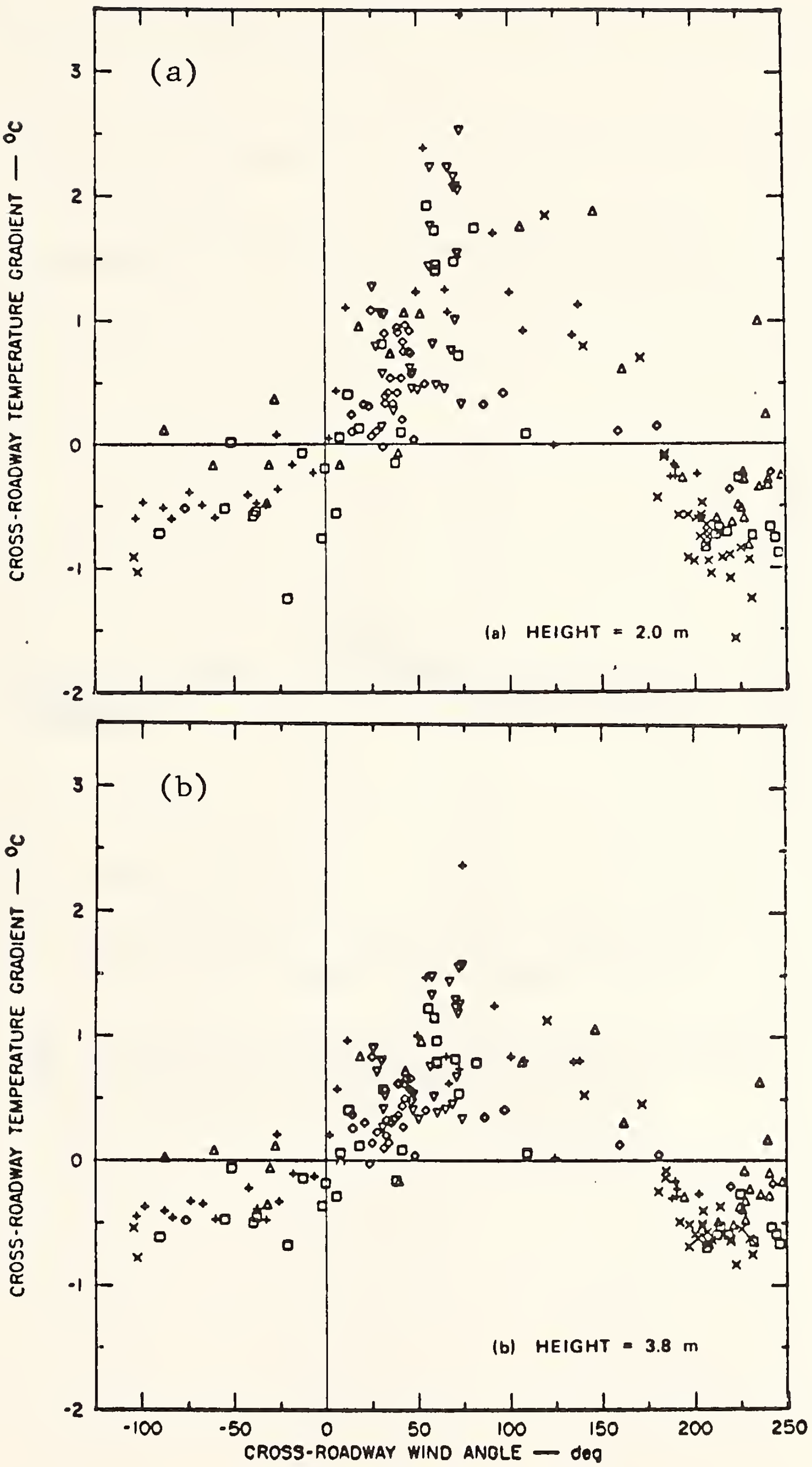

FIGURE 35 15-MIN VALUES OF CROSS-ROADWAY TEMPERATURE GRADIENT vs WIND DIRECTION RELATIVE TO ROADWAY, AT THREE HEIGHTS ABOVE ROAD SURFACE

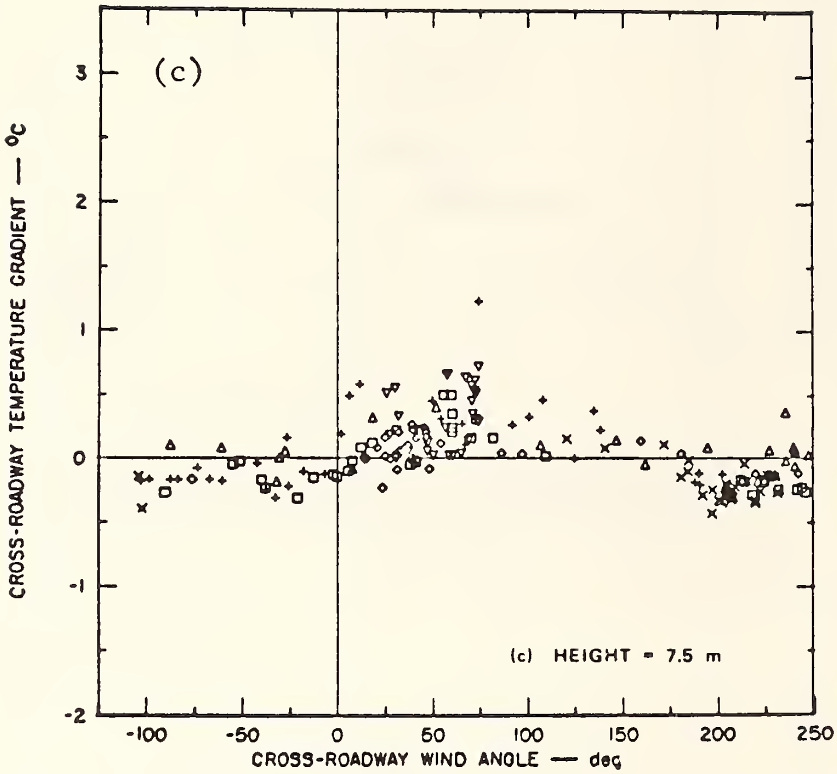

FIGURE 35 15-MIN VALUES OF CROSS-ROADWAY TEMPERATURE GRADIENT vs WIND DIRECTION RELATIVE TO ROADWAY, AT THREE HEIGHTS ABOVE ROAD SURFACE (Concluded) atmospheric surface layer by roadway vehicles after changes in the downwind (vertical) temperature profile.

If the third hypothesis were valid, then under lapse conditions (i.e., temperature decrease with height), the effect of vehicle-induced atmospheric mixing would be to lower near-ground temperatures downwind. Downwind temperatures would thus be lower than their upwind counterparts. With inversion conditions, the reverse would apply and downwind temperatures would be higher than those upwind. However, examination of the data in Figure 34 shows that there is no bimodal distribution by stability. (Note that all six days were characterized by both lapse and inversion conditions.) Rather, downwind temperatures are virtually always higher than upwind temperatures at each of the three heights. We therefore conclude that while this phenomenon is present, it is not the controlling factor in the cross-roadway temperature structure. However, it may explain why southerly winds (positive cross-road component) have maximum cross-road temperature gradients that are significantly larger (1°C greater at 2 m) than the northerly winds: in the study area, the local wind flow is controlled by a land-bay breeze circulation. Southerly winds blow at night with stable or inversion conditions over land, while the northerly bay breeze blows by day with lapse conditions over land.

The data in Figure 35 suggest that ΔT_{horiz} depends strongly on wind direction relative to the roadway. Therefore, those data were first disaggregated into 12 wind direction classes, as follows:

Class	Wind Direction Range (θ_{road}, °)	
I	000.0-014.9	165.0-179.9
II	015.0-029.9	150.0-164.9
III	030.0-044.9	135.0-149.9
IV	045.0-059.9	120.0-134.9
V	060.0-074.9	105.0-119.9
VI	075.0-089.9	090.0-104.9
VII	345.0-360.0	180.0-194.9
VIII	330.0-344.9	195.0-209.9

Class	Wind Direction Range (θ_{road}, °)	
IX	315.0-329.9	210.0-224.9
X	300.0-314.9	225.0-239.9
XI	285.0-299.9	240.0-254.9
XII	270.0-284.9	225.0-269.9

Wind direction classes were then combined (I and VII, II and VIII, and so on) and the cross-road temperature gradient at 2 m was correlated with each of the following six independent variables:

(1) TTI (upwind)--The total turbulence intensity (TTI) at 2 m on the tower farthest upwind of the roadway. TTI is a good indicator of the degree of mechanical mixing in the ambient atmosphere. It is defined here by the following relationship:

$$TTI \equiv [(u')^2 + (v')^2 + (w')]^{1/2} \quad ,$$

where u, v, and w are the longitudinal, lateral, and vertical wind components, respectively. The prime notation denotes the departure from the period average.

(2) u_{road}--The cross-roadway wind speed component.

(3) TTI × u_{road}--When reference is made to Gaussian line-source dispersion concepts (e.g., Turner, 1967), this product is analogous to the dispersion term given by the transport wind and diffusion coefficient.

(4) Total vehicle volume--This term is approximately proportional to the waste heat emission rate for cruising automobiles. Actually (Cope, 1973), the energy release rate extrapolated to 1974 is a constant 1.33×10^6 cal mi^{-1} from 30 to 40 mph and thereafter increases linearly at 1.41×10^4 cal mi^{-1} mph^{-1} from 40 to 70 mph.

(5) $\sum_{i=1}^{6}$ (volume × speed)--The product of vehicle volume and speed summed over all six lanes of the roadway. Since the energy out put does have some speed dependence, this term also represents an approximation of the heat released by the roadway vehicles.

(6) $\dfrac{\Sigma \text{ (volume} \times \text{speed)}}{TTI \times u_{road}}$ --Scaling factor for the disperion of heat from roadway vehicles, similar to the Gaussian line source dispersion formulation.

The results of the various correlations are summarized in Table 20. Of the six independent variables, clearly the cross-road wind speed component has the highest and most consistent correlation with ΔT_{horiz}.

Table 20

MATRIX OF THE LINEAR CORRELATION COEFFICIENT BETWEEN THE DEPENDENT VARIABLE ΔT_{horiz} AND SIX INDEPENDENT VARIABLES FOR EACH OF SIX WIND DIRECTION (θ_{road}) CATEGORIES

Wind direction classes	I,VII	II,VIII	III,IX	IV,X	V,XI	VI,XII
Number of data points	20	27	42	35	31	12
Independent variables	Correlation Coefficients					
(1) TTI (upwind)	-0.10	0.06	0.06	-0.17	-0.03	-0.07
(2) Cross-road wind speed (u_{road})	0.51	0.70	0.73	0.66	0.81	0.82
(3) TTI $\times$ u_{road}	0.40	0.61	0.60	0.52	0.67	0.49
(4) Total vehicle volume	0.19	-0.57	0.05	-0.02	0.27	0.78
(5) $\sum_{i=1}^{6}$ (volume $\times$ speed)	0.22	-0.52	0.02	-0.12	0.40	0.57
(6) $\frac{\Sigma \text{ (volume} \times \text{speed)}}{\text{TTI} \times u_{road}}$	0.46	0.47	0.71	0.65	0.48	0.93

The ambient TTI is virtually uncorrelated, while the traffic variables alone are poorly and inconsistently correlated. In fact, in no case do any of the five other independent variables show a higher correlation than u_{road} alone.

The positive correlation of ΔT_{horiz} with u_{road} is contrary to intuition, unless the vertical mixing induced by thermal instabilities from vehicle heat emissions and vehicle-induced mechanical mixing dominates under light wind conditions, thereby effectively dispersing vehicle thermal emissions more than under higher wind conditions when more "conventional" dispersion (i.e., mechanical mixing) dominates. This could possibly also explain an apparent leveling off of ΔT_{horiz} at the larger values of u_{road} (see Figure 34).

This examination of thermal structure has revealed some interesting observations on the magnitude and nature of cross-roadway temperature gradients. It has pointed out some of the complexities of near-roadway dispersion but has not provided a definitive understanding of the effects of vehicle motions and thermal emissions. These are addressed further in the following sections in examinations of the variation of near-roadway turbulence characteristics and trace-gas dispersion in relation to meteorological and traffic variables; later in this section, we discuss the combined implications of temperature, turbulence, and tracer analyses.

2. Turbulence Structure

Cross-roadway variations in the total turbulence intensity were investigated to obtain a better understanding of the effect of roadway traffic on the local dispersion of traffic-generated pollutants. The previous discussion indicated that both thermal and mechanical effects of the traffic stream may be important, and that they apparently combine to produce a direct relationship between wind speed and local dispersion (contrary to the indirect or inverse relationship that exists elsewhere).

Possible vehicle effects on dispersion near the roadway were examined by looking at the difference in the TTI between the upwind tower and first the median tower, then the downwind tower. Figure 36 (a-d) illustrates the variation of 15-min values of the TTI difference (ΔTTI_{horiz}) between upwind and downwind towers as a function of the cross-roadway wind angle (θ_{road}), where

$$\Delta TTI_{horiz}(i) \equiv TTI_4(i) - TTI_2(i) \quad , \qquad (10a)$$

and i is the level (height) and the subscripts denote tower location. Figure 37 (a-c) shows the TTI difference between the upwind and median (#3) towers as a function of θ_{road}, where

$$\Delta TTI_{horiz}(i) \equiv TTI_u(i) - TTI_3(i) \qquad (10b)$$

and the subscript u denotes the upwind tower location (either #2 or #4).

There is considerable scatter in the data in Figure 36 at all levels, with a slight inference of a dependence of ΔTTI on the wind/roadway angle. The large scatter does suggest the need to consider the dependence on other independent parameters, such as vehicle speed and volume, wind/roadway orientation, and stability. The gradient is somewhat larger at the lower levels, although not significantly. Values range from +0.5 to -0.5 m s^{-1} with the largest scatter at the lower levels.

The TTI difference between the upwind and median sensors (Figure 37) shows that the two lower levels have virtually the same distribution: the median tower always has the greater turbulence intensity but has large scatter from 0 to -1.3 m s^{-1}. However, the situation changes between the 3.8-m level and the 7.5-m level; the horizontal gradient of turbulence intensity drops by about a factor of two. Also, there are now a few cases where the upwind tower has greater turbulence. This suggests the need to consider vehicle effects on variations in the gradient. Data from the median tower do suggest, however, that a uniformly well-mixed layer is present on the road up to a height of at least 4 m, and then damps out significantly by 7.5 m.

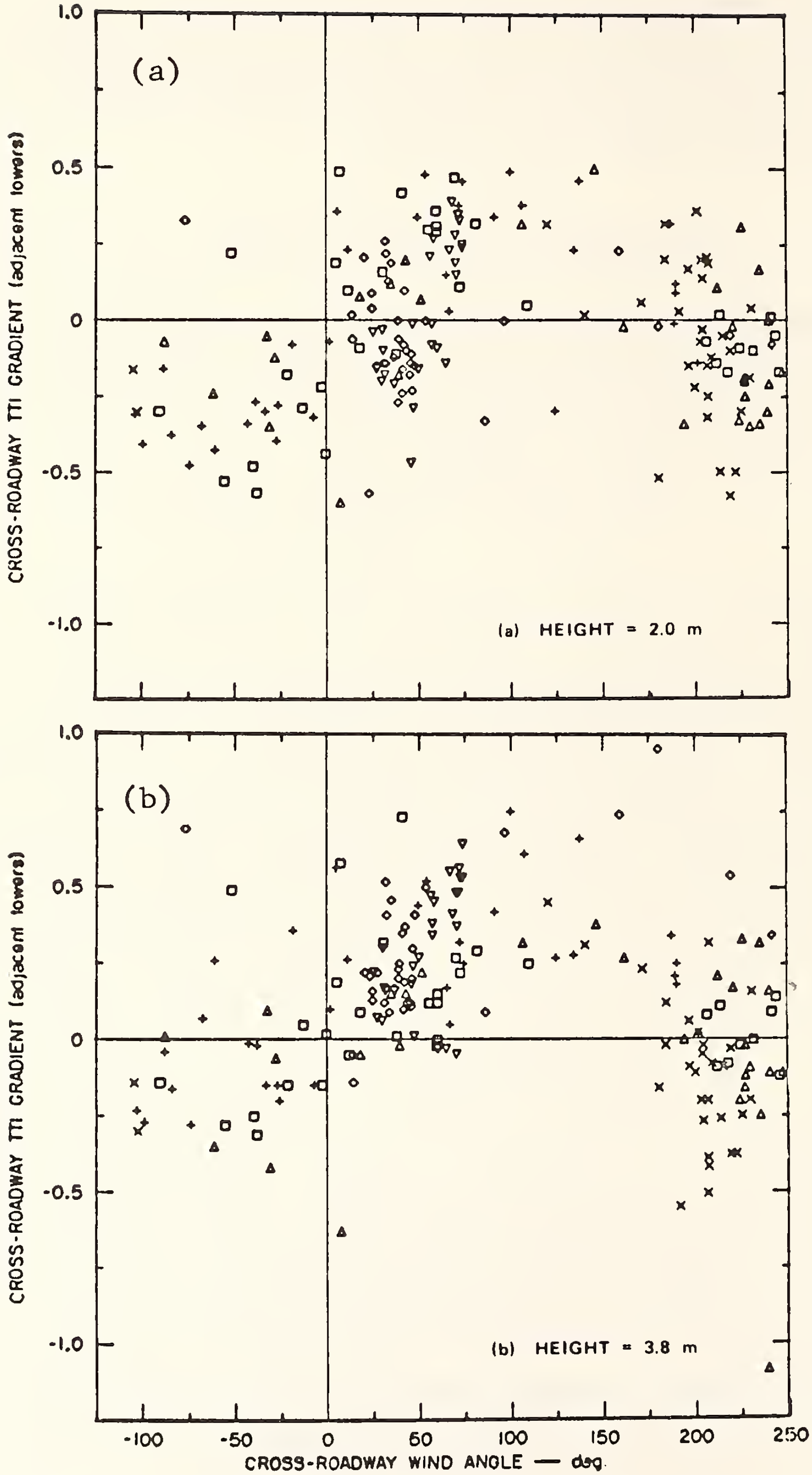

FIGURE 36 CROSS-ROADWAY DIFFERENCE IN THE TURBULENCE INTENSITY AS A FUNCTION OF THE CROSS-ROAD WIND ANGLE, AT FOUR HEIGHTS ABOVE THE ROAD SURFACE

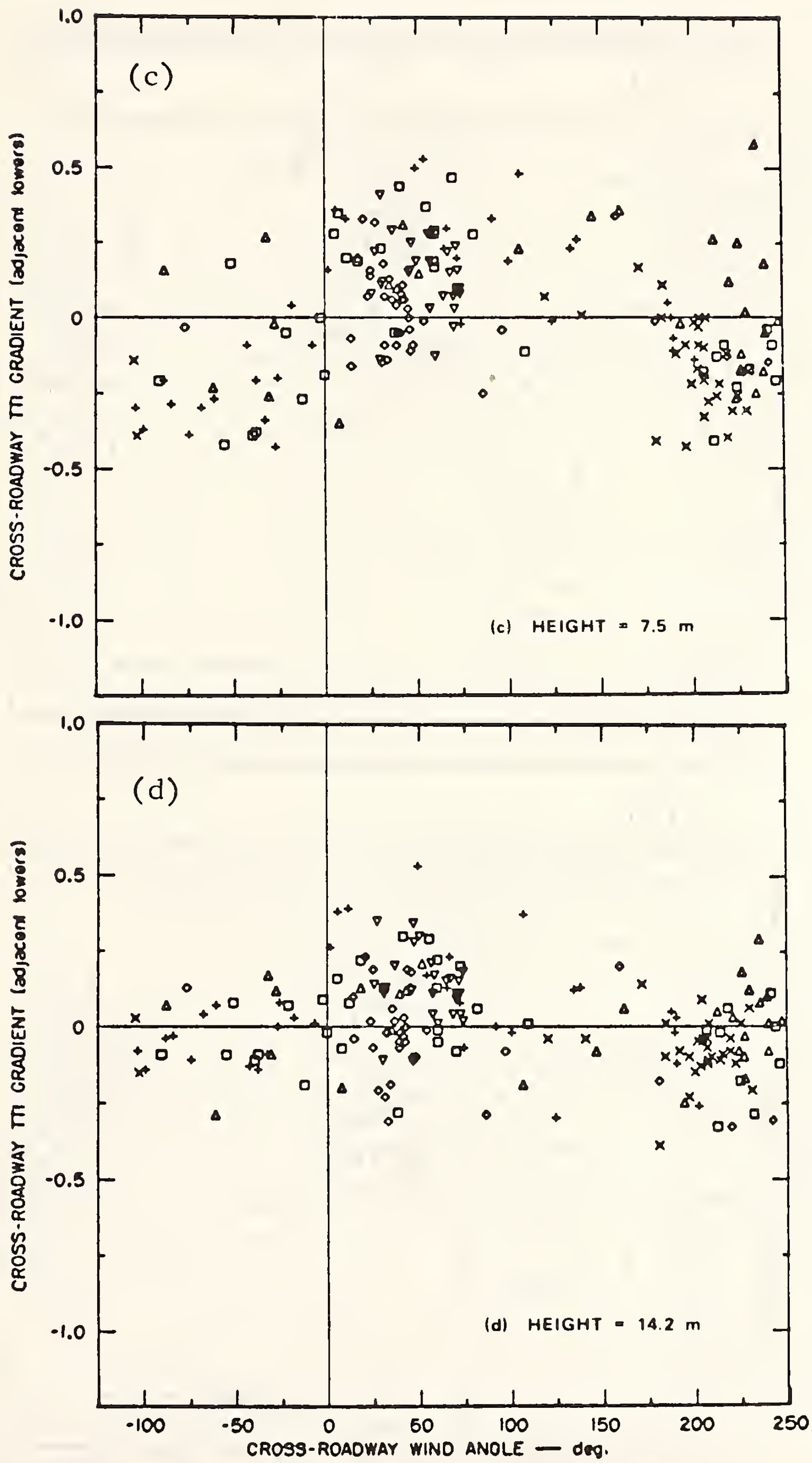

FIGURE 36 CROSS-ROADWAY DIFFERENCE IN THE TURBULENCE INTENSITY AS A FUNCTION OF THE CROSS-ROAD WIND ANGLE, AT FOUR HEIGHTS ABOVE THE ROAD SURFACE (Concluded)

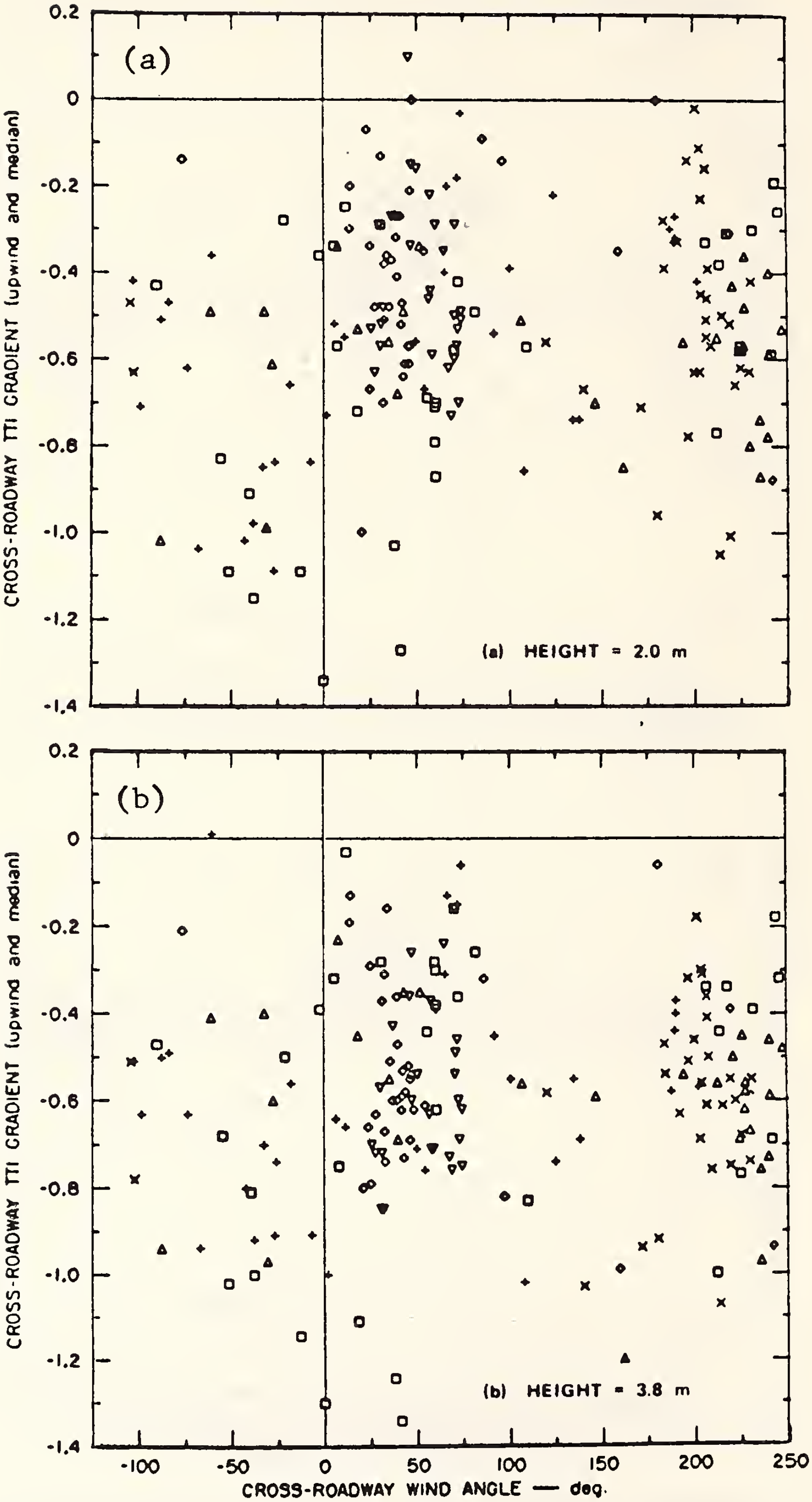

FIGURE 37 DIFFERENCE IN TURBULENCE INTENSITY BETWEEN THE UPWIND AND MEDIAN TOWERS AS A FUNCTION OF THE CROSS-ROAD WIND ANGLE, AT THREE HEIGHTS ABOVE THE ROAD SURFACE

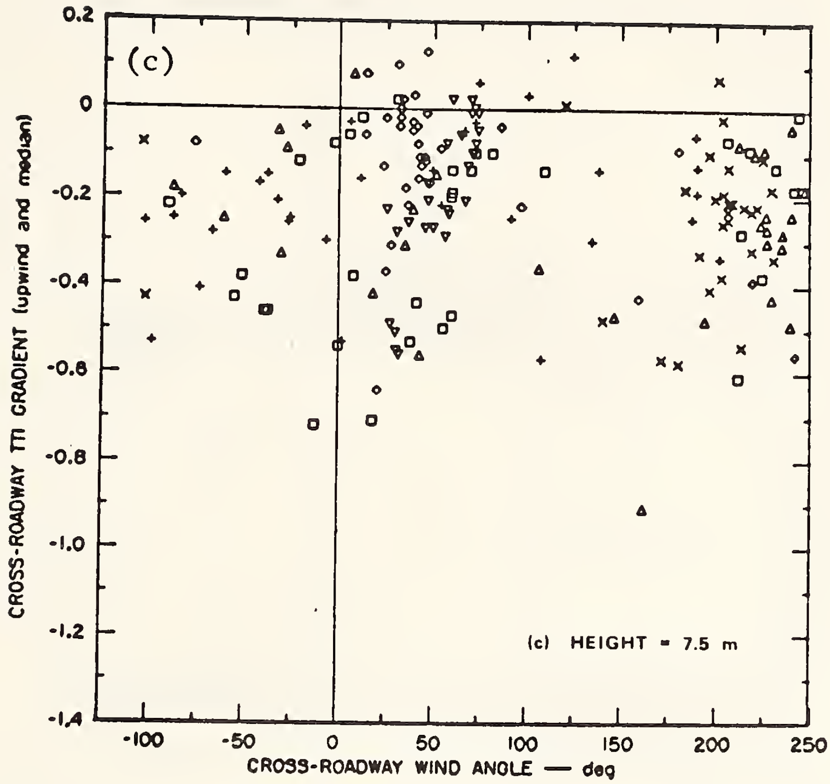

FIGURE 37 DIFFERENCE IN TURBULENCE INTENSITY BETWEEN THE UPWIND AND MEDIAN TOWERS AS A FUNCTION OF THE CROSS-ROAD WIND ANGLE, AT THREE HEIGHTS ABOVE THE ROAD SURFACE (Concluded)

The absolute value of the cross-roadway turbulence intensity is possibly largely affected by the magnitude of the TTI of the ambient flow. Figures 38 (a-d) and 39 (a-c) show the variation of the normalized horizontal gradient of turbulence intensity ($\Delta NTTI_{horiz}$) against the cross-roadway wind angle, where

$$\Delta NTTI_{horiz}(i) \equiv \Delta TTI_{horiz}(i)/TTI_u(i) \quad . \qquad (11)$$

Figure 38 presents normalized differences between the up- and downwind sensors, while Figure 39 is for the upwind and median sensors. Normalizing provides some perspective into the magnitude of the roadway effect. Note in Figure 38 that the cross-roadway difference in turbulence intensity frequently equals and often exceeds the ambient level for the

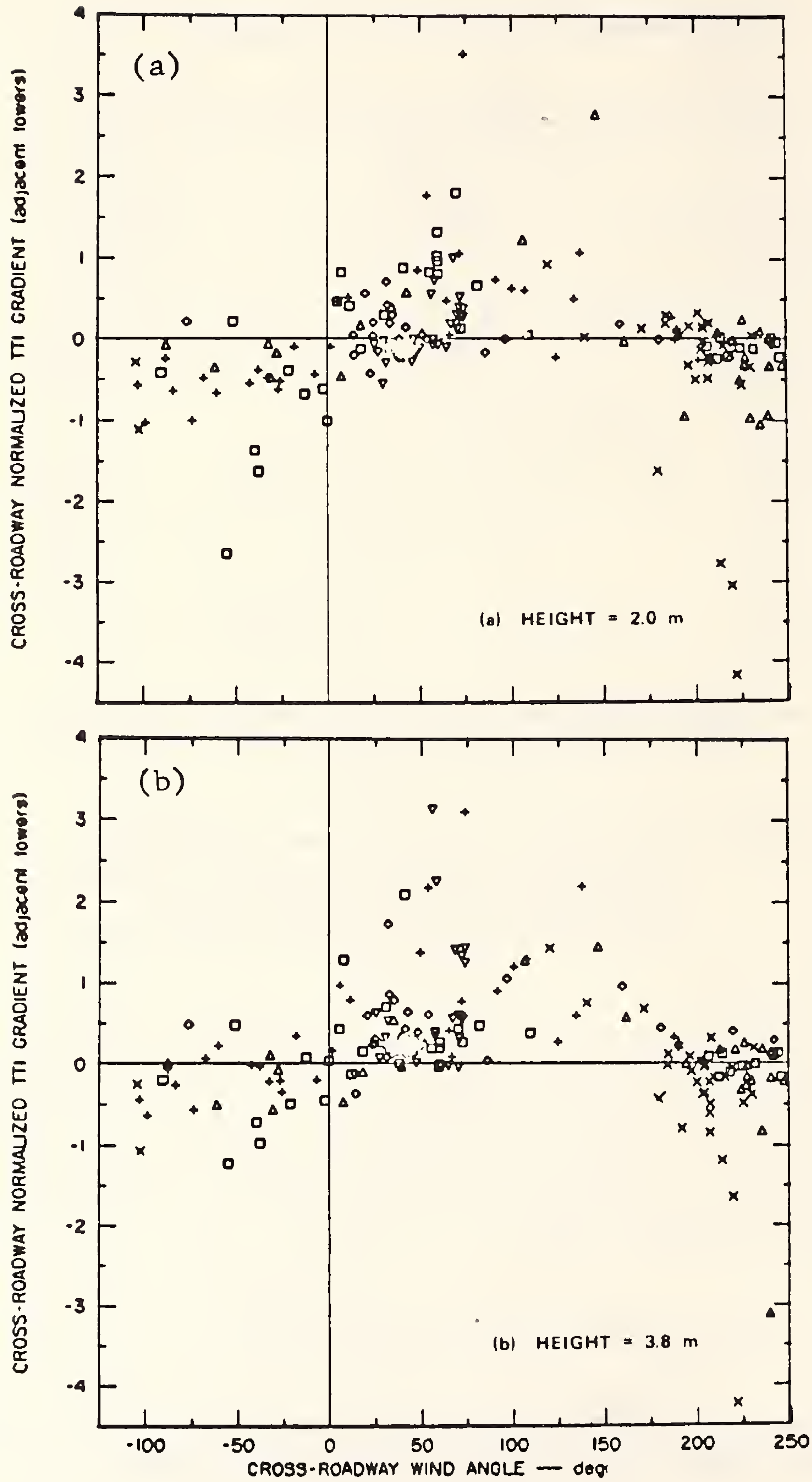

FIGURE 38 WIND DIRECTIONAL VARIATION OF THE RATIO OF THE CROSS-ROAD TURBULENCE INTENSITY DIFFERENCE TO THE UPWIND TURBULENCE INTENSITY, AT FOUR HEIGHTS ABOVE THE ROADWAY SURFACE

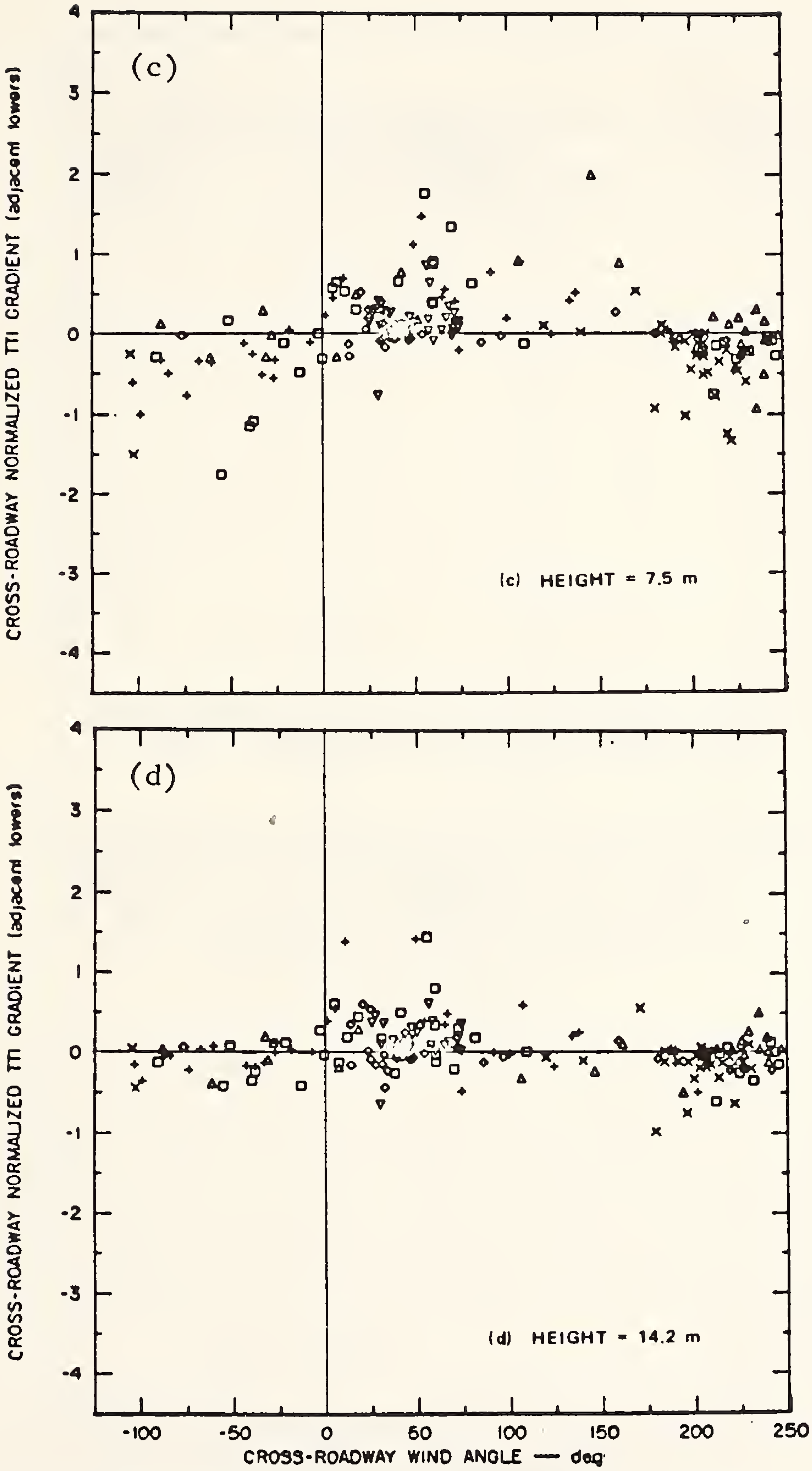

FIGURE 38 WIND DIRECTIONAL VARIATION OF THE RATIO OF THE CROSS-ROAD TURBULENCE INTENSITY DIFFERENCE TO THE UPWIND TURBULENCE INTENSITY, AT FOUR HEIGHTS ABOVE THE ROADWAY SURFACE (Concluded)

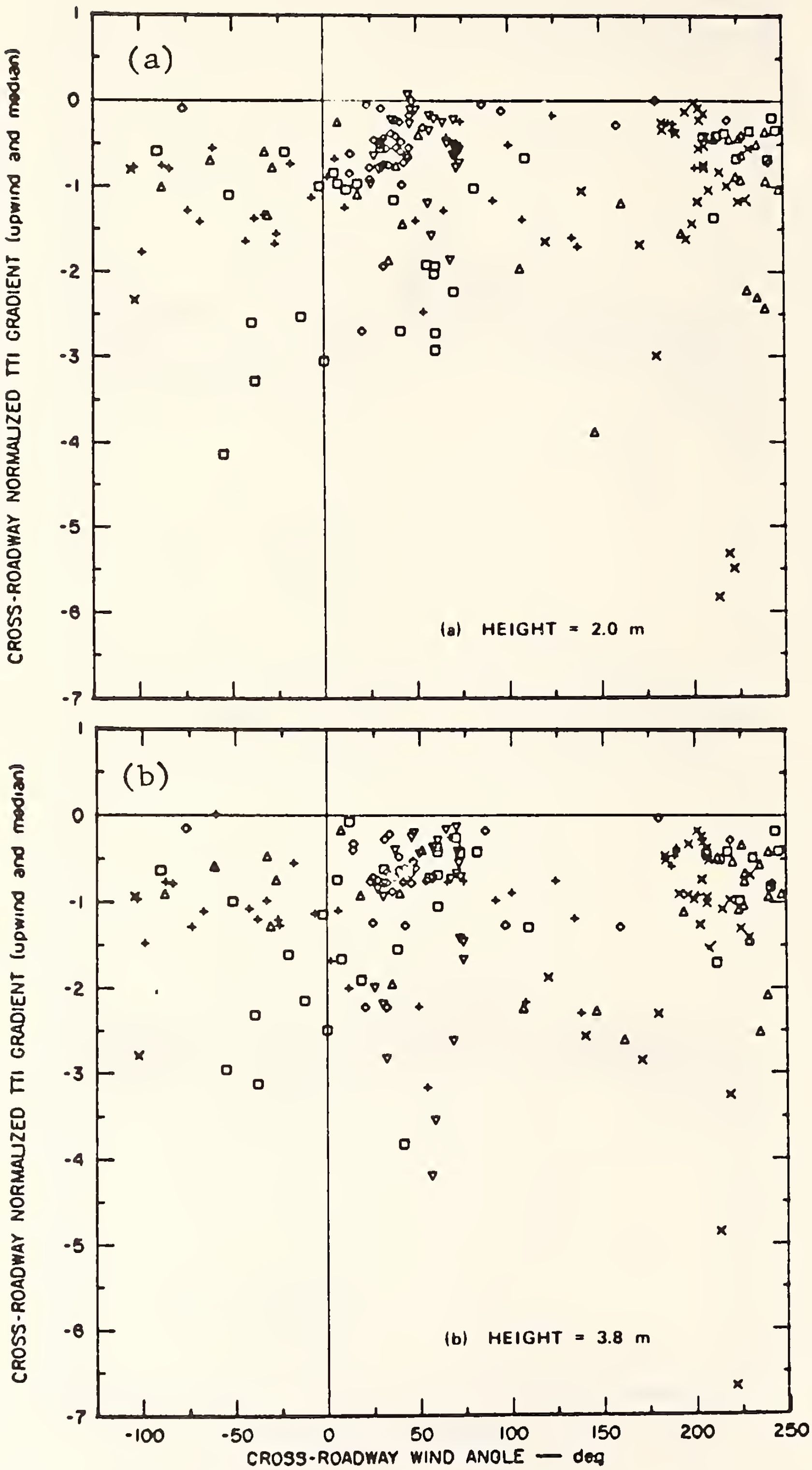

FIGURE 39 WIND DIRECTIONAL VARIATION OF THE RATIO OF THE UPWIND-MEDIAN TURBULENCE INTENSITY DIFFERENCE TO THE UPWIND TURBULENCE INTENSITY, AT THREE HEIGHTS ABOVE THE ROADWAY SURFACE

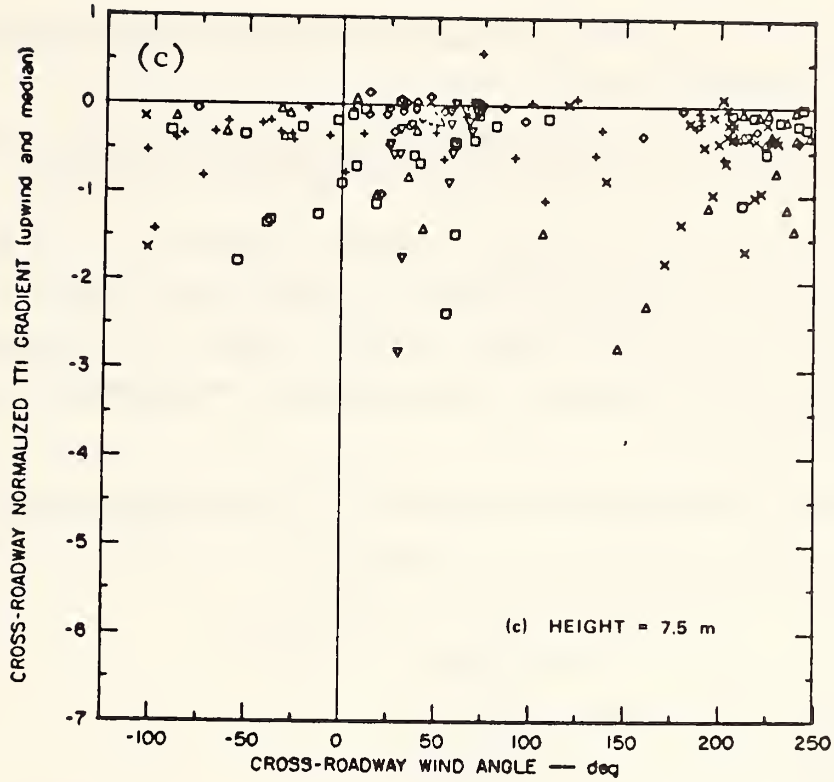

FIGURE 39 WIND DIRECTIONAL VARIATION OF THE RATIO OF THE UPWIND-MEDIAN TURBULENCE INTENSITY DIFFERENCE TO THE UPWIND TURBULENCE INTENSITY, AT THREE HEIGHTS ABOVE THE ROADWAY SURFACE (Concluded)

lower three heights (up to 7.5 m); at the 14.2-m level the general range of $\Delta NTTI_{horiz}$ is about half the ambient level with no apparent wind directional dependence. As shown in Figure 39, $\Delta NTTI_{horiz}$ values are always negative (i.e., greater turbulence in the median) and frequently range up to three and greater at the two lower levels. At 7.5 m, $\Delta NTTI_{horiz}$ values drop by nearly a factor of two over those at the lower levels.

Furthermore, normalizing results in a more pronounced variation of the gradient between upwind and downwind sensors as a function of wind/roadway angle. The distribution is similar to that shown earlier for the temperature gradient variations. For "positive" wind angles, $\Delta NTTI$

peaks about 90° relative to the road; for "negative" wind angles there is not as pronounced a peak.

Normalization of the upwind-median gradient of turbulence intensity has reduced the scatter, particularly at the 7.5-m level. Nearer the ground, however, there is still considerable scatter. At all levels there is still no apparent dependence on wind/roadway angle. But since the median tower is located between traffic lanes, it is probably dominated by traffic features, thus minimizing any dependence on ambient wind direction.

To examine the possible dependence of cross-roadway differences in the turbulence intensity on meteorological and traffic parameters, we correlated the following dependent variables

- $\Delta TTI_{horiz}(1)$--upwind/downwind
- $\Delta TTI_{horiz}(1)$--upwind/median
- $\Delta NTTI_{horiz}(1)$--upwind/downwind
- $\Delta NTTI_{horiz}(1)$--upwind/median

with the following independent variables

(1) $A \equiv TTI_u(1)$, upwind turbulence intensity at 2 m

(2) $B \equiv u_{ref}$; upwind reference wind speed

(3) $C \equiv u_{road}$; cross-roadway wind speed component

(4) $D \equiv \Delta T_{horiz}(1)$; cross-roadway temperature gradient at 2 m

(5) $E \equiv \phi CC(E) + \phi CC(W)$; sum of eastbound and westbound (by lanes) vehicle occupancy--occupancy is defined as the ratio of vehicle volume to vehicle speed

(6) $F \equiv [V\phi L(E) \times SP(E)] + [V\phi L(W) \times SP(W)]$; sum of the eastbound and westbound (by lanes) products of vehicle speed and vehicle volume

(7) $G \equiv V\phi L(E + W)$; sum of eastbound and westbound traffic volumes

(8) $\phi \equiv \phi CC(u)$; occupancy of the upwind traffic steam

(9) $P \equiv V\phi L(u) \times SP(u)$; product of volume and speed (by lanes) for upwind traffic stream

(10) $Q \equiv u_{net}$; vector sum of ambient wind flow and vehicle-induced drag flow of the upwind traffic stream; drag flow computed as the product of vehicle density, vehicle speed, and drag coefficient (approximately 0.6)

(11) $R \equiv V\phi L(u)$; volume of the upwind traffic stream

(12) $S \equiv DRAG(u)$; vehicle drag flow of the upwind traffic stream

(13) $T \equiv v_{net}$; vector sum of roadway-parallel ambient wind component and vehicle-induced drag flow of the upwind traffic stream.

The symbols are cited in Table 21 in a summary of correlation coefficients (r) while the letters alone are given in Appendix A which includes both the data of Table 21 and the mean and standard deviation of all independent and dependent variables. Furthermore, in the analyses summarized in both Table 21 and Appendix A, the data are stratified according to six wind direction categories (as before in the ΔT analysis) based on the 12 wind classes given earlier:

Category	Class
1	I, VII
2	II, VIII
3	III, IX
4	IV, X
5	V, XI
6	VI, XII

The results summarized in Table 21 shows that the up/downwind gradient of turbulence intensity at 2 m is consistently well correlated with only one parameter, the cross-road temperature gradient; the average r is about 0.53. This further suggests that thermal vehicle emissions are the cause of the large cross-road temperature gradients observed. Interestingly, the upwind/median gradient of turbulence intensity is strongly correlated with the reference wind speed; the average r is about 0.52. None of the other independent parameters shows any consistently significant correlation. (Note, however, that this is not unexpected in the case of ΔT_{horiz} since it is defined as the difference between two geographically-fixed locations, while the upwind/median TTI gradient is always taken as upwind minus median values.)

Table 21

MATRIX OF THE LINEAR CORRELATION COEFFICIENT
BETWEEN CROSS-ROADWAY TURBULENCE GRADIENTS (Dependent Variable)
AND VARIOUS METEOROLOGICAL AND TRAFFIC PARAMETERS
(15-min averages) FOR EACH OF SIX WIND-DIRECTION CATEGORIES

Wind direction category	1	2	3	4	5	6
Number of data points	20	27	42	35	31	12
Dependent variable = $\Delta NTTI_{horiz}(1)$ -- upwind/downwind						
$TTI_u(1)$	-.05	-.22	.15	.11	-.02	.09
u_{ref}	.06	.36	.23	-.32	-.12	-.17
u_{road}	.20	.40	.24	-.15	.21	.54
$\Delta T_{horiz}(1)$	.37	.27	.10	.70	.59	.83
ØCC (total)	.09	.12	.07	-.23	.17	.60
VØL x SP (total)	-.01	-.00	.00	-.14	.02	.66
VØL (total)	.05	.06	.05	-.21	.16	.70
Dependent variable = $\Delta TTI_{horiz}(1)$ -- upwind/downwind						
$TTI_u(1)$	.02	-.28	-.38	-.36	-.06	-.01
u_{ref}	-.22	.21	-.11	-.32	.19	-.20
u_{road}	.14	.34	.18	-.19	.56	.34
ΔT_{horiz}	.38	.41	.73	.31	.76	.72
ØCC (total)	.08	.12	.03	.29	.37	.59
VØL x SP (total)	-.06	.13	-.22	-.11	.05	.64
VØL (total)	.01	.15	-.07	.18	.27	.68
Dependent variable = $\Delta NTTI_{horiz}(1)$ -- upwind/median						
$TTI_u(1)$	-.51	-.22	.21	.25	.24	.78
u_{ref}	.67	.57	.57	.58	.42	.56
u_{road}	.48	.49	.47	.61	.31	.08
$\Delta T_{horiz}(1)$	-.10	-.02	-.26	.05	-.08	-.11
ØCC(u)	.25	-.05	.02	-.12	.19	-.06
VØL(u) x SP(u)	.26	.14	-.04	.24	-.17	-.13
u_{net}	-.41	-.20	.17	.14	-.03	.19
VØL(u)	.26	.05	-.02	.03	.08	-.14
DRAG(u)	.26	.05	-.02	.03	.08	-.14
v_{net}	.47	.23	-.09	-.05	.16	-.09
Dependent variable = $\Delta TTI_{horiz}(1)$ -- upwind/median						
$TTI_u(1)$	-.57	-.34	.05	.48	.17	.55
u_{ref}	.59	.53	.65	.41	.14	.52
u_{road}	.50	.47	.68	.47	.12	.20
$\Delta T_{horiz}(1)$	-.07	.09	.30	.07	.04	-.04
ØCC(u)	-.01	-.03	-.02	-.16	-.05	-.04
VØL(u) x SP(u)	-.07	.05	-.25	.18	-.47	-.09
u_{net}	-.19	-.17	.22	.27	.37	.13
VØL(u)	-.04	.01	-.16	-.05	-.31	-.10
DRAG(u)	-.04	.01	-.16	-.05	-.31	-.10
v_{net}	.32	.25	-.11	-.20	-.27	-.04

3. Trace Gas Dispersion

The objective of the dispersion analysis was to compare diffusion rates between the upwind and downwind tracers as a method for examining possible effects of the traffic flow. Differences between the two reflect the influence of the intervening traffic stream on pollutant dispersion. The general layout of the near-roadway samplers was shown earlier in Figure 22; Table 22 summarizes the fetch between each of the surface samplers and the two tracer release points.

Using $\bar{\theta}$ and u_{road}, together with the tracer release rates (Q, g m^{-1} s^{-1}), the vertical Gaussian diffusion coefficient σ_z(m) near ground level (i.e., 2 m) was computed from the line source equation, where

$$\sigma_z = \frac{\sqrt{2/\pi}\, Q}{u_{road}\ \chi} \tag{12}$$

and χ is the tracer concentration (g m^{-3}). The use of the Gaussian line source formulation is not intended to imply that the two-dimensional pollutant distribution near the roadway is adequately described by Gaussian concepts. Rather, the surface level diffusion coefficient so derived is used as a <u>scaling parameter</u> of atmospheric mixing.

For each test, σ_z values were computed for each of the downwind surface samplers when $\bar{\theta}$ was not within 20° of the roadway orientation. Values of u_{road} were taken from the 3.8-m level of the near downwind tower (#2 or #4). Then, the diffusion data for each test and each tracer were analyzed for their functional dependence on the fetch (x) from the release lane according to the following relationship:

$$\sigma_z = \sigma_{z-o} + a\ x^b \quad . \tag{13}$$

The term σ_{z-o} may be thought of as scaling the effect of the initial mixing of the tracer gas on the near-ground concentration at the release point. The coefficients a and b describe the distance-dependence of the near-ground diffusion coefficient. In determining σ_{z-o}, a, and b,

Table 22

HORIZONTAL ORTHOGONAL DISTANCE BETWEEN TRACER LINE SOURCE AND GROUND LEVEL SAMPLERS

Sampler Number	Direction (m)			
	North of Highway		South of Highway	
	SF_6	F13B1	SF_6	F13B1
1	97.0	122.0		
2	81.7	106.7		
3	66.5	91.5		
4	51.2	76.2		
T11	36.0	61.0		
5	25.3	50.3		
T21	16.2	41.2		
7*	16.2	41.2		
6	11.6	36.6		
9*†	-11.4	13.3	11.4	-13.3
T31	-11.4	13.3	11.4	-13.3
13			35.5	11.6
T41			40.0	16.2
11*			40.0	16.2
14			49.2	25.3
T51			59.9	36.0
15			75.1	51.2
16			90.3	66.5
17			105.6	81.7
18			120.8	97.0

*These three samplers were located 22.9 m perpendicular (to the west) to the principal sampling line.

†Negative distance signifies sampler is upwind of line source.

a standard nonlinear regression technique in the SRI computer library was used. Table 23 summarizes these values for both the upwind and downwind tracers, and also tabulates the number of samples per analysis and the

Table 23

SUMMARY OF METEOROLOGICAL CONDITIONS AND REGRESSION ANALYSIS OF DIFFUSION DATA (Equations 12 and 13)

DATE	TIME	$\bar{\theta}_{road}$ (deg)	u_{road} (m s^{-1})	v_{road} (m s^{-1})	N(up)	σ_{z-o}(up) (m)	a	b	N(dn)	σ_{z-o}(dn) (m)	a	b
17JAN75	1400	158.00	1.26	-3.06	10	.659E+00	.671E+00	.436E+00	8	.150E+01	.251E-02	.161E+01
17JAN75	1500	157.00	.93	-2.16	4	-.664E+01	.188E+01	.494E+00	4	-.858E+01	.906E+01	.113E+00
17JAN75	1600	84.00	1.51	.17	8	-.163E+01	.254E+01	.655E-01	5	-.115E+01	.577E+00	.605E+00
17JAN75	1700	107.00	1.17	-.35	7	.113E+01	.146E+01	.147E+00	6	.266E+01	.444E-02	.155E+01
17JAN75	1800	104.00	.79	-.19	6	-.885E+01	.807E+01	.191E+00	4	.176E+01	.343E+00	.720E+00
17JAN75	1900	81.00	.20	.03	4	-.972E+01	.336E+00	.116E+01	4	.140E+02	.138E+00	.128E+01
21JAN75	700	39.00	.41	.50	10	.203E+01	.131E+00	.100E+01	8	-.934E+01	.296E+01	.508E+00
21JAN75	800	44.00	.70	.74	10	-.537E+02	.887E+01	.690E+00	6	-.415E+02	.288E+02	.192E+00
21JAN75	900	77.00	1.13	.27	8	.103E+01	.844E-01	.102E+01	6	.790E+01	.258E-01	.112E+01
21JAN75	1000	109.00	.85	-.29	10	-.381E+01	.200E+01	.586E+00	8	.276E+01	.388E-02	.195E+01
21JAN75	1100	78.00	.66	.15	8	.794E+00	.124E+00	.127E+01	6	-.681E+01	.663E+00	.958E+00
24JAN75	700	38.00	.84	1.07	9	-.144E+01	.957E+00	.424E+00	7	-.212E+01	.151E+01	.275E+00
24JAN75	800	22.00	.42	1.02	6	-.569E+02	.126E+02	.366E+00	6	-.206E+02	.186E+01	.745E+00
24JAN75	900	85.00	.90	.08	10	-.179E+01	.118E+01	.548E+00	8	-.103E+02	.758E+01	.176E+00
24JAN75	1000	100.00	.27	-.05	11	-.971E+02	.474E+02	.383E+00	9	-.497E+02	.276E+02	.405E+00
24JAN75	1100	113.00	.79	-.33	10	.205E+01	.694E-01	.118E+01	8	.520E+00	.853E-01	.125E+01
24JAN75	1200	100.00	.97	-.16	10	.168E+01	.107E-01	.173E+01	8	-.582E+00	.569E+00	.758E+00
28JAN75	700	36.00	1.48	2.00	9	-.122E+01	.579E+00	.483E+00	7	.869E+00	.284E-01	.960E+00
28JAN75	800	29.00	1.36	2.42	9	.238E+01	.389E-02	.136E+01	7	.302E+01	.266E-01	.105E+01
28JAN75	900	27.00	1.27	2.46	7	.128E+01	.104E-01	.117E+01	5	.282E+01	.916E-02	.127E+01
28JAN75	1100	34.00	.47	.69	9	-.161E+01	.145E+00	.118E+01	7	.283E+01	.151E-01	.160E+01
28JAN75	1200	105.00	.75	-.19	9	.483E+01	.495E-01	.155E+01	8	.266E+01	.720E-04	.309E+01
30JAN75	1200	61.00	.30	.17	6	-.205E+01	.240E-01	.205E+01	4	-.489E+02	.155E+02	.521E+00
30JAN75	1300	30.00	.30	.52	9	.615E+01	.186E+00	.122E+01	7	.141E+01	.150E+00	.139E+01
30JAN75	1400	116.00	.97	-.46	8	-.369E+02	.290E+02	.172E+00	6	.162E+02	-.186E+00	.761E+00
30JAN75	1500	112.00	1.49	-.59	8	.959E+00	.802E-01	.100E+01	6	.201E+01	.161E-01	.152E+01
30JAN75	1600	96.00	1.71	-.17	10	.119E+01	.309E-01	.115E+01	8	-.222E+01	.137E+01	.310E+00
30JAN75	1700	99.00	1.28	-.19	9	.449E+00	.175E+00	.715E+00	8	-.295E+01	.148E+01	.415E+00
30JAN75	1800	124.00	1.07	-.71	10	-.614E-02	.376E+00	.442E+00	8	-.370E+00	.572E+00	.430E+00
5FEB75	1800	64.00	1.18	.57	8	-.236E+01	.138E+01	.354E+00	7	.739E-01	.438E+00	.517E+00
5FEB75	1200	36.00	1.42	1.93	12	-.100E+01	.492E+00	.552E+00	10	.869E+00	.147E-01	.129E+01
5FEB75	1300	50.00	2.47	2.04	11	.154E+01	.103E-01	.111E+01	11	.848E+00	.797E-01	.846E+00
5FEB75	1400	49.00	2.19	1.87	13	.106E+01	.655E-02	.127E+01	11	-.250E+00	.281E+00	.635E+00
5FEB75	1500	62.00	3.56	1.86	11	.814E+00	.298E-01	.940E+00	9	-.557E+00	.634E+00	.466E+00
5FEB75	1600	70.00	3.40	1.21	10	.506E+00	.122E+00	.647E+00	8	.989E+00	.150E-01	.109E+01
5FEB75	1700	70.00	2.19	.78	9	-.128E-01	.176E+00	.651E+00	8	.162E+01	.351E-01	.106E+01

hourly meteorological conditions. Table 24 summarizes hourly traffic and meteorological data, and the diffusion coefficients at x = 40 m and x = 60 m for the upwind tracer, and x = 40 m for the downwind tracers as computed from the nonlinear fit to Eq. (13) (see Table 23). Note that the separation of the east- and westbound center lanes is 20 m.

The ratio of the upwind dispersion coefficient [σ_z (up)] to the downwind coefficient [σ_z (dn)] at a fetch of 40 m ranged from about 0.3 to 3.0. In examining these variations more extensively, hourly cases with ambient wind speeds of less than 1 m s^{-1} were also excluded as possibly being nonrepresentative. This left 19 h that satisfied the two meteorological criteria. The coefficient averages (at x = 40 m) were 5.5 and 4.9 m for the downwind and upwind lanes, respectively. The average difference in coefficients normalized by the downwind coefficient was 7%. The coefficient of variation of the upwind-lane data was 101% and for the downwind data, 103%. Four standard statistical tests (e.g., see Panofsky and Brier, 1965) were made to evaluate the significance of the downwind coefficients being apparently larger than the upwind.

The analysis-of-variance technique used to determine the between-group (upwind and downwind) variation states that each observation (X_{ij}) is made up of four components:

- The grand mean of all observations (M)
- The experimental error (e_{ij})
- The within-group variation (W_j)
- The between-group variation (B_i).

This may be expressed as:

$$X_{ij} = M + e_{ij} + W_j + B_i \quad . \tag{14}$$

The between-group variation is the variable used to test the null hypothesis that the between-sample variation is only a reflection of the variation of items in a common parent population. The statistic used to verify this hypothesis is Snedecor's F test and the critical value for rejecting the null hypothesis in the 5% level.

Table 24

METEOROLOGICAL, TRAFFIC, AND DISPERSION DATA SUMMARY

DATE	TIME	WIND/ROAD ANGLE (DEG)	WIND SPEED (M/S)		DISPERSION COEFFICIENTS (M)			VOLUP	VOLDN	TTIUP (M/S)	SIGWUP (M/S)	SIGPHIUP (DEG)
			U	V	X(DN)=40M	X(UP)=40M	X(UP)=60M	(veh/hr)				
17JAN75	1400	158	1.26	-3.06	2.5	4.0	4.7	2803.	2705.	.85	.22	6.04
17JAN75	1700	107	1.17	-.35	4.0	3.7	3.8	3065.	3779.	.74	.15	4.20
17JAN75	1800	104	.79	-.19	6.6	7.5	8.8	2161.	2798.	.43	.11	15.60
17JAN75	1900	81	.20	.03	29.3	14.5	29.0	1909.	1581.	.39	.13	7.70
21JAN75	700	39	.41	.50	9.9	7.3	10.0	2830.	5199.	.54	.18	11.34
21JAN75	900	77	1.13	.27	9.5	4.6	6.5	2441.	1859.	.67	.15	13.83
21JAN75	1000	109	.85	-.29	7.9	13.6	18.2	2276.	1875.	.85	.20	15.12
21JAN75	1100	78	.66	.15	15.9	14.3	23.3	2382.	1983.	.82	.26	21.61
24JAN75	700	38	.84	1.07	2.1	3.1	4.0	2773.	5355.	.61	.06	5.00
24JAN75	900	85	.90	.08	4.2	7.1	9.3	2936.	1850.	.44	.15	14.96
24JAN75	1000	100	.27	-.05	73.6	97.6	130.3	2449.	1875.	.96	.31	22.53
24JAN75	1100	113	.79	-.33	9.1	7.4	10.7	2521.	1983.	.79	.23	15.76
24JAN75	1200	100	.97	-.16	8.7	8.0	14.3	2427.	1853.	.80	.25	10.77
28JAN75	700	36	1.48	2.00	1.8	2.2	3.0	2593.	5118.	.75	.21	6.75
28JAN75	800	29	1.36	2.42	4.3	3.0	3.4	2312.	3794.	.91	.25	8.40
28JAN75	900	27	1.27	2.46	3.8	2.1	2.6	1878.	2524.	.89	.28	10.50
28JAN75	1100	34	.47	.69	8.3	9.7	16.6	1983.	2169.	1.27	.34	19.61
28JAN75	1200	105	.75	-.19	15.0	20.1	33.5	2129.	1835.	1.55	.34	17.15
30JAN75	1200	61	.30	.17	56.9	44.6	105.1	2267.	2034.	.77	.29	21.23
30JAN75	1300	30	.30	.52	26.7	22.9	33.7	2262.	2108.	1.14	.33	22.13
30JAN75	1400	116	.97	-.46	7.0	8.0	12.0	2729.	2197.	1.13	.28	15.24
30JAN75	1500	112	1.49	-.59	6.3	4.2	5.8	3428.	3389.	.71	.19	6.42
30JAN75	1600	96	1.71	-.17	2.1	3.4	4.7	3133.	3513.	.49	.13	4.83
30JAN75	1700	99	1.28	-.19	3.9	2.9	3.7	3080.	3513.	.77	.05	2.89
30JAN75	1800	124	1.07	-.71	2.4	1.9	2.3	1909.	2702.	1.43	.04	2.96
5FEB75	1200	36	1.42	1.93	2.6	2.8	3.7	2215.	1954.	1.17	.26	8.49
5FEB75	1300	50	2.47	2.04	2.7	2.2	2.5	2303.	2108.	1.17	.26	7.39
5FEB75	1400	49	2.19	1.87	2.7	1.8	2.3	2454.	2408.	1.14	.27	8.89
5FEB75	1500	62	3.56	1.86	3.0	1.8	2.2	3518.	3033.	.97	.28	6.08
5FEB75	1600	70	3.40	1.21	1.8	1.8	2.2	3747.	2770.	.85	.27	12.54
5FEB75	1700	70	2.19	.78	3.4	1.9	2.5	3930.	2670.	.34	.16	22.09
5FEB75	1800	64	1.18	.57	3.0	2.7	3.5	2685.	1601.	.26	.09	23.97

DN = Downwind traffic stream (i.e., all lanes)
UP = Upwind traffic stream (i.e., all lanes)

A summary of the computational procedures used in the analysis is shown in Table 25, and the data are summarized in Table 26.

The F ratio for the data is:

$$F = \frac{MS_B}{MS_{Rem}} = 3.19 \quad . \tag{15}$$

For a 5% test, the critical value for the F ratio is $F_{0.95}$ (1,18) = 4.14. This value does not contradict the null hypothesis at the 5% level and suggests that the values from the two groups may have come from the same population.

A "Studentized" range statistic was calculated from the data to determine whether the means of the two data sets (columns) came from the same population. This statistic is defined by

$$q = \frac{\overline{X}_2 - \overline{X}_1}{\sqrt{MS_{rem}/r}} \quad , \tag{16}$$

where $\overline{X}_2$ and $\overline{X}_1$ are the means of the two samples. The q statistic is approximated by the "Studentized" range distribution having parameters r = number of columns and df = degrees of freedom for MS_{rem}. The symbol $q_{0.95}$ (r,df) designates the 95 percentile point on the q distribution and is

$$q(2,18) = \frac{5.51 - 4.94}{\sqrt{0.94/2}} = 0.83 \quad . \tag{17}$$

The critical value for a 5% test is $q_{0.95}$ (2,18) = 2.97. Thus the hypothesis that the means came from the same population would not be rejected.

Student's "t" test is similar to Student's range distribution when only two columns are used; this statistic also tests the

Table 25

SUMMARY OF COMPUTATIONAL PROCEDURE FOR ANALYSIS OF VARIANCE

Equations

$(1) = (\sum_i \sum_j X_{ij})^2/rc \quad (2) = \sum_i \sum_j (X_{ij})^2 \quad (3) = \sum_j (\sum_i X_{ij})^2/r \quad (4) = \sum(\sum X_{ij})^2/c$

where X_{ij} represents the dispersion coefficients of column i on run j.;

$i=1,\ldots,r$ and $j=1,\ldots,c$.

	Sum of Squares (SS)	Degrees of Freedom (df)	Mean Square (MS)	F Ratio
Within group variation	$SS_w = (3) - (1)$	c-1	$\frac{SS_w}{c-1}$	
Between group variation	$SS_B = (4) - (1)$	r-1	$\frac{SS_B}{r-1}$	SS_B/SS_{rem}
Remainder	$SS_{rem} = SS_T - SS_W - SS_B$	(c-1) (r-1)	$\frac{SS_{rem}}{(c-1)(r-1)}$	
Total	$SS_T = (2) - (1)$	rc-1		

Table 26

ANALYSIS OF VARIANCE

(a) Analysis of Variance of up and Downwind Dispersion Coefficients at 40 m

	σ_z(40-dn)	σ_z(40-up)	Σr_i
	2.5	4.0	65
	4.0	3.7	7.7
	9.1	7.4	16.5
	8.7	8.0	16.7
	1.8	2.2	4.0
	4.3	3.0	7.3
	3.8	2.1	5.9
	8.3	9.7	18.0
	26.7	22.9	49.6
	7.0	8.0	15.0
	6.3	4.2	10.5
	2.1	3.4	5.5
	3.9	2.9	6.8
	2.6	2.8	5.4
	2.7	2.2	4.9
	2.7	1.8	4.5
	3.0	1.8	4.8
	1.8	1.8	3.6
	3.4	1.9	5.3
Σc_j	104.7	93.8	198.5
Mean ($\overline{x}$)	5.51	4.94	
Standard deviation (S)	5.65	5.00	
Number of runs (N)	19	19	

(b) Computed Values from Equations in Table 25

(1) = 1037 (3) = 2045
(2) = 2065 (4) = 1040

Source of Variation	SS	df	MS	F(1,18)
SS_W	1008	18	56.0	
SS_B	3	1	3	3.19
SS_{rem}	17	18	0.94	
SS_T	1028	37	27.8	

hypothesis that the two sample means came from the same population. The t score is

$$t = \frac{\bar{X}_2 - \bar{X}_1}{\sigma\sqrt{1/N_1 + 1/N_2}} \quad \text{where} \quad \sigma = \sqrt{\frac{N_1 S_1^2 + M_2 S_2^2}{M_1 + N_2 - 2}} \quad . \tag{18}$$

N_1 and N_2 are the size of the two samples and S_1 and S_2 are the standard deviations of the two samples. The distribution of t is Student's distribution with degrees of freedom df = $N_1 + N_2 - 2$. The calculated statistic is

$$t(36) = \frac{5.51 - 4.94}{5.48\sqrt{2/38}} = 0.45 \quad .$$

The critical value for a 5% test is $t_{0.95}$ (36) = 1.69. Again the hypothesis that the means came from the same population would not be rejected.

Lastly, the rank difference test was used to evaluate the significance of the frequency with which $\sigma_z(40 - dn)$ is greater than $\sigma_z(40 - up)$. Since we are concerned with relative differences (and not absolute) between dispersion coefficients, the rank test considered the normalized difference: $[\sigma_z(40 - dn) - \sigma_z(40 - up)]/\sigma_z(40 - dn)$. Of the 19 cases, 12 showed positive differences, 6 were negative, and 1 was zero (i.e., equal). To test the significance of $\sigma_z(40 - dn)$ being apparently larger:

- Compute the normalized differences
- Rank the differences without regard to sign
- Sign the rank values by the sign of the difference
- Total the rank values for the fewest cases of the same sign.

This sum is 56.5. The 5% limit is then calculated from:

$$\frac{N(N + 1)}{4} - 1.960 \left[\frac{N(N + 1)(2N + 1)}{24}\right]^{1/2} = 40 \tag{19}$$

Thus the apparently larger $\sigma_z(40 - dn)$ values are not significant at the 5% level.

While the statistical tests do not confirm the significance of enhanced dispersion from the downwind lanes, we evaluated the dependence of the absolute value, ratios, and differences in the dispersion coefficients on a variety of independent meteorological and traffic variables. Table 27 summarizes the correlation coefficients (r). Differences in and ratios of the dispersion coefficients correlated "best" with u_{road} alone: r ranges from -0.23 to -0.35. All other parameters correlated even more poorly. The individual dispersion coefficients correlated quite well with the meteorological parameters: r values of 0.84 and 0.90 were associated with the ratio σ_ϕ/u_{road}, where σ_ϕ is the standard deviation of the elevation angle of the ambient wind; the addition of traffic volume in the numerator of the term does not increase the correlation.

C. Carbon Monoxide Emissions

An additional advantage of the use of gas tracers is that it permits the determination of vehicle pollutant emission rates when both the pollutant and trace gas ambient concentrations are measured, in addition to the trace gas emission rate. When two tracers are used (each emitted on only one side of the roadway), then vehicle pollutant emissions can be determined for both traffic streams.

For an inert vehicle pollutant and inert gas tracers, the following relationship between emissions (Q, g m^{-1} s^{-1}) and concentrations (χ, g m^{-3}) hold, provided the pollutant and tracer are released at the same location and measured at common points:

$$\frac{\chi\ (CO - W)}{Q\ (CO - W)} = \frac{\chi\ (SF_6)}{Q\ (SF_6)} \quad , \qquad (20)$$

and

$$\frac{\chi\ (CO - E)}{Q\ (CO - E)} = \frac{\chi\ (F13B1)}{Q\ (F13B1)} \quad . \qquad (21)$$

Table 27

LINEAR CORRELATION COEFFICIENTS

Independent Variables	Dependent Variables*					
	$\frac{\sigma(40\text{-up})-\sigma(dn)}{\sigma(40\text{-up})}$	$\frac{\sigma(60\text{-up})-\sigma(dn)}{\sigma(60\text{-up})}$	$\frac{\sigma(40\text{-up})}{\sigma(dn)}$	$\frac{\sigma(60\text{-up})}{\sigma(dn)}$	$\sigma(40\text{-up})$	$\sigma(dn)$
$\frac{\phi cc(up)-\phi cc(dn)}{T\phi T\ \phi cc}$	0.06	0.15	-0.05	-0.01	--	--
$\frac{V\phi L(up)-V\phi L(dn)}{T\phi T\ V\phi L}$	0.02	0.10	-0.03	0.02	--	--
u_{road}	-0.23	-0.27	-0.23	-0.35	-0.59	-0.57
$\frac{\phi cc(up)-\phi cc(dn)}{u_{road}*T\phi T\ \phi cc}$	0.10	0.20	0.01	0.07	--	--
$\frac{V\phi L(up)-V\phi L(dn)}{u_{road}*T\phi T\ V\phi L}$	0.06	0.14	-0.01	0.07	--	--
$\frac{T\phi T\ V\phi L}{u_{road}}$	0.20	0.26	0.13	0.27	0.77	0.83
σ_{ϕ}	0.07	0.18	-0.03	0.11	--	--
σ_{w}	0.02	0.26	0.07	0.16	--	--
$\frac{\sigma_{\phi}}{u_{road}}$	0.16	0.24	0.06	0.23	0.84	0.90
$\frac{\sigma_{w}}{u_{road}}$	0.21	0.29	0.12	0.28	0.84	0.87
$\frac{TTI}{u_{road}}$	0.24	0.31	0.14	0.29	0.84	0.86
$\frac{\sigma_{\phi}*T\phi T\ V\phi L}{u_{road}}$	0.15	0.24	0.06	0.21	0.84	0.90
$\frac{\sigma_{w}*T\phi T\ V\phi L}{u_{road}}$	0.22	0.30	0.13	0.29	0.84	0.88
$\frac{TTI*T\phi T\ V\phi L}{u_{road}}$	0.26	0.31	0.15	0.29	0.84	0.86

*"up and "dn" refer to upwind and downwind traffic stream, respectively, while "40" and "60" refer to distance, in metres, from the center of the respective traffic streams

The letters E and W refer to the eastbound and westbound traffic lanes, respectively. Background concentrations of all gases are assumed to have been subtracted. Of the eight parameters in Eqs. (20) and (21), only the four terms on the right-hand side are known. Furthermore, for those sampler locations downwind of the roadway:

$$\chi\ (CO) = \chi\ (CO - E) + \chi\ (CO - W) \quad . \tag{22}$$

As a model assumption we represent the <u>relative</u> speed dependence of emissions in the two traffic streams by the following:

$$\frac{Q\ (CO - E)}{Q\ (CO - W)} = \frac{V\ (E)}{V\ (W)} \left[\frac{S\ (W)}{S\ (E)}\right]^{\beta} \tag{23}$$

where V denotes traffic volume, and S traffic speed in each direction. The exponent β was taken equal to 0.946 as used by District 04 of the California Department of Transportation (Morse, 1974). Note that the only use of Eq. (23) is to allocate the total computed CO emissions to the east and westbound directions. Combining Eqs. (20)-(23), the following equation is derived:

$$Q\ (CO - E) = \chi\ (CO) \Bigg/ \left\{\frac{\chi\ (F13B1)}{Q\ (F13B1)} + \frac{\chi\ (SF_6) V\ (W)}{Q\ (SF_6) V\ (E)} \left[\frac{S\ (E)}{S\ (W)}\right]^{\beta}\right\} , \tag{24}$$

$$Q\ (CO - W) = Q\ (CO - E)\ \frac{V\ (W)}{V\ (E)} \left[\frac{S\ (E)}{S\ (W)}\right]^{\beta} \quad .$$

CO emission rates were computed in the above manner using the experimental data, with the following exceptions:

- January 17--malfunction of the CO analyzer
- Those hours with average wind directions within 20° of the roadway orientation
- Those hours where the average 2- and 3.8-m wind speed was less than 1 m s^{-1}.

For comparison, directional CO emissions were also computed using the cruise-mode data given for California autos in EPA Report APTD-1497 (1975); these data are tabulated below:

Speed (mph)	CO Emissions Rate (gm/veh-mi)
15	69.1
30	29.5
45	24.6
60	25.5

Linear interpolation was used between these values. Also, the data were updated (from a 1971 vehicle mix to a 1974-75 mix) using CALTRANS factors and assuming a 5% heavy-duty mix; the final factor thus applied was 0.726.

Figure 40 is a comparison of the CO emissions computed by the two methods. Note that each point on the figure represents an average of all the downwind samples obtained for each hour. For the eastbound direction, the average ratio of all "tracer" CO emission computations to those predicted by the emissions model is 1.00; in the westbound direction the ratio is 1.03. However, there is considerable variance in the individual comparisons. An average normalized difference between the two methods was defined by:

$$\text{Av. diff.} \equiv \frac{1}{N}\sum\frac{|X_1 - X_2|}{X_1} \tag{25}$$

where X_1 is the tracer-derived value and X_2 is from the emission model. For the eastbound data, the average difference is 0.35 and the average westbound difference is 0.36. Standard linear correlations were also computed for each data set: the correlation coefficient for the eastbound data was 0.81, while the westbound value was 0.36.

The results given here suggest that the emission model tested provided a good estimate of actual CO emissions as determined by the

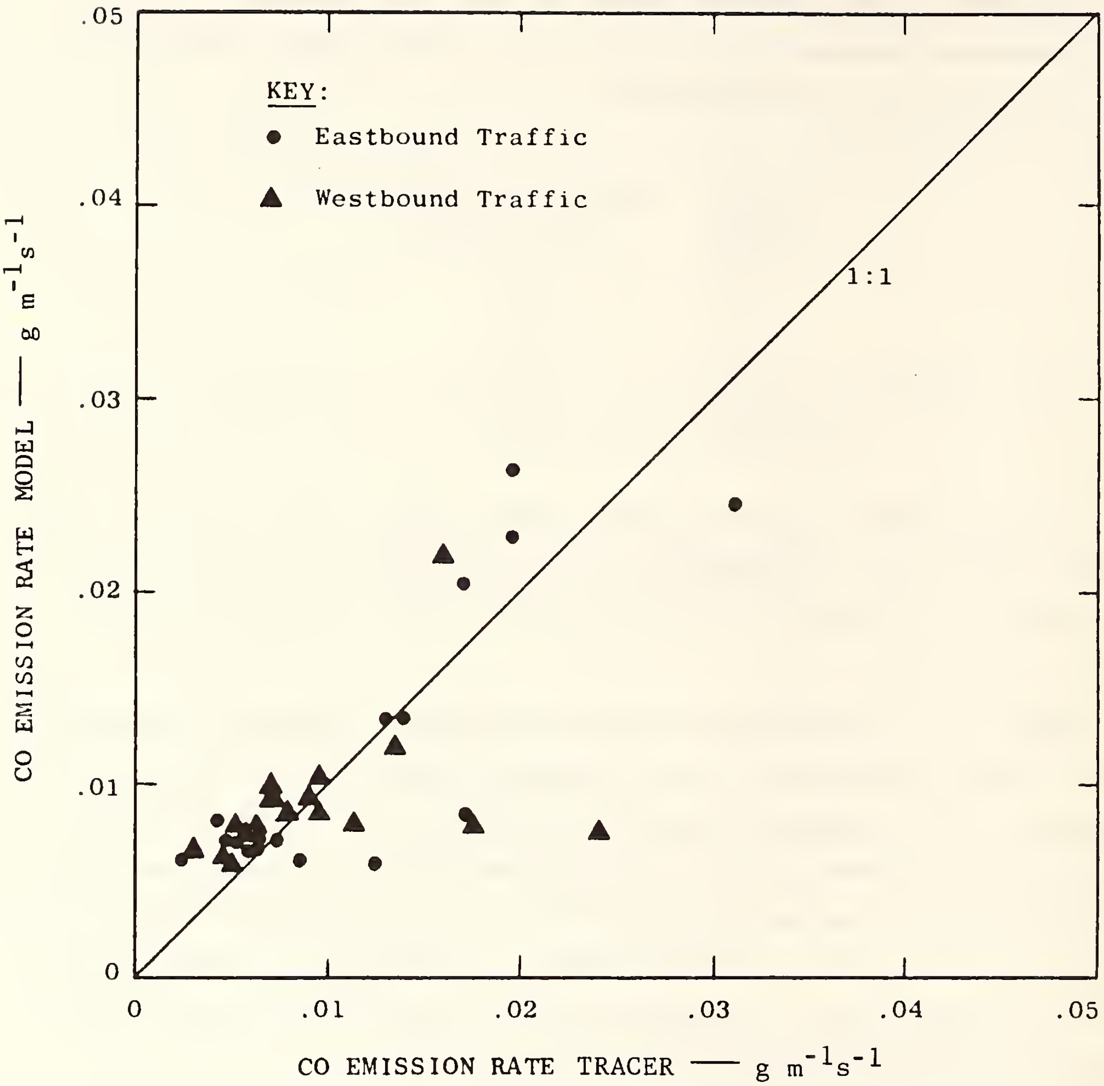

FIGURE 40 COMPARISON OF MODEL PREDICTION OF CO EMISSION RATE WITH COMPUTATION BASED ON TRACER AND AMBIENT CO MEASUREMENTS

tracer method. Differences between the two may be explainable in part by a temperature dependence of emissions not considered here (see EPA, 1975, AP-42, Supplement No. 5).

D. Summary of Observations

Analysis of the data has produced important results in the areas of near-roadway ambient temperature field and turbulence characteristics, tracer gas dispersion, and vehicular CO emission rates.

Temperatures measured about 10.5 m from either edge of the roadway showed significant cross-roadway gradients (ΔT). At the 2-m level, south-to-north gradients* ranged up to 2.5°C for southerly winds and up to -1.5°C for northerly winds. At 3.8 m, ΔT ranged from +1.5 to -0.75°C for northerly and southerly winds, respectively, while at 7.5 m the range was from +0.75 to -0.4°C. To better understand the cause and significance of the temperature gradient data they were first stratified into six 15° (arc) categories according to the absolute value of the angle between the wind vector and the roadway. Then the ΔT data were correlated within each of the six categories with each of six independent variables:

(1) Upwind turbulence intensity

(2) Cross-roadway wind speed

(3) The product of (1) and (2)

(4) Vehicle volume

(5) The produce of vehicle volume and speed

(6) The quotient of (5) and (3).

The only consistently significant linear correlation coefficient ($\bar{r} = 0.71$) was found between ΔT and the cross-roadway wind speed (u_{road}). Examination of a scatter plot of ΔT versus u_{road} shows that at low wind speeds ΔT is nearly zero, and that ΔT increases with increasing u_{road}-values.

Values of the three-component or total intensity of turbulence (TTI) were compared at several heights among near-upwind, median, and near-downwind sensor locations. The south-to-north turbulence graident between sensors 10.5 m to either edge of the roadway ranged from +0.50 to -0.50 s^{-1} at the 2, 3.8, and 7.5-m levels with southerly and northerly winds, respectively; at 14.2 m the range was ±0.35 m s^{-1}. When ΔTTI was normalized by dividing by the upwind turbulence intensity at corresponding heights, the range of maximum normalized values showed a similar height dependence: ±1.5 at 2 m, +2.0 to -1.0 at 3.8 m, +1.5 to -1.0 at 7.5 m, and ±0.75 at 14.2 m. Similar comparisons were also made among the upwind

---

*ΔT = T(north) - T(south).

(near-roadway) values and the turbulence data measured in the roadway median. The median-upwind gradient ranged up to $-1.10\ m\ s^{-1}$ at 2 m >, up to $-1.20\ m\ s^{-1}$ at 3.8 m, and up to $-0.60\ m\ s^{-1}$ at 7.5 m. Normalized gradients range up to -3.5 at both the 2 and 3.8-m levels, and up to -2.0 at 7.5 m.

Again, the data were grouped into six wind direction categories and correlations made with various independent traffic and meteorological variables; 13 independent variables were defined using the following basic parameters:

(1) Upwind turbulence intensity

(2) Upwind wind speed

(3) Cross-roadway wind speed component

(4) Cross-roadway temperature gradient

(5) Vehicle volume

(6) Vehicle speed

(7) The computed vehicle drag-induced ambient flow.

The south-north turbulence gradient correlated consistently over the six wind direction categories with only one parameter, the south-north temperature gradient. Even so, the average correlation coefficient of 0.55 (and 0.40 for normalized ΔTTI) is not particularly notable. The average correlation for winds > 45° to the road increased to 0.68 for the normalized turbulence gradient and remained at 0.55 for the unnormalized gradient. Interestingly, the upwind-median gradient of turbulence also correlated consistently well with only one independent variable, the upwind wind speed (u_{ref}). Surprisingly, the cross-roadway component correlated less well. The average correlation coefficient for ΔTTI and u_{ref} was 0.47 for all categories and only 0.32 for wind ≥ 45° to the road. The normalized ΔTTI correlated with u_{ref} at 0.56 for all directions and at 0.51 for the more oblique directions.

The validity of using the three-component intensity of turbulence to investigate possible roadway influences was also tested. For example, it might be argued that the gradient of the cross-roadway component of turbulence might be a better indicator; yet the use of a single component also has limitations. Therefore, the total turbulence intensity was correlated with both the cross-road and along-road turbulence components at two locations: the 2-m levels on the south (near-roadway) and median towers. The correlation with the cross-road and along-road components on the south tower was 0.93 and 0.96, respectively; in the median, correlations of 0.80 and 0.76 were noted. This test implies that the total turbulence intensity is an excellent indicator of horizontal component fluctuations for the near-roadway sensors, and a good indicator for the median sensors. However, future, deeper studies of these data might profit from a systematic analysis of all components.

Concentration data from the two tracer gases were used together with ambient wind data to compute dispersion coefficients at each of the ground-level sampler locations downwind of the roadway. For each run, the functional distance-dependence of the dispersion coefficient was computed separately for gas released on both the upwind and downwind sides of the road; cases with wind speeds of less than 1 m s^{-1} or wind-roadway angles of less than 20° were excluded. Then, dispersion coefficient magnitudes were compared for each of the 19 cases at a common distance (40 m) downwind of the two traffic lanes where (i.e., 40 m downwind of the upwind release lane and 40 m downwind of the downwind release lane) tracer gas was released. The coefficient averages were 5.5 and 4.9 m for the downwind and upwind lanes, respectively. The average of the difference in coefficients normalized by the downwind coefficient was 7%. The coefficient of variation for the upwind-lane data was 101%; for the downwind data, 103%. Four standard statistical tests were made to evaluate the significance of the downwind coefficients being larger than the upwind. In no case could the null hypothesis be rejected even at the 5% limit. Thus, statistically, we cannot disprove that the upwind and downwind data samples come from the same population.

The trace gas data were also used with the traffic and ambient CO data to compute the in-situ vehicular emission rate for both traffic directions; comparisons were made with a cruise mode emission model. For the eastbound direction, the average ratio of "tracer-computer" CO emissions to model predictions was 1.00; in the westbound direction the ratio was 1.03. The average normalized absolute difference between the two emission values was 35% eastbound and 36% westbound. The correlation coefficient for the eastbound values was 0.81, with 0.36 for the westbound.

E. Implications and Discussion

The near-roadway vertical temperature data are important for two reasons: first, they indicate the thermal stability of the air near the roadway and thus describe the diffusion characteristics of the air into which vehicular pollutants are emitted; second, they serve as a tracer of vehicle pollutant emissions. Before the full utility of the temperature data can be assessed, it is first necessary to understand the causes of the observed cross-roadway temperature gradients. Three processes are potential contributors: vehicle waste heat emissions, differences in the atmospheric sensible heat flux between the clay soil of upwind fetches and the concrete and asphalt surfaces of the eastbound and westbound lanes, respectively, and vertical mixing induced by air flow over the traffic stream and the subsequent transport of heat to (inversion conditions) or away (lapse conditions) from the ground.

To aid this analysis, the vertical temperature profile data discussed earlier were examined in more detail. First, the 15-min vertical wind profiles for the near-roadway upwind tower were analyzed to obtain eddy diffusivity values (K, cm^2, s^{-1}). Because of the relatively few anemometers and the possible influence of traffic and other surface discontinuities, the eddy diffusivity for momentum (K_m) was estimated from the value of the friction velocity (u^*, cm s^{-1}) obtained from the logarithmic wind profile equation, where

$$u^* = k\, z\, \frac{\Delta u}{\Delta z} \quad , \tag{26}$$

and

$$K_m = k\, u^*\, z \quad . \tag{27}$$

Here, k is the Karman constant (0.428), u is wind speed, and z height. Next the atmospheric sensible heat flux density (H, cal cm^{-2} s^{-1}) upwind of the roadway was computed from:

$$H = -\rho \ c_p \ K_h \left(\frac{\Delta T}{\Delta z} + \Gamma\right) \quad , \tag{28}$$

where ρ is density (g cm^{-3}), c_p the specific heat at constant pressure (0.24 cal g^{-1} $°C^{-1}$), and Γ the dry adiabatic lapse rate (9.8°C km^{-1}). The eddy diffusivity for heat (K_h) has been assumed to equal that for momentum. Table 28 summarizes K and H values for each 15-min period; K is given as the value at 3-m height.

The importance of the effect of vertical mixing over and downwind of the roadway on the cross-road temperature gradient is clarified by examination of the ambient heat flux data. Earlier it was noted that ΔT values were consistently greater with southerly winds. Referring to Table 28, 72% of the south-wind cases occur under stable atmospheric conditions. Thus, on the downwind side, the effect of enhanced vertical mixing over the roadway is to increase near-surface temperatures and, as a result, increase the cross-road temperature gradient. With northerly winds, lapse conditions dominate (84%) thereby decreasing near-surface temperatures downwind of the road and also decreasing ΔT values.

To summarize, the effect of vehicle-induced vertical mixing is to increase the magnitude of the cross-road temperature difference under stable conditions and to decrease the difference under lapse conditions. But this effect only moderates the magnitude of ΔT. The source of heat, however, must be either the vehicles or the roadway pavement. If the latter effect dominated, then we would expect to incur warmer temperatures downwind part of the day and cooler temperatures at other times (provided the daily average surface temperature is the same for pavement and soil--a reasonable assumption). This type of a diurnal pattern is not observed. To understand the significance of vehicle waste heat emissions, the heat flux density averaged over the roadway/median area was computed and evaluated against ambient fluxes.

Table 28

SUMMARY OF COMPUTED HEAT FLUX AND DIFFUSIVITY VALUES

					-----AMBIENT-----		----------ROADWAY----------			NET
DATE	TIME (PST)	AVE WD (DEG)	UROAD (M/S)	VROAD (M/S)	K (M*M/S)	H (LY/MIN)	K (M*M/S)	H (LY/MIN)	DT/DZ (DEG/M)	DT/DZ (DEG/M)
17 JAN 75	1330	310.	-.80	-2.26	.258	.054	2.274	.223	-.0470	-.0584
17 JAN 75	1345	319.	-1.10	-2.07	.258	.051	2.394	.235	-.0474	-.0576
17 JAN 75	1400	323.	-1.70	-2.63	.236	.044	2.398	.234	-.0475	-.0565
17 JAN 75	1415	317.	-1.62	-3.22	.271	.050	2.398	.234	-.0469	-.0569
17 JAN 75	1430	311.	-1.06	-2.85	.294	.046	2.657	.259	-.0469	-.0553
17 JAN 75	1445	309.	-.99	-2.97	.384	.072	2.746	.268	-.0458	-.0581
17 JAN 75	1500	312.	-1.20	-3.01	.321	.053	3.222	.311	-.0469	-.0549
17 JAN 75	1515	315.	-1.12	-2.52	.271	.031	3.487	.337	-.0479	-.0523
17 JAN 75	1530	305.	-.59	-2.29	.339	.023	3.865	.350	-.0445	-.0475
17 JAN 75	1545	318.	-1.03	-1.98	.265	.012	3.044	.270	-.0437	-.0456
17 JAN 75	1600	345.	-.94	-.66	.178	.004	2.911	.259	-.0448	-.0454
17 JAN 75	1615	17.	-2.22	-.16	.134	.010	2.978	.265	-.0456	-.0473
17 JAN 75	1630	347.	-2.52	-1.69	.249	.017	3.093	.273	-.0437	-.0465
17 JAN 75	1645	343.	-2.33	-1.82	.381	.010	3.235	.285	-.0421	-.0436
17 JAN 75	1700	332.	-1.86	-2.07	.443	-.016	3.291	.291	-.0416	-.0393
17 JAN 75	1715	320.	-1.38	-2.47	.453	-.037	3.159	.280	-.0414	-.0359
17 JAN 75	1730	325.	-1.72	-2.47	.561	-.078	3.000	.264	-.0396	-.0279
17 JAN 75	1745	350.	-1.38	-.80	.393	-.069	3.224	.281	-.0415	-.0314
21 JAN 75	515	163.	.97	.74	.226	-.213	.306	.030	-.0302	.1842
21 JAN 75	545	130.	.42	1.16	.300	-.179	.883	.087	-.0395	.0412
21 JAN 75	600	119.	.16	1.01	.262	-.135	1.415	.139	-.0444	-.0013
21 JAN 75	615	129.	.30	.92	.204	-.146	2.463	.234	-.0468	-.0175
21 JAN 75	730	173.	1.08	.55	.152	-.074	3.819	.337	-.0453	-.0354
21 JAN 75	1215	305.	-.74	-2.89	.326	.075	1.780	.175	-.0443	-.0632
21 JAN 75	1245	305.	-.81	-3.05	.335	.076	1.919	.188	-.0446	-.0627
24 JAN 75	530	99.	-.34	1.71	.544	-.185	.646	.063	-.0284	.0545
24 JAN 75	545	93.	-.42	1.30	.480	-.205	.893	.088	-.0344	.0452
24 JAN 75	615	136.	.61	1.28	.381	-.063	2.324	.220	-.0435	-.0310
24 JAN 75	630	154.	.90	.94	.320	-.131	3.219	.287	-.0433	-.0236
24 JAN 75	645	166.	1.05	.73	.297	-.150	3.467	.313	-.0445	-.0232
24 JAN 75	700	150.	.92	1.10	.275	-.099	3.591	.316	-.0437	-.0300
24 JAN 75	715	151.	.77	.90	.299	-.095	3.565	.310	-.0428	-.0296
24 JAN 75	730	149.	.71	.89	.374	-.109	3.998	.351	-.0429	-.0296
24 JAN 75	745	144.	.55	.86	.395	-.179	3.898	.346	-.0431	-.0208
24 JAN 75	1130	9.	-1.35	-.27	.092	.012	2.093	.206	-.0503	-.0533
24 JAN 75	1145	341.	-1.53	-1.28	.144	.021	2.059	.203	-.0493	-.0544
24 JAN 75	1200	320.	-.92	-1.61	.173	.030	2.081	.205	-.0486	-.0556
24 JAN 75	1215	330.	-1.13	-1.39	.146	.029	1.950	.192	-.0488	-.0564
24 JAN 75	1230	335.	-.99	-1.02	.132	.020	1.993	.196	-.0493	-.0544
24 JAN 75	1245	5.	-1.49	-.42	.123	.020	1.902	.186	-.0492	-.0546
28 JAN 75	515	128.	.77	2.41	.415	-.220	.380	.037	-.0250	.1228
28 JAN 75	530	137.	1.38	2.73	.333	-.071	.672	.066	-.0350	.0029
28 JAN 75	545	139.	1.19	2.24	.365	-.054	.996	.098	-.0385	-.0173
28 JAN 75	600	138.	1.19	2.34	.415	-.061	1.404	.137	-.0404	-.0224
28 JAN 75	615	129.	.77	2.37	.331	-.056	2.539	.240	-.0447	-.0342
28 JAN 75	630	137.	1.16	2.33	.475	-.073	3.420	.313	-.0430	-.0329
28 JAN 75	645	139.	1.25	2.30	.425	-.049	3.420	.313	-.0435	-.0368
28 JAN 75	700	146.	1.59	2.27	.376	-.039	3.550	.306	-.0417	-.0363
28 JAN 75	715	152.	1.83	2.07	.363	-.027	3.394	.297	-.0422	-.0383
28 JAN 75	730	153.	1.58	1.75	.263	-.020	3.550	.311	-.0435	-.0408
28 JAN 75	745	155.	1.77	1.77	.249	-.013	3.785	.332	-.0440	-.0423
28 JAN 75	800	151.	1.73	2.04	.356	-.013	3.326	.307	-.0445	-.0427
28 JAN 75	815	155.	1.81	1.86	.342	-.001	3.022	.293	-.0465	-.0464
28 JAN 75	830	156.	1.62	1.60	.282	.010	2.643	.256	-.0467	-.0485
28 JAN 75	845	150.	1.44	1.74	.311	.010	2.317	.226	-.0459	-.0478
28 JAN 75	900	164.	1.71	1.25	.168	.011	2.317	.226	-.0485	-.0509
28 JAN 75	915	148.	1.20	1.59	.235	.029	2.046	.201	-.0472	-.0539
28 JAN 75	930	142.	1.18	1.90	.340	.057	1.917	.188	-.0444	-.0578
28 JAN 75	945	145.	1.10	1.61	.229	.033	1.872	.183	-.0464	-.0547
28 JAN 75	1000	131.	.46	1.24	.419	.098	1.906	.186	-.0427	-.0653
28 JAN 75	1015	132.	.39	.97	.371	.085	1.798	.178	-.0439	-.0648
30 JAN 75	1415	346.	-.82	-.57	.135	.028	2.267	.219	-.0487	-.0549
30 JAN 75	1430	348.	-1.53	-.96	.185	.060	2.267	.219	-.0477	-.0609
30 JAN 75	1445	334.	-1.28	-1.35	.198	.047	2.413	.233	-.0478	-.0574
30 JAN 75	1500	341.	-1.50	-1.23	.187	.046	2.909	.281	-.0485	-.0564
30 JAN 75	1515	341.	-1.59	-1.33	.196	.065	3.328	.318	-.0483	-.0582
30 JAN 75	1530	341.	-1.80	-1.49	.207	.059	3.493	.309	-.0447	-.0532
30 JAN 75	1545	346.	-1.96	-1.34	.220	.083	2.894	.256	-.0438	-.0580
30 JAN 75	1600	0.	-2.11	-.79	.140	.045	2.920	.257	-.0449	-.0527
30 JAN 75	1615	9.	-1.97	-.41	.135	.042	2.915	.257	-.0450	-.0523
30 JAN 75	1630	360.	-1.87	-.72	.172	.076	3.259	.289	-.0450	-.0568
30 JAN 75	1645	354.	-1.51	-.74	.321	.175	3.213	.285	-.0431	-.0695
30 JAN 75	1700	2.	-1.26	-.42	.388	.125	3.354	.299	-.0426	-.0604
30 JAN 75	1715	350.	-1.77	-1.02	.480	.018	3.104	.275	-.0410	-.0437
30 JAN 75	1730	353.	-1.70	-.91	.479	-.009	2.889	.256	-.0406	-.0391

Waste heat emissions from automobiles have been estimated on the basis of the fuel consumption rate for steady driving--see Figure 41 (Cope, 1973). Motor gasoline has an energy equivalent of about 3.13 $\times 10^7$ cal gal^{-1} (Bureau of Mines, 1975), and we assume that 85% of the energy is released as sensible heat. Furthermore, the fuel consumption in a 1974/75 vehicle mix is taken to be 1.046 the 1970-71 value. Thus, for cruise speeds below 40 mph, the per vehicle waste heat emission rate is 1.33×10^6 cal mi^{-1}; above that speed the heat emission increases at a rate of 1.41×10^4 cal mi^{-1} mph^{-1}. The resultant heat flux density is then given as the product of the speed-dependent emission rate and vehicle volume divided by the roadway width (36.6 m including median).

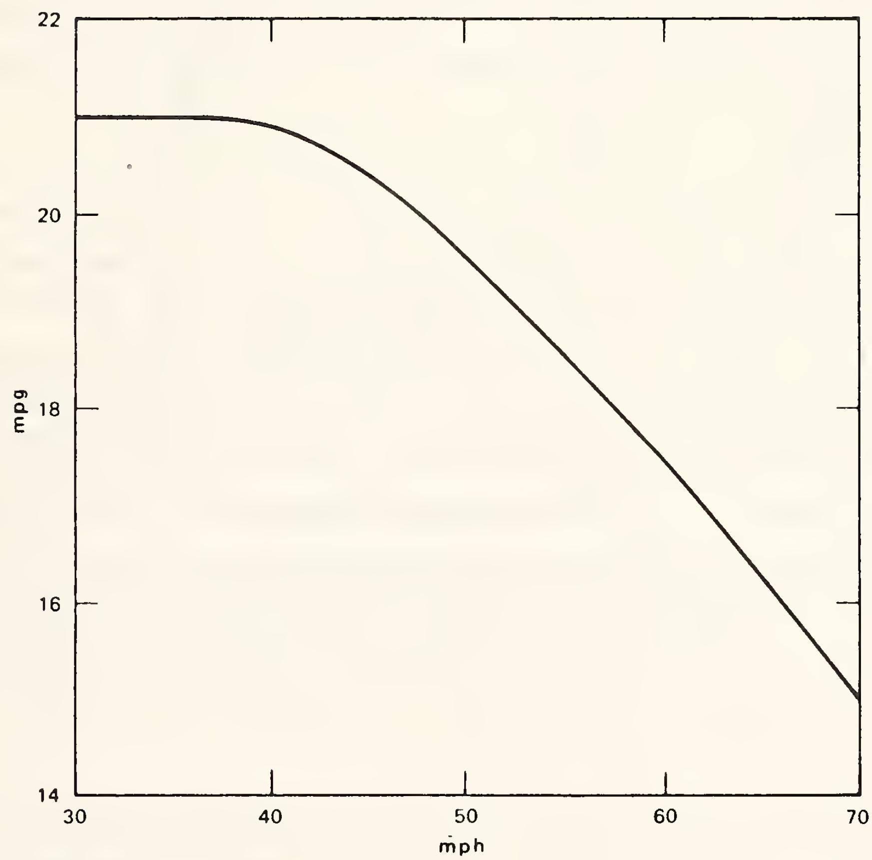

SOURCE: Cope, 1973

SA-2761-56

FIGURE 41 AVERAGE EFFECT OF SPEED ON AUTOMOBILE FUEL CONSUMPTION — 1970/71 MODELS

Table 24 in Section III lists these heat flux-density data (1 ly min^{-1} $\equiv$ 1 cal cm^{-1} min^{-1}). The vehicle heat emission rate is generally in the range of 0.2 to 0.3 ly min^{-1} with a peak value of 0.35 ly min^{-1}; for comparison, the peak solar flux density is 0.79 ly min^{-1}, while the ambient sensible fluxes are generally a factor of 5 less than the vehicle fluxes.

To better understand the implications of these data, the magnitude of the temperature lapse rates that result from the vehicle heat emissions alone were estimated using Eq. (28). The eddy diffusivity above and close to the roadway surface was assumed to result primarily from the effect of vehicle motions. Considering K as the product of a turbulent velocity (v^*) and a characteristic length scale (ℓ), we let v^* equal the vehicle speed and ℓ equal the square root of the vehicle frontal area ($\ell \approx 2$ m). Temperature lapse rates estimated this way are summarized in Table 28, and are generally in excess of the autoconvective lapse rate. It is unrealistic to exclude the advection of sensible heat from the regions upwind of the roadway. To estimate the combined effects of ambient and vehicular heat fluxes and diffusivities, we have taken the arithmetic sum of each and estimated a "net" vertical temperature gradient from Eq. (28); see Table 28. The combined effect is to further enhance instability by day; even for most periods of stable ambient conditions (except when traffic volumes are very low), the vehicle heat emission is sufficient to create an unstable state over the roadway.

These findings are confirmed by the observational data given in Figure 42, where cumulative frequency distributions of the vertical temperature differences (2 - 3.8 m, 3.8 - 7.5 m, and 7.5 - 14.2 m) are given for both the upwind and downwind sides of the road. The decrease in stability downwind of the roadway is apparent at all levels, although it is most pronounced near the surface.

The effect of waste heat in vertically dispersing exhaust emissions can often be visualized during cold weather when low atmospheric temperatures condense the water vapor in the exhaust. Figure 43 is an example of the rise of the exhaust plume as photographed on an overcast day (near-neutral stability), very low wind speeds, and a temperature

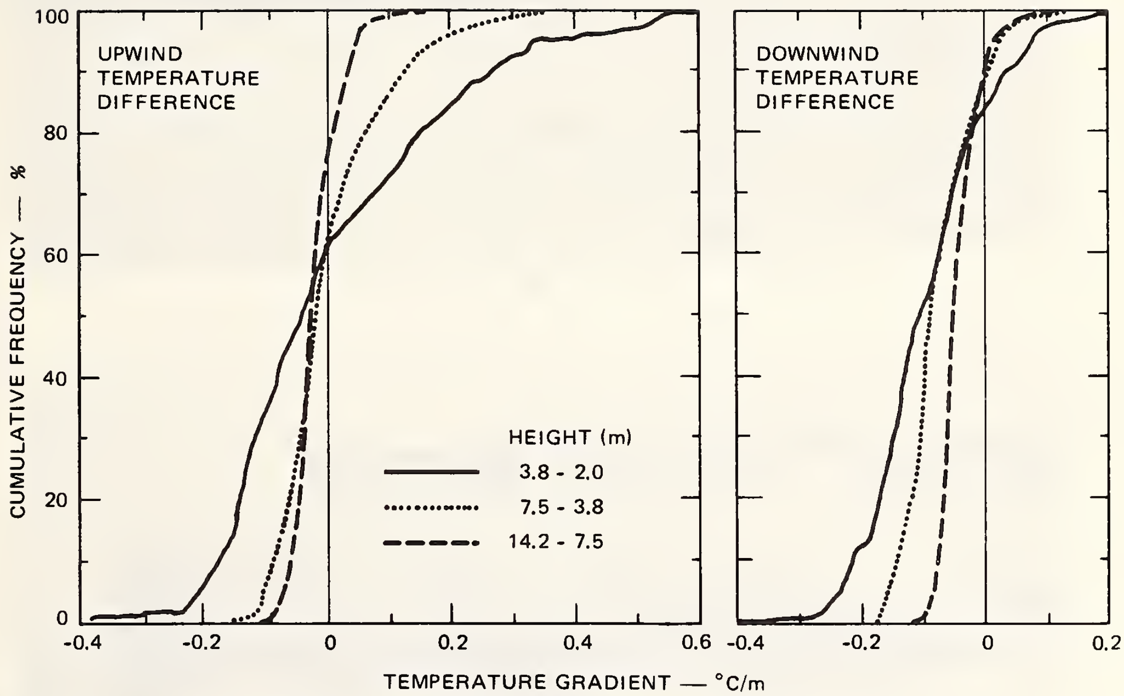

FIGURE 42 CUMULATIVE FREQUENCY DISTRIBUTIONS OF VERTICAL TEMPERATURE GRADIENTS

(a)

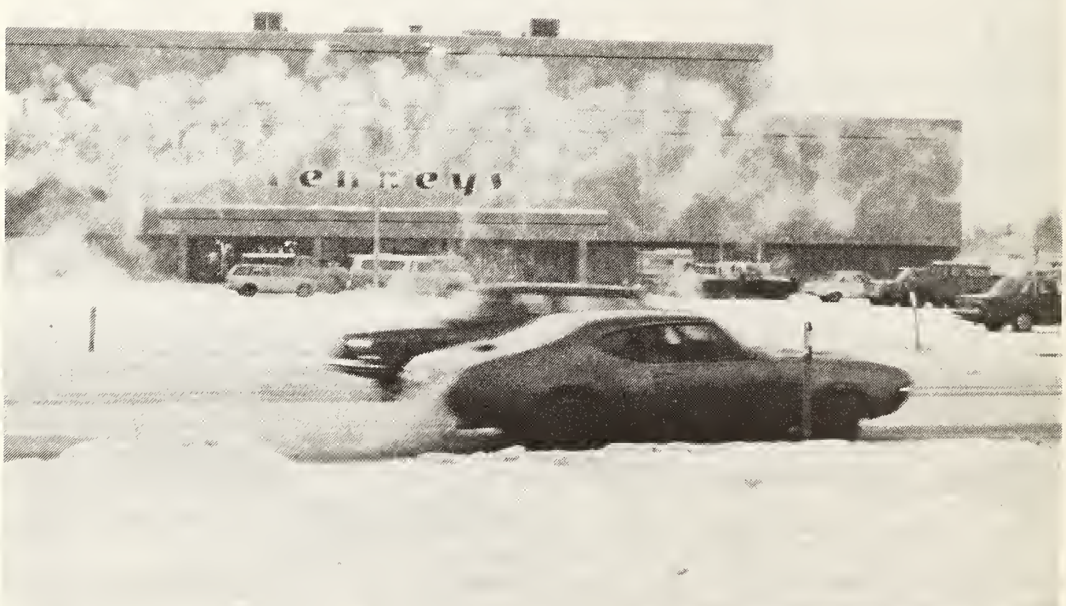

(b)

FIGURE 43 EXAMPLES OF VERTICAL DISPERSION OF VEHICLE EXHAUST PLUME DUE TO WASTE HEAT EMISSION

Stability: Near Neutral; Winds: Very Light; Temperature: -23° C around -23°C (-10°F). In Figure 43(b), the elevated plume can be seen from a vehicle that just passed out of the photo to the left; in Figure 43(a), the rise of an idling vehicle is depicted.

The wind and turbulence data are not as easy to interpret as either the temperature or tracer gas data. While measurements of the latter reflect the integral effect of a passive additive released at a specific location, the wind and turbulence data are more influenced by local effects and therefore may not provide a true picture of the general flow regime.

Nonetheless, certain observations stand out:

- Turbulence levels in the median and downwind of the roadway are consistently higher (by a factor up to 3.5) than the upwind ambient values.
- Cross-roadway turbulence differences showed no correlation with either traffic or <u>ambient</u> meteorological factors.
- The difference in turbulence levels between upwind and median locations is <u>not</u> correlated with either vehicle speed, volume, or occupancy and is only fairly well correlated with wind speed.
- While the cross-roadway turbulence difference gradually decreases with height, the upwind-median difference is similar at 2 and 3.8 m and then falls off sharply at 7.5 m.

While turbulence levels are greatly increased by the roadway, they are not correlated with traffic parameters. This suggests that either the turbulence generation mechanism is insensitive to traffic volume and speed variations over the ranges observed or that other effects need to be considered; in fact, both concepts may be true.

Further examination of the tracer dispersion data supports the traffic-insensitivity concept. As noted before, <u>differences</u> in the dispersion from the up- and downwind lanes did not correlate to any notable degree with any of the traffic or meteorological parameters tested. Yet the individual dispersion coefficients from both traffic streams correlated very well with meteorological parameters <u>alone</u>:

	Correlation σ (upwind)	Coefficients σ (downwind)
σ_w/u_{road}	0.84	0.87
σ_ϕ/u_{road}	0.84	0.90
Volume	-0.43	-0.42
Occupancy	-0.43	-0.40
Vol $\times$ σ_ϕ/u_{road}	0.84	0.90
σ_ϕ/vol $\times$ u_{road}	0.52	0.48

But again, the individual dispersion coefficients did not correlate well with traffic parameters alone and the correlation with the meteorological parameters was not improved. Furthermore, the dispersion values correlated negatively with vehicle volume and occupancy alone.

Considering the dispersion of the exhaust gases of a single isolated vehicle: the tailpipe emissions are first entrained and rigorously mixed within the wake behind the vehicle. At the same time the aerodynamic drag of the vehicle imparts a mean flow in the direction of the vehicle movement. Thus, it can be hypothesized that the effect of the vehicle motion is primarily to disperse the emissions in a plane oriented vertically and parallel to the roadway. But, since the roadway is in effect an infinite line source, the transport and diffusion parallel to the road have no effect on pollutant concentrations normal to the roadway. [Some lateral mixing occurs because of the streamline divergence of the flow about the obstacle, i.e., vehicle. The extent of this region has been estimated to be of the order of one obstacle width for fully turbulent flow (e.g., Dabberdt, 1968). The net effect for a multilane roadway, however, would be minimal.] The vehicle-induced vertical mixing does affect the concentration.

The remaining question is thus whether the presence of multiple vehicles in longitudinal proximity increases the vertical extent or intensity of the vertical dispersion. Based on the turbulence and tracer-dispersion observations from the atmospheric tests, the implication is that there is no such amplification that depends on either vehicle spacing (i.e., volume) or speed*. This in turn suggests that while the turbulence generated by a second car may further mix the pollutants emitted by the first car, the wake of the first car may already be thoroughly mixed such that the further mixing has no effect on the concentration; the turbulence in the wake of the first car is normally sufficiently damped so that there is no dynamic interaction with the wake of the following car that could lead to an increase in the depth of the mixed zone. However, the mean depth of the mixed zone is a function of vehicle density and speed insofar as these factors affect the thermal instability over the roadway (as discussed earlier).

The lateral (i.e., cross-roadway) dispersion is apparently not enhanced by increasing vehicle density or speed. However, apart from the dynamic effects of vehicle motion, it may be necessary to consider the static effect that a "wall" of vehicles imparts on the cross-roadway wind and turbulence structure and subsequently on the cross-roadway pollutant dispersion. Heretofore this "shelterbelt" effect has not been considered in understanding near-roadway dispersion. The literature on shelterbelt effects is primarily devoted to studies of simple, static shelters: normally one or two rows of either a solid or porous obstruction. Before this study, moving shelters had not been considered.

Plate (1971) has summarized the results of a number of shelterbelt studies that have dealt with effects on flow in the lee of the obstruction, streamline separation, drag, and turbulence. Plate describes in

---

*The possible effects caused by variations in traffic density are more systematically analyzed in Chapter IV using wind tunnel data. No significant effect is apparent. However, it appears that there is some enhancement of the vertical dispersion with roadway-parallel winds when the traffic density is decreased; see the discussion beginning on page 157 for more details.

Effects of traffic speed are also examined in Chapter IV using wind tunnel measurements; see the discussion beginning on page 170. Higher-speed (50 mph) traffic apparently reduces ambient concentrations by an overall average of about 7% compared with lower-speed (12.5 mph) traffic. The reduction is greater at the more distant sampling locations, while no systematic difference could be found over the roadway.

some detail the complexities in the flow field about a simple wedge-shaped obstruction oriented normal to the ambient flow (Figure 44). Seven different flow regimes are identified:

- The undisturbed surface layer profile upwind of the obstruction.
- A layer displaced by streamline separation at the wedge.
- A low-velocity zone far downwind.
- An upper transition layer.
- An inner transition layer.
- A recirculation region in the immediate lee of the obstruction.
- An outer, potential flow regime.

Recirculation in Zone 6 occurs only if the obstruction is solid--not the case for traffic on a roadway. Several studies (e.g., Nägeli, 1941) have been made of the effects of shelterbelt porosity on wind speed reduction downwind (both the magnitude of the reduction and its extent); Figure 45 illustrates the sheltering at different porosities. The maximum velocity

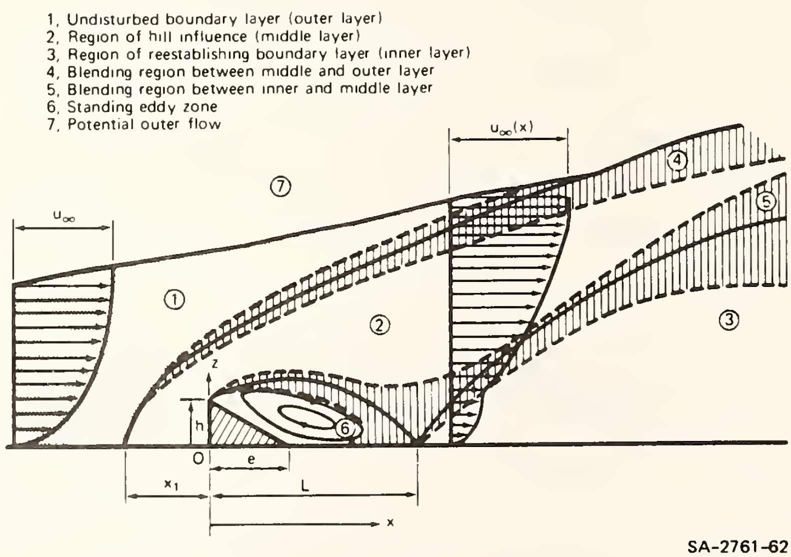

FIGURE 44 THE FLOW ZONES OF A BOUNDARY LAYER DISTURBED BY A SHELTERBELT

(From Plate and Lin, 1965)

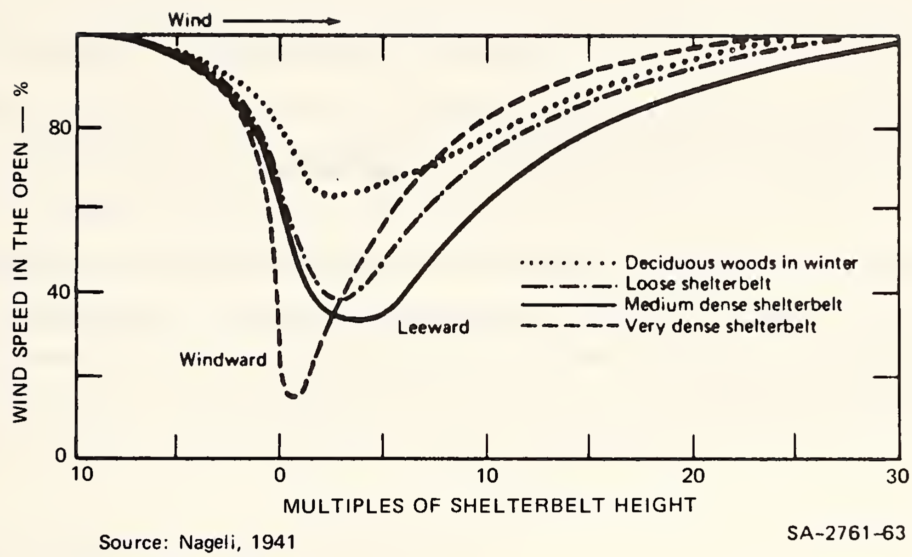

FIGURE 45 SHELTERING AT DIFFERENT POROSITIES

reduction at a single point occurs with a near-solid obstruction, while the maximum sheltering (i.e., spatial integral of velocity deficit) has been observed with porosities of 30% to 50%.

The resulting shear in the mean vertical gradients of velocity enhance the turbulent wind fluctuations and the net transfer of momentum and mass. Plate reports that the intensity of turbulence in the "blending" region (Zones 4 and 5) increases at a rate proportional to $(u_\infty^2 - u_b^2)(u_\infty - u_b)$, where u_∞ is the ambient cross-shelter wind speed and u_b is wind speed through a porous shelter. Referring to Figure 45 we see that the following peak turbulence levels are likely to result:

Shelter Type	Relative Turbulence Intensity
Solid wall	100%
High density	83
Medium density	57
Low density	53

As an approximation, turbulence levels in the lee of a stationary shelter having a porosity typical of a roadway are about one-half those in the lee of a solid wall and are relatively insensitive to porosity changes.

These shelterbelt concepts are useful inasmuch as they provide some insight into the dispersion effects generated by simple, stationary obstructions. The roadway situation is more complex for several reasons, particularly because the drag flow created by traffic motion makes the problem three-dimensional and the relatively simple picture given above may not strictly apply.

IV ANALYSIS OF WIND, TRAFFIC, AND GROUND-ROUGHNESS EFFECTS ON NEAR-ROADWAY DISPERSION USING WIND TUNNEL TEST DATA

Various statistical tests and data analytic procedures were applied to the wind tunnel data to establish the significance of effects of traffic, winds, and surface roughness and geometry on the dispersion of roadway gases. These methods included factor analysis and multiple regression, and scatter plots and linear regression.

A. Application of Factor Analysis

1. Introduction

Factor analysis has been demonstrated to be a useful diagnostic technique in other studies of pollution dispersion (e.g., Peterson, 1970). In this study, we have applied the method to provide preliminary estimates of the dependence of pollution concentrations on a number of independent (or "environmental") variables. This approach was first applied to test series Q-W to estimate the relationship when traffic density and direction were varied among the series. Next, the method was applied to test series C, D, I, J, and Q to evaluate the relationship when significant surface-roughness variations existed between the five series. Before proceeding to the results, we first briefly review factor analysis as applied here and then define each of the environmental variables considered in the analysis. More extensive discussions of factor analysis abound in the literature: an excellent nontechnical introduction is given by Rummel (1967), while Rozeboom (1966) and Harman (1967) provide modest and extensive technical reviews, respectively.

The technique used to investigate the relationship between the pollutant concentrations and the environmental variables is a combination of factor analysis and multiple regression. Factor analysis was performed on the data from the probe locations (actually the χ/Q values: the concentrations divided by the emission rate) to consolidate the information from probes to two sets of "factor scores." The environmental variables were then regressed on each of these factor scores separately for each test.

Factor analysis begins with the assumption that the ith variable (in this case the X/Q value for the ith probe) is a linear combination of up to n factors (where n is the number of probes) and one unique factor:

$$z_i = a_{i1}F_1 + a_{i2}F_2 + \ldots a_{ij}F_j + d_iU_i \quad . \tag{29}$$

Each factor but the unique one is simply a linear combination of the variables:

$$F_j = b_{j1}z_1 + b_{j2}z_2 + \ldots + b_{ji}z_i \quad . \tag{30}$$

The unique factor is unrelated to the zs.

The data-reduction element of factor analysis results from the fact that two or three factors can usually account for most of the variation in the z_i-terms. A further simplification is a consequence of the method by which the factors are extracted, which in the ideal case results in each variable depending heavily on only one factor; that is, in Eq. (29) only one a_{ij} will be large for each row. Thus the factors identify "clusters" of variables that tend to move in similar patterns.

The statistical procedure used to perform the factor analysis first calculates the matrix of as, the factor matrix. The factor matrix implies the matrix of bs, the factor score coefficient matrix. The factor-score coefficient matrix can then be applied to the X/Q-data to calculate the value of the factors, the factor scores for each observation. The result in our analysis was a reduction from the 12 or 14 X/Q-values to two factor scores for each case. These factor scores summarize for each observation the movement in the two most important patterns of variation in the X/Q-values.

Multiple regression analysis was used to relate the environmental variables to these two factor scores. For environmental variables ev_i and factor score fsc_j, the model is:

$$FS_j = C_{oj} + C_{1j}EV_{ij} + C_{2j}EV_{2j} + \ldots C_{nj}EV_{nj} \quad j = 1,2 \quad . \tag{31}$$

The size of the regression coefficients (the Cs) reveals which environmental variables have the greatest effect on the X/Q-values. A check on the validity of this two-stage process is performed by applying the Cs to the environment variables to predict factor scores, and then applying the factor matrix (which defines the X/Q-values in terms of the factors) to the factor scores to predict or reconstruct X/Q-values for each probe location. The predicted X/Q-values are then regressed on the observed values to assess the predictive accuracy of the model.

A total of 12 environmental variables were proposed; some are direct measures of the independent meteorological and traffic variables, others are derived from them. The symbols used to identify these variables and their definitions are summarized below:

Environmental Variable	Definition
VEHSPD	Vehicle speed (mph)
ABSPRD	Absolute value of the orthogonal component of the wind parallel to the roadway (mph)
SINWDA or ABSIN	Sin of the acute angle between the wind vector and roadway axis (n.d.)
WDSPD	Vector (or total) wind speed (mph)
PARALRD	Signed value of the orthogonal wind component parallel to the roadway (mph)
VSPDWSPD	Ratio of vehicle to wind speeds (n.d.)
DCRS	A measure of the dispersion velocity perpendicular to the roadway axis: the product of the cross-roadway wind component (transport term) and the friction velocity (USTAR, diffusion term) (mph^2)

DPRL	A measure of the dispersion velocity parallel to the roadway axis: the product of ABSPRD and USTAR (mph^2)
DCSPRL	The arithmetic sum of DCRS and DPRL (mph^2)
USTAR	The friction velocity: determined from the logarithmic wind profile, and controlled by the values of WDSPD and the aerodynamic roughness of the surface (mph)
CROSSRD	Signed value of the orthogonal wind component perpendicular to the roadway (mph)

2. Evaluation of Traffic Effects

Two different sampling probe arrays were used throughout the Q-W test series; one for parallel winds (i.e., 0° and 15° wind/roadway angles), and another for oblique winds. Of the 20 probe locations for each array, 12 were common; these are illustrated in Figure 46. Table 29 is a matrix of the correlation coefficients among the 12 probes for all 144 tests that comprise the seven series. Because four pairs of probes correlated at values greater than 0.97, probe numbers 2, 4, 10, and 11 were deleted from subsequent analysis. Two sets of factors were found sufficient to explain the variance in the data; the orthogonally-rotated factors are plotted in Figures 47a and 47b.

The factor analysis only provides a means for determining patterns in the data; it does not explicitly ascribe physical significance or meaning to those patterns. To do this we have done multiple linear regressions between the environmental variables and the factor scores (using the factor patterns common to all data series); the results are summarized in Table 30. In the first case, all seven series were combined. Factor score one (FS1) was significantly correlated with four environmental variables, and FS2 with three variables. The regression equations are:

$$\begin{aligned} FS1 = & -0.0620\ ABSPRD - 1.263\ ABSIN \\ & +0.0340\ VSPDWSPD - 0.0756\ CROSSRD + 1.380 \end{aligned} \tag{32}$$

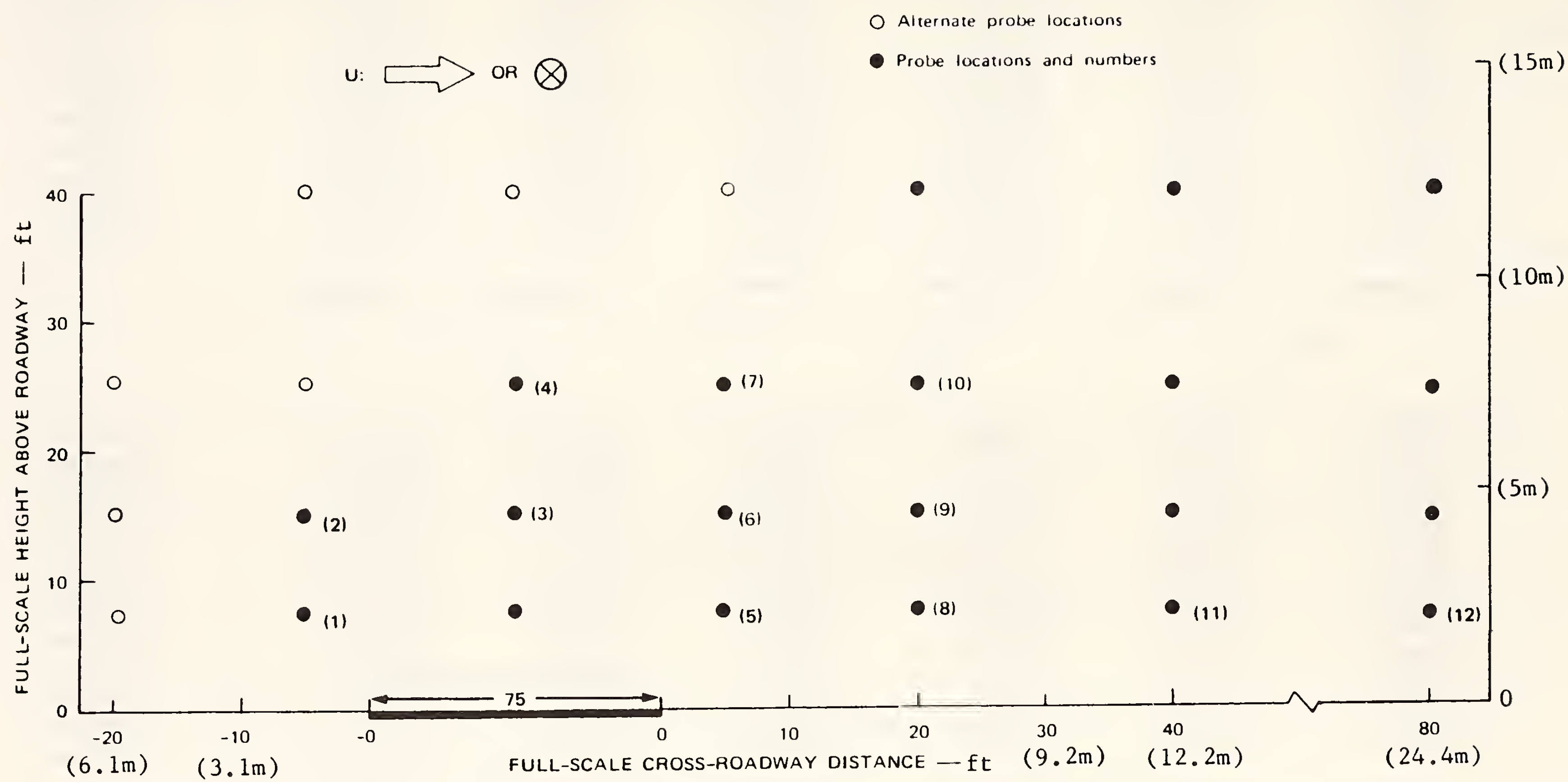

FIGURE 46 LOCATION OF SAMPLING PROBES FOR WIND TUNNEL DATA SERIES Q, R, S, T, U, V, AND W

(Note: Probe locations shown are only those used for both parallel and oblique wind directions.)

Table 29

CORRELATION MATRIX AMONG POLLUTANT CONCENTRATIONS FOR DATA SERIES Q - W

	PROBE1	PROBE2	PROBE3	PROBE4	PROBE5	PROBE6
PROBE1	1.00000	.97036	.89882	.90825	.61105	.77415
PROBE2	.97036	1.00000	.90911	.93594	.54196	.72718
PROBE3	.89882	.90911	1.00000	.98058	.73422	.90766
PROBE4	.90825	.93594	.98058	1.00000	.67179	.85222
PROBE5	.61105	.54196	.73422	.67179	1.00000	.92615
PROBE6	.77415	.72718	.90766	.85222	.92615	1.00000
PROBE7	.83007	.81140	.96064	.93375	.82114	.96354
PROBE8	.47536	.43145	.65097	.59384	.93967	.85130
PROBE9	.65150	.61194	.83152	.77068	.92451	.96321
PROBE10	.77018	.74011	.92131	.88360	.84724	.96873
PROBE11	.37559	.31935	.54561	.50149	.88343	.77438
PROBE12	.12196	.08206	.30287	.27010	.69367	.54834

	PROBE7	PROBE8	PROBE9	PROBE10	PROBE11	PROBE12
PROBE1	.83007	.47536	.65150	.77018	.37559	.12196
PROBE2	.81140	.43145	.61194	.74011	.31935	.08206
PROBE3	.96064	.65097	.83152	.92131	.54561	.30287
PROBE4	.93375	.59384	.77068	.88360	.50149	.27010
PROBE5	.82114	.93967	.92451	.84724	.88343	.69367
PROBE6	.96354	.85130	.96321	.96873	.77438	.54834
PROBE7	1.00000	.74833	.91183	.98429	.66492	.43730
PROBE8	.74833	1.00000	.93200	.81158	.97491	.85945
PROBE9	.91183	.93200	1.00000	.95776	.87696	.70274
PROBE10	.98429	.81158	.95776	1.00000	.74297	.53734
PROBE11	.66492	.97491	.87696	.74297	1.00000	.93446
PROBE12	.43730	.85945	.70274	.53734	.93446	1.00000

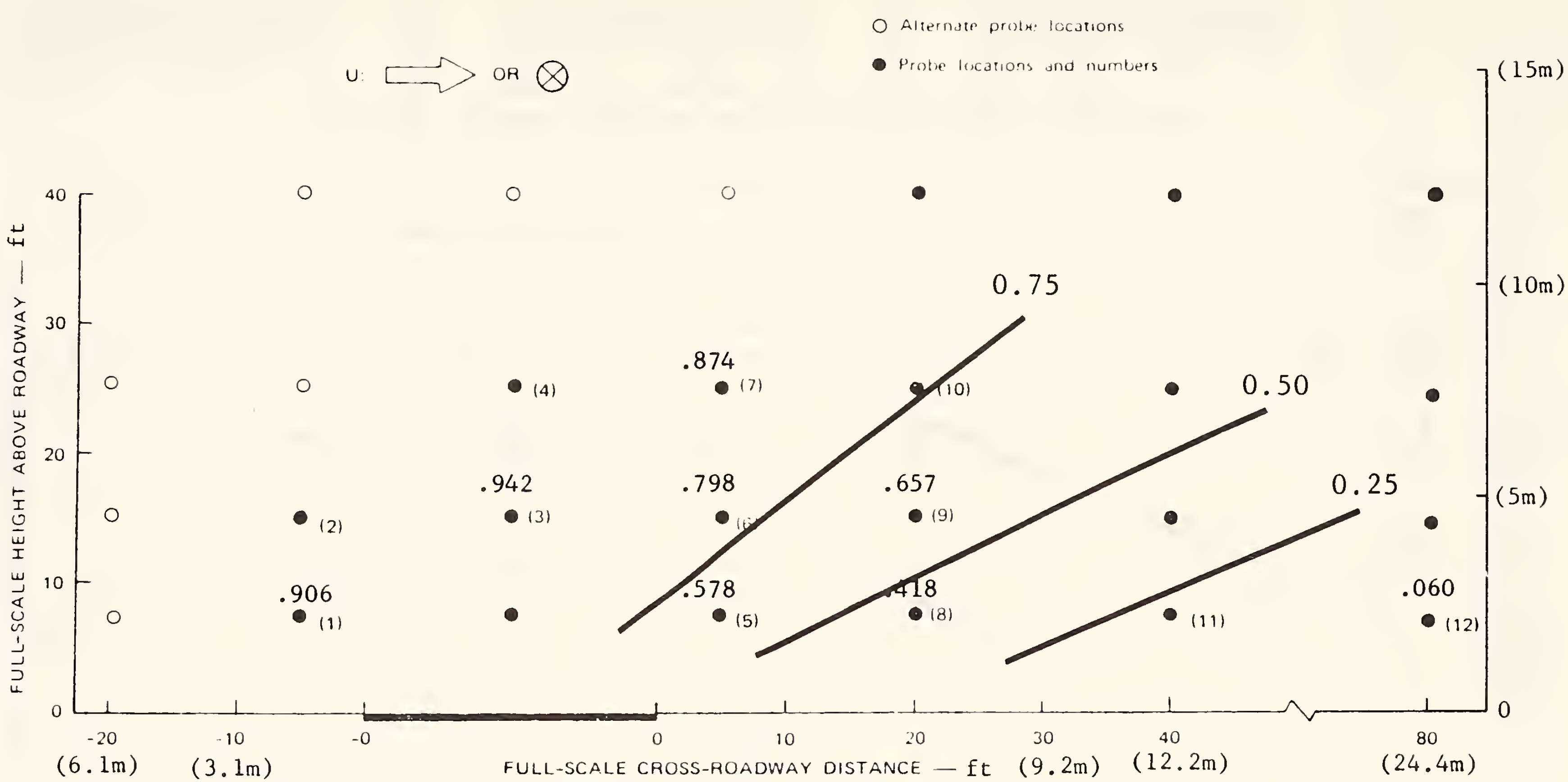

FIGURE 47a DISTRIBUTION OF FIRST FACTOR FROM FACTOR ANALYSIS (WITH VARIMAX ROTATION) FOR DATA SETS Q, R, S, T, U, V, AND W

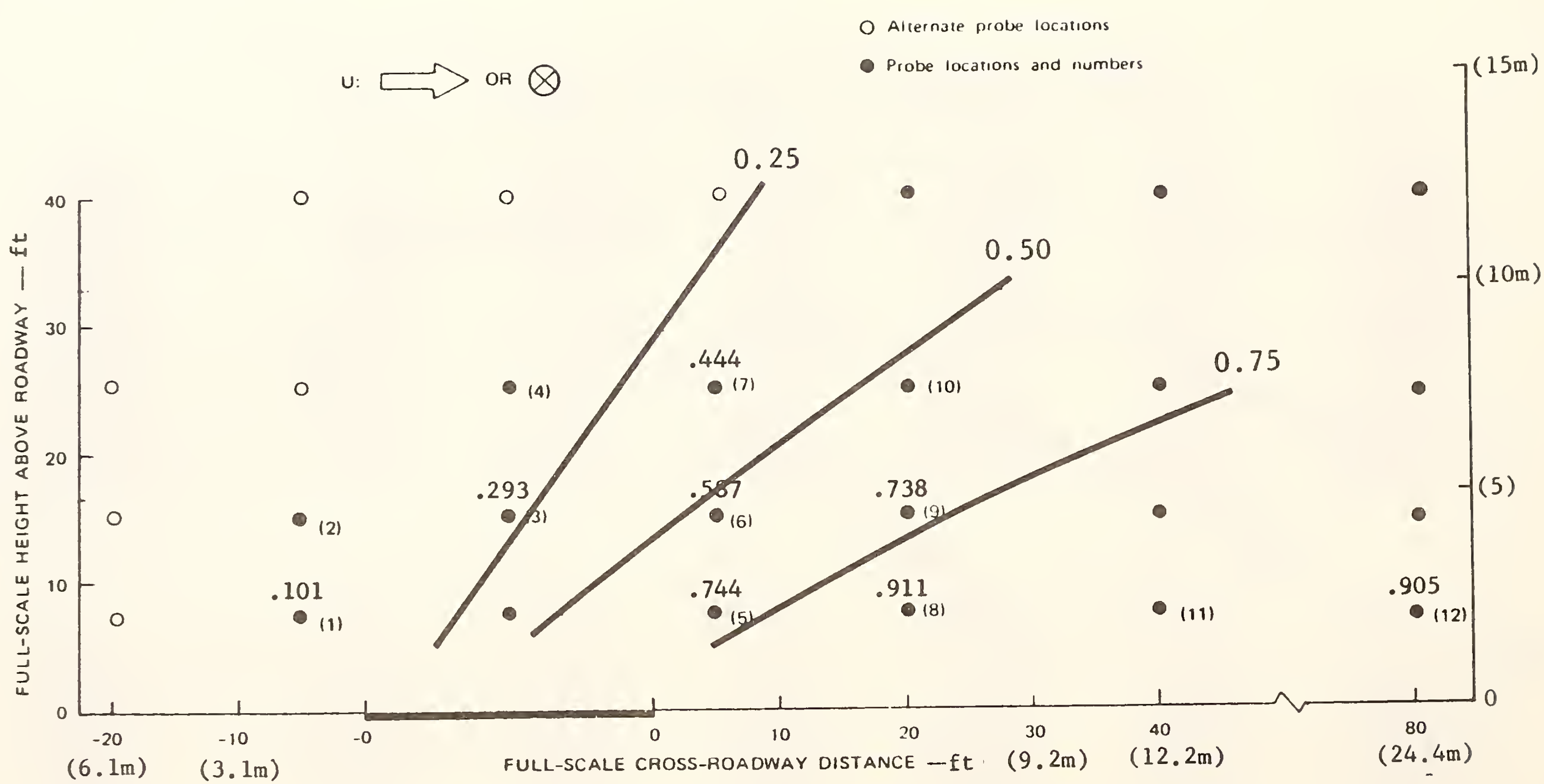

FIGURE 47b DISTRIBUTION OF SECOND FACTOR FROM FACTOR ANALYSIS (WITH VARIMAX ROTATION) FOR DATA SETS Q, R, S, T, U, V, AND W

Table 30

RESULTS OF MULTIPLE LINEAR REGRESSION OF FACTOR SCORES WITH ENVIRONMENTAL VARIABLES FOR TEST SERIES Q-W, SHOWING BOTH THE COEFFICIENTS (b) AND CONSTANT OF THE REGRESSION AND THE CUMULATIVE EXPLAINED VARIANCE (r^2)

Environmental Variables	Data Series Q,R,S,T,U,V,W				Data Series Q			
	Factor Score 1		Factor Score 2		Factor Score 1		Factor Score 2	
	b	r^2	b	r^2	b	r^2	b	r^2
VEHSPD			-.0130	.502	.0092	.770		
ABSPRD	-.0620	.695			-.1237	.686		
ABSIN	-1.263	.740	.9716	.457	-4.196	.604		
WDSPD								
PARALRD								
VSPDWSPD	.0340	.766						
DCRS								
DPRL								
DCSPRL							-.0175	.368
USTAR			-.6330	.350	.6433	.730		
CROSSRD	-.0756	.583						
SIGN								
CONSTANT	1.380		1.400		1.327		1.055	

Environmental Variables	Data Series R				Data Series S			
	Factor Score 1		Factor Score 2		Factor Score 1		Factor Score 2	
	b	r^2	b	r^2	b	r^2	b	r^2
VEHSPD								
ABSPRD					-.0679	.811		
ABSIN					-2.978	.672	1.431	.344
WDSPD								
PARALRD								
VSPDWSPD								
DCRS								
DPRL	.0145	.927	-.0100	.563				
DCSPRL								
USTAR								
CROSSRD								
SIGN								
CONSTANT	-1.547		0.350		1.609		-0.960	

Environmental Variables	Data Series T				Data Series U			
	Factor Score 1		Factor Score 2		Factor Score 1		Factor Score 2	
	b	r^2	b	r^2	b	r^2	b	r^2
VEHSPD			.0486	.539				
ABSPRD	-.0410	.861			-.0870	.751		
ABSIN			1.147	.712				
WDSPD								
PARALRD							.0505	.622
VSPDWSPD								
DCRS					.0432	.707		
DPRL	-.0283	.619					-.0106	.385
DCSPRL	.0279	.762						
USTAR								
CROSSRD	-.2476	.435			-.3135	.906		
SIGN							.4286	.715
CONSTANT	0.962		-2.472		1.348		-0.176	

Table 30 (Concluded)

Environmental Variables	Data Series V				Data Series W			
	Factor Score 1		Factor Score 2		Factor Score 1		Factor Score 2	
	b	r^2	b	r^2	b	r^2	b	r^2
VEHSPD	.0287	.701	.0401	.619			-.320	.631
ABSPRD	-.1009	.934			-.1198	.890		
ABSIN	-1.894	.899						
WDSPD							-.2389	.750
PARALRD								
VSPDWSPD								
DCRS					.1359	.818		
DPRL					-.0069	.755		
DCSPRL							-.0201	.560
USTAR								
CROSSRD					-.6893	.569		
SIGN								
CONSTANT	1.125		-1.098		2.363		3.030	

$$FS2 = -0.0130\ VEHSPD + 0.9716\ ABSIN \\ -0.6330\ USTAR + 1.400 \tag{33}$$

Thus, when all the data are taken together, four variables explain 76.6% of the variance in the first factor score and three variables explain 50.2% of the variance in the second factor score. To understand how effectively these factor scores derived from environmental variables can be used to reconstruct the original data, (1) Eqs. 32 and 33 were used to "predict" the two factor scores, (2) the factor scores and factor matrix were used in Eqs. 29 and 30 to estimate the original data (3) the original and reconstructed concentration data were correlated at all probe locations, and (4) the procedure was repeated for each of the seven individual test series. Table 31 summarizes the correlation coefficients

Table 31

CORRELATION COEFFICIENTS FOR OBSERVED WIND TUNNEL DATA (TEST SERIES Q-W) AND NORMALIZED CONCENTRATION DATA AS RECONSTRUCTED FROM FACTOR ANALYSIS AND REGRESSION OF FACTOR SCORES WITH ENVIRONMENTAL VARIABLES

Probe ID (N)	All Data (144)	Q-Series (30)	R-Series (18)	S-Series (15)	T-Series (15)	U-Series (16)	V-Series (18)	W-Series (32)
1	0.85	0.84	0.94	0.91	0.93	0.86	0.94	0.65
3	0.91	0.92	0.98	0.92	0.92	0.95	0.98	0.93
5	0.82	0.77	0.34	0.27	0.91	0.81	0.95	0.62
6	0.88	0.92	0.92	0.75	0.92	0.89	0.96	0.76
7	0.89	0.96	0.99	0.96	0.85	0.86	0.94	0.87
8	0.83	0.68	0.46	0.26	0.88	0.81	0.94	0.52
9	0.85	0.80	0.48	0.34	0.87	0.82	0.92	0.69
12	0.75	0.67	0.75	0.60	0.84	0.70	0.87	0.06
Min	0.75	0.67	0.34	0.26	0.84	0.70	0.87	0.06
Max	0.91	0.96	0.99	0.92	0.93	0.95	0.98	0.93
Mean	0.85	0.82	0.73	0.63	0.89	0.84	0.94	0.64

between observed and reconstructed data. As indicated, the mean correlations for each series range from 0.63 to 0.94, with a grand average of 0.85 for all test series. Tables 30 and 31 essentially provide two outputs: (1) an indication of which environmental variables are significantly correlated with the observed variations in the concentration patterns, and (2) the degree to which the environmental variables can effectively reproduce the observed patterns. Because of the nature of factor analysis, no unique set of factors is derived. Others could be found that would characterize the data equally well. As a consequence, the regression with the environmental variables should also not be viewed as absolute. However, it does provide a good measure of which environmental variables are important and for what series. Thus, for example, we see that vehicle speed (among other variables) is particularly important for series Q, T, V, and W. Subsequent analyses have been geared to quantify this variable's impact on concentrations. In examining Table 30, it is also important to bear in mind that several variables are highly correlated. Table 32 is thus given to quantify this commonality among environmental variables.

3. Evaluation of Configuration Effects

Test series C, D, I, J, and Q were also evaluated using factor analysis. The objective was to identify those environmental variables that were important when surface conditions were significantly changed between test series. Fourteen sampling locations were common to all tests/series (Figure 48). Again, two sets of factors were sufficient to explain the variance in the data; the orthogonally-rotated factors are shown in Figures 49a and 49b. The corresponding factor scores were again correlated with environmental variables, as summarized in Table 33. Interestingly, vehicle speed does not correlate with the factor scores as it did in test series Q-W, although the ratio of vehicle to wind speed does correlate. Table 34 lists the correlation matrix for the environmental variables, while Table 35 provides the correlations among the concentration data at the various probe locations. The regressions among the environmental variables and factor scores were again used with

Table 32

CORRELATION MATRIX AMONG ENVIRONMENTAL VARIABLES FOR DATA SERIES Q - W

	FACSC1	FACSC2	VEHSPD	ABSPRD	ABSIN	WDSPD
FACSC2	-.02595					
VEHSPD	.20543	.07294				
ABSPRD	-.20667	-.41660	-.14787			
ABSIN	-.50477	.33953	.00487	-.57439		
WDSPD	-.65614	-.41187	-.22328	.69315	-.01908	
PARALRD	.01556	-.04085	-.11026	.13287	-.12668	.07512
VSPDWSPD	.55681	.30922	.63918	-.45972	.02644	-.66632
DCRS	-.63343	-.10558	-.20084	-.09558	.59389	.53872
DPRL	.00379	-.42177	-.18511	.48253	-.39443	.33350
DCSPRL	-.11428	-.44566	-.22440	.46952	-.28763	.43727
USTAR	-.41802	-.59137	-.44597	.40947	-.02076	.58777
SIGN	-.12606	.09089	.07638	-.11004	.20977	-.03416
CROSSRD	-.76368	.04193	-.11880	-.16128	.72099	.54380

	PARALRD	VSPDWSPD	DCRS	DPRL	DCSPRL	USTAR
FACSC2						
VEHSPD						
ABSPRD						
ABSIN						
WDSPD						
PARALRD						
VSPDWSPD	-.08387					
DCRS	-.06497	-.37783				
DPRL	.04098	-.22771	-.14548			
DCSPRL	.02928	-.30043	.03954	.98284		
USTAR	.00935	-.61562	.52694	.57745	.68146	
SIGN	-.05731	.08126	.09765	-.11132	-.09422	.00115
CROSSRD	-.07538	-.36033	.90280	-.23603	-.07004	.30245

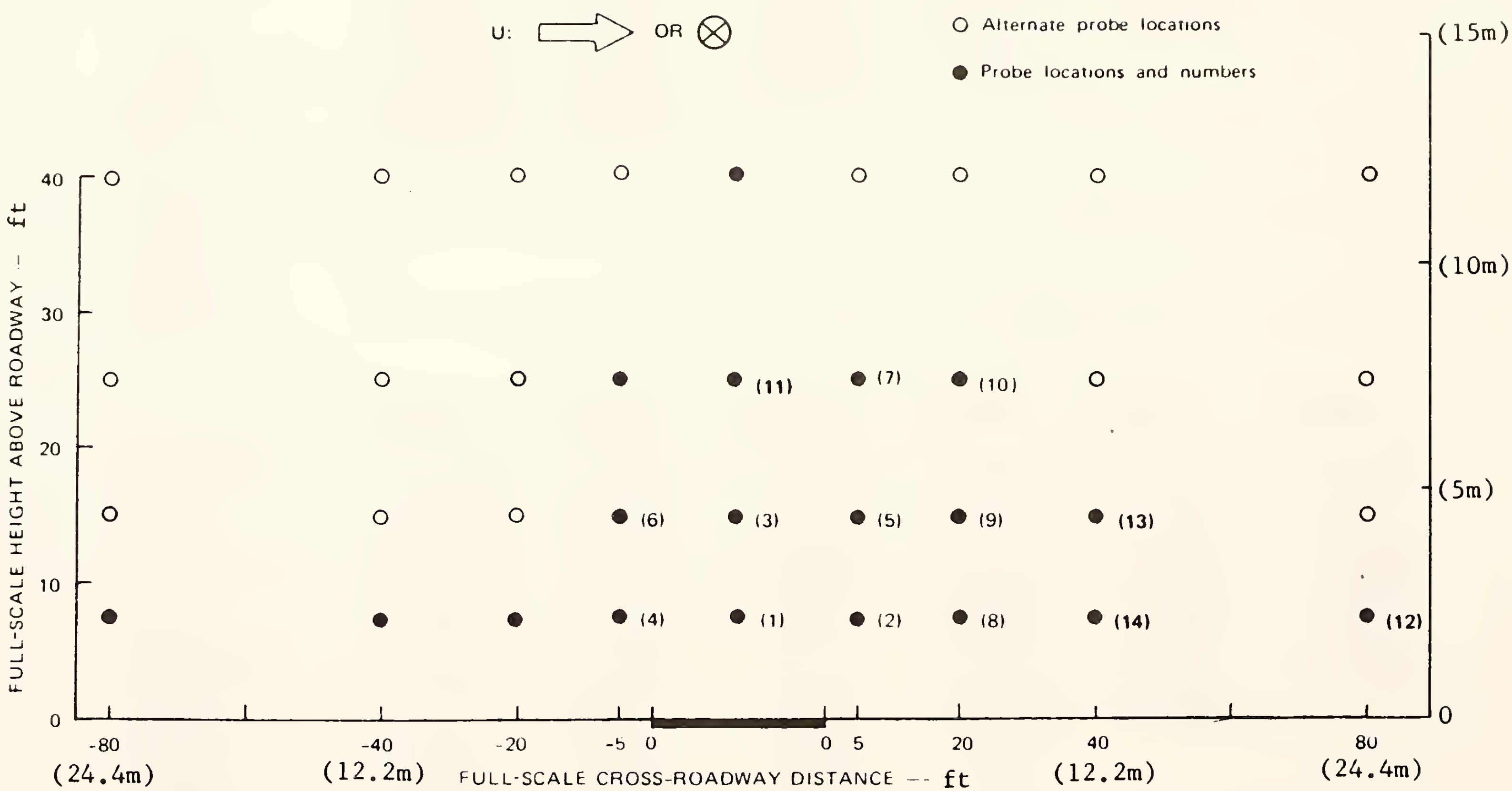

FIGURE 48 LOCATION OF SAMPLING PROBES FOR WIND TUNNEL DATA SERIES C, D, I, J, AND Q

(Note: Probe locations shown are only those used for *both* parallel and oblique wind directions.)

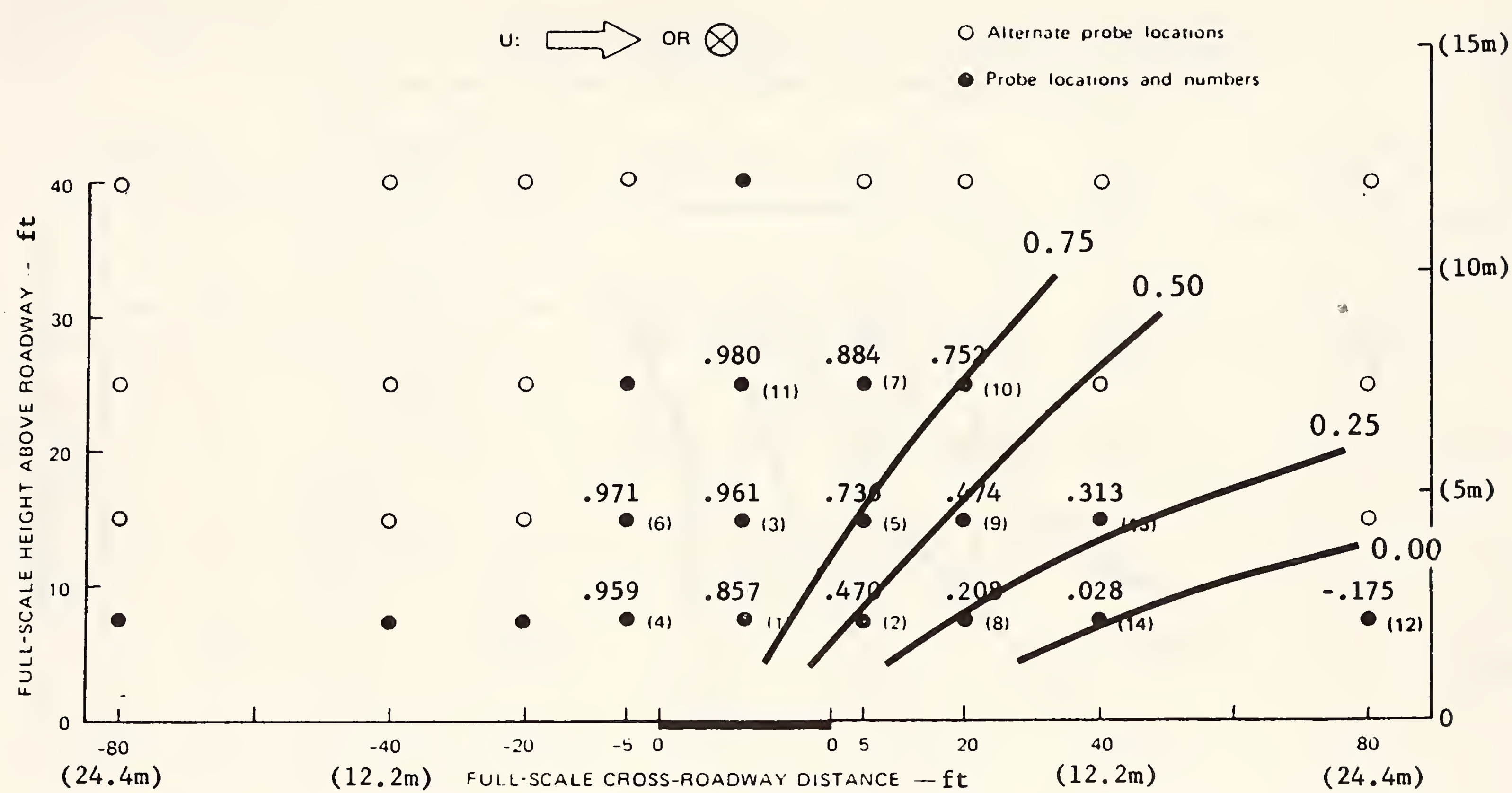

FIGURE 49a DISTRIBUTION OF FIRST FACTOR FROM FACTOR ANALYSIS (WITH VARIMAX ROTATION) FOR DATA SETS C, D, I, J, AND Q

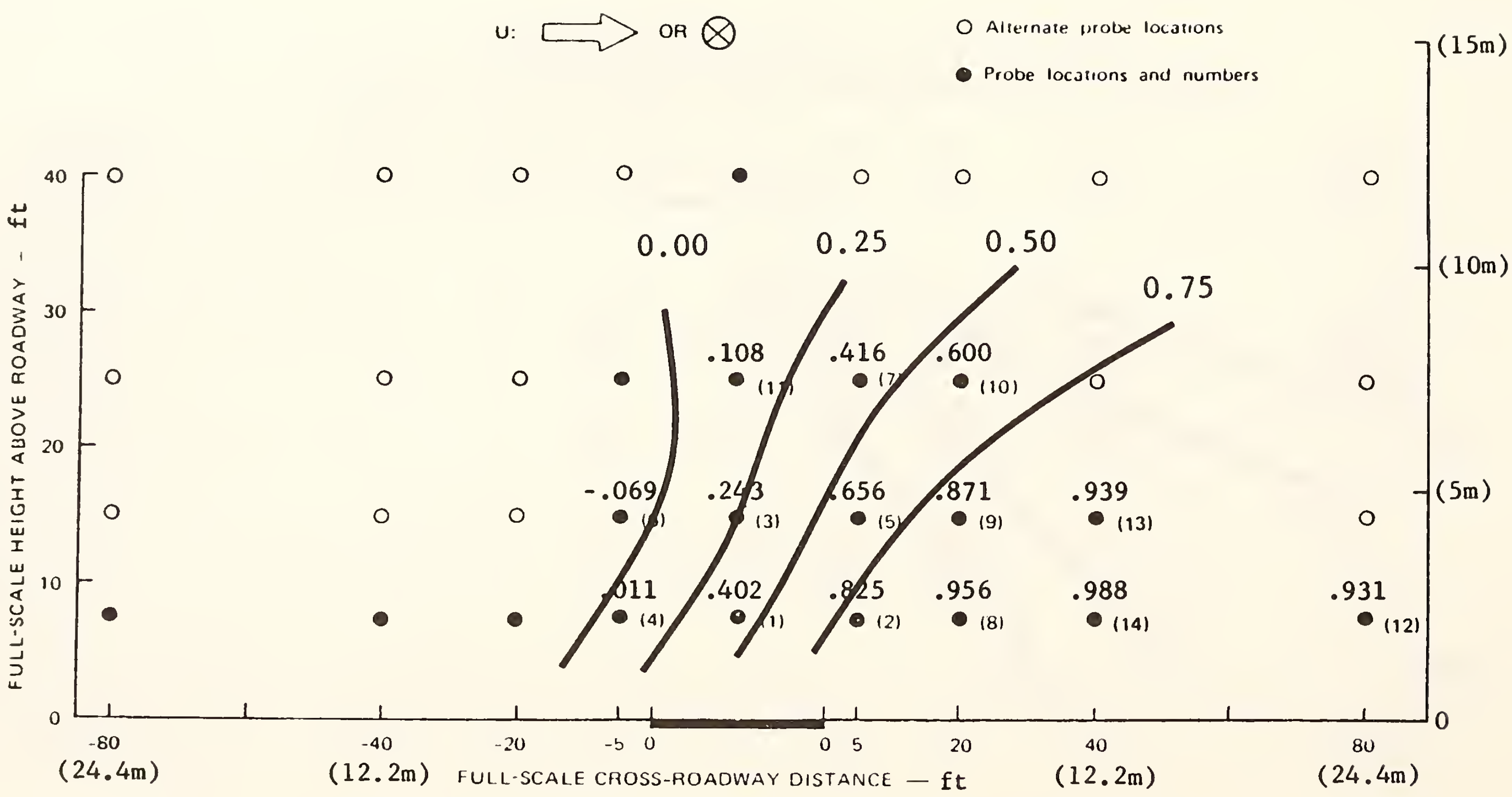

FIGURE 49b DISTRIBUTION OF SECOND FACTOR FROM FACTOR ANALYSIS (WITH VARIMAX ROTATION) FOR DATA SETS C, D, I, J, AND Q

Table 33

RESULTS OF MULTIPLE LINEAR REGRESSION OF FACTOR SCORES WITH ENVIRONMENTAL VARIABLES FOR TEST SERIES C,D,I,J, AND Q SHOWING BOTH THE COEFFICIENTS (b) AND CONSTANT OF THE REGRESSION AND THE CUMULATIVE EXPLAINED VARIANCE (r^2)

Environmental Variables	Data Series C,D,I,J,Q				Data Series C			
	Factor Score 1		Factor Score 2		Factor Score 1		Factor Score 2	
	b	r^2	b	r^2	b	r^2	b	r^2
VEHSPD								
ABSPRD	-.0775	.711						
SINWDA	-2.3933	.587	1.6438	.518	-2.2392	.828	1.5152	.844
WDSPD					-.2348	.665	-.1751	.744
PARALRD					-.0967	.962		
VSPDWSPD	.0580	.522						
DCRS					.0368	.943	-.0373	.883
DPRL			-.0250	.629				
DCSPRL			.0280	.593				
USTAR			.7617	.452				
CROSSRD	-.0048	.412	-.1295	.577				
CONSTANT	1.6599		1.2705		3.7327		.8484	

Environmental Variables	Data Series D				Data Series I			
	Factor Score 1		Factor Score 2		Factor Score 1		Factor Score 2	
	b	r^2	b	r^2	b	r^2	b	r^2
VEHSPD								
ABSPRD					-.1594	.831	.1580	.864
SINWDA	-3.3133	.870	.8374	.848	1.2124	.636		
WDSPD			-.2836	.762				
PARALRD	-.1690	.952						
VSPFWSPD								
DCRS							.0137	.650
DPRL	-.0090	.684						
DCSPRL					-.0037	.944	.0031	.582
USTAR					1.1215	.470	-1.3135	.955
CROSSRD	-0.0604	.604			-3.584	.853	.1961	.781
CONSTANT	2.9246		1.9712		-1.2001		1.2467	

Environmental Variables	Data Series J				Data Series Q			
	Factor Score 1		Factor Score 2		Factor Score 1		Factor Score 2	
	b	r^2	b	r^2	b	r^2	b	r^2
VEHSPD								
ABSPRD	-.1169	.894			-.0875	.723	.0810	.468
SINWDA	-4.2711	.653	3.1671	.506	-4.2851	.563	1.2876	.559
SDSPD							-1.6333	.443
PARALRD								
VSPDWSPD								
DCRS								
DPRL								
DCSPRL			.0480	.654				
USTAR			-.0555	.365				
CROSSRD							.0707	.764
CONSTANT			3.0121	.658			2.1237	1.011

Table 34

CORRELATION MATRIX AMONG POLLUTANT CONCENTRATIONS FOR TEST SERIES C, D, I, J, AND Q

	PROBE1	PROBE2	PROBE3	PROBE4	PROBE5	PROBE6	PROBE7
PROBE1	1.00000	.76871	.94981	.83033	.88472	.81842	.90049
PROBE2	.76871	1.00000	.63797	.47345	.88749	.40717	.74321
PROBE3	.94981	.63797	1.00000	.91070	.86849	.90815	.95127
PROBE4	.83033	.47345	.91070	1.00000	.70292	.97552	.83586
PROBE5	.88472	.88749	.86849	.70292	1.00000	.64657	.94417
PROBE6	.81842	.40717	.90815	.97552	.64657	1.00000	.80835
PROBE7	.90049	.74321	.95127	.83586	.94417	.80835	1.00000
PROBE8	.58567	.92502	.42812	.21359	.75981	.15771	.56270
PROBE9	.74117	.93897	.66600	.45505	.93752	.38524	.79693
PROBE10	.84584	.83360	.86576	.71455	.97767	.66054	.96848
PROBE11	.89144	.53155	.97636	.93370	.78162	.95761	.91565
PROBE12	.23246	.65791	.06838	-.15852	.47213	-.22421	.21923
PROBE13	.62278	.91218	.52351	.31463	.85419	.23120	.68002
PROBE14	.43148	.83773	.26489	.05602	.64903	-.01823	.41729

	PROBE8	PROBE9	PROBE10	PROBE11	PROBE12	PROBE13	PROBE14
PROBE1	.58567	.74117	.84584	.89144	.23246	.62278	.43148
PROBE2	.92502	.93897	.83360	.53155	.65791	.91218	.83773
PROBE3	.42812	.66600	.86576	.97636	.06838	.52351	.26489
PROBE4	.21359	.45505	.71455	.93370	-.15852	.31463	.05602
PROBE5	.75981	.93752	.97767	.78162	.47213	.85419	.64903
PROBE6	.15771	.38524	.66054	.95761	-.22421	.23120	-.01823
PROBE7	.56270	.79693	.96848	.91565	.21923	.68002	.41729
PROBE8	1.00000	.91336	.70150	.31671	.86530	.94440	.96926
PROBE9	.91336	1.00000	.90708	.55228	.72497	.97750	.85784
PROBE10	.70150	.90708	1.00000	.79929	.41020	.82685	.59205
PROBE11	.31671	.55228	.79929	1.00000	-.05792	.40195	.14174
PROBE12	.86530	.72497	.41020	-.05792	1.00000	.82190	.93934
PROBE13	.94440	.97750	.82685	.40195	.82190	1.00000	.93190
PROBE14	.96926	.85784	.59205	.14174	.93934	.93190	1.00000

Table 35

CORRELATION MATRIX AMONG ENVIRONMENTAL VARIABLES FOR DATA SERIES C, D, I, J, AND Q

	FACSC1	FACSC2	VEHSPD	ABSPRD	SINWDA	WDSPD
FACSC2	-.00009					
~~VEHSPD~~	~~.25929~~	~~.29921~~				
ABSPRD	-.09592	-.40834	-.09913			
SINWDA	-.54228	.26893	.01887	-.63726		
~~WDSPD~~	~~-.51944~~	~~-.54775~~	~~-.18129~~	~~.64527~~	~~-.03051~~	
PARALRD	.08249	-.30019	-.24971	.52538	-.47119	.25361
VSPDWSPD	.51223	.52299	.68436	-.38414	.03607	-.60656
~~DCRS~~	~~-.46626~~	~~-.30908~~	~~-.11749~~	~~-.16429~~	~~.55988~~	~~.51220~~
DPRL	-.04099	-.39440	-.08998	.51953	-.38753	.36372
DCSPRL	-.12283	-.44871	-.11062	.49076	-.28931	.45367
~~USTAR~~	~~-.34465~~	~~-.67252~~	~~-.34493~~	~~.35576~~	~~-.01957~~	~~.56925~~
CROSSRD	-.64186	-.13639	-.07898	-.26660	.75050	.51065

	PARALRD	VSPDWSPD	DCRS	DPRL	DCSPRL	USTAR
FACSC2						
VEHSPD						
ABSPRD						
SINWDA						
WDSPD						
PARALRD						
VSPDWSPD	-.23570					
DCRS	-.17174	-.29272				
DPRL	.43353	-.17884	-.08851			
DCSPRL	.40345	-.23024	.08699	.98460		
USTAR	.30272	-.50180	.57666	.62698	.72828	
CROSSRD	-.31942	-.30602	.85266	-.23851	-.08889	.27620

the two sets of factors to reconstruct the concentrations. Reconstructed and observed concentration data were again correlated at each sampling location for all series; the correlations are summarized in Table 36. Individual series have correlations at individual probes that range from a low of 0.63 to a high value 0.99, with the grand average using all data being 0.84. Thus, the factor model together with the regression among environmental variables and factor scores provides a convenient way to

Table 36

CORRELATION COEFFICIENTS FOR OBSERVED WIND TUNNEL DATA AND NORMALIZED CONCENTRATION DATA AS RECONSTRUCTED FROM FACTOR ANALYSIS AND REGRESSION OF FACTOR SCORES WITH ENVIRONMENTAL VARIABLES

Probe ID (N)	All Data (102)	C-Series (20)	D-Series (20)	I-Series (16)	J-Series (16)	Q-Series (30)
1	.877	.982	.981	.893	.962	.818
2	.824	.942	.920	.963	.779	.808
3	.896	.985	.983	.946	.958	.915
4	.770	.923	.962	.850	.894	.817
5	.898	.976	.968	.971	.762	.960
6	.792	.969	.959	.915	.864	.803
7	.883	.963	.963	.914	.850	.965
8	.827	.960	.942	.965	.736	.723
9	.871	.964	.947	.988	.677	.898
10	.854	.947	.946	.936	.634	.939
11	.876	.967	.970	.949	.947	.902
12	.799	.895	.910	.935	.849	.715
13	.844	.938	.923	.988	.723	.827
14	.824	.948	.926	.965	.860	.713
Min	.770	.895	.910	.850	.634	.715
Max	.898	.982	.981	.988	.962	.965
Mean	.845	.874	.951	.941	.821	.843

quantify the patterns of observed pollutant concentrations in the presence of variations of surface conditions and environmental variables.

B. Parametric Analyses of Traffic Effects

1. Effects Due to Traffic Density

Differences in traffic density have been suspected by some to have important effects on the initial dispersion of vehicular pollutants. On the other hand Chapter III indicates that we could not find a significant effect for variations in traffic density ranging from moderate to heavy for a major suburban freeway. The wind tunnel data were analyzed to further evaluate this possible effect. Experimental tests conducted in different series were similar except for differences in the density of the traffic. Normalized pollutant concentrations were inter-compared for test series C, V, and W (rough terrain, at-grade configurations, narrow right-of-way) and for test series Q and R (smooth terrain, at-grade configuration). Three variations in traffic density existed: (1) high density on all four lanes, (2) low density on all four lanes, and (3) high density on two lanes and low density on the opposing two lanes.

Normalized concentrations at three locations from 18 pairs of Q- and R-tests are plotted as a scatter diagram in Figure 50. The three locations are: (1) Probe 3-15 ft (4.57 m) above the center of the roadway; (2) Probe 8-7.5 ft (2.29 m) above ground and 57.5 ft (17.53 m) to the side of roadway center; and (3) Probe 12-7.5 ft above ground and 117.5 ft (35.82 m) to the side of roadway center. Referring to the correlation matrix in Table 29 it is seen that these three locations are representative of concentrations in the near-road, midfield, and distant areas. Table 37 summarizes the various comparisons made between the Q- and R-series data.

Comparing the Q-series data (hi-hi density) with the R-series data (hi-lo density), there is little, if any, overall difference that can be ascribed to traffic density variation. Indeed, the slope of the linear regression curve for all data is 0.932, while the intercept is zero.

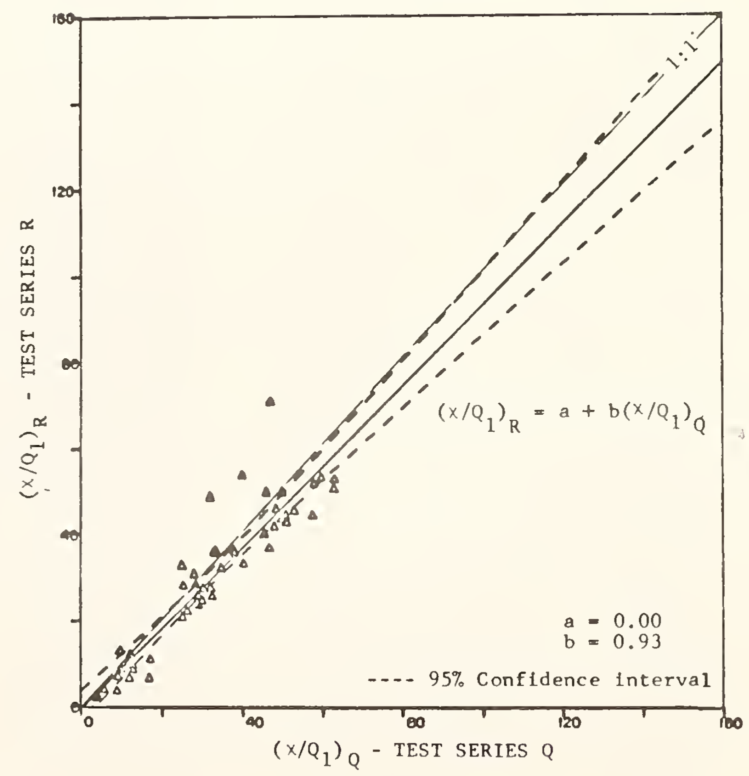

FIGURE 50 COMPARISON OF NORMALIZED CONCENTRATIONS (χ/Q_1) FROM TEST SERIES Q (HI-HI TRAFFIC DENSITY) AND TEST SERIES R (HI-LO)

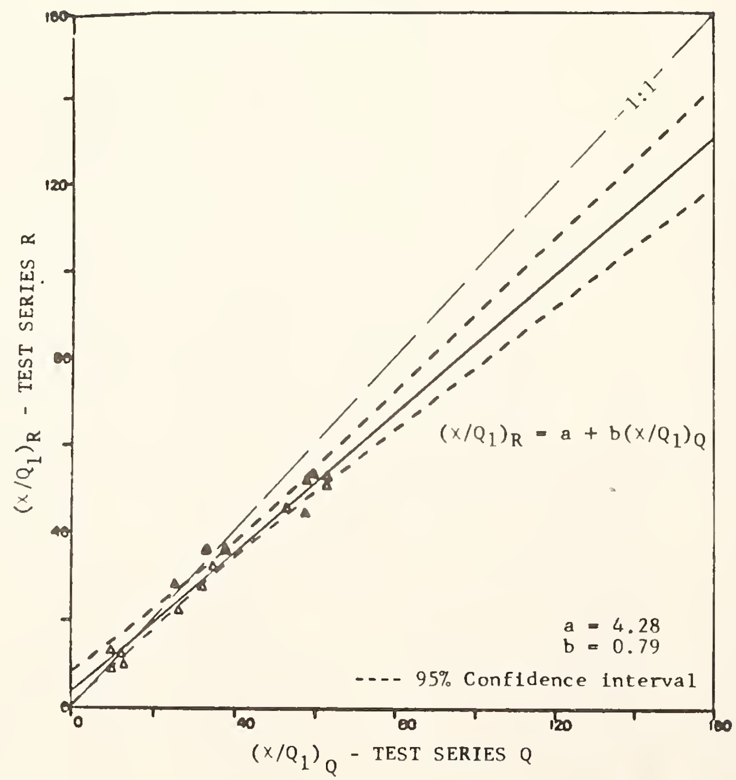

FIGURE 51 COMPARISON OF NORMALIZED CONCENTRATIONS (χ/Q_1) FROM TEST SERIES Q AND R FOR PARALLEL WIND-ROAD ANGLES

Table 37

COMPARISON OF WIND TUNNEL CONCENTRATION
DATA FROM TEST SERIES Q AND R

Test Series	X*	Y*	Data Description	N	r	b*	a*	$\overline{(\chi/Q_\ell)}$		rms	
	Q	R						Q	R	$(\Delta\chi/Q_\ell)$	$(\bar{Q}/\bar{R})$
Right-of-way	Infinite	Infinite	All data	54	0.926	0.932	0.00	31.33	29.21	6.38	1.07
Surface roughness	Smooth	Smooth	Probe #3	18	0.987	0.856	-1.24	23.04	18.49	2.94	1.25
Traffic density	Hi-Hi	Hi-Lo	Probe #8	18	0.473	0.609	16.75	45.47	44.42	7.82	1.02
Traffic direction	Two-way	Two-way	Probe #12	18	0.802	0.937	0.82	25.49	24.71	5.56	1.03
			Oblique winds	36	0.917	1.043	-2.74	28.66	27.14	7.03	1.06
			Parallel winds	18	0.977	0.793	4.28	36.67	33.35	3.17	1.10

*Y = a + b X

Moreover, the perfect or 1:1 curve lies wholly within the 95% confidence intervals indicated on the figure by the dashed curves. Stratifying the data according to wind direction (i.e., oblique and parallel with respect to the roadway axis) shows little influence except that the slope of the regression for parallel winds is about 0.79 (Figure 51). However, the ratio of the concentration average for the two series is only 1.10. Thus, the parallel-wind cases indicate a tendency for the higher density traffic to result in slightly higher average ambient concentrations. This is contrary to intuition in that it would normally be assumed that the more dense traffic flow would result in increased turbulent mixing and, consequently, lower concentrations. Examining the difference for oblique wind angles, a different finding results: virtually no difference in pollutant concentrations can be attributed to traffic density. The linear regression curve in Figure 52 indicates slightly higher concentrations for the lower traffic-density cases (slope = 1.04), while the ratio of the mean concentrations for the two series (1.06) indicates a slight, opposite tendency. The effect reflected in parallel-wind cases is again apparent when concentrations over all wind angles are compared at the near-road probe (Figure 53): both the slope of the regression (0.86) and the ratio of concentrations for the two series (1.25) indicate higher concentrations associated with the higher-density traffic flow. If anything, the data indicate slightly greater dispersion and lower concentrations may occur with the lower density traffic--particularly for parallel wind-road angles (all probes) and locations over the roadway (all wind angles).

Evaluations of possible dispersion effects due to variations in traffic density were also made using data from test series C, V, and W; all three have high surface roughness. Traffic density ranged from lo-lo (C series), through hi-lo (V series), to hi-hi (W series). The overall dispersion pattern is more complicated here than with the Q and R series (smooth surface) in that the large surface roughness elements located close to the roadway edges (ca. 30 m) create a form of street canyon about the roadway. With a parallel wind the air is channeled through the canyon, while an oblique wind creates a helical circulation

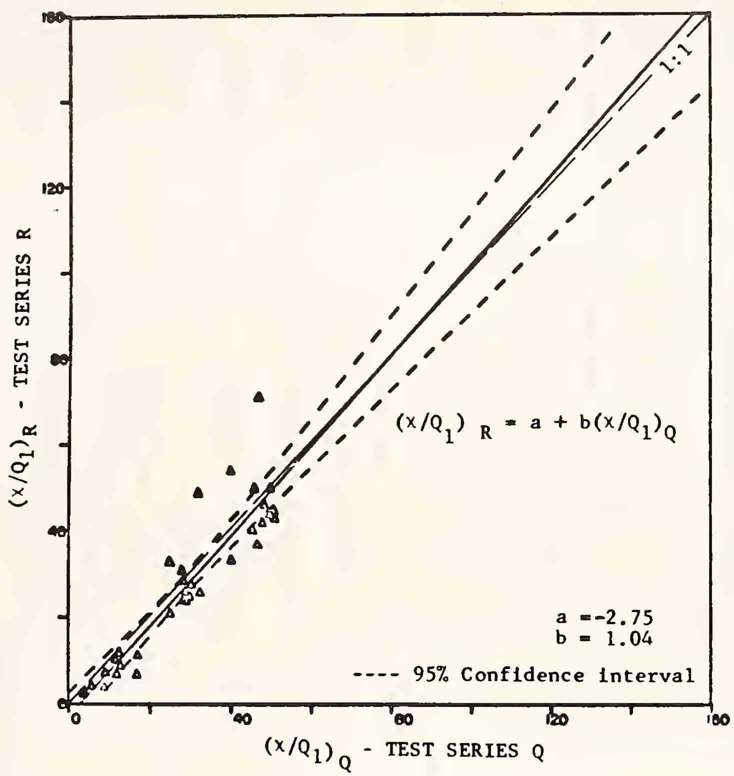

FIGURE 52 COMPARISON OF NORMALIZED CONCENTRATIONS (χ/Q_1) FROM TEST SERIES Q AND R FOR OBLIQUE WIND-ROAD ANGLES

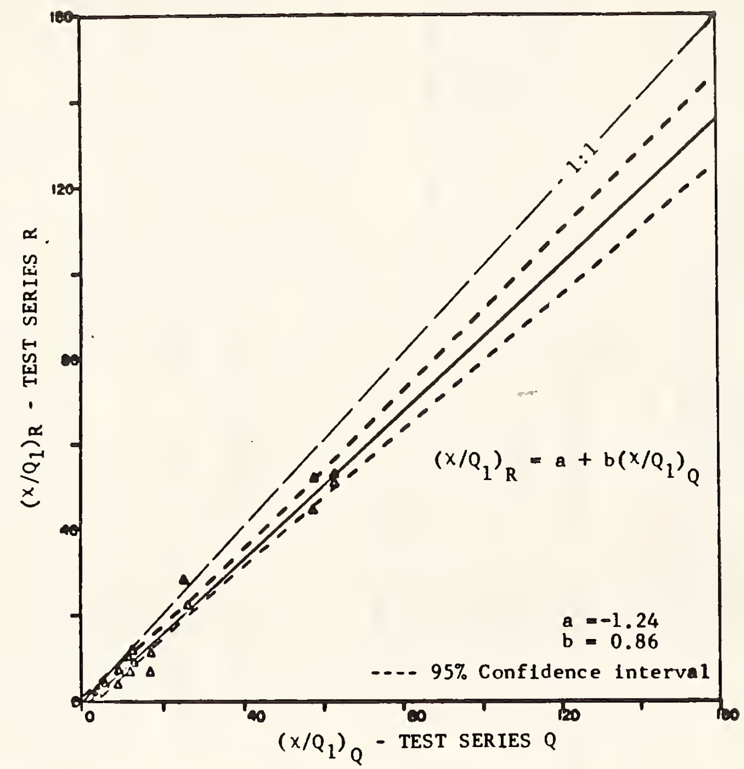

FIGURE 53 COMPARISON OF NORMALIZED CONCENTRATIONS (χ/Q_1) FROM TEST SERIES Q AND R AT PROBE NUMBER 3 (LOCATED OVER ROADWAY CENTER)

across the roadway resulting in a wind flow reversal at roadway level. In all cases, near-roadway concentrations are increased substantially for rough surfaces over the smooth-surface configuration. This indicates decreased dispersion near the roadway and may have the secondary effect of magnifying vehicular influences.

Table 38 summarizes the intercomparisons of the three test series. Again the results are mixed. In Figure 54, normalized concentrations are plotted for the C (lo-lo traffic density) and V series (hi-lo). No influence due to traffic density is seen for either the whole data set or when stratified by probe location or wind angle.

Contrary to the comparison of lo-lo and hi-lo traffic, the concentrations resulting from hi-hi traffic (series W) appear systematically lower than their "hi-lo" counterparts by an average of 14%. Figure 55 illustrates this comparison for all wind angles and probe locations. As shown in Table 38, these differences are independent of probe location although they are apparently more pronounced (Figure 56) for oblique winds (average difference of 16%) than parallel winds (10%). Comparing the regression and 1:1 lines in both Figures 55 and 56 indicates that the two series have comparable values at low concentrations, but that the hi-hi concentrations are less than the hi-lo values for mid and high concentrations. This same pattern holds for all three probe locations. Thus, the indication is that a traffic influence is present for very dense traffic and that the magnitude of the effect is greatest when ambient wind speeds are low--that is, when concentrations are high.

This same pattern of influence is also seen when the lo-lo cases (series C) are compared with the hi-hi (series W), as illustrated in Figure 57. Surprisingly, however, the magnitude of the traffic influence is not as large as with the hi-lo/hi-hi comparison. While no fast conclusions can be drawn, two inferences appear reasonable: (1) in view of the overall similarity and equality of the C- and W-series data, it appears that the influence of traffic on dispersion is only present when the density is very high in both directions as with the W-series data; and (2) that the differences among the hi-lo/hi-hi and lo-lo/hi-hi comparisons reflect the range of experimental uncertainty and not some additional physical phenomenon.

Table 38

COMPARISON OF WIND TUNNEL CONCENTRATION DATA
FROM TEST SERIES C, V, AND W

Test Series	X*	Y*	Data Description	N	r	b*	a*	$(\overline{X/Q_\ell})$		rms	
	C	V						C	V	$(\Delta X/Q_\ell)$	$(\bar{C}/\bar{V})$
Right-of-way	Narrow	Narrow	All data	54	0.972	0.951	2.59	60.75	60.34	8.80	1.01
Surface roughness	Rough	Rough	Probe #3	18	0.977	1.080	-3.92	74.83	76.90	9.29	0.97
Traffic density	Lo-Lo	Hi-Lo	Probe #8	18	0.972	0.789	11.50	74.76	70.50	6.61	1.06
Traffic direction	Two-way	Two-way	Probe #12	18	0.967	0.934	3.11	32.76	33.62	5.02	0.97
			Oblique winds	36	0.962	0.923	3.19	60.47	58.98	8.85	1.03
			Parallel winds	18	0.984	0.982	2.88	61.33	63.07	8.05	0.97

Test Series	X*	Y*	Data Description	N	r	b*	a*	$(\overline{X/Q_\ell})$		rms	
	V	W						V	W	$(\Delta X/Q_\ell)$	$(\bar{V}/\bar{W})$
Right-of-way	Narrow	Narrow	All data	54	0.979	0.791	5.37	60.30	53.09	6.11	1.14
Surface roughness	Rough	Rough	Probe #3	18	0.975	0.758	9.11	76.85	67.39	7.45	1.14
Traffic density	Hi-Lo	Hi-Hi	Probe #8	18	0.971	0.770	8.45	70.45	62.68	5.36	1.12
Traffic direction	Two-way	Two-way	Probe #12	18	0.972	0.713	5.23	33.59	29.18	3.38	1.15
			Oblique winds	36	0.976	0.760	6.20	58.93	50.97	5.52	1.16
			Parallel winds	18	0.985	0.821	5.62	63.02	57.33	6.37	1.10

Test Series	X*	Y*	Data Description	N	r	b*	a*	(X/Q_ℓ)		rms	
	C	W						C	W	$(\Delta X/Q_\ell)$	$(\bar{C}/\bar{W})$
Right-of-way	Narrow	Narrow	All data	57	0.963	0.818	6.80	55.81	52.44	7.70	1.06
Surface roughness	Rough	Rough	Probe #3	19	0.968	0.873	6.81	67.65	65.86	7.52	1.03
Traffic density	Lo-Lo	Hi-Hi	Probe #8	19	0.947	0.667	16.95	70.63	64.04	6.99	1.10
Traffic direction	Two-way	Two-way	Probe #12	19	0.942	0.688	7.37	29.14	27.42	4.23	1.06
			Oblique winds	33	0.969	0.780	7.25	55.95	50.86	5.88	1.10
			Parallel winds	24	0.964	0.850	7.34	55.61	54.61	8.98	1.02

*$Y = a + b\,X$

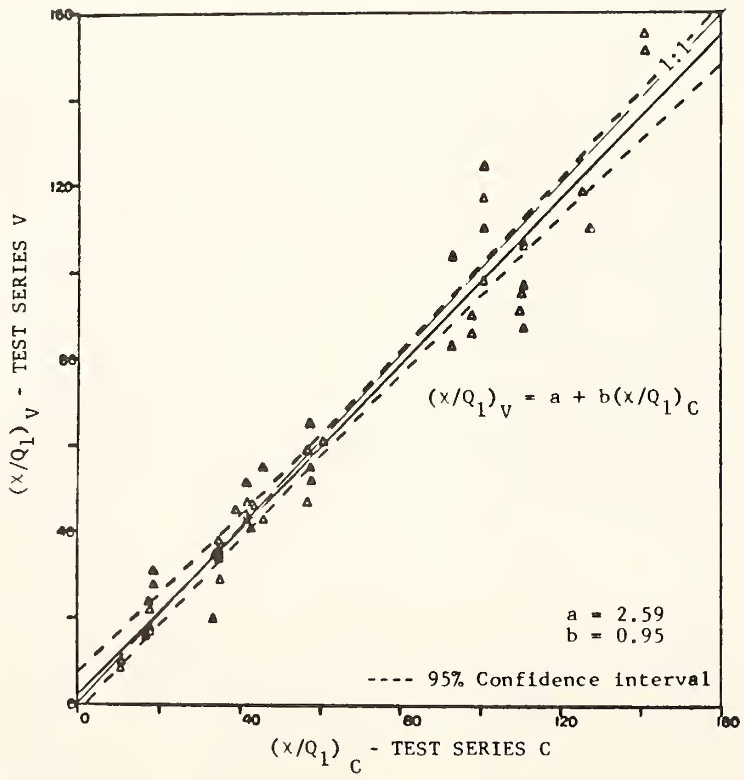

FIGURE 54 COMPARISON OF NORMALIZED CONCENTRATIONS (χ/Q_1) FROM TEST SERIES C (LO-LO TRAFFIC DENSITY) AND TEST SERIES V(HI-LO)

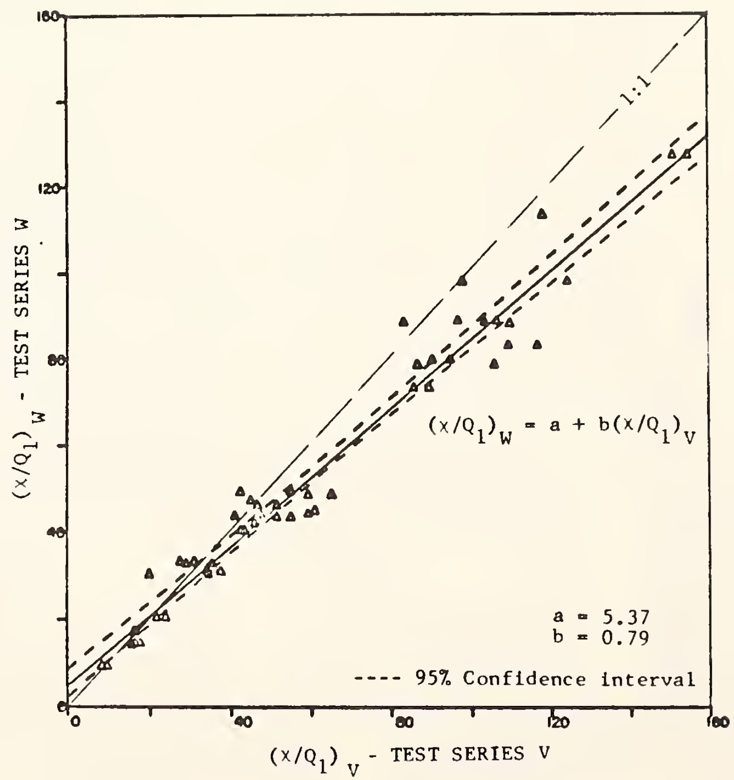

FIGURE 55 COMPARISON OF NORMALIZED CONCENTRATIONS (χ/Q_1) FROM TEST SERIES V (HI-LO TRAFFIC DENSITY) AND TEST SERIES W (HI-HI)

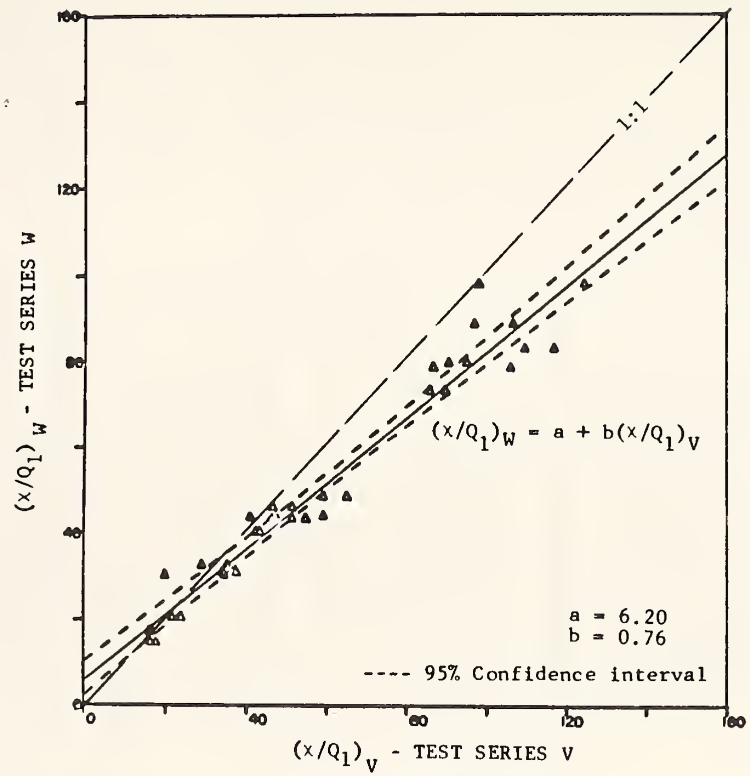

FIGURE 56 COMPARISON OF NORMALIZED CONCENTRATIONS (χ/Q_1) FROM TEST SERIES V AND W FOR OBLIQUE WIND ANGLES

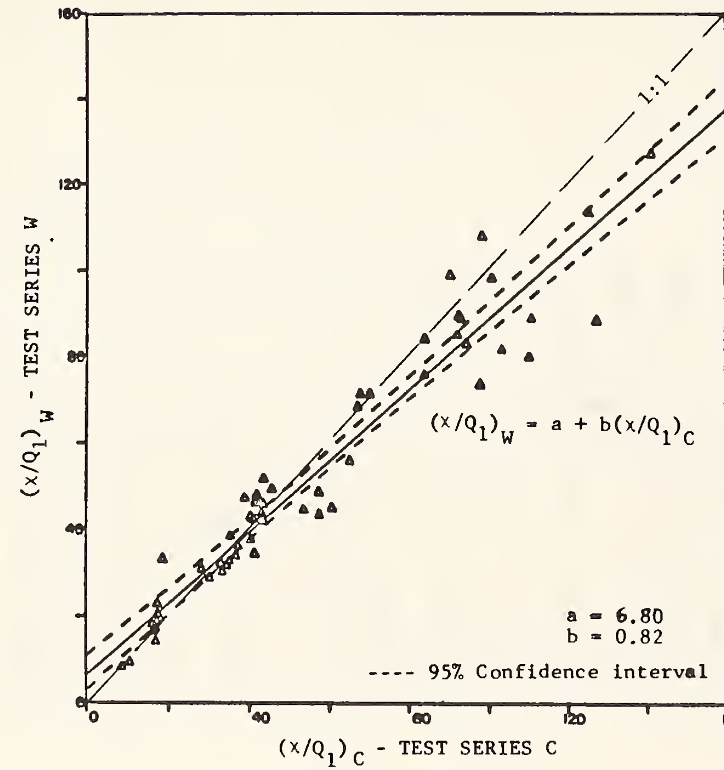

FIGURE 57 COMPARISON OF NORMALIZED CONCENTRATIONS (χ/Q_1) FROM TEST SERIES C (LO-LO TRAFFIC DENSITY) AND TEST SERIES W (HI-HI)

2. Effects Due to Traffic Direction

Table 39 and Figures 58 and 59 summarize the results of a comparison of normalized concentrations from test series S (smooth terrain, hi-hi traffic density, one-way traffic flow) and test series Q (smooth, hi-hi, two-way traffic). The comparison points out several noteworthy items. First, there is a large amount of scatter in the data: the rms difference between the two data series is 33% of the average value of the normalized concentration, although their means differ only by 12%. Second, the scatter in the data is largest at probes 8 and 12. The scatter is reduced considerably when the data are stratified by wind direction category; this is reflected by the correlation coefficients in Table 39.

The most pronounced difference is over the roadway--at probe 3. There the scatter in the data is small, and the concentrations with two-way traffic are 22% higher than with one-way traffic. This contrasts to an average 12% difference for all data.

In summary, traffic direction has a significant effect on concentrations over the roadway. Oddly enough, the concentrations there are lower with one-way traffic than they are with two-way. This may mean that the drag flow induced by the stream of vehicles is more effective in increasing the vertical dispersion than the increased mechanical turbulence that results from the interaction of two opposing traffic streams. This could indeed be the case if the mechanical mixing from the unidirectional traffic stream were sufficiently vigorous to (initially) uniformly diffuse the exhaust in the air layer immediately above the roadway (i.e., the so-called mixing cell); then the added turbulence within the mixing cell from two-way traffic would not affect the magnitude of the dispersion. On the other hand, the vertical wind profile generated by the Couette-type drag flow from the vehicle movement would have an effect on the vertical extent and intensity of the dispersion.

3. Effects of Traffic Speed

Concentration data from test series Q, R, and S were grouped into pairs of tests with similar roughness, traffic density, and wind speed

Table 39

COMPARISON OF WIND TUNNEL CONCENTRATION DATA
FROM TEST SERIES S AND Q

Test Series	X*	Y*	Data Description	N	r	b*	a*	$(\overline{\chi/Q_\ell})$		rms	
	S	Q						S	Q	$(\Delta\chi/Q_\ell)$	$(\bar{S}/\bar{Q})$
Right-of-way	Infinite	Infinite	All data	45	0.829	0.892	7.39	32.33	36.23	11.40	0.89
Surface roughness	Smooth	Smooth	Probe #3	15	0.938	1.118	2.88	28.73	35.00	9.46	0.82
Traffic density	Hi-Hi	Hi-Hi	Probe #8	15	0.382	0.281	36.11	44.08	48.49	9.68	0.91
Traffic direction	One-way	Two-way	Probe #12	15	0.634	0.602	10.63	24.18	25.18	8.49	0.96
			Oblique winds	27	0.794	0.744	10.58	30.26	33.08	10.65	0.91
			Parallel winds	18	0.878	1.080	2.65	35.44	40.94	11.15	0.87

*Y = a + b X

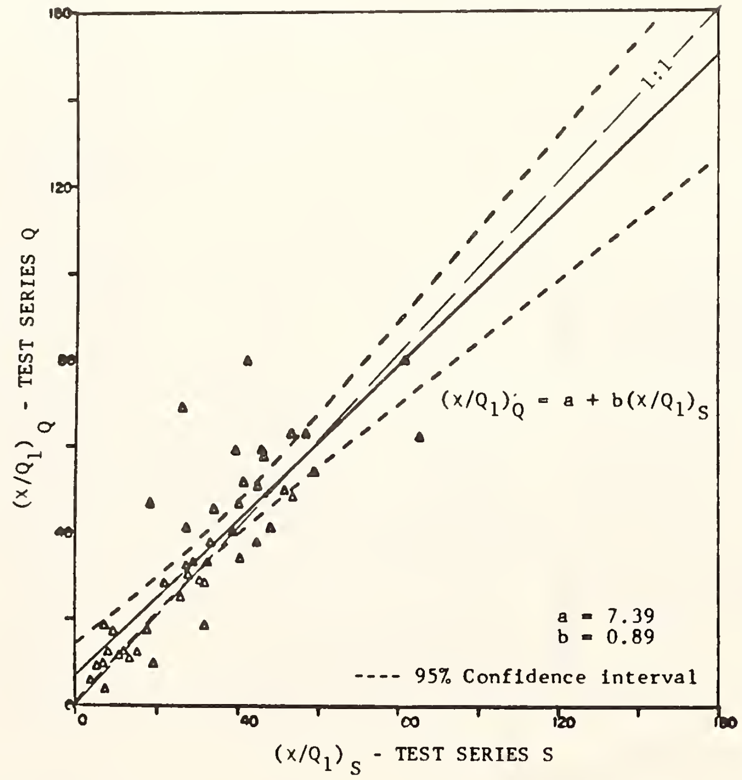

FIGURE 58 COMPARISON OF NORMALIZED CONCENTRATIONS (χ/Q_1) FROM TEST SERIES Q (TWO-WAY TRAFFIC) AND TEST SERIES S (ONE-WAY)

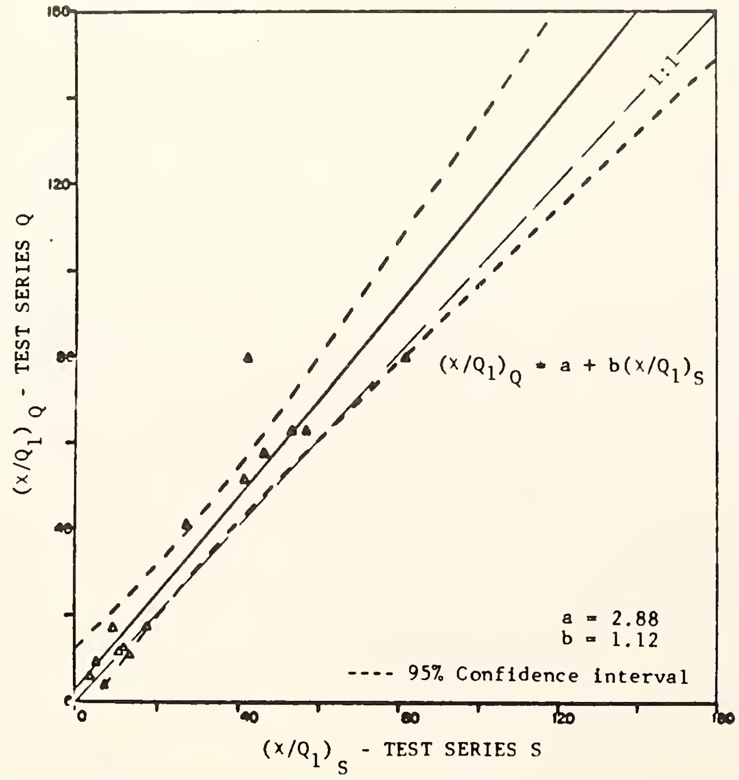

FIGURE 59 COMPARISON OF NORMALIZED CONCENTRATIONS (χ/Q_1) FROM TEST SERIES Q AND S FOR PROBE NUMBER 3

and direction, but different traffic speeds (i.e., 12.5 and 50 mph). As before, data from the twenty-two test pairs were analyzed at three locations--over the roadway (probe 3), adjacent to the roadway (probe 8), and distant (probe 12). Figures 60 and 61 are scatter plots of the data for parallel and oblique wind directions, respectively; also plotted are the linear regression line, 95% confidence intervals, and the equality (1:1) line. Statistics for these and other data stratifications are summarized in Table 40. The slope of the regression line for both the parallel and oblique data sets is 0.80, indicating a tendency for concentrations to be lower with the higher vehicle speeds. This trend is also reflected in the mean concentration values for the two data sets: the average concentration at the lower vehicle speed is about 7% higher than the value for the 50-mph speed. *

The effect from traffic speed is not so obvious when the data are grouped according to location. Figure 62 compares the data at a location immediately above the roadway. The mean values indicate a contrary tendency in that the lower-speed concentration average is actually 4% less than the higher-speed value. Referring again to the figure, there appears to be one value that is an outlier. When this is deleted, the averages for the two groups are virtually identical. The linear regression line, on the other hand, indicates concentrations associated with the lower traffic speed are higher than with the higher speed (as indicated earlier in Figures 60 and 61). However, the 1:1 line falls almost entirely within the 95% confidence intervals. In summary, it appears that over the roadway there are mixed indications regarding the impact of traffic speed on concentration.

Adjacent to the roadway edge (Figure 63) and farther away, there is more systematic indication that the higher-speed vehicles decrease concentration levels. Both the slope of the regression lines and the mean values support this effect. As seen in Figure 63, however, the data are scattered and so the precise magnitude of the impact cannot be quantified with confidence. But nearly all of the data pairs indicate some degree of reduction in concentration with the higher speed, with an average reduction of the order of 10%.

*See Vol. II, page 104

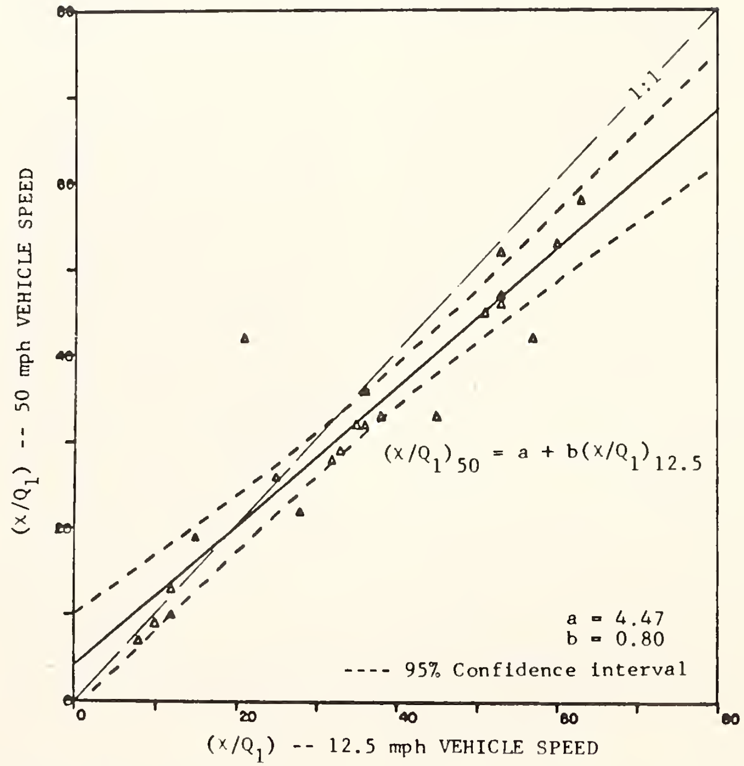

FIGURE 60 COMPARISON OF NORMALIZED CONCENTRATIONS WITH 12.5- AND 50-MPH VEHICLE SPEEDS, AND PARALLEL WINDS

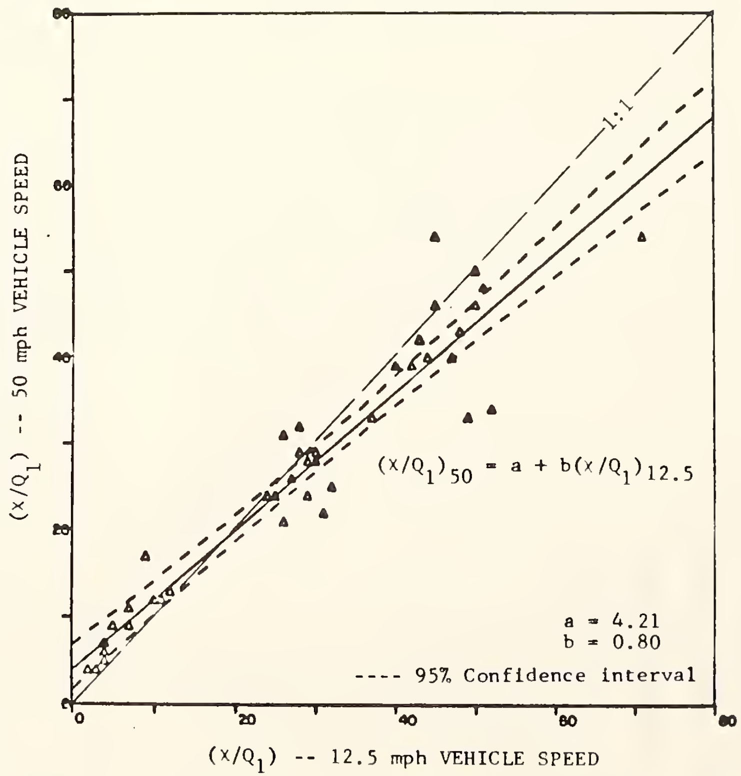

FIGURE 61 COMPARISON OF NORMALIZED CONCENTRATIONS WITH 12.5- AND 50-MPH VEHICLE SPEEDS, AND OBLIQUE WINDS

Table 40

COMPARISON OF WIND TUNNEL CONCENTRATION DATA
AT TRAFFIC SPEEDS OF 12.5 mph AND 50 mph

Data Description	N	r	b*	a*	$(\overline{\chi/Q_\ell})$		$\Delta(\chi/Q_\ell)$	$(\bar{X}/\bar{Y})$
					X(12.5 mph)*	Y(50 mph)*		
All data	66	0.950	0.801	4.24	30.88	28.97	4.81	1.07
Probe #3	22	0.954	0.818	4.47	19.77	20.64	5.28	0.96
Probe #8	22	0.784	0.683	10.42	46.77	42.36	4.93	1.10
Probe #12	22	0.882	0.716	5.23	26.09	23.91	3.61	1.09
Oblique winds	42	0.931	0.801	4.47	36.46	26.29	4.42	1.05
Parallel winds	24	0.931	0.801	4.47	36.46	33.67	5.41	1.08

*Y = a + b X

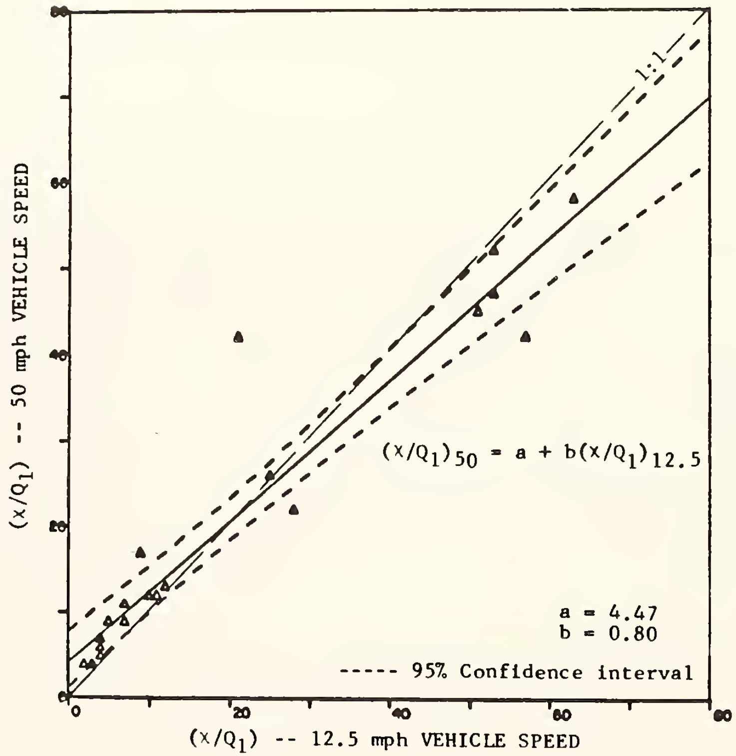

FIGURE 62 COMPARISON OF NORMALIZED CONCENTRATIONS WITH 12.5- AND 50-MPH VEHICLE SPEEDS, AT PROBE NUMBER 3 (OVER ROADWAY)

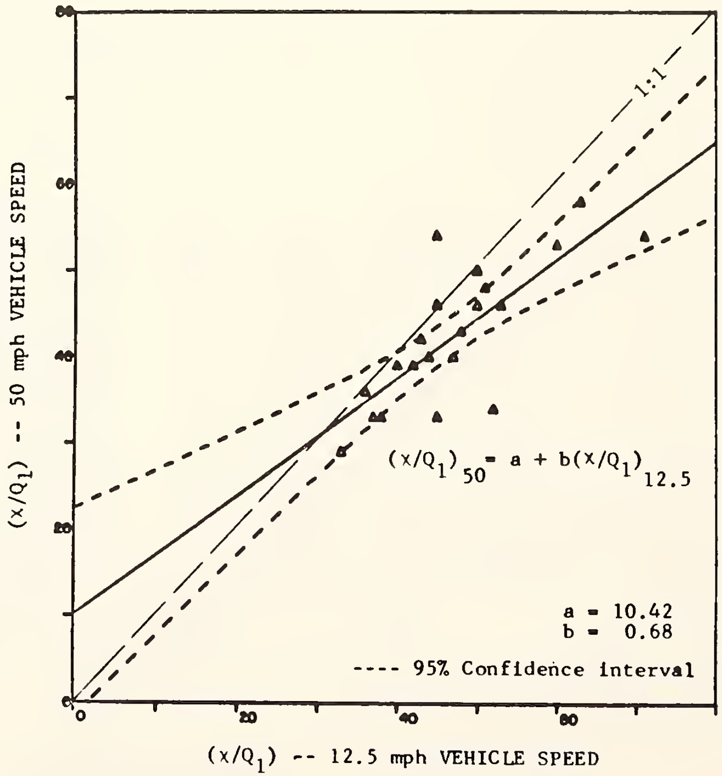

FIGURE 63 COMPARISON OF NORMALIZED CONCENTRATIONS WITH 12.5- AND 50-MPH VEHICLE SPEEDS, AT PROBE NUMBER 8 (ADJACENT TO ROADWAY)

C. Summary

Factor analysis and multiple-regression analysis techniques have been used to evaluate further the significance of traffic variations on near-roadway dispersion patterns. In the first phase of this analysis, the roadway configuration was not varied; the simple grade-level roadway was used to avoid the aerodynamic complexities of the other test configurations. Seven such test series were analyzed; the series differed only in the density and direction of the traffic streams and the roughness of the surrounding terrain. Multiple-regression analyses among the factor scores and a variety of wind and traffic parameters indicated two important findings:

- When factor scores are derived from the concentration data from all sampling locations for all seven tests and multiple correlations are calculated between the factor scores and the environmental variables (e.g., wind, traffic speed) for all tests, the effect of wind speed is a minor determinant of the concentration patterns.
- When the factor scores calculated from the composite data set are correlated with the environmental variables for each of the individual test series, vehicle speed is a significant determinant for several of the seven tests considered.

The second phase of this analysis was directed toward achieving a closer evaluation of the effect of vehicle speed variations alone. Five test series were selected for this analysis: one of the original seven used earlier and four additional series. The five had virtually identical traffic and meteorological conditions, but differed principally in the nature of the roughness of the ground surface for these grade-level configurations. The analysis did not indicate vehicle speed to be a significant determination of the concentration patterns, neither when the multiple regression was performed for the composite data set nor when each of the five sets were treated individually.

Together, these two analyses indicate that vehicle speed can be an important determinant of pollution dispersion on and near the roadway, but only for certain selected roadway configurations. For the test series considered here, these configurations were those where the roadway right-of-way was narrow with very rough terrain (i.e., typical of multiple story residential dwellings) on both sides.* However, as a general conclusion, these analyses indicated an overall insensitivity of the pollution patterns near the roadway to variations in traffic speed.

A third examination of possible traffic influences on dispersion was made using parametric analyses of data from various grade-level test series to further explore differences in the concentration patterns that might be due to traffic variations when all other roadway, surface, and meteorological conditions were the same. In this way, the effects of traffic density, traffic direction, and traffic speed were analyzed separately with the following results:

- When the surrounding terrain is smooth to both sides of the roadway, variations in traffic density showed no effect on concentrations.
- When the surrounding terrain was very rough, high-density traffic in both directions has corresponding normalized concentration levels that averaged about 10% lower than with low-density traffic in either one or both directions. This likely reflects the constraint on the air flow by the neighboring roughness elements.
- Surprisingly, two-way traffic (high density, and smooth terrain) was accompanied by concentrations over the roadway that averaged 18% higher than with one-way traffic; however, the scatter in the data was quite large. Variations in traffic speed show no effect on concentrations over the roadway, while farther away 10% average reductions are noted with 50-mph speeds compared to 12.5-mph traffic speeds. The pattern was independent of the wind/roadway orientation. Comparison of concentrations from idling vehicles and traffic moving steadily at 50 mph indicated an overall increase in concentrations from the idling vehicles of about 25%; the increase was independent of sampling location and wind conditions.

*Note that cut sections were not included in the 11 test series included in these two analyses.

V ROADMAP: A NEW, EMPIRICAL ROADWAY ATMOSPHERIC DISPERSION MODEL FOR AIR POLLUTION

A. ROADMAP Description

One objective of this study was to develop a simulation model that would both: (1) represent the interrelationship among independent atmospheric and geometric variables and the dependent variable, pollutant concentration near the roadway, and (2) be readily applicable, yet accurate. These characteristics of the model are important to satisfy the contractual requirement that the "final product ... be a practical, versatile, and objective procedure to evaluate local contributions to the nearby air quality and to aid in air quality management." The development and application of ROADMAP is described here, while its role and application in the evaluation of air quality impacts is the focus of Volume II of the final report.

In considering the framework for such a model, four approaches were considered: (1) gradient transfer, (2) Gaussian, (3) statistical, and (4) empirical. The first three methods were eventually rejected for various reasons: The gradient transfer method requires the specification of the eddy diffusivity at each of a large number of grid points; these values are not known nor could they easily be estimated. But more fundamentally, the flux-gradient assumption that is the basis of this approach cannot be expected to apply near the roadway where the steady-state vertical wind profile structure is destroyed by the aerodynamic effects of the cars and roadway configuration. (Moreover, there are additional drawbacks that would arise in trying to implement the methodology without benefit of a sophisticated computer.) The common Gaussian line source equation suffers from not being able to jointly simulate (with reliability) configuration effects and acute wind-roadway angles. Statistical models, although capable of reproducing observed concentration patterns, do not provide the user with a model that aids in understanding the physics of the dispersion process; also, their application to other site types may be less reliable than the other approaches. The empirical approach, however, overcomes most of the limitations of the three other models in that it is: flexible, easily applied, inexpensive, and (for most configurations tested) reliable.

The foundation of the model is the approach used to represent the dispersion of pollutants from an extended line source (end effects are not considered). The model treats the total dispersion as the vector sum of two components; one is the dispersion along the horizontal wind component normal (perpendicular or lateral) to the roadway, the other is the dispersion along the horizontal wind component parallel (longitudinal) to the roadway:

$$\frac{\chi_T U}{Q_\ell} = \vec{i}\left(\frac{\chi_n u}{Q_\ell}\right) + \vec{j}\left(\frac{\chi_p v}{Q_\ell}\right) \qquad (34)$$

where

$\vec{i}$ = unit vector normal to roadway
$\vec{j}$ = unit vector parallel to roadway
U = vector wind speed (m/s)
u = wind component normal to roadway (m/s)
v = wind component parallel to roadway (m/s)
Q_ℓ = line source emission flux density (g/m-s)
χ_T = total pollutant concentration (g/m^3)
χ_n = concentration from lateral dispersion (g/m^3)
χ_p = concentration from longitudinal dispersion (g/m^3).

When Θ is introduced as the angle between the longitudinal axis of the line source and the wind vector, then

$$u = U \sin \Theta \quad , \qquad (35a)$$

and

$$v = U \cos \Theta \quad . \qquad (35b)$$

Substituting Eq. (35) into Eq. (34) and squaring both sides,

$$\left[\frac{\chi_T U}{Q_\ell}\right]^2 = \left[\frac{\chi_n U \sin \Theta}{Q_\ell}\right]^2 + \left[\frac{\chi_p U \cos \Theta}{Q_\ell}\right]^2 . \tag{36}$$

For convenience, the first right-hand term in Eq. (36) is designated the "perpendicular" term and the second, the "parallel" term.

The form of the perpendicular term is specified in analogy to the Gaussian line source equation for a perpendicular wind,

$$\left[\frac{\chi_n U}{Q_\ell}\right] = \frac{\sqrt{2/\pi}}{k\sigma_z} \left\{ \exp\left[\frac{-1}{2}\left(\frac{z + z' - H}{\sigma_z}\right)^2\right] + \exp\left[\frac{-1}{2}\left(\frac{z + z' + H}{\sigma_z}\right)^2\right] \right\} \tag{37}$$

where

- z = height above ground for grade-level roadways and elevated roadways, and the height above the road surface for depressed sections (m)
- k = constant; for depressed and grade-level sections, it is equal to two, and for elevated sections it is one (n.d.)
- σ_z = vertical Gaussian dispersion function (m)
- z' = height offset (e.g. due to plume rise) (m)
- H = roadway height above grade-level; equal to zero for grade-level and depressed sections (m)

A unique feature of Eq. (37) is the term z' which serves as a height-modifier to represent the possible change in the height of the plume centerline as a function of distance downwind. This offset could result either from the aerodynamic influence (i.e., shelterbelt) of the traffic stream or from the buoyancy effect of vehicular waste heat emissions. In principle, both σ_z and z' may vary both with distance (x) away from the roadway and atmospheric stability, but not with height. Distance, x, is measured perpendicular to the highway with the origin located at the center of the line source (Q_ℓ). In normal practice, each traffic stream is treated as a separate line source; however, roadways with four or more lanes in each direction may need to be represented by multiple line sources for each stream, while narrow roadways may be represented by a single line source for both streams. (For the case of the 101 study, each of the two three-lane traffic streams was represented by a single line source with x=0 in the middle of each center lane.)

The parallel dispersion term was formulated to represent the general features of the Gaussian point source equation when the latter is integrated for a wind aligned parallel to a semi-infinite line source (see Dabberdt and Sandys, 1976). The resulting formulation may be thought of as a type of expanding-box model where the sides and top of the box are given as exponential functions of height (z) and cross-roadway distance (x). The form chosen assumes the same functional dependence on height as the perpendicular term, but a different cross-roadway dispersion representation (f):

$$\left[\frac{\chi_p U}{Q_\ell}\right] = \frac{1}{k\sigma_{z-o} f} \left\{ \exp\left[\frac{-1}{2}\left(\frac{z+z'-H}{\sigma_z}\right)^2\right] + \exp\left[\frac{-1}{2}\left(\frac{z+z'+H}{\sigma_z}\right)^2\right] \right\}, \quad (38)$$

where

$$\sigma_z = \sigma_{z-o} + a_1 x^{b_1} \quad , \quad (39a)$$

$$z' = z'_o + a_2 x^{b_2} \quad , \quad (39b)$$

$$f = a_3 \left(c_3 + \frac{2x}{W}\right)^{b_3} \quad (39c)$$

and

W = roadway width (m).

When the model is applied to both traffic streams, W is defined as the total roadway width (i.e., from shoulder-to-shoulder). On the other hand, physical separation of the traffic streams or marked dissimilarities in the traffic volumes (and hence emissions) may suggest application of the model separately for each direction. In this case, W would, of course, be redefined accordingly.

As indicated later in the analyses of the test data, the height-offset term (z') may be either positive or negative. [Note: When assessing the net effect of this term, it is useful to consider the square of $z+z'\pm H$ rather than z' alone.] The vertical dispersion term σ_z consists of two parts: first, there is the initial mixing that results from vehicle aerodynamic effects that is given by σ_{z-o}; the second term then describes the vertical growth of the pollutant 'plume' as it is dispersed by the ambient wind downwind of the source. *The lateral dispersion function* $f\sigma_{z-o}$ *is an empirical analogy to the vertical dispersion term. Like its vertical counterpart, the lateral term also has a minimum value given by the value of f at the roadway edge. In effect, then, both the vertical and lateral dispersion terms have minima over the roadway that cause ROADMAP to reduce to a box model over the roadway. With these minima for* σ_z *and* $f\sigma_{z-o}$*, concentrations can be estimated over the roadway itself.*

Evaluation of the coefficients in Eqs. (39a-c) is described in the following section. Also discussed is the procedure used to evaluate ROADMAP predictions.

B. Model Evaluation Procedure

A least-squares technique was used to estimate the coefficients of the model. Suppose the generalized nonlinear equation is of the form

$$Y = f(X_1, X_2, \ldots, X_K, \beta_1, \beta_2, \ldots \beta_p) \quad , \tag{40}$$

where f is a nonlinear function of k independent variables $X_1, \ldots, X_K$ and p coefficients $\beta_1, \ldots, \beta_p$. We want to choose estimated values of the coefficients such that the sum of squared errors is minimized. If we have T observations on $Y, X_1, \ldots, X_K$, then the sum of squared errors is

$$S = \sum_{t=1}^{T} [Y_t - f(X_{1t}, \ldots X_{Kt}, \beta_1, \ldots, \beta_p)]^2 \quad . \tag{41}$$

To minimize S with respect to the βs, one differentiates the right side of this equation with respect to each coefficient and sets the derivatives equal to zero:

$$\sum_{t=1}^{T} 2[Y_t - f(X_{1t},\ldots,X_{Kt},\beta_1,\ldots,\beta_p)] \frac{\partial f}{\partial \beta_i} = 0 \text{ ,for } i = 1,\ldots,p \quad . \qquad (42)$$

Rather than solving these equations simultaneously, the SPSS program (Nie et al., 1975) used employs the steepest-descent method, an iterative process, to find the minimum of S. This method moves from one set of coefficient values for $\beta_1,\ldots\beta_p$ to a new set in such a way that the derivatives (calculated numerically) $\frac{-\partial s}{\partial \beta_1}$,... $\frac{-\partial s}{\partial \beta_p}$ are as large as possible, so that those values of $\beta_1,\ldots\beta_p$ that minimize S are reached rapidly.

Two potential pitfalls exist with this method. First, the minimum of S found may be a local rather than a global minimum. Suppose that the graph of the sum of squared errors for a nonlinear function with one coefficient to be estimated looks like:

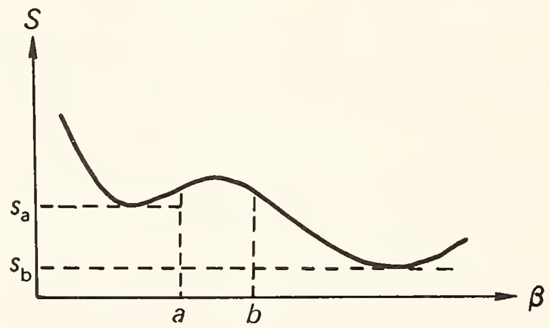

If the initial trial coefficient-estimate is a, the minimum found by this method will be at S_a, a local minimum, while if the initial estimate is b, the global minimum S_b ($<S_a$) will be reached. This example illustrates the importance of the initial coefficient estimates to the method's ability to find a global minimum. The only way to test the kind of

minimum a particular set of coefficient estimates represents is by repeating the estimation procedure for different sets of initial estimates and comparing the resulting sums of squared residuals. Even so, there is no guarantee that the smallest of these sums represents a global minimum. The second pitfall is that the coefficient estimates may not converge at all. Because of the form of the partial derivatives, it may be impossible to obtain coefficient estimates that represent even a local minimum of the sum of squared errors.

The only measure of the efficiency of the solution provided by the SPSS program (aside from the explained variance) is the number of digits of accuracy, d. Let $\Phi(\beta)$ be the sum of squared errors at the point $\beta = (\beta_1, \ldots \beta_p)$. A point $\beta^* = (\beta_1^*, \ldots \beta_p^*)$ is a d-digit solution if $\Phi(\beta^*) < \Phi(\beta)$ for all β that satisfy: $10^{-d} < \mathrm{rel}_{AX}(\beta^*, \beta) \leq 10^{-d+1}$, where

$$\mathrm{rel}_{AX}(\beta^*, \beta) = \max_{1 \leq i \leq p} \left(\frac{|\beta_i^* - \beta_i|}{\max(|\beta_i^*|, |\beta_i|, AX} \right) \tag{43}$$

In the runs of the program to estimate the model, AX was set to 0.1 and d to 3. When it is impossible to find a 3-digit solution (because of rounding errors or the nature of the model), the program stops and prints an accuracy estimate with the final coefficients.

In practice, the procedure to evaluate the nine coefficients of the model (a_1, b_1, σ_{z-o}, a_2, b_2, z_o', a_3, b_3, and c_3) consisted of the following four steps:

Step 1--The experimental tests were first stratified according to atmospheric stability. All wind tunnel tests were representative of neutral conditions, while the atmospheric tests included stable, neutral, and unstable conditions.

Step 2--Coefficients a_1, b_1, σ_{z-o}, a_2, b_2, and z_o' were estimated using Eq. (37) and those test data with near-orthogonal wind/roadway angles (Θ). For the wind tunnel tests, Θ-values $\geq 60°$ were used, while for the atmospheric tests $\Theta \geq 63°$. The variance (r^2) explained by the estimated coefficients and Eq. (37) was also determined for the large-Θ cases.

Step 3--Next, coefficients a_3, b_3, and c_3 were estimated using Eq. (38), along with the other coefficient estimates from Step 2, and those test data with near-parallel wind/roadway angles. For the wind tunnel tests, Θ-values $\leq 15°$ were used, while for the atmospheric tests $\Theta \leq 24°$. Again, r^2 was determined.

Step 4--Eqs. (37) and (38) were substituted into the general model form, Eq. (36), together with the nine coefficient estimates from Steps 2 and 3. In this way, the component ROADMAP model was used to predict normalized concentrations for all observed data. Observations and predictions were then compared for all data, as well as for various subsets including those cases not included in the coefficient estimates of Steps 2 and 3; the latter provide an independent test of ROADMAP performance.

Results of the evaluation procedure and the attendant implications are discussed in detail in Section VI.

VI ROADMAP ANALYSIS OF WIND TUNNEL AND ATMOSPHERIC DATA

A. Grade-Level Configurations

1. Wind Tunnel Tests

Table 41 summarizes the results of the ROADMAP analyses for wind tunnel test series Q, C, D, I, and J. The Q series is most compatible with the ideal concept of a simple grade-level configuration. The terrain was smooth, stability was neutral, and the traffic exhibited equal density and speeds in each of the two directions. As such, the Q series provides a good basis for both evaluating ROADMAP and assessing the representivity of the wind tunnel simulations. The latter is described in Part 3 of this subsection.

Figure 64 illustrates the variation of σ_z, z', and $f\sigma_{z-o}$ with normal distance (x) from the roadway center for the Q-series data. The gradual increase in σ_z with x is not unusual. However, z' is nearly independent of x with a value of about -1 m, indicating a slight and constant offset in the plume-centerline height above ground level. The lateral dispersion function $f\sigma_{z-o}$ represents the combined effect of initial vertical mixing at the roadway and the horizontal diffusion perpendicular to the along-roadway wind component (v). The marked increase in the lateral dispersion with increasing x results in relatively low concentrations even near the roadway edge (located at x = 11.4 m for all wind tunnel tests). This contrasts with the more limited lateral dispersion assumed in line source models that integrate the Gaussian point source. HIWAY (Zimmerman and Thompson, 1975), for example, has been evaluated by Dabberdt et al. (1976) and has been found to consistently and significantly overpredict when v is small (i.e., small θ).

Table 41 provides r^2-values associated with estimation of the coefficients. Using data with $\theta = 90°$ only, the perpendicular term explains

Table 41

SUMMARY OF ROADMAP ANALYSES FOR GRADE-LEVEL ROADWAY CONFIGURATIONS

Test Series	Perpendicular Dispersion Term									Parallel Dispersion Term						Two-Component Model				
	θ	N	a_1	b_1	c_1	a_2	b_2	c_2	R^2	θ	N	a_3	b_3	c_3	R^2	θ	N	R^2	m^*	$s^†$
Q	90	5	0.656	0.448	0.358	1.62	0.026	-2.78	0.910	0,15	13	0.0324	3.90	2.23	0.641	All 0,15 30 60,90	30 13 8 9	0.656 0.488 0.850 0.924	0.0676 0.141 0.0547 0.0086	0.635 0.477 0.616 0.899
C	60,90	8	1.07	0.731	-3.25	36.8	-17.5	-1.49	0.154	0,15	8	-0.810	2.01	0.196	0.735	All 0,15 30 60,90	20 8 4 8	0.241 0.115 0.378 0.348		
D	60,90	8	0.154	0.878	2.15	-18.4	0.0029	19.1	0.825	0,15	8	0.0070	3.49	4.09	0.615	All 0,15 30 60,90	20 8 4 8	0.631 0.493 0.801 0.824		
I	90	4	0.0282	1.41	2.89	-8.09	0.0258	7.77	0.818	0,15	8	0.0939	2.78	1.50	0.827	All 0,15 30 90	16 8 4 4	0.494 0.579 0.369 0.818		
J	90	4	0.0956	0.957	0.642	-0.0166	1.46	-1.10	0.957	0,15	8	0.0060	3.84	3.94	0.215	All 0,15 30 90	16 8 4 4	0.266 0.376 0.909 0.957	0.148 0.183 0.066 0.018	0.730 2.54 1.78 0.958
101-CO Neutral	≥63	4	0.411	0.641	-1.90	1.47	-0.0733	-2.68	0.763	≤18	3	-0.0181	1.79	11.9	0.085	All >18,<63	13 6	0.354 0.824	0.111 0.084	0.872 1.06
101-CO Stable	69,87	2	0.274	0.844	0.856	-0.781	0.371	3.87	0.469	--	0	0.0181 (from 101-CO, neutral)	1.79	11.9	--	All <69	7 5	0.514 0.444	0.008 0.000	0.496 0.513
101-CO Unstable	67,79	2	0.330	0.686	-0.872	2710.	-3.87	-2.42	0.584	9,24	2	-5.15	0.372	-1.27	0.144	All >24,<67	9 5	0.642 0.645	0.040 0.035	0.724 0.710
Upwind Neutral‡	≥63	4	-6.94	-0.0783	6.78	-0.006	1.58	-1.82	0.684	≤18	3	0.0533	0.914	1.02	0.127	All >18,<63		0.476 0.538	0.121 0.156	0.862 0.788
Downwind Neutral‡	≥63	4	0.0030	1.54	0.765	-0.150	0.621	-0.729	0.636	≤18	3	0.0538	1.95	4.50	0.296	All >18,<63		0.564 0.644	0.140 0.155	0.813 0.862
Upwind Stable‡	69,87	2	0.295	0.775	0.236	-33.4	-1.74	-1.23	0.385	--	0	0.0533 (from upwind, neutral)	0.914	1.02	--	All <69		0.432 0.529		
Downwind Stable‡	69,87	2	0.739	0.534	0.993	1.79	0.0375	-1.90	0.643	--	0	0.0538	1.95	4.50	--	All <69		0.288 0.238	0.025 0.034	0.734 0.700
Upwind Unstable‡	67,79	2	-217.	-1.92	2.60	-0.0210	0.992	-1.63	0.422	≤24	3	0.0061	2.37	4.99	0.384	All >24,<67		0.321 0.272	0.082 0.098	0.746 0.664
Downwind Unstable‡	67,79	2	0.154	0.242	1.15	-0.360	0.830	2.90	0.300	≤24	3	1.37	0.0962	-1.51	0.008	All >24,<67		0.317 0.334	0.137 0.145	0.487 0.505

*m - intercept

†s slope

‡tracer data

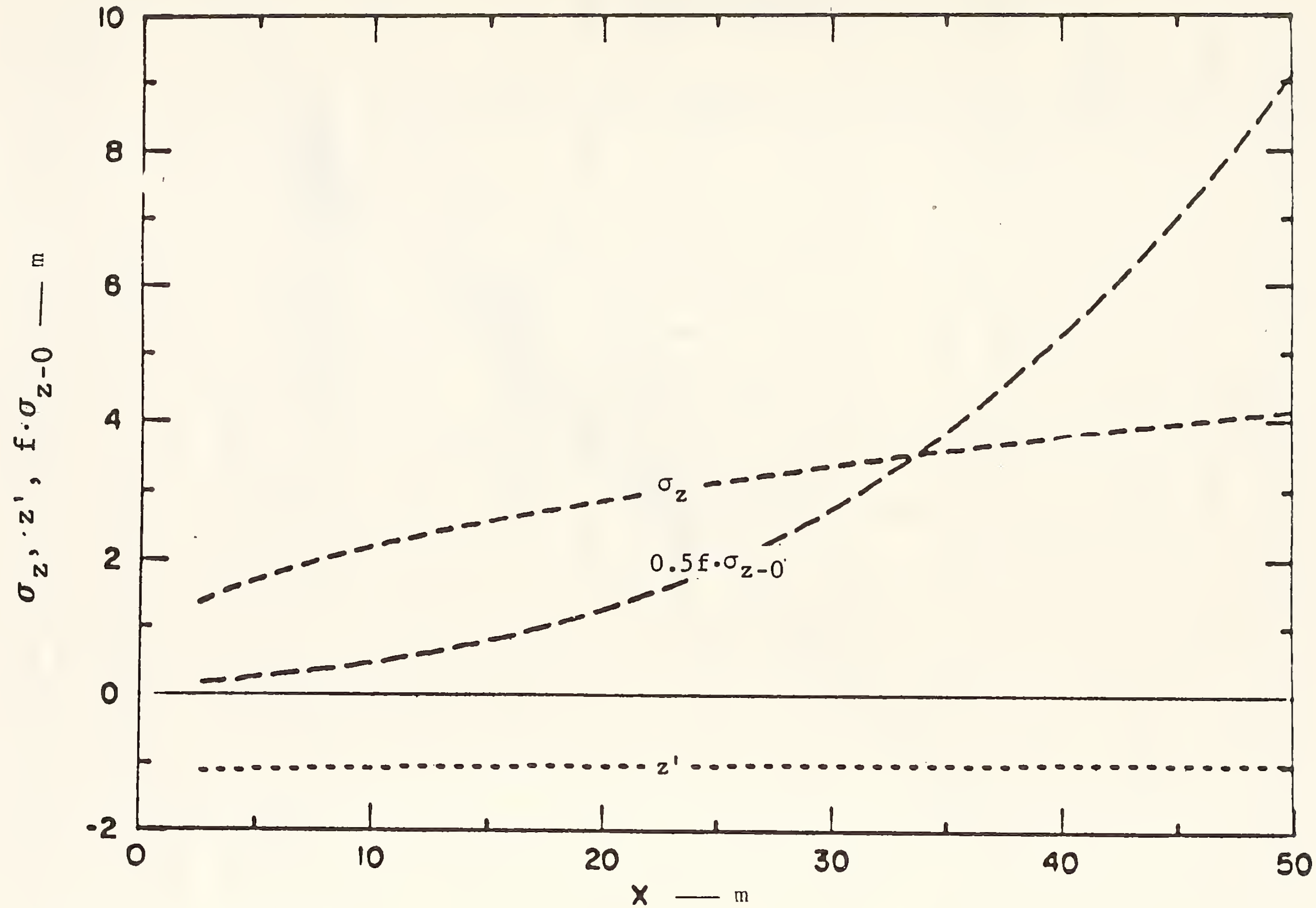

FIGURE 64 VARIATION OF ROADMAP DISPERSION PARAMETERS WITH CROSS-ROADWAY DISTANCE FOR WIND TUNNEL SERIES Q

91% of the variance (r = 0.954)*; for $\theta = 0°$ and 15°, the parallel term alone explains 64% of the variance (r = 0.801). When the two-component model is used to predict all observations, $r^2 = 0.66$ (r = 0.810); for data with $\theta = 30°$ only, $r^2 = 0.850$ (r = 0.922). Figure 65† illustrates the comparison of Q-observations and ROADMAP predictions for all wind/roadway angles tested. The observations represent sampling points that range in x from 0.01 m (roadway center‡) to 36 m, and in z from 2.29 m to 12.20 m; the four different sampling heights are indicated by different symbols on the figure. Also shown on the figure is the linear regression line, equation, and 95%-confidence intervals. Figures 66 and 67 illustrate the model/data comparison for θ-values of 0°, 15° and 30°, 60°, 90°, respectively.

Test series C had a vastly different setting. The ground was very rough, and the roughness elements encroached on the right-of-way to form what may be thought of as a porous street canyon (Figure 12). Figure 68 illustrates σ_z, z', and $f \cdot \sigma_{z-o}$. Comparing these functions with the Q-series values: (1) z' is again independent of x, although its magnitude has changed from about -1 m to about -2 m; (2) σ_z-values are also increased (about 250%, at x = 35 m) reflecting the increased surface roughness, and (3) the lateral mixing occurs at a rate essentially twice that for the smoother surface. However, the importance and meaning of the σ_z and z' terms is uncertain for the C series in view of the large unexplained variance. As seen in Table 41, the perpendicular term explains but 15% of the variance in the data for the 60° and 90° cases; even when the two-component model is used (i.e., when the parallel term is considered)§, r^2 increases to only 0.35 (r = 0.59) for $\theta = 60°$ and 90°. On the other hand, the parallel term alone has an associated $r^2 = 0.74$ (r = 0.86) for

---

*r is the linear correlation coefficient.

†Note that in Figures 65 through 104, the intercepts of the scattergrams are not necessarily zero and the scales of the ordinates and abscissas are usually different; these inconsistencies have been introduced in an attempt to enhance the data-area of each figure.

‡x was not set precisely equal to zero to avoid potential mathematical instabilities in the analysis.

§Note that the 90°-calculations do not include the parallel term.

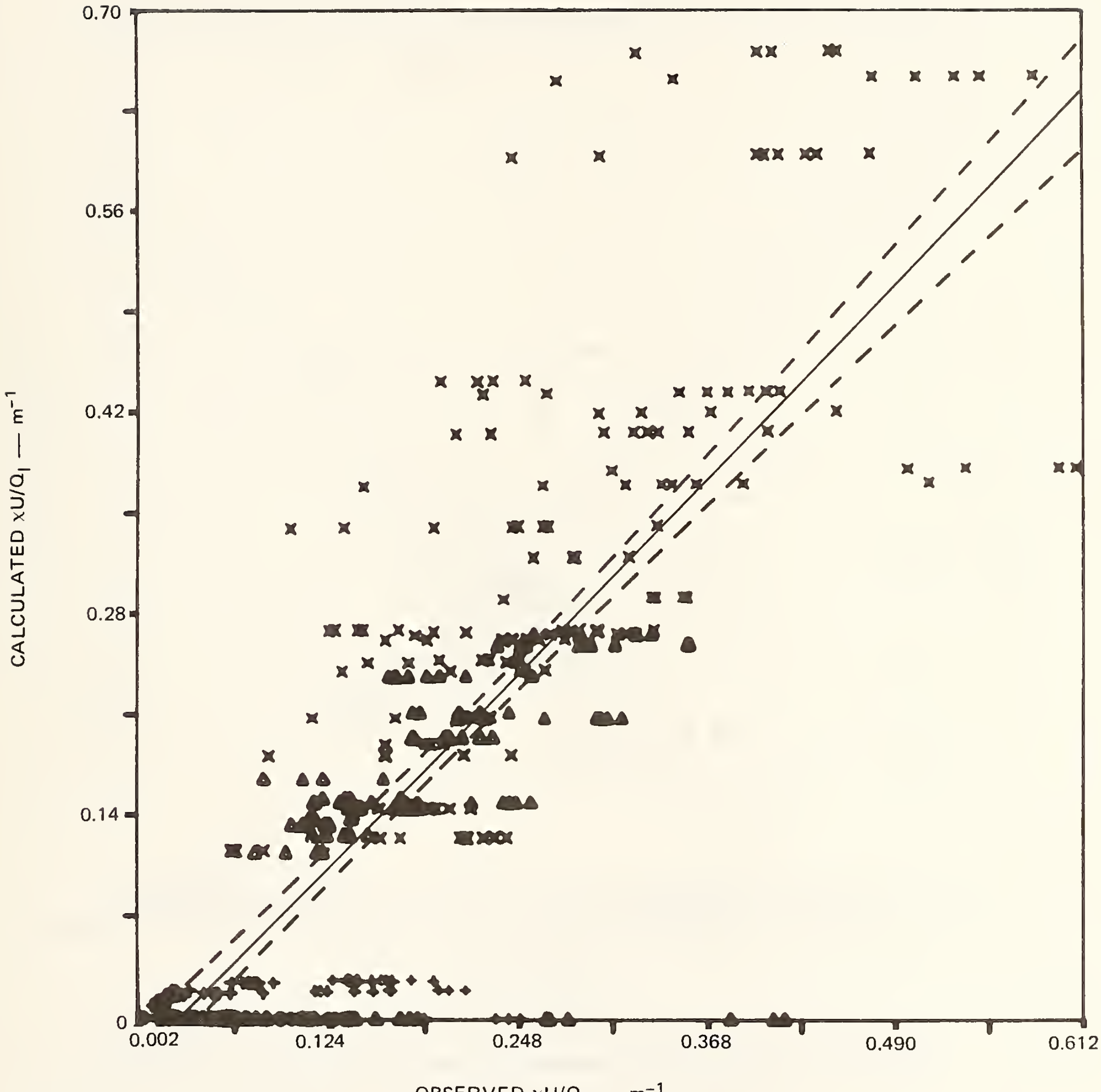

FIGURE 65 COMPARISON OF OBSERVED NORMALIZED CONCENTRATION WITH ROADMAP CALCULATION FOR WIND TUNNEL SERIES Q, ALL WIND ANGLES

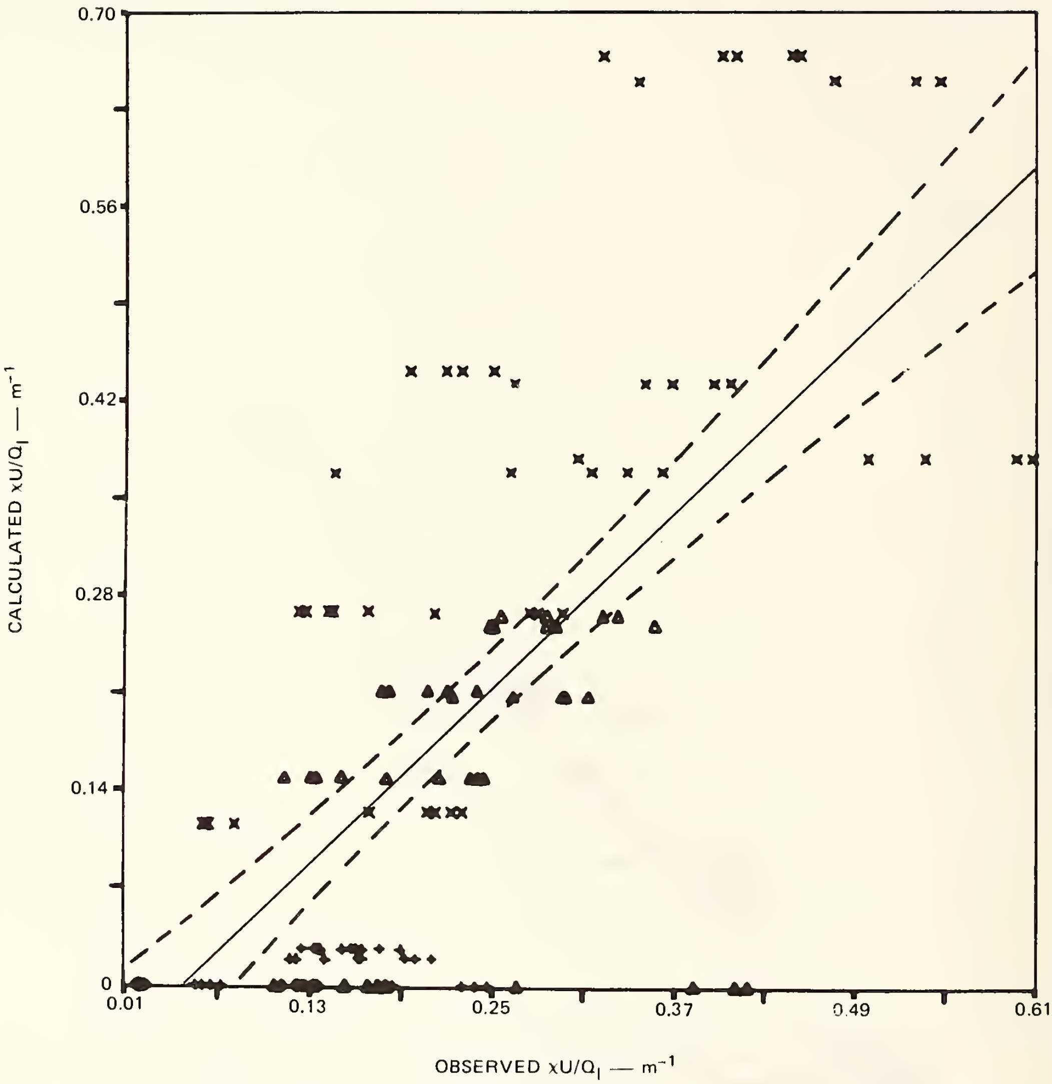

FIGURE 66 COMPARISON OF OBSERVED NORMALIZED CONCENTRATION WITH ROADMAP CALCULATION FOR WIND TUNNEL SERIES Q; θ = 0° AND 15°

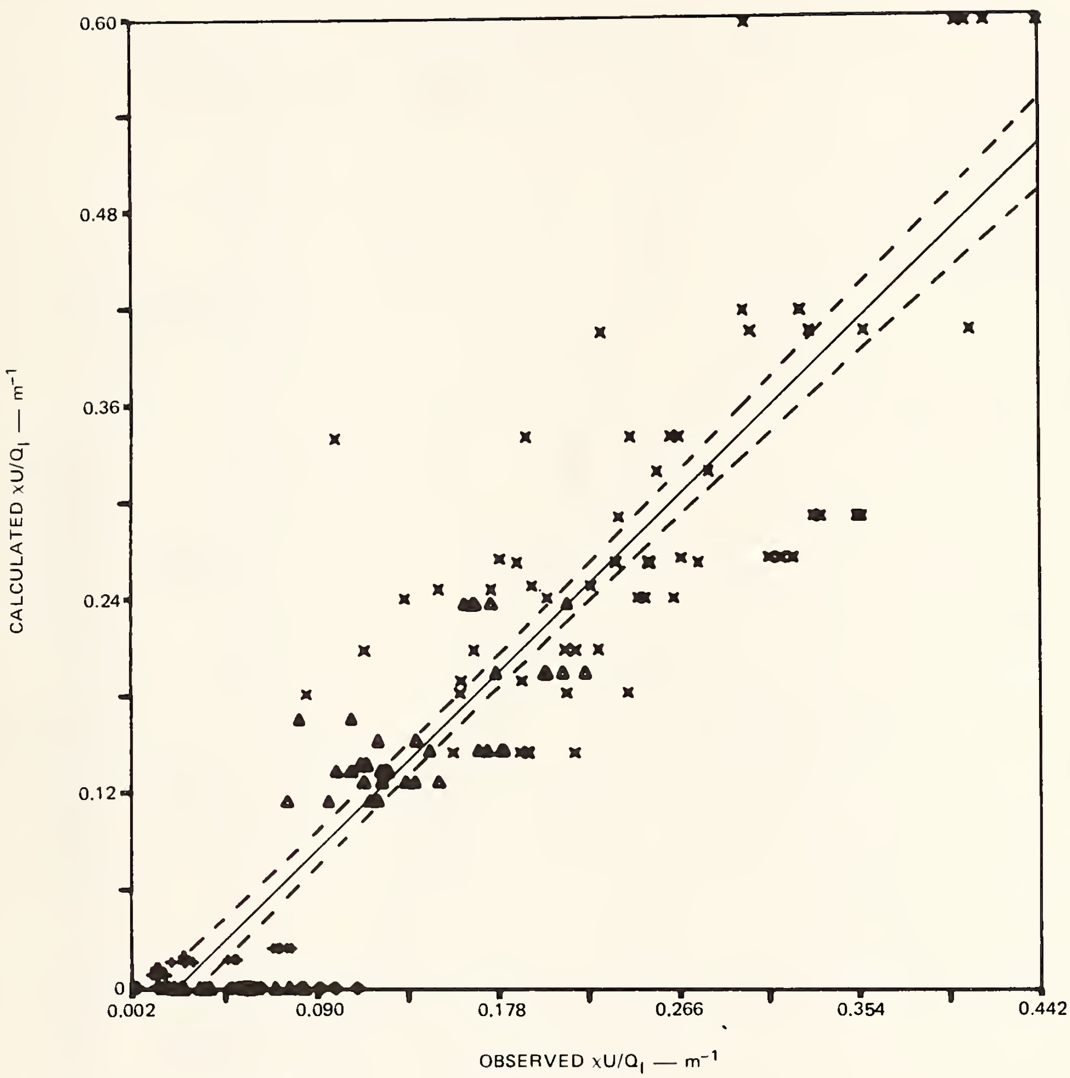

FIGURE 67 COMPARISON OF OBSERVED NORMALIZED CONCENTRATION WITH ROADMAP CALCULATION FOR WIND TUNNEL SERIES Q; θ = 30°, 60°, AND 90°

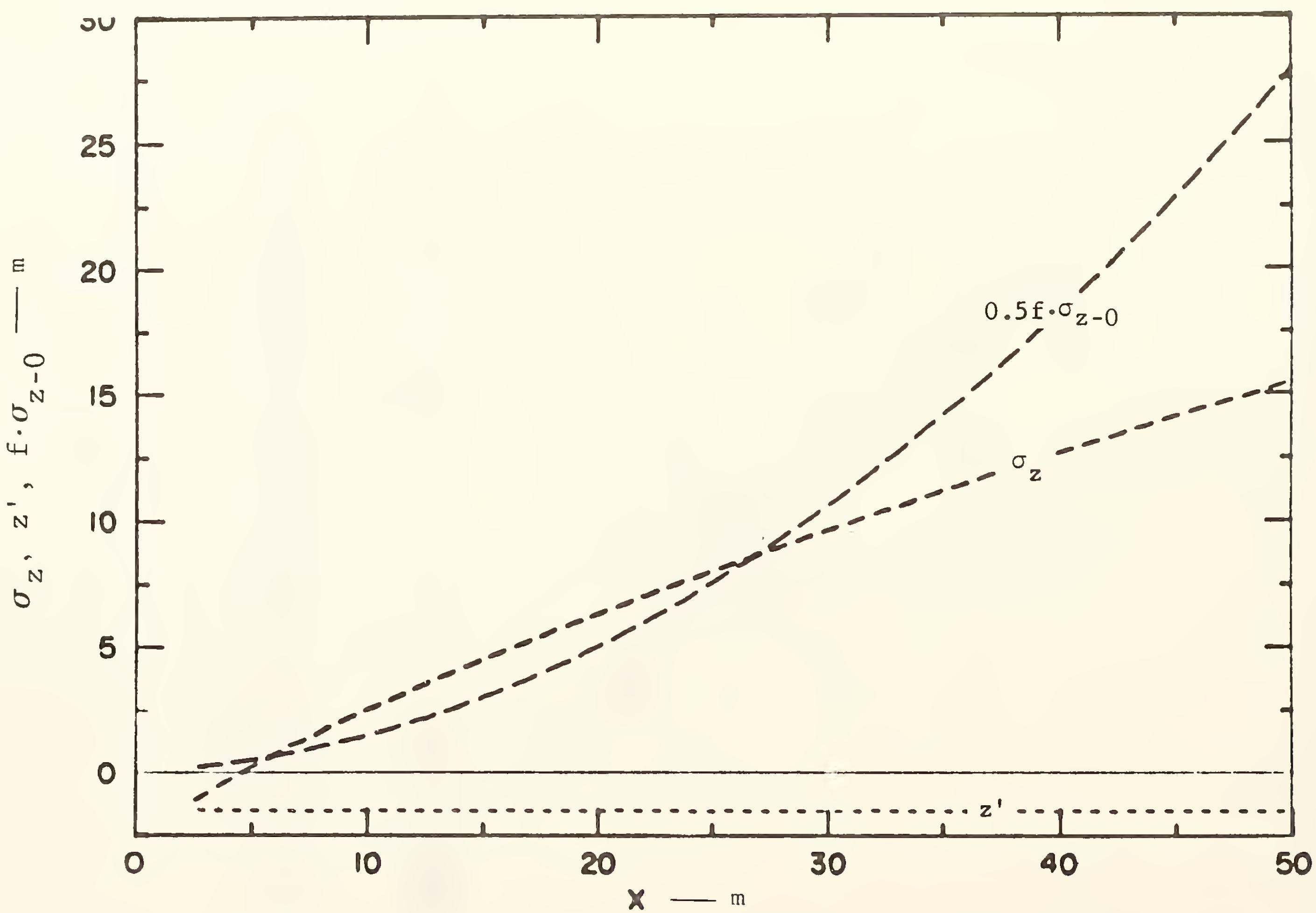

FIGURE 68 VARIATION OF ROADMAP DISPERSION PARAMETERS WITH CROSS-ROADWAY DISTANCE FOR WIND TUNNEL SERIES C

the eight cases with $\theta = 0°$ and $15°$. But when the full two-component model is used, r^2 drops to 0.12 ($r = 0.34$) for $\theta = 0°$ and $15°$. Figure 69 compares the two-component model with all θ-cases; the associated $r^2 = 0.24$ ($r = 0.49$). For the 30°-wind angle cases, the model performs similar to the 60° and 90° cases; $r^2 = 0.38$ ($r = 0.61$). All this suggests that there may exist two markedly distinct dispersion regimes: one for small θ-values, where the wind flow is channeled through the "canyon" and where the parallel dispersion term alone properly simulates the data, and a second regime for more oblique wind/roadway angles, where the two-component dispersion concept is valid.

Comparing the C-series values of normalized concentration with those from the Q series indicates that the rougher ground surface results in decreases up to about 50% for acute wind/roadway angles ($\leq 30°$). For orthogonal winds, two important features are observed: (1) the rough terrain results in only a 15% reduction in the peak near-roadway concentration, compared to the smooth-terrain situation, and (2) the location of the peak shifts from the downwind shoulder for smooth terrain to the <u>upwind</u> shoulder for rough terrain. This is a manifestation of a recirculation flow pattern that develops in the notch formed by the open right-of-way and the nearby roughness elements. Figure 70 is a schematic illustration from Johnson et al. (1971) of this so-called "street-canyon" effect. It depicts how the ambient flow above the obstacles is disturbed at the notch with a backflow of air at road level that transports roadway emissions to the upwind edges of the roadway.

Test series D differed only in one important respect from series C: the open space from the side of the roadway to the large roughness elements was considerably wider (about 120 m). As a result, we can expect the turbulence structure of the ambient flow approaching the roadway to be representative of the rough ground, but the street-canyon recirculation may not be present. Indeed, the ROADMAP results given in Table 41 reflect these two hypotheses. The perpendicular dispersion term alone has an r^2-value of 0.825 ($r = 0.91$) for the eight 60°- and 90°- cases, while r^2 for the parallel term and the 0°- and 15°-data is 0.615 ($r = 0.78$). Figure 71 compares observed D-series data with ROADMAP predictions.

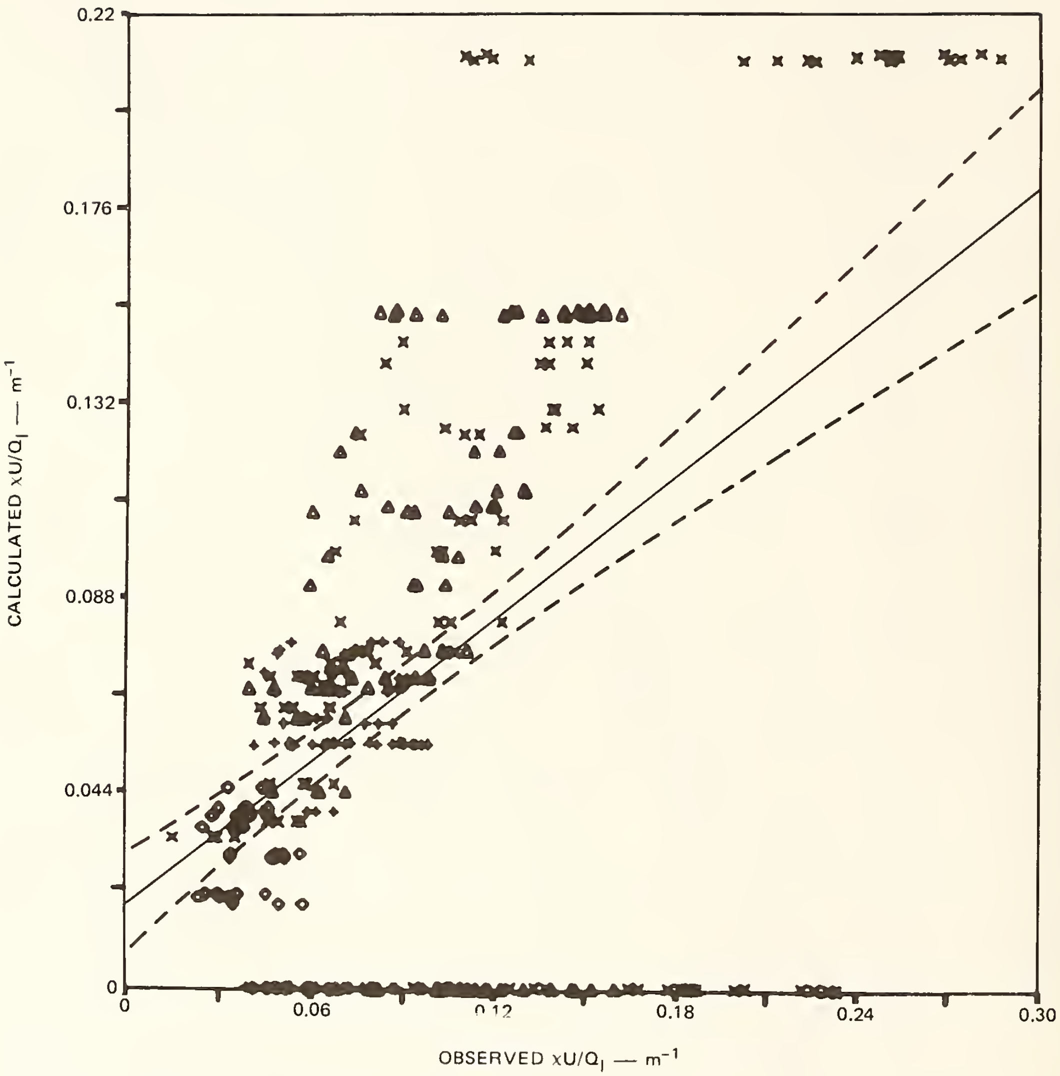

FIGURE 69 COMPARISON OF OBSERVED NORMALIZED CONCENTRATION WITH ROADMAP CALCULATION FOR WIND TUNNEL SERIES C, ALL WIND ANGLES

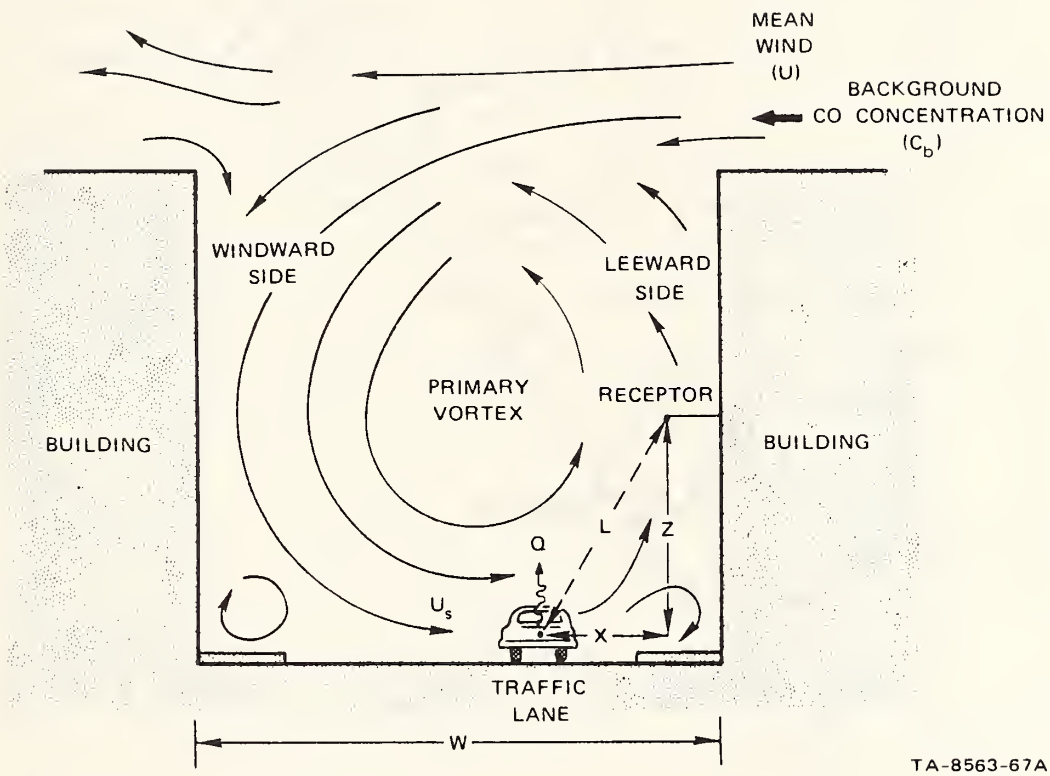

FIGURE 70 SCHEMATIC OF CROSS-STREET CIRCULATION BETWEEN BUILDINGS

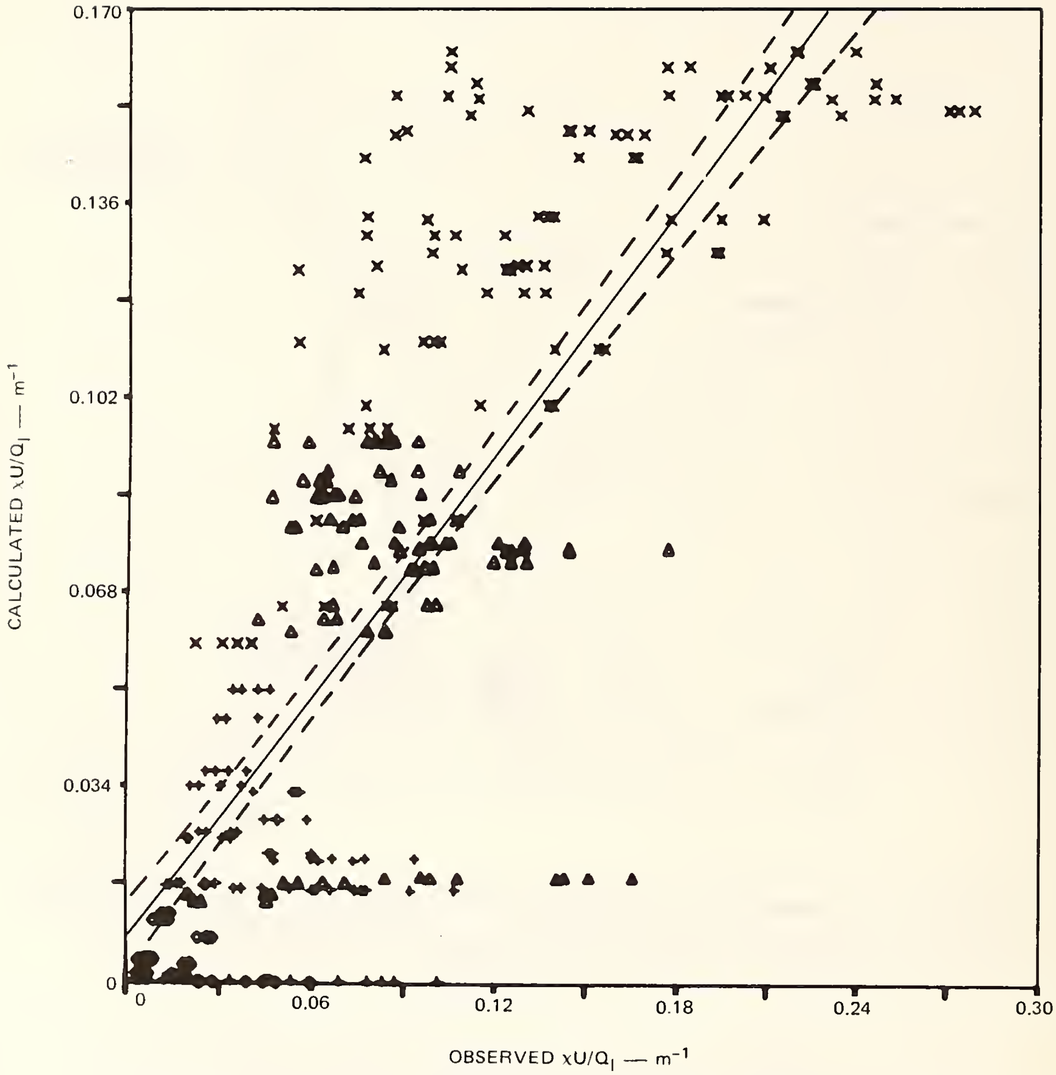

FIGURE 71 COMPARISON OF OBSERVED NORMALIZED CONCENTRATION WITH ROADMAP CALCULATION FOR WIND TUNNEL SERIES D; ALL WIND ANGLES

For all θ-values, the model provides an explained variance of 63% ($r = 0.79$); for the $\theta = 30°$ cases alone (i.e., those not used in the estimation of coefficients), the r^2-value is 0.80 ($r = 0.89$). Figure 72 graphs the x-dependence of σ_z, z', and $f \cdot \sigma_{z-o}$. Values of σ_z are consistently about 50% larger than for the smooth-ground case (series Q); z' is again nearly independent of x at a value of about 0.5 m. The lateral dispersion function $f \cdot \sigma_{z-o}$ is very similar to the Q series, or about one-half its C-series value. This indicates that the broad open area adjacent to the roadway produces a dispersion pattern for small θ values that is more typical of smooth ground that it is of the rough ground. As a consequence, the concentration patterns for the D series are similar to the Q series, although the magnitudes are decreased by about 50% because of the increase in σ_z. Unlike the C series, the concentration peak for winds orthogonal to the roadway is located beyond the downwind edge of the roadway.

Test series I is a variation on series C in that the rough upwind terrain is close to the roadway edge (60 m), but the downwind terrain is smooth. The perpendicular term explains 82% of the variance ($r = 0.90$) in in the 90°-data, while the parallel term has an r^2-value of 0.83 ($r = 0.91$) for the 0°- and 15°-data. Together, the two components yield an r^2-value of 0.49 ($r = 0.70$) for all wind angles (0°, 15°, 30°, and 90°) (Figure 73). The variation in σ_z, z', and $f \cdot \sigma_{z-o}$ is given in Figure 74. Both σ_z and $f \cdot \sigma_{z-o}$ are similar though slightly larger than with the D series; z' is again nearly constant, but at a value of about -1 m. Peak concentrations for all wind directions are of comparable magnitude (within 10°) and similar location to the D-series values. As expected, the decrease in concentration levels downwind over the smooth terrain is less rapid than with the C series. For example, the concentration level with the I series at $\theta = 90°$ falls to 50% of the peak value in more than double the distance than for the C series. Generally, the downwind dispersion pattern is similar to the D-series pattern.

The J-series configuration consists of smooth terrain upwind of the roadway, and rough terrain that begins some 30 m downwind of the roadway edge. For the four orthogonal wind cases, ROADMAP simulates 96% of the

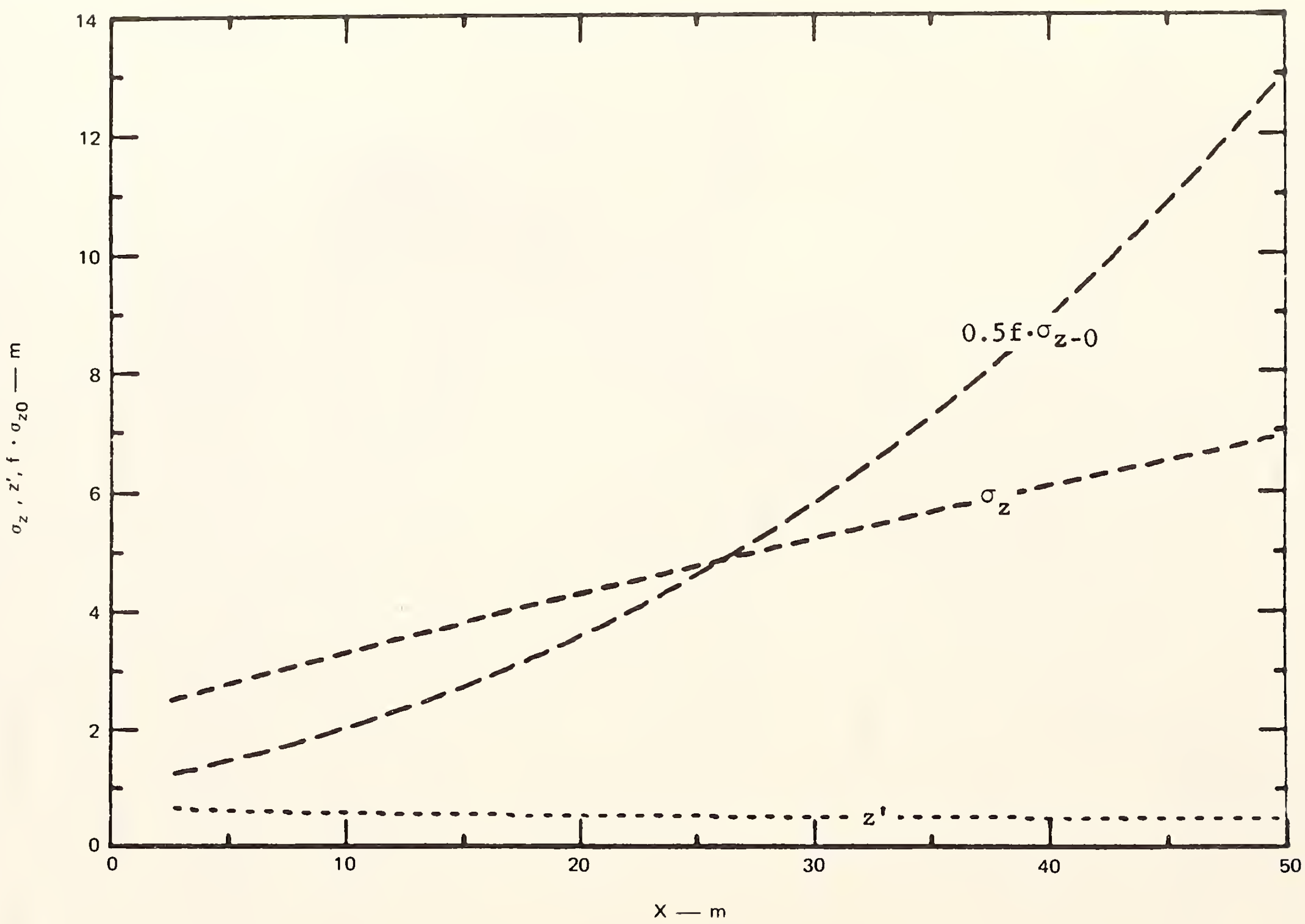

FIGURE 72 VARIATION OF ROADMAP DISPERSION PARAMETERS WITH CROSS-ROADWAY DISTANCE FOR WIND TUNNEL SERIES D

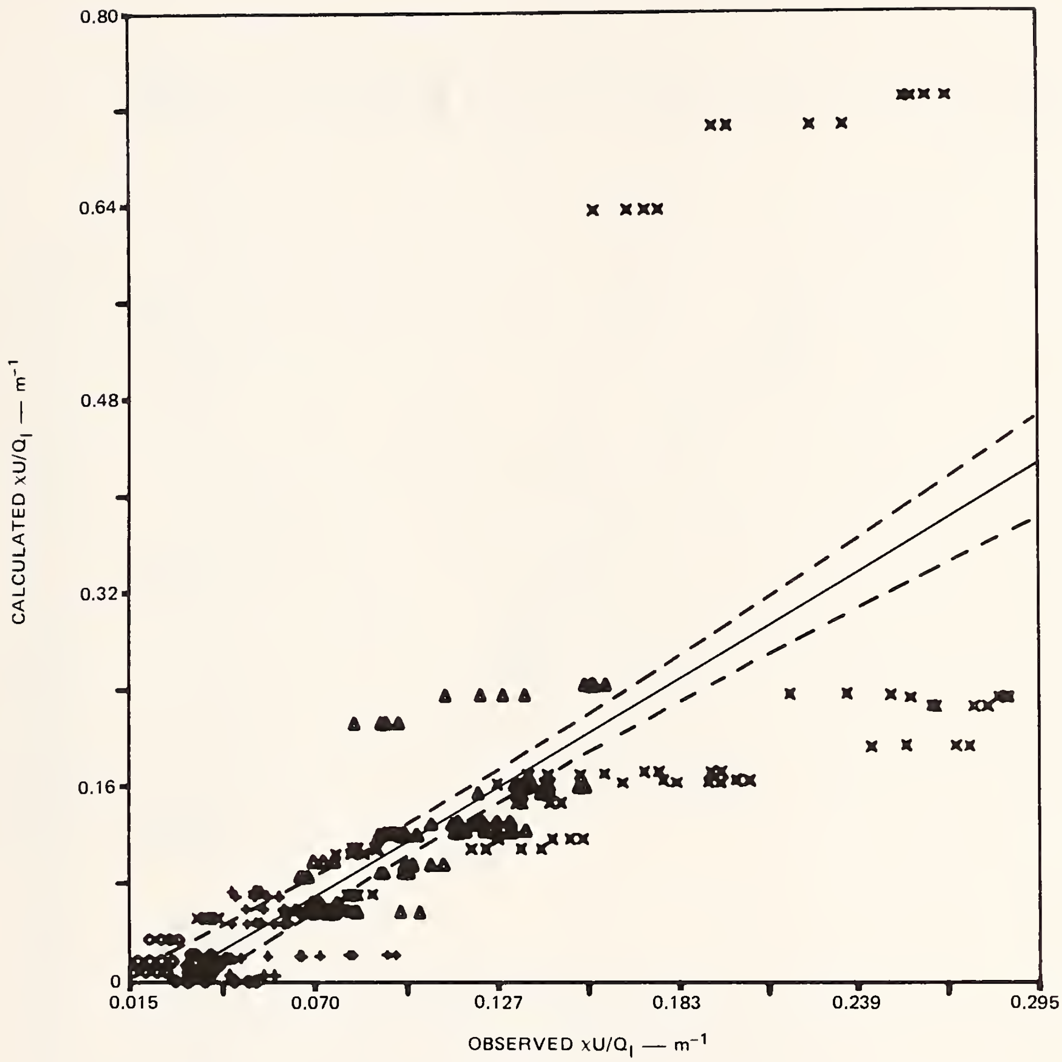

FIGURE 73 COMPARISON OF OBSERVED NORMALIZED CONCENTRATION WITH ROADMAP CALCULATION FOR WIND TUNNEL SERIES I; ALL WIND ANGLES

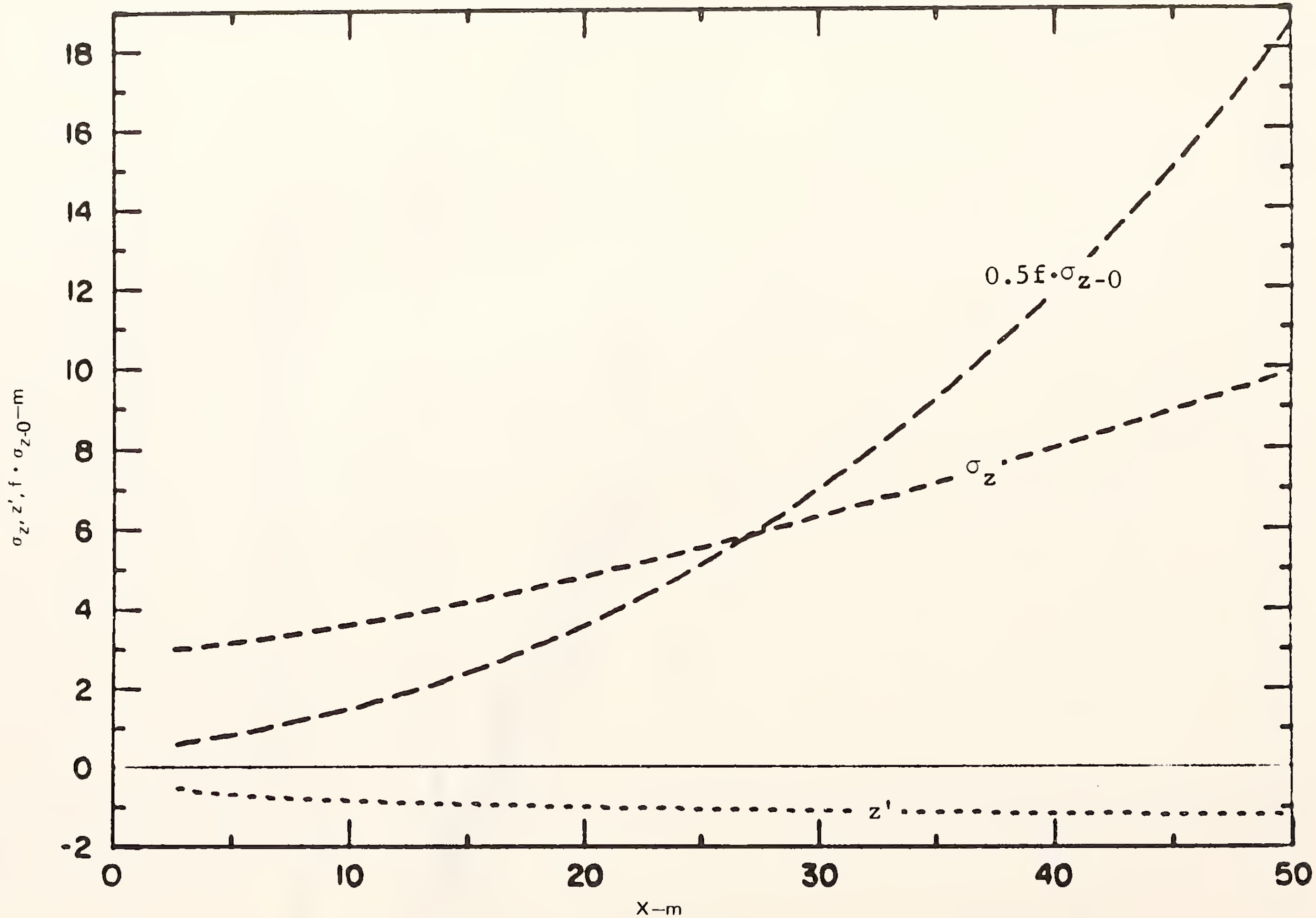

FIGURE 74 VARIATION OF ROADMAP DISPERSION PARAMETERS WITH CROSS-ROADWAY DISTANCE FOR WIND TUNNEL SERIES I

variance (r = 0.98) in the observed data. The parallel term does far less well with r^2 = 0.22 (r = 0.46). The two-component model derived from the 0°-, 15°-, and 90°-data is, however, able to predict 91% of the variance (r = 0.95) in the 30°-data cases and 38% (r = 0.61) in the 0°- 15°-data. Figure 75 compares observations with predictions for all θ values; the corresponding r^2 is only 0.27 (r = 0.52). These results indicate that the model adequately simulates the large wind-angle cases ($\theta \geq 30°$, but not the small wind-angle cases; Figures 76 and 77 illustrate these findings. However, this contrasts markedly with the I series where the roughness discontinuity was upwind of the roadway. Apparently, the nearby presence of the large obstacles downwind of the roadway restricts the lateral dispersion, which controls the concentration pattern for small wind angles. This is clearly seen in Figure 78 where values of $f \cdot \sigma_{z-o}$ are three times smaller than they are for the I-series data (Figure 74). The abrupt increase in surface roughness is also reflected in z', which increases sharply (with negative sign) away from the roadway to reflect the lifting of the roadway "plume" as the air flows up and over the obstacles. A further consequence of this configuration is that peak concentrations are equal to or greater than the comparable peaks for the Q and C series. With near-parallel winds, the J-series peak is 25% greater than the Q-series peak; with orthogonal winds, the J-series peak is about 35% larger.

2. Atmospheric Test

a. Neutral Atmospheric Stability

Seventeen of the 45 available hours with concentration data at the 101 location were classified as having neutral atmospheric stability. Three meteorological parameters measured over hourly periods were used to classify the stability: (1) the standard deviation of the horizontal (azimuth) wind direction, σ_θ, (2) the standard deviation of the vertical (elevation) wind angle, σ_ϕ, and (3) the gradient Richardson number*, Ri.

---

*The Richardson number is the non-dimensional ratio of buoyancy and momentum forces, and is defined in the gradient form as:

$$Ri = \frac{g}{T} \frac{\Delta T/\Delta z}{(\Delta U/\Delta z)^2}$$

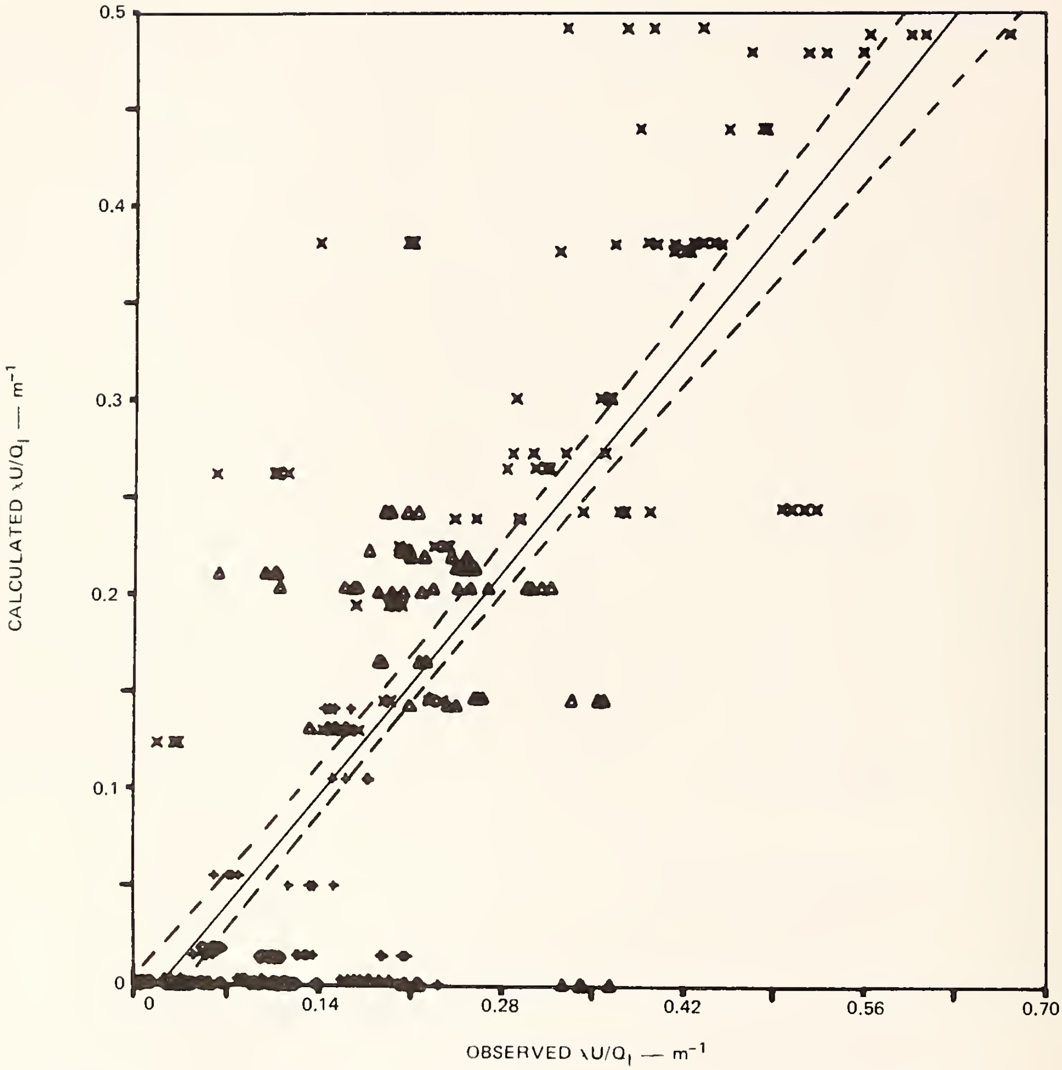

FIGURE 75 COMPARISON OF OBSERVED NORMALIZED CONCENTRATION WITH ROADMAP CALCULATION FOR WIND TUNNEL SERIES J; ALL WIND ANGLES

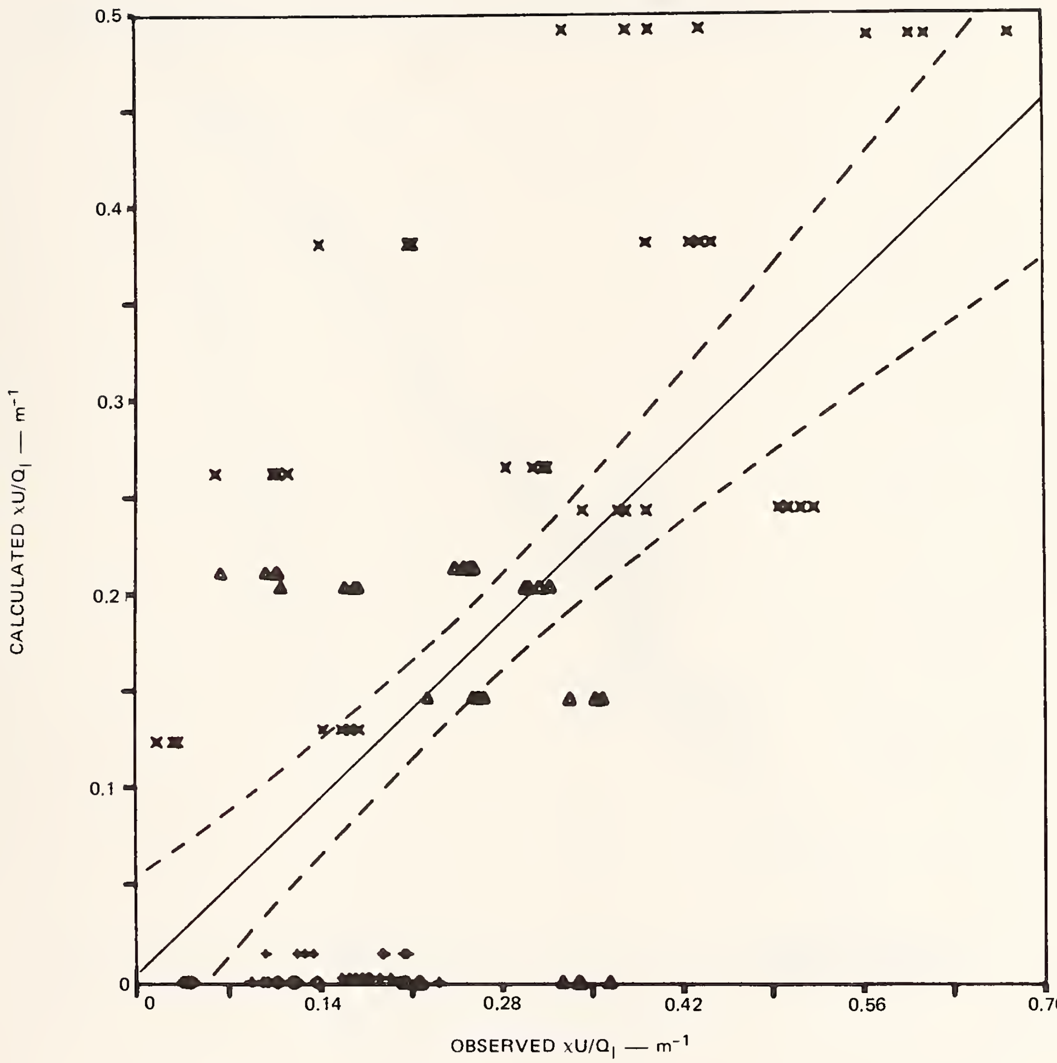

FIGURE 76 COMPARISON OF OBSERVED NORMALIZED CONCENTRATION WITH ROADMAP CALCULATION FOR WIND TUNNEL SERIES J; θ = 0° AND 15°

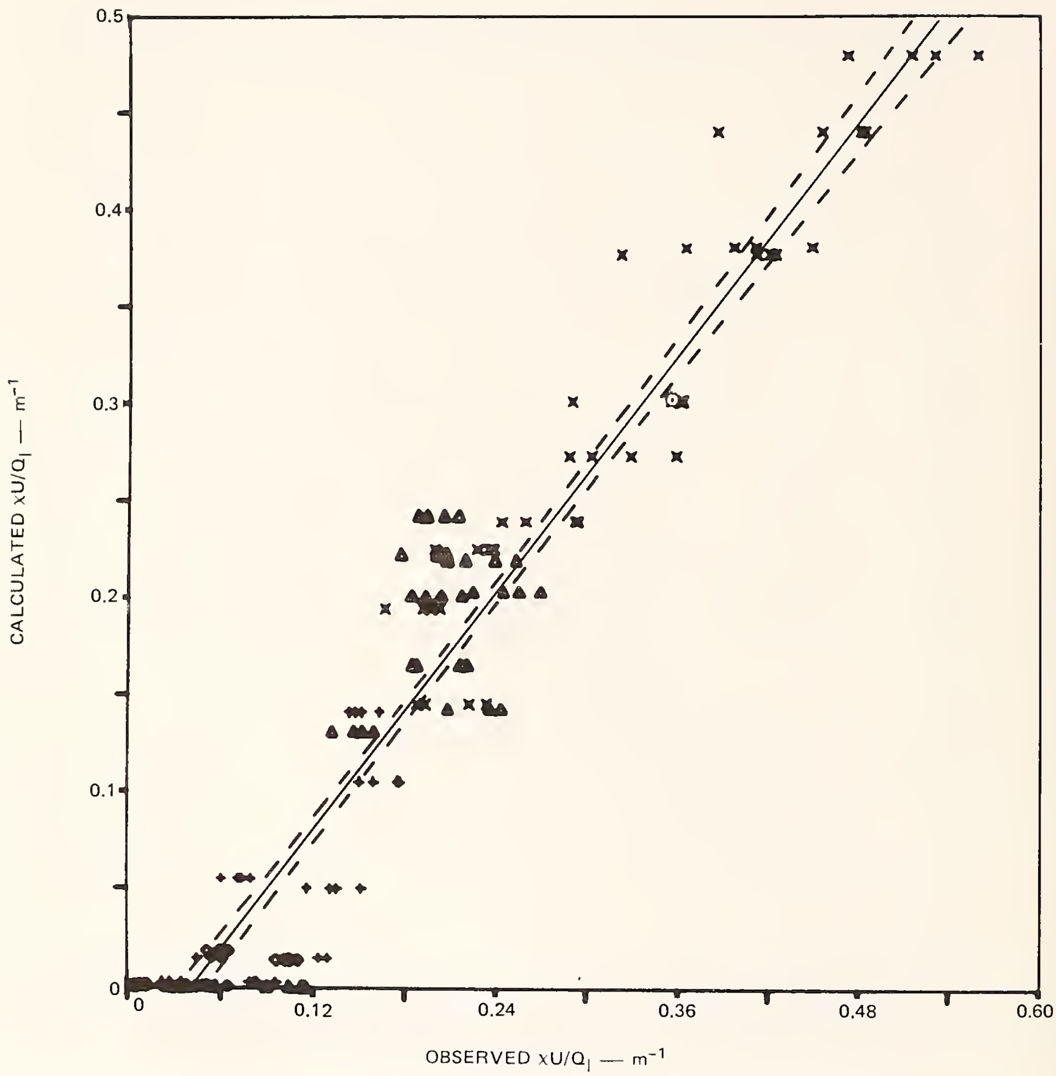

FIGURE 77 COMPARISON OF OBSERVED NORMALIZED CONCENTRATION WITH ROADMAP CALCULATION FOR WIND TUNNEL SERIES J; θ = 30° AND 90°

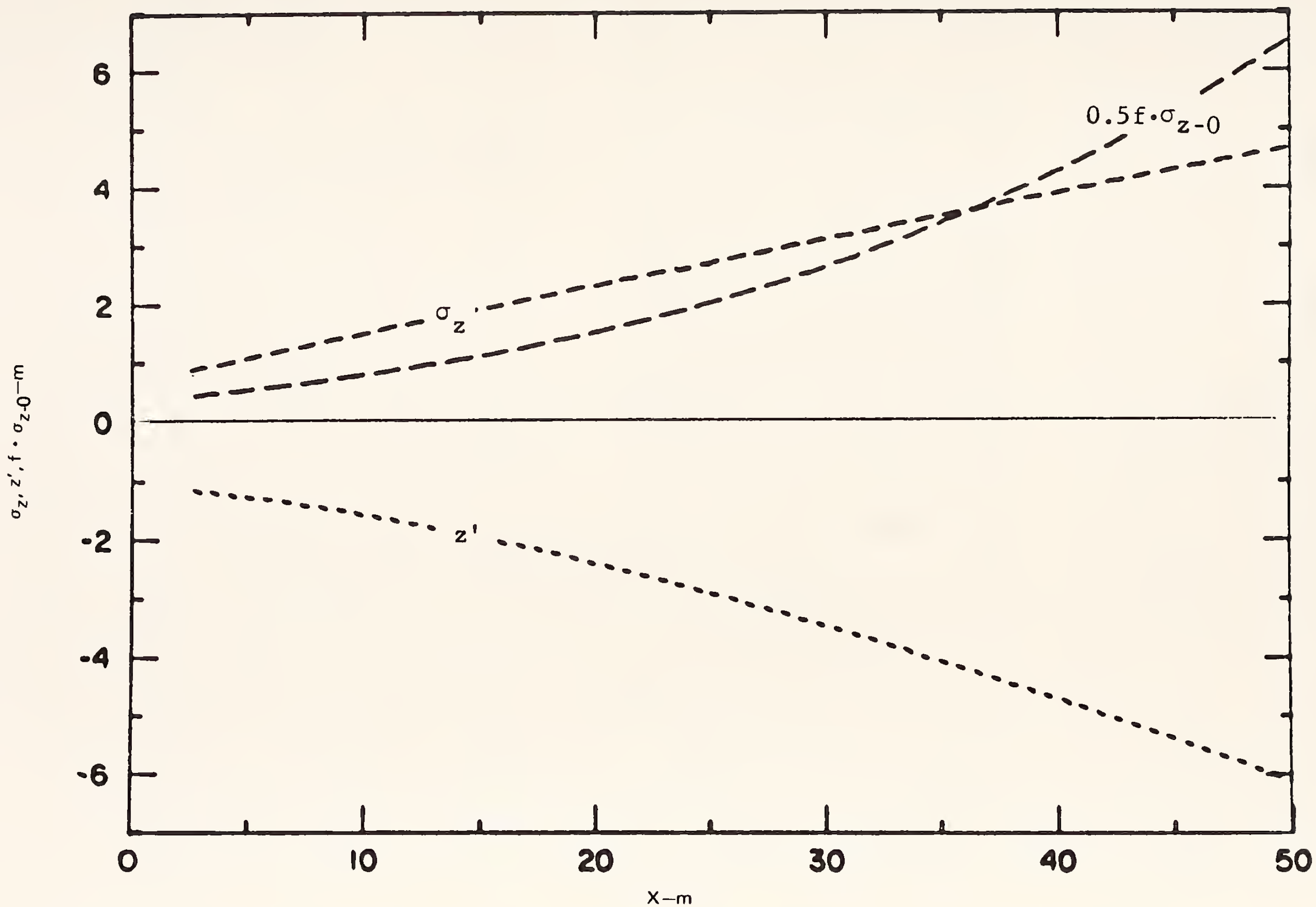

FIGURE 78 VARIATION OF ROADMAP DISPERSION PARAMETERS WITH CROSS-ROADWAY DISTANCE FOR WIND TUNNEL SERIES J

The first of these (σ_θ) has been most often used by others in the past (see Ludwig and Dabberdt, 1976), although the vertical sigma term (σ_ϕ) is equally or perhaps more appropriate to describing line-source dispersion. In principle, Ri is the most appropriate measure, but it can be a difficult parameter to measure accurately considering instrumentation and site-representivity aspects. Therefore, all three terms were used with the result that the 17 hours classified as neutral had the following ranges for each term: (1) $5.6° \leq \sigma_\theta \leq 15.6°$; (2) $2.9° \leq \sigma_\phi \leq 12.5°$; and (3) $-0.83 \leq Ri \leq 0.37$.

Both the CO and tracer data were used in the ROADMAP analyses (see Table 41). Regarding the CO data, while the hourly emission rates are known for each traffic direction, there is no way to ascertain the respective contribution to the total CO concentration measured at each sampling location. The tracer data, however, do permit us to directly measure the dispersion of emissions from each direction. But while the CO emissions are virtually continuous, the tracer emissions are not, which can induce sampling errors when the hourly meteorological conditions are not steady. Thus, the CO and tracer data provide a good basis for evaluating near-roadway dispersion.

Figure 79 plots the cross-roadway variation of the three dispersion parameters as computed from the CO data. Several important inferences can be drawn: first, the lateral dispersion function, $f \cdot \sigma_{z-o}$, is nearly constant with x and is about an order of magnitude smaller than the comparable wind tunnel test (series Q). This indicates that the crosswind diffusion is more pronounced for the atmospheric case or, alternately stated, the resulting crosswind concentrations are more uniform. This increased lateral mixing for the atmospheric case may result from the low-frequency meander of the wind that usually occurs in nature, but that was not simulated in the wind tunnel. Second, the height-offset term is essentially constant with lateral distance (x) and has a negative value ($z' \approx -1.5$ m). This indicates that concentration values at heights above 0.75 m (i.e., where $z = -0.5z'$) are greater than they would be in the absence of the height-offset term (here equal to -1.5 m). Conversely, concentrations closer to the ground than 0.75 m would be less than

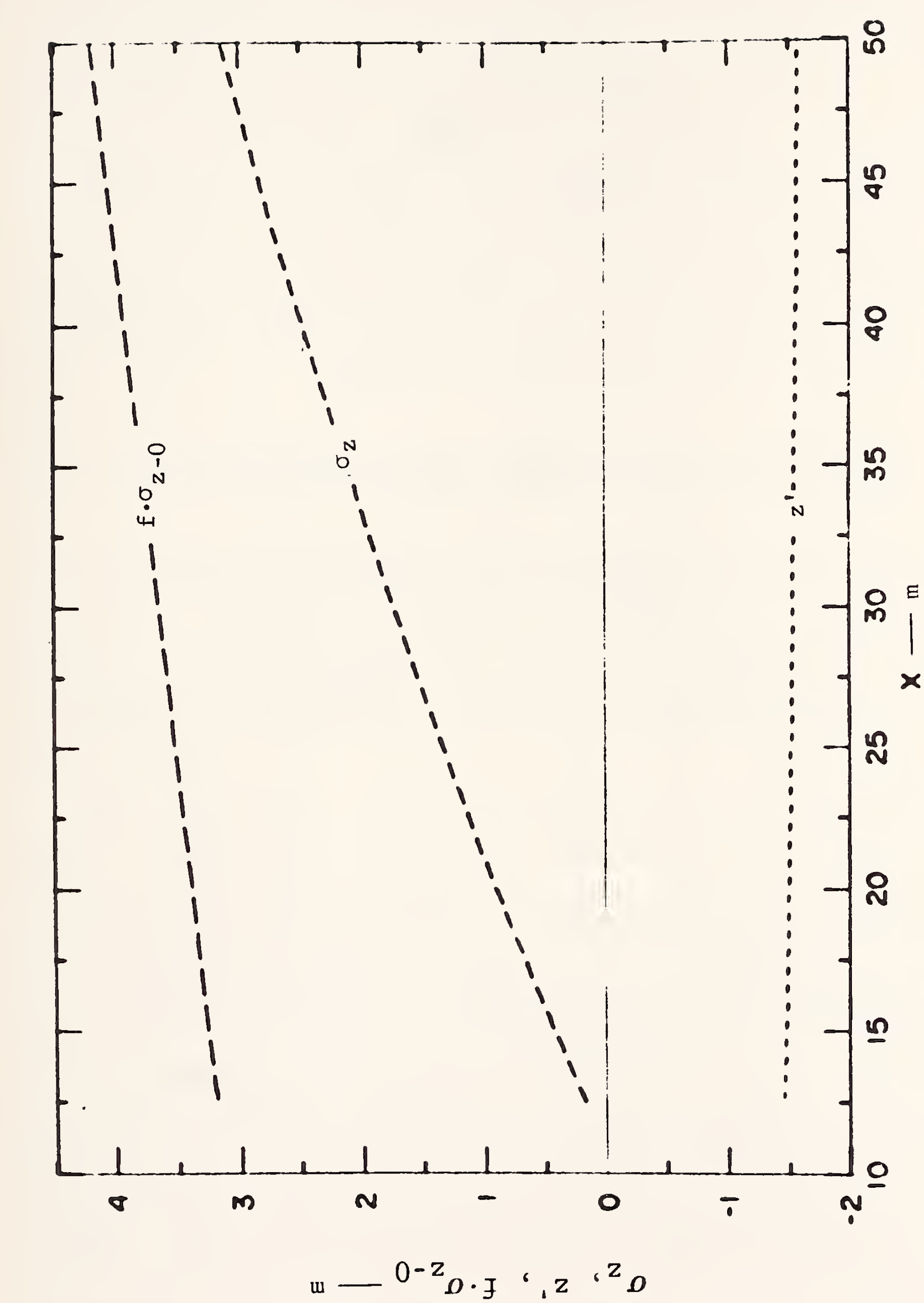

FIGURE 79 VARIATION OF ROADMAP DISPERSION PARAMETERS BASED ON CO DATA WITH CROSS-ROADWAY DISTANCE FOR HIGHWAY 101 GRADE-LEVEL TEST, NEUTRAL ATMOSPHERIC CONDITIONS

equivalent values with no height-offset term. The physical basis of the height-offset term can be traced to one or more of three effects: (1) "plume rise" attributable to vehicle waste heat emissions and/or sensible heat emissions from the roadway surface, (2) mechanical mixing of the air over the roadway due to vehicle wake effects or the influence of noise barriers or vegetation, and (3) modification of the mean air flow over the site resulting from natural topography or the configuration of the roadway section. Under the test conditions that existed (i.e., neutral atmospheric stability and grade-level roadway), the concentrations at the four measurement heights range from significantly greater to nominally larger than those that would be expected with a similar model, but without the height-offset term*; sample calculations are given in the tabulation below for two roadway-receptor distances:

Table 42

RELATIVE CONCENTRATION VALUES FOR TWO ROADWAY-RECEPTOR DISTANCES AT FOUR MEASUREMENT HEIGHTS

Height above Ground (m)	Relative Concentration Values			
	x = 20 m		x = 40 m	
	Without z'-term	With z' = -1.5 m	Without z'-term	With z' = -1.5 m
1.0	0.57	0.87	0.35	0.37
3.8	0.00	0.05	0.12	0.25
7.5	0.00	0.00	0.00	0.06
14.2	0.00	0.00	0.00	0.00

Atmospheric stability also plays an apparent role in modifying the value of the height-offset term, as is discussed in subsequent sections.

The third inference drawn from Figure 79 is the x-dependence of the vertical dispersion term (σ_z) which is reasonable, although somewhat smaller than expected, particularly near the roadway edge. In analyzing the CO data to estimate the dispersion functions, concentration measurements from the sampling tower in the median strip were not used. This

---

*The comparison in Table 42 is not strictly appropriate in that the σ_z- and z'-terms used in the calculations were derived simultaneously from statistical analysis of the data. Eliminating the z'-term would more properly require the recalculation of σ_z.

was necessary because of the often asymmetrical nature of the roadway emissions (by direction); for example, one hour might have uniform emission rates in both directions and the median samplers would provide representative CO data, while another hour with the same total roadway emission rate might have negligible traffic on the upwind traffic lanes with the result that the median samplers would measure little or no CO.

Four of the 17 neutral hours were used to evaluate σ_z and z' using the perpendicular dispersion term; the θ-values ranged from 63° to 72°. The accompanying r^2-value was an encouraging 0.763 (r = 0.873). Three hours with θ values of 4°, 15°, and 18° were used with the parallel dispersion term to estimate f; the accompanying r^2-value was 0.085 (r = 0.292). Four of the remaining 10 hours could not be used in the ROADMAP evaluation because the measured CO values were very low due to the minimal traffic volume. When ROADMAP was evaluated against all 13 hours of data, r^2 = 0.354 (r = 0.595); these results are plotted in Figure 80. For the 6 hours not used in estimating the dispersion functions ($18° < \theta < 63°$), r^2 = 0.824 (r = .908); and for the 10 hours where $\theta > 18°$, r^2 = 0.698 (r = 0.835).

Figures 81 and 82 plot the x-variation of σ_z, z', and $f \cdot \sigma_{z-o}$ for the upwind and downwind traffic streams, respectively, as determined from the tracer data. The general features compare well with the comparable functions estimated earlier from the CO data. The height-offset terms are both similar in magnitude and variation to the previous estimate. There are some minor differences in the vertical dispersion functions: first, they are both initially larger than estimated from the CO data; but, second, they increase less quickly downwind so that they are both smaller at x = 50 m. The estimates of the lateral dispersion functions are of the same order of magnitude as given earlier, but they are both initially smaller. This may be a reflection of the tracer having been released only from one lane, while CO is emitted from all lanes. As summarized in Table 41, the two-component ROADMAP performs equally as well overall for both the upwind and downwind tracer-cases as it did in the CO analysis.

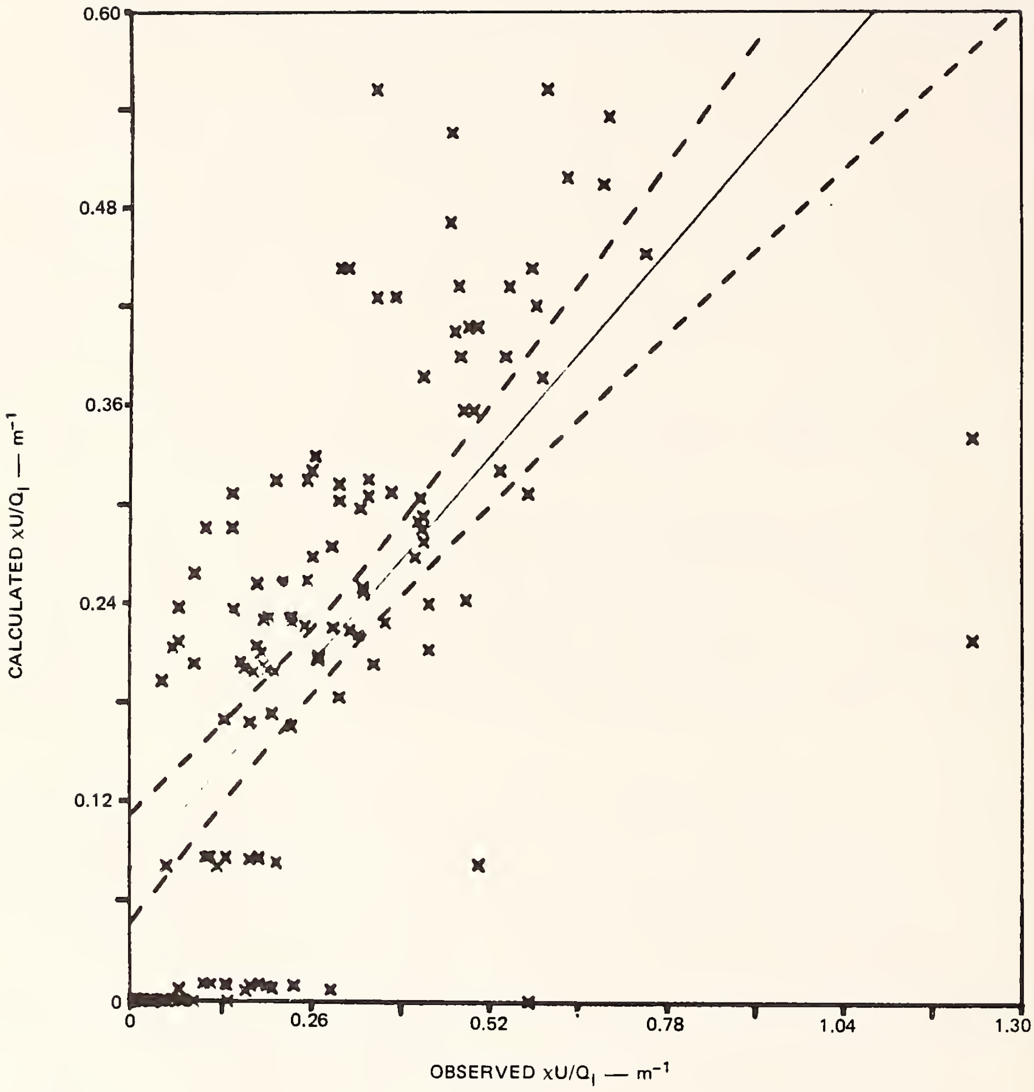

FIGURE 80 · COMPARISON OF OBSERVED NORMALIZED CONCENTRATION WITH ROADMAP CALCULATION FOR HIGHWAY 101 GRADE-LEVEL TESTS, NEUTRAL ATMOSPHERIC CONDITIONS, ALL WIND ANGLES

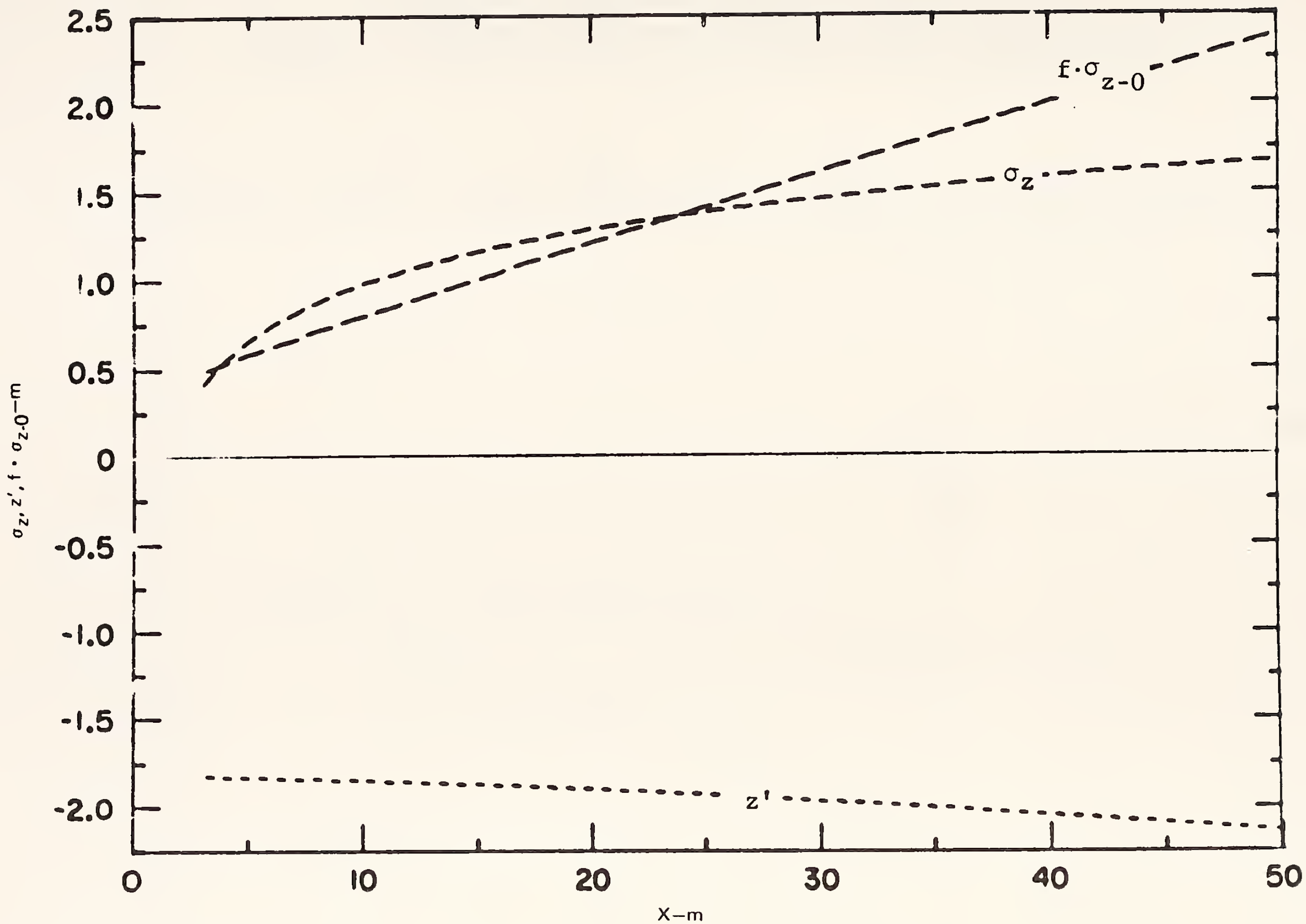

FIGURE 81 VARIATION OF ROADMAP DISPERSION PARAMETERS WITH CROSS-ROADWAY DISTANCE FOR UPWIND TRAFFIC LANES ON HIGHWAY 101; NEUTRAL ATMOSPHERIC CONDITIONS

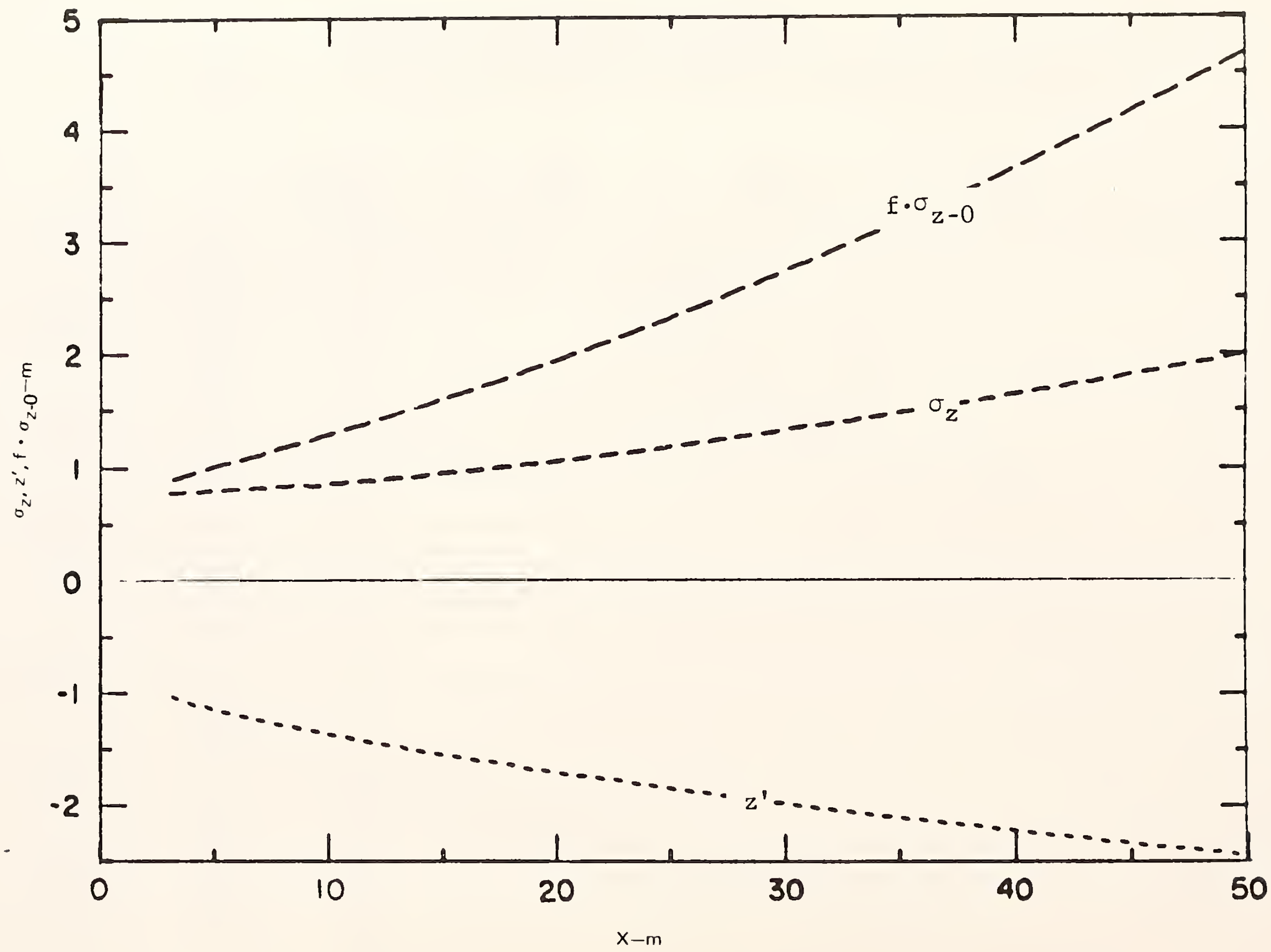

FIGURE 82 VARIATION OF ROADMAP DISPERSION PARAMETERS WITH CROSS-ROADWAY DISTANCE FOR DOWNWIND TRAFFIC LANES ON HIGHWAY 101; NEUTRAL ATMOSPHERIC CONDITIONS

b. Stable Atmospheric Conditions

Seven hours were grouped into a "stable" category and had the following ranges in the measured meteorological parameters used in the grouping process (1) $17.1° \leq \sigma_\theta \leq 47.9°$, (2) $4.4° \leq \sigma_\phi \leq 24.0°$, and (3) $0.00 \leq Ri \leq 0.12$. Unfortunately, there were neither more stable hours available nor less variability among those available; while the analysis provides a good contrast to the neutral (and later, unstable) conditions, the results cannot be compared directly with other analyses that have used a more restrictive and conventional categorization of stability (see, for example, Ludwig and Dabberdt, 1977, for several such classification methods).

Figure 83 plots the cross-roadway variation of the three dispersion parameters. They were estimated from the CO data for two of the hourly periods with large θ-values. The height-offset term, z', has an initial value of +2.0 m at x = 10 m and tapers down to 0.5 m at x = 50 m. This has the effect of greatly reducing the near-ground concentrations, particularly close to the roadway. This pattern may be the result of vertical transport and mixing from the emission of buoyant exhaust gases in a stable ambient environment. The heat is mixed and diffused as the exhaust plume is transported away from the road, and the magnitude of the effect diminishes accordingly. The vertical mixing term, σ_z, is significantly larger than for the neutral case. This may be the result of two factors: (1) the larger σ_ϕ-values of the ambient wind, and (2) the vertical motion from vehicular waste heat emissions. The latter may explain the particularly larger σ_z-values near to the roadway (compared to Figure 79). As discussed later, the $f \cdot \sigma_{z-o}$ term could not be derived from the stable data.

The perpendicular dispersion term with the estimates of σ_z and z' was able to explain 47% of the variance (r = 0.68) of the observed concentrations for the two large θ cases. None of the other five hours had a θ value sufficiently small to estimate f from the parallel dispersion term. Therefore, a first approximation to f was obtained by using the neutral-case values of a_3, b_3, and c_3. As a result, the two-component

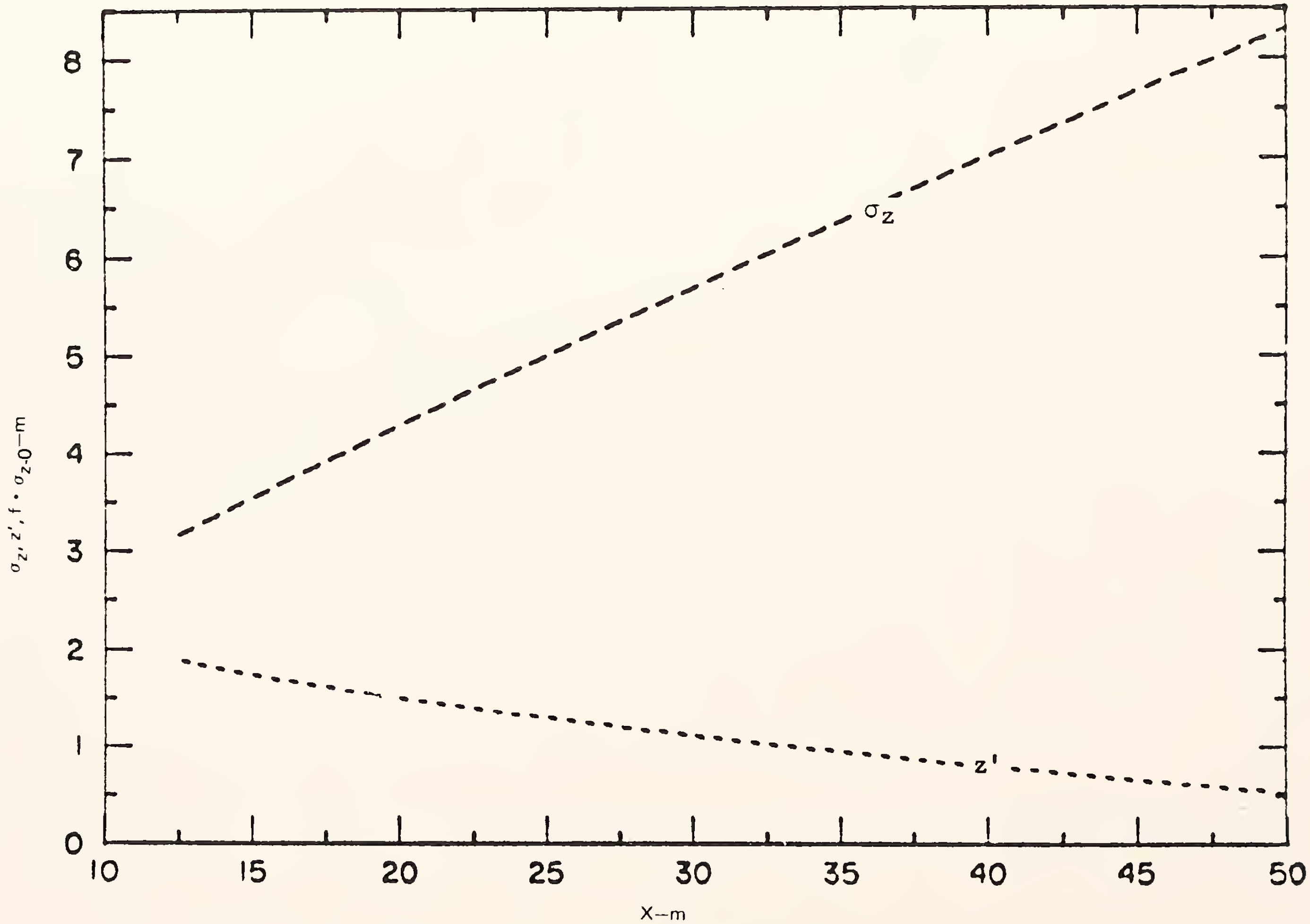

FIGURE 83 VARIATION OF ROADMAP DISPERSION PARAMETERS WITH CROSS-ROADWAY DISTANCE FOR HIGHWAY 101 GRADE-LEVEL TEST, STABLE ATMOSPHERIC CONDITIONS

ROADMAP had $r^2 = 0.514$ ($r = 0.72$) for all seven cases (Figure 84), and $r^2 = 0.444$ ($r = 0.67$) for the five cases where $37° \leq \theta \leq 55°$.

Figures 85 and 86 illustrate the x-dependence of the dispersion functions from the upwind and downwind tracer data, respectively. As before, the $f \cdot \sigma_{z-o}$-data could not be evaluated or compared in that they all had to be estimated from the neutral-stability analyses. The σ_z values are comparable to those estimated earlier from the CO analysis (Figure 83). The z' values differ markedly; data from the tracer released on the upwind lanes shows a moderate and constant negative value ($z' \approx -1.5$ m), while the downwind tracer data indicate a small, positive value that increases slightly with x. Insofar as all of the σ_z and z' estimates are derived from only two hourly cases, it may not be valid to attempt to attribute too much importance to these upwind-downwind differences. However, both z' estimates are equal to, or more positive than, their neutral-stability counterparts (as seen also in the comparison of CO analyses).

c. Unstable Atmospheric Conditions

Nine hourly periods were grouped together and represent what may be called moderately unstable conditions, although not in the strict sense of the Hanna-Gifford or Pasquill-Turner definitions. As before, σ_θ, σ_ϕ, and Ri were used to stratify the data and eliminate those few hours that were very unstable. Even so, the range in the three parameters is still large: (1) $16.8° \leq \sigma_\theta \leq 40.9°$, (2) $7.4° \leq \sigma_\theta \leq 22.2°$, and (3) $-4.61 \leq$ Ri ≤ -0.03. As discussed earlier and can be seen in these broad ranges, no single parameter was able to consistently stratify the data properly.

Two of the nine cases ($\theta = 67°$ and $79°$) were used to estimate σ_z and z' from the CO data using the perpendicular dispersion term. This single component was able to represent 58% of the variance in the data for these two cases ($r = 0.76$). Figure 87 is a plot of the three dispersion functions. The σ_z term is larger than the neutral case, yet surprisingly smaller than the stable case. The height-offset term is independent of x at a value of -2.4 m. No firm explanation is offered,

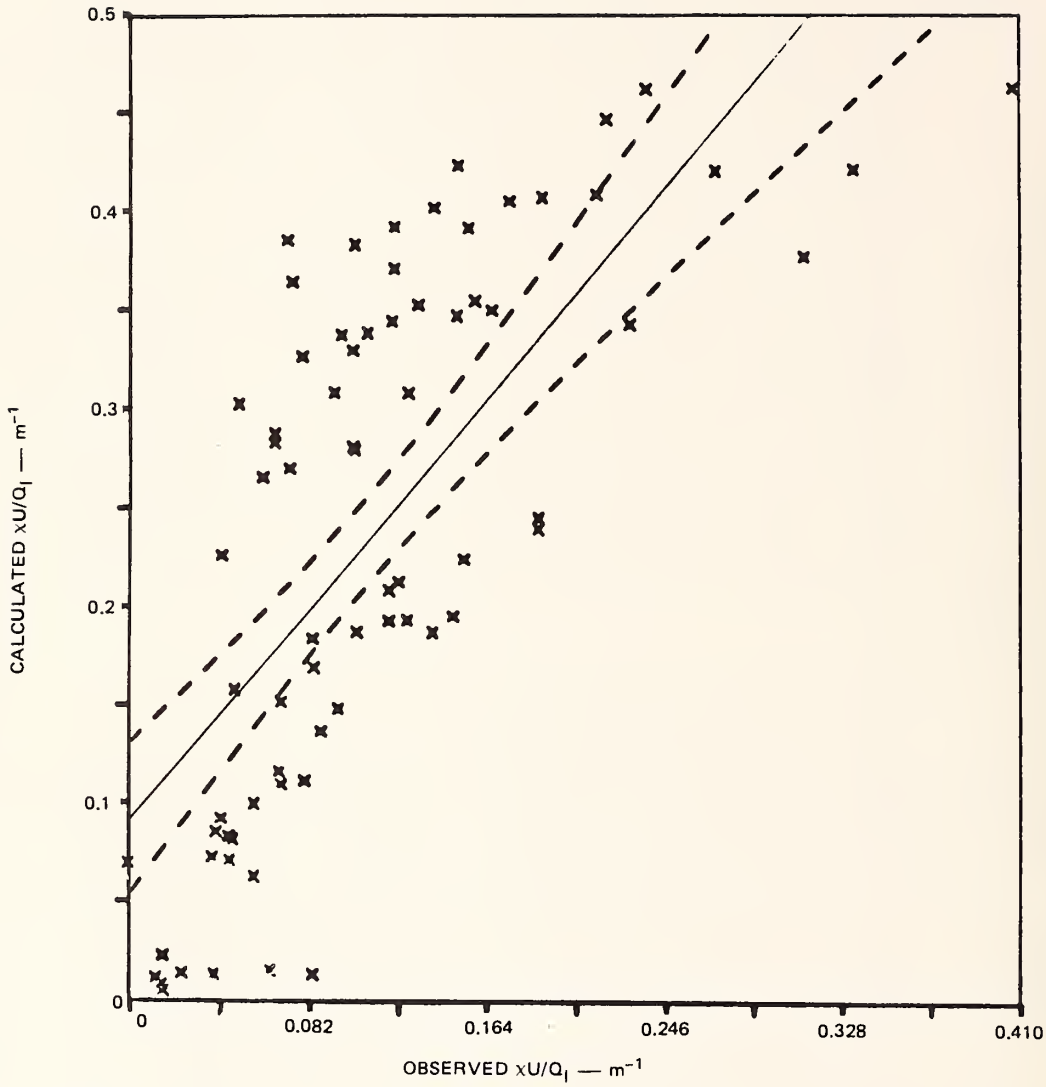

FIGURE 84 COMPARISON OF OBSERVED NORMALIZED CONCENTRATION WITH ROADMAP CALCULATION FOR HIGHWAY 101 GRADE-LEVEL TESTS, STABLE ATMOSPHERIC CONDITIONS, ALL WIND ANGLES

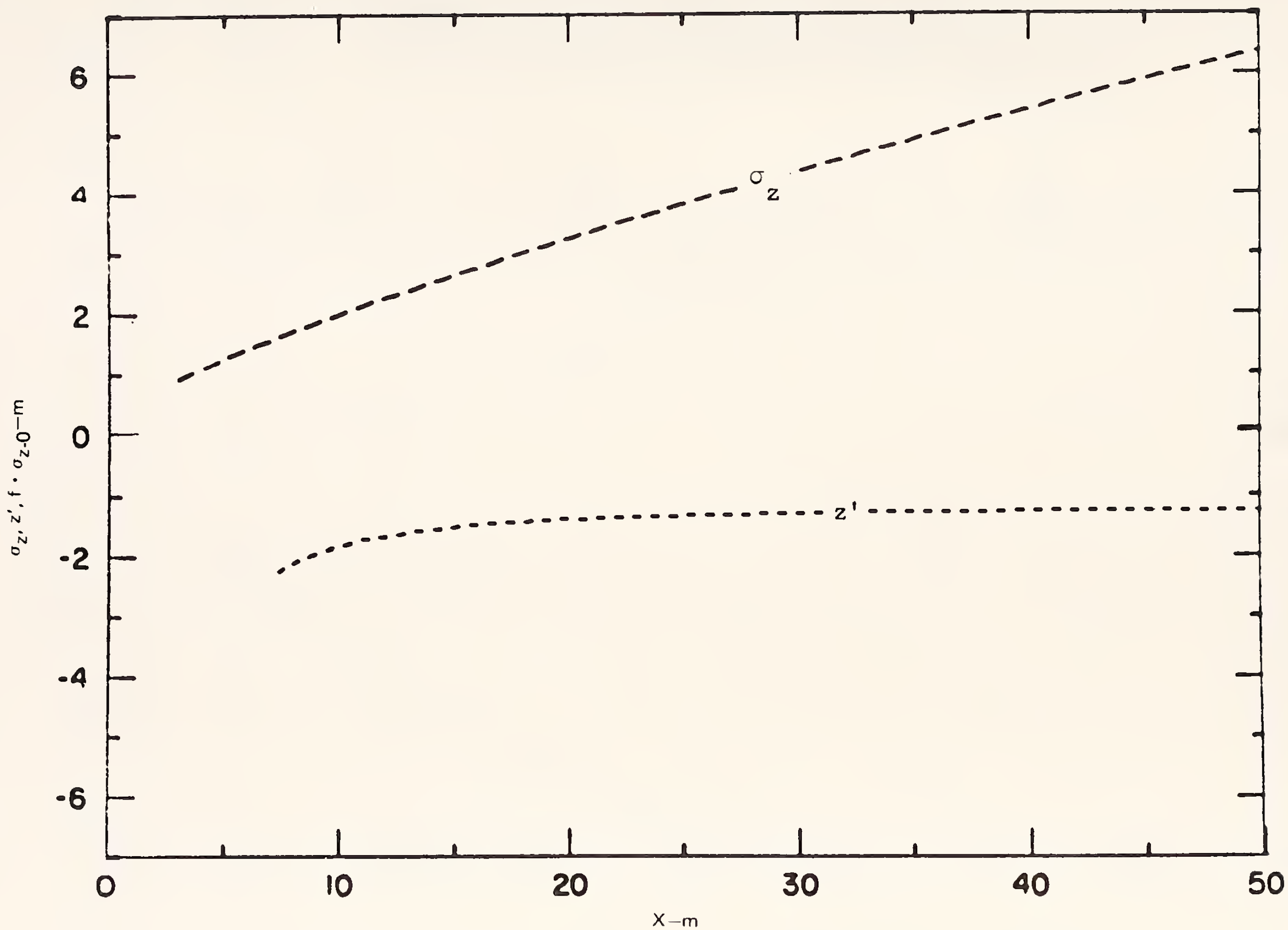

FIGURE 85 VARIATION OF ROADMAP DISPERSION PARAMETERS WITH CROSS-ROADWAY DISTANCE FOR UPWIND TRAFFIC LANES ON HIGHWAY 101; STABLE ATMOSPHERIC CONDITIONS

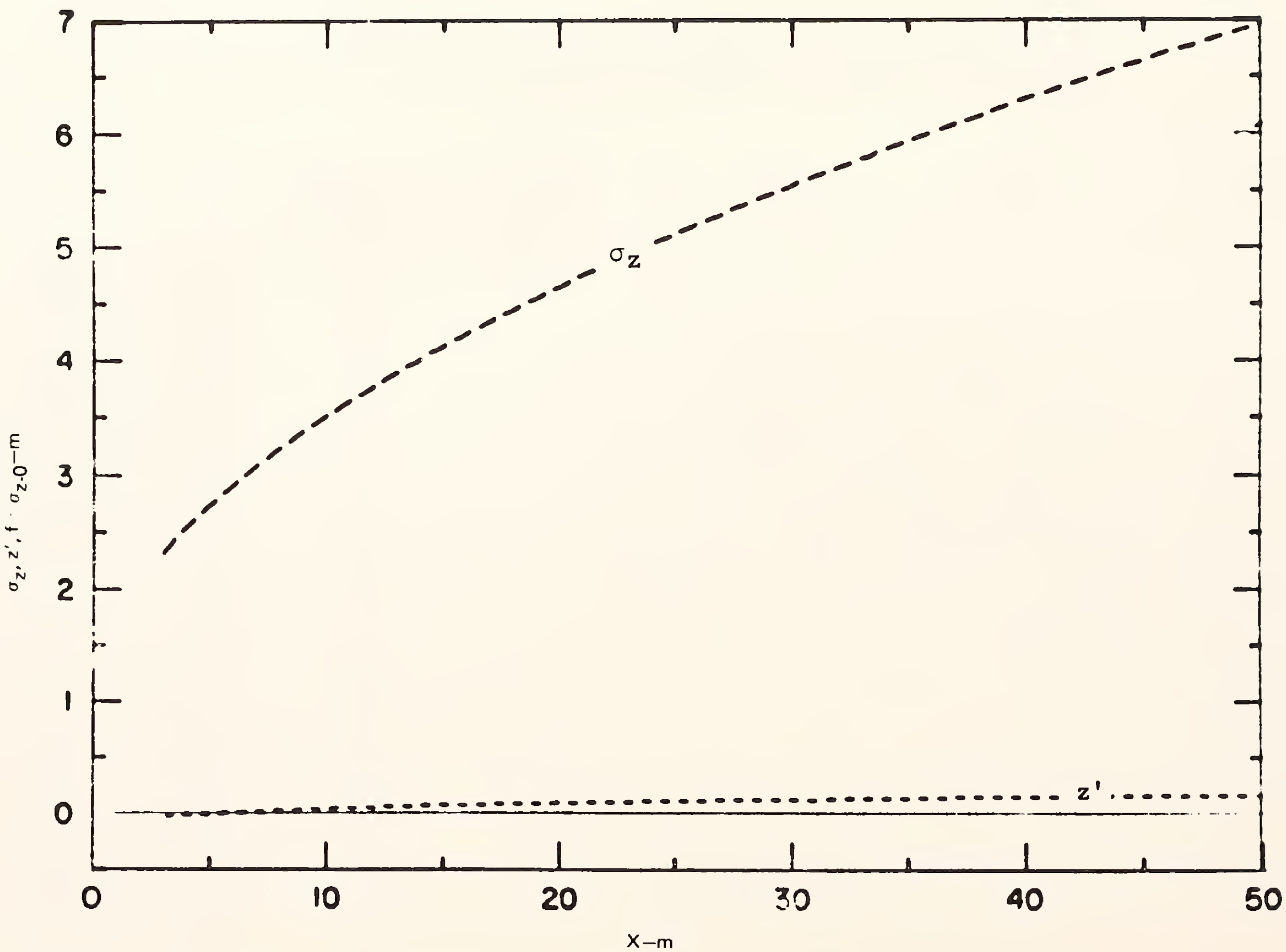

FIGURE 86 VARIATION OF ROADMAP DISPERSION PARAMETERS WITH CROSS-ROADWAY DISTANCE FOR DOWNWIND TRAFFIC LANES ON HIGHWAY 101; STABLE ATMOSPHERIC CONDITIONS

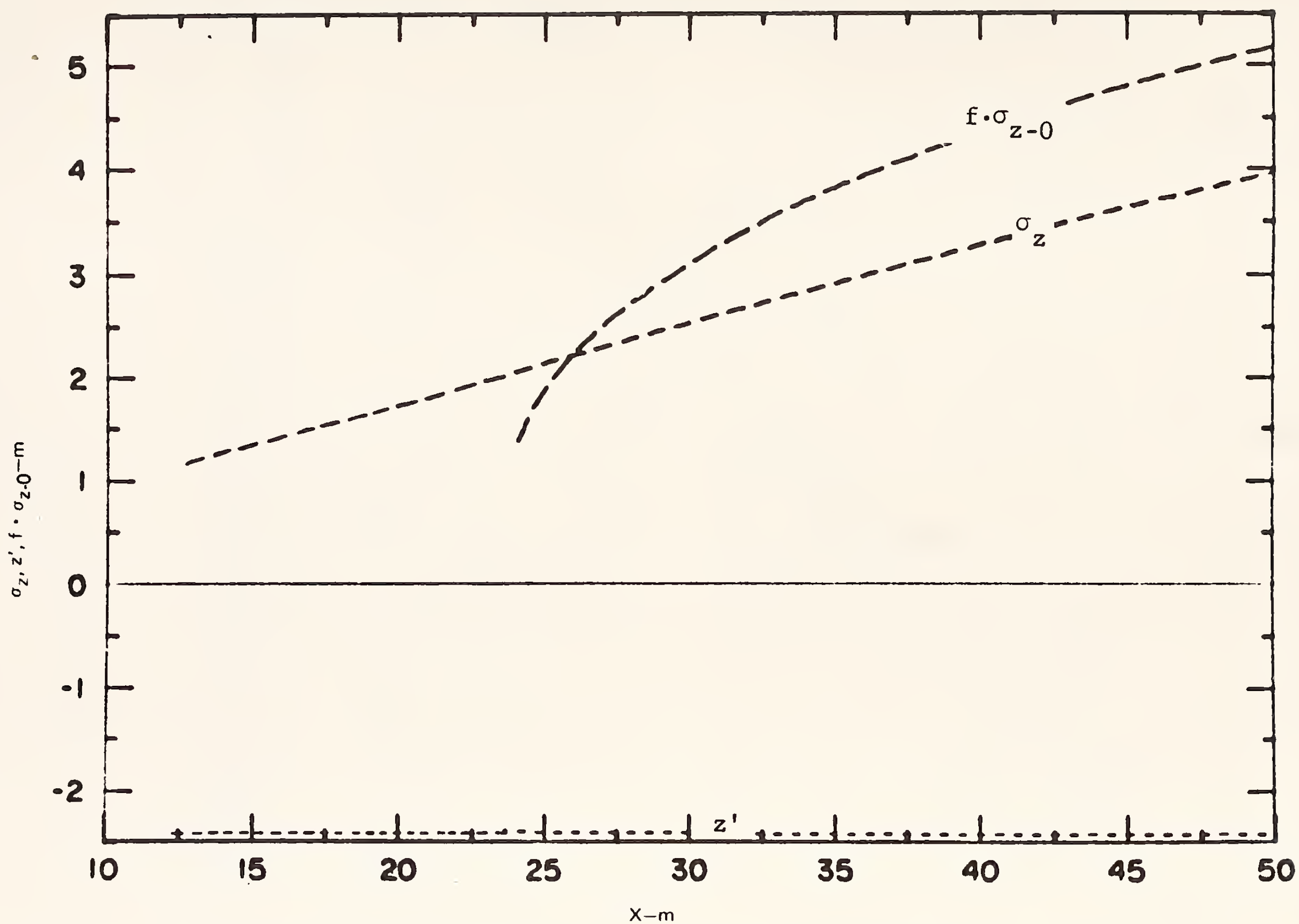

FIGURE 87 VARIATION OF ROADMAP DISPERSION PARAMETERS WITH CROSS-ROADWAY DISTANCE FOR HIGHWAY 101 GRADE-LEVEL TEST, UNSTABLE ATMOSPHERIC CONDITIONS

although it may be suggested that the unstable conditions result in a "looping" effect (similar to plume dispersion from a stack) that brings the emissions plume to the ground with higher-than-expected concentrations.

Two of the remaining seven cases had sufficiently small wind/roadway angles (θ = 9° and 24°) to permit estimation of f using the parallel dispersion term. The function ($f\sigma_{zo}$) is plotted in Figure 87; the magnitude for $x \geq 25$ m appears consistent with the earlier analyses, although the negative values for $x < 20$ m are unrealistic and may result from the small data base. (Note, however, that when this function is used in the two-component model it is squared and does not cause computational instability insofar as there are no samples with x values corresponding to $f\sigma_{z-o} = 0$). Nonetheless, the two-component ROADMAP performs quite well over the entire range of θ: $r^2 = 0.642$ ($r = 0.80$) for all θ-values, and $r^2 = 0.645$ ($r = 0.80$) for $24° < \theta < 67°$. The observed and predicted values for all nine cases are compared in Figure 88.

Figures 89 and 90 illustrate the comparable variations in σ_z, z', and $f\sigma_{z-o}$ as estimated from the upwind and downwind tracer data, respectively. The upwind-based estimate of z' is very similar to the CO-based estimate, although the downwind-estimate is significantly different. Both the downwind-based σ_z- and $f\sigma_{zo}$-terms are relatively invariant with x, so while the initial values are similar to the CO-based estimates the values downwind are substantially smaller. The upwind estimates are more like the CO-based values. As with the stable cases before, it appears that the small number of hourly periods available (i.e., two) to estimate the dispersion functions makes it difficult to make definitive comparisons among upwind- and downwind-tracer estimates and CO estimates.

3. Evaluation of Wind Tunnel Data

A first-order evaluation of the representivity of the wind tunnel simulations can be made by comparing concentration data from the wind tunnel tests with their atmospheric counterparts. None of the tunnel

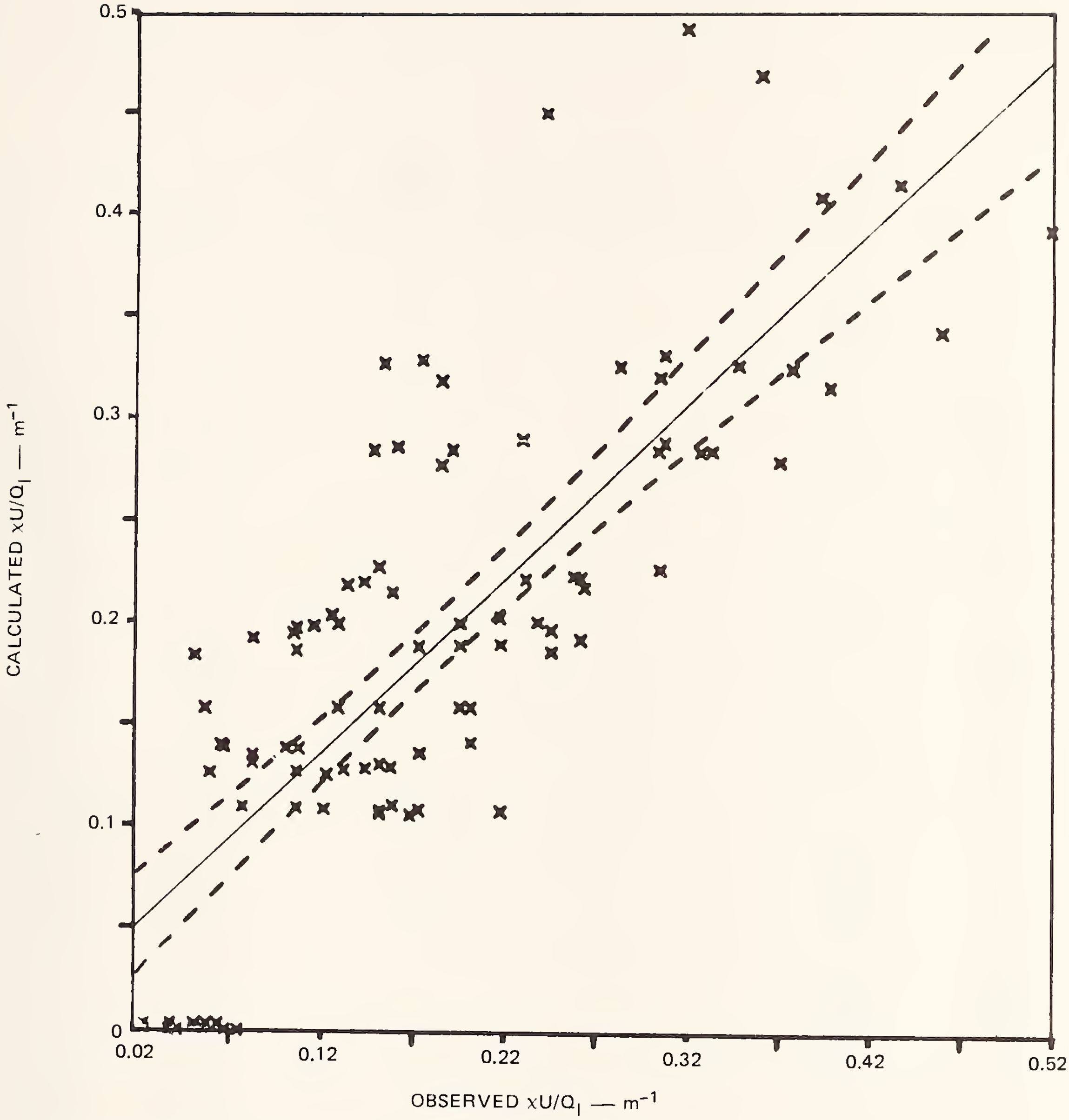

FIGURE 88 COMPARISON OF OBSERVED NORMALIZED CONCENTRATION WITH ROADMAP CALCULATION FOR HIGHWAY 101 GRADE-LEVEL TESTS, UNSTABLE ATMOSPHERIC CONDITIONS, ALL WIND ANGLES

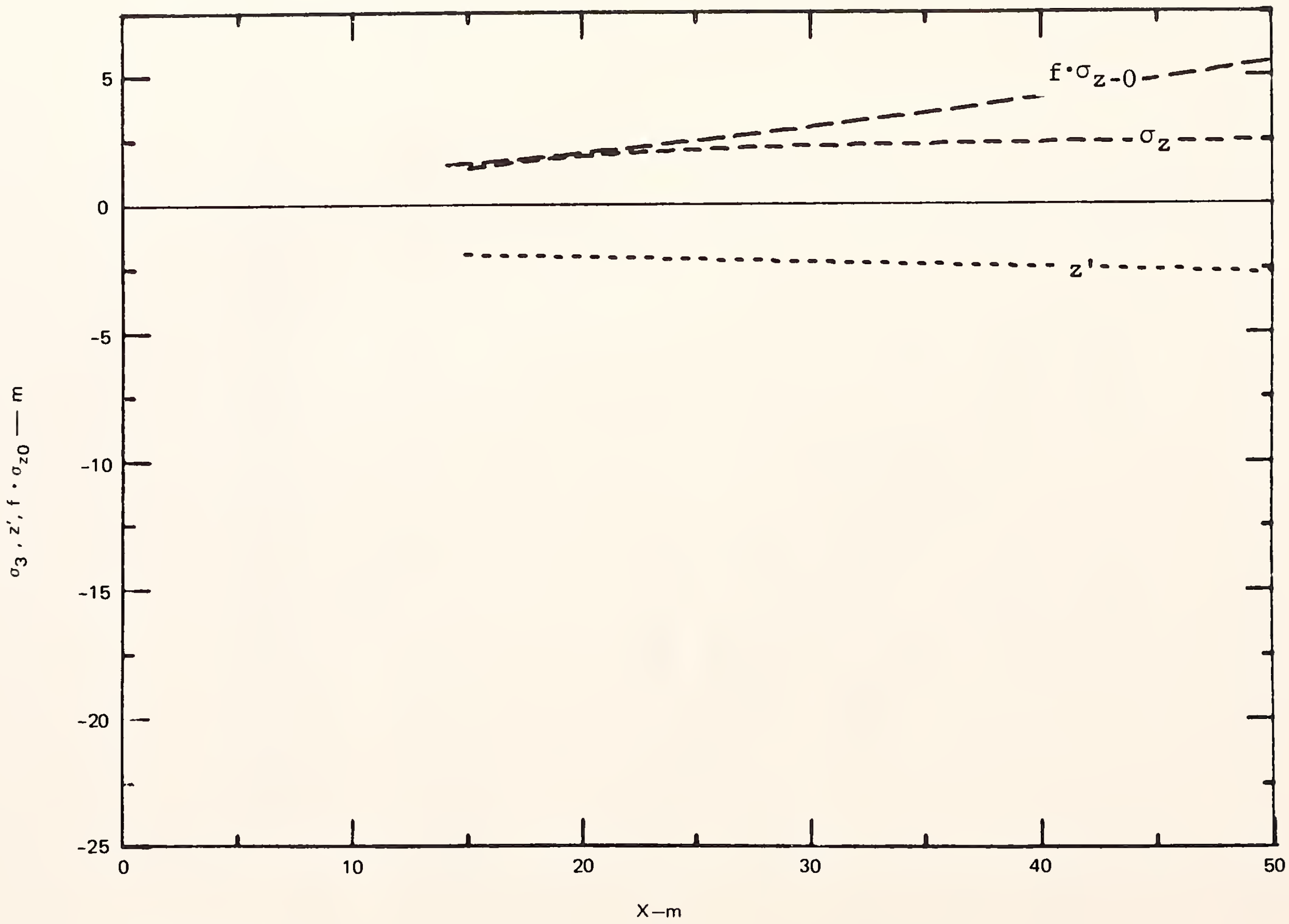

FIGURE 89 VARIATION OF ROADMAP DISPERSION PARAMETERS WITH CROSS-ROADWAY DISTANCE FOR UPWIND TRAFFIC LANES ON HIGHWAY 101; UNSTABLE ATMOSPHERIC CONDITIONS

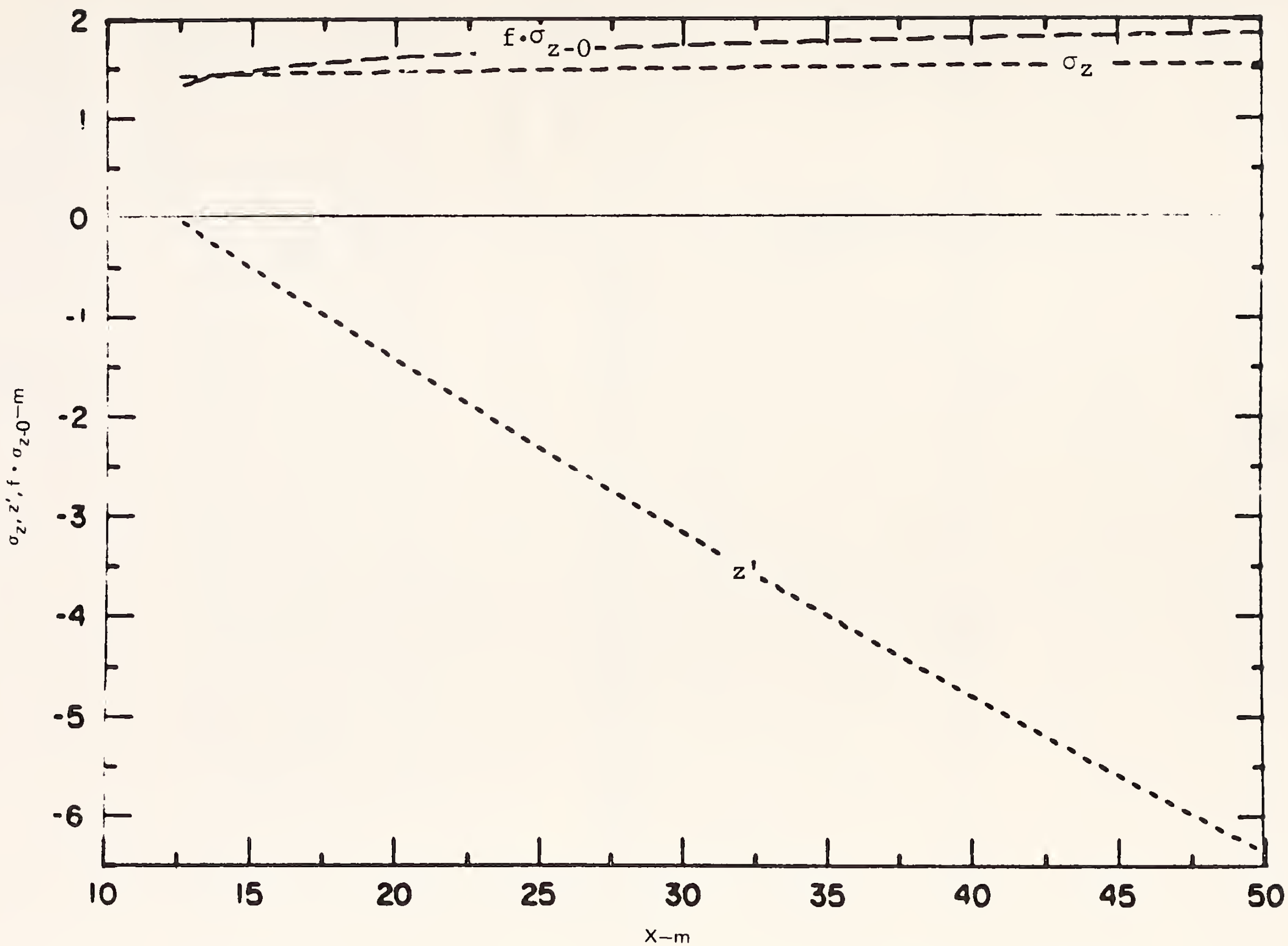

FIGURE 90 VARIATION OF ROADMAP DISPERSION PARAMETERS WITH CROSS-ROADWAY DISTANCE FOR DOWNWIND TRAFFIC LANES ON HIGHWAY 101; UNSTABLE ATMOSPHERIC CONDITIONS

tests was designed explicitly to replicate the atmospheric tests; however, there is a reasonable consistency between tunnel and field grade-level tests. Accordingly, dispersion patterns obtained from the atmospheric study on Route 101 were compared with wind tunnel results from test series Q (smooth terrain, and two-way, high-density traffic). There are three major discrepancies between the tunnel and field tests:

1. The scale model has four traffic lanes to six for the field test,
2. There is no azimuthal meander of wind direction in the tunnel, and
3. The uniformity of traffic speed, volume, and emissions in the scale-model tests contrasts markedly with atmospheric conditions.

Figure 64 illustrated the variation of the three dispersion parameters for the wind tunnel test. The σ_z and z' terms are quite similar in shape and magnitude to their atmospheric equivalents shown later in Figure 79. In contrast, the lateral term ($f\sigma_{z-o}$) is distinctly different; near the roadway edge it is very small indicating high concentrations, but further away it increases rapidly indicating a corresponding drop in concentrations. This is consistent with the steady-wind concept (i.e., no meander). In the atmospheric test, $f\sigma_{z-o}$ is nearly independent of x, indicating a more uniform horizontal x-distribution with parallel winds--typical of a meander situation.

Concentration values were computed using the dispersion coefficients for the two tests in order to compare objectively the dispersion patterns at each of 16 common receptor locations (Figure 91). Comparisons were made over a 4 x 4-receptor matrix with z = 1, 2, 4, and 8 m and x = 20, 30, 40, and 50 m; two wind-roadway angles have been considered: $\theta = 0°$ and 90°. Considering first the parallel-wind situation, the atmospheric data yield an average $u/Q = 0.14\ m^{-1}$ and the wind tunnel average is $0.124\ m^{-1}$. The higher-concentration receptors (i.e., small x and z) indicate wind tunnel concentrations about 60% greater than the atmospheric values, but further away from the roadway the atmospheric values drop off very little in comparison to the wind tunnel concentrations which rapidly approach zero. The low-correlation value of 0.44 reflects this convolution.

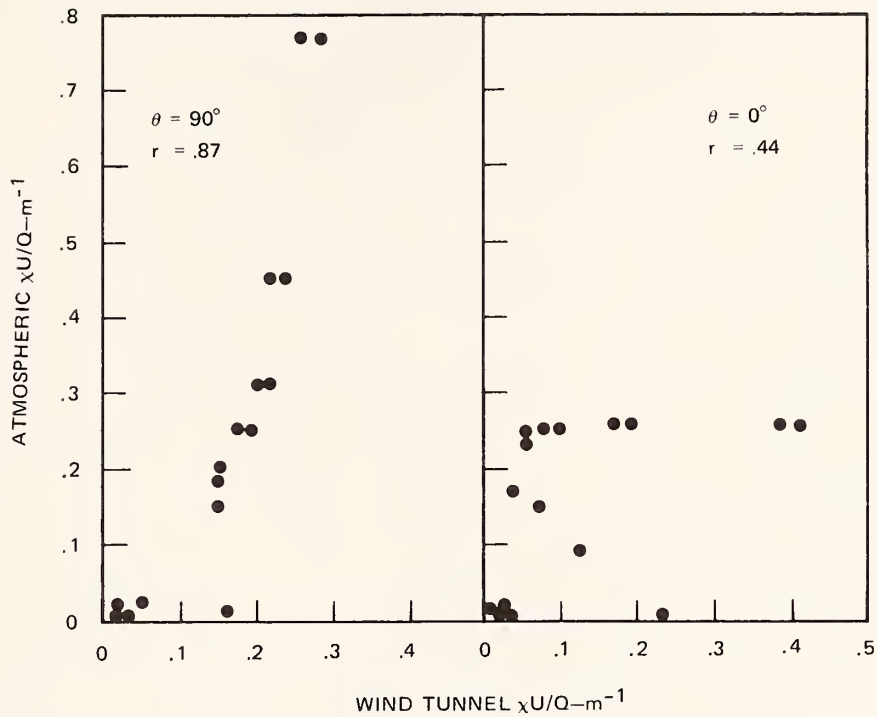

FIGURE 91 ROADMAP VALUES OF NORMALIZED CONCENTRATIONS FROM COMPARABLE ATMOSPHERIC AND WIND TUNNEL ANALYSES

Considering the oblique wind conditions, the average concentration is nearly two-thirds greater for the atmospheric data while the correlation coefficient is significant at 0.87. From these preliminary comparisons we conclude that the relative dispersion pattern given by the wind tunnel simulations is representative of atmospheric conditions when the wind-roadway angle has a strongly oblique component, but the lateral dispersion is underestimated in the wind tunnel for near-parallel wind-roadway angles.

B. Cut-Section Configurations

1. Wind Tunnel Tests

Table 43 summarizes the results of the ROADMAP analyses for wind tunnel test series E and F. Both series had 6.1-m deep cuts, two-way,

Table 43

SUMMARY OF ROADMAP ANALYSES FOR CUT-SECTION CONFIGURATIONS

Series	Perpendicular Dispersion Term									Parallel Dispersion Term						Two-Component Model				
	θ	N	a_1	b_1	c_1	a_2	b_2	c_2	R^2	θ	N	a_3	b_3	c_3	R^2	θ	N	R^2	m^*	$s^\dagger$
E	90	4	0.0006	2.53	2.24	-0.0155	1.47	-3.65	0.898	0,15	8	0.0103	3.19	4.33	0.444	All	16	0.415	0.071	0.828
																0,15	8	0.324	0.091	0.843
																30	4	0.479	0.076	0.711
																90	4	0.898	0.015	0.998
F	90	4	0.00004	3.22	2.53	-0.734	0.496	-0.522	0.941	0,15	8	0.0036	3.37	3.97	0.448	All	16	0.740	0.057	0.556
																0,15	8	0.756	0.073	0.518
																30	4	0.699	0.054	0.498
																90	4	0.941	0.010	0.979
280-CO			0.774	0.386	0.685	-0.0285	1.49	-0.705	0.339	--	$0^\ddagger$	$0.0103^\ddagger$	$3.19^\ddagger$	$4.33^\ddagger$	--	All		0.172	0.121	0.857
Neutral																≥ 45		0.214	0.106	1.01
280-CO			0.796	0.557	-0.945	-1560.	-4.16	-4.17	0.089	--	$0^\ddagger$	$0.0103^\ddagger$	$3.19^\ddagger$	$4.33^\ddagger$	--	All		0.095	0.094	0.597
Unstable																≥ 45		0.190	0.073	0.871
																≥ 67		0.445	0.029	0.890

*m - intercept

†s - slope

‡from E-Series

low-density traffic, and smooth grade-level terrain throughout. The E configuration had side walls that were vertical and situated about 8 m from the roadway edges (Figure 14), while for the F-configuration (Figure 15) the sides sloped at a 30°-angle that begins only 3 m from the roadway.

The perpendicular dispersion term of the two-component model was used in the previous way to estimate $\sigma_z(x)$ and $z'(x)$ for the E-configuration tests. Height $z = 0$ in the model corresponded to the roadway level; data values were taken both within, above, and downwind of the cut. Referring to Table 43, the perpendicular term explained 90% of the variance ($r = 0.95$) in the 90° wind-angles cases. The parallel dispersion term produced $r^2 = 0.44$ ($r = 0.67$) for the 0° and 15° data. Together, the two-component model has an r^2-value of 0.42 ($r = 0.64$) for all wind-angle cases (Figure 92), $r^2 = 0.32$ ($r = 0.57$) for the 0°-15°-data, and $r^2 = 0.48$ ($r = 0.69$) for the 30°-data. The model represents the more oblique wind angles ($\theta \geq 30°$) quite well, but not the near-parallel cases. For example, the two-component ROADMAP has an $r^2 = 0.66$ ($r = 0.81$) for 30°- and 90°-data (Figure 93), but the two-component model was less effective in simulating the 0°-15°-data than the parallel dispersion term alone: the respective r^2-values decreased to 0.32 from 0.44. This implies that the wind flow is channeled along the axis of the cut section for small wind/road angles, such that: (1) there is no real cross-roadway transport out of the cut for small θ values, but (2) the dispersion can be effectively simulated by the two-component approach for more oblique winds.

Figure 94 illustrates the increase in the magnitude of z' (negative sign) to account for the air flow out of the cut. The magnitude and variation of σ_z is similar to series C ("porous cut"), but the magnitude and gradient of the $f \cdot \sigma_{z-o}$ function are quite different. Near the cut, $f \cdot \sigma_{z-o}$ is initially larger than for the C series, but it increases gently with increasing x such that at $x = 35$ m the E-series value is only half the C-series value.

Perhaps more important than what is observed and predicted downwind of the roadway centerline is the magnitude of the upwind concentrations for the E configuration, for within the cut and just upwind of the

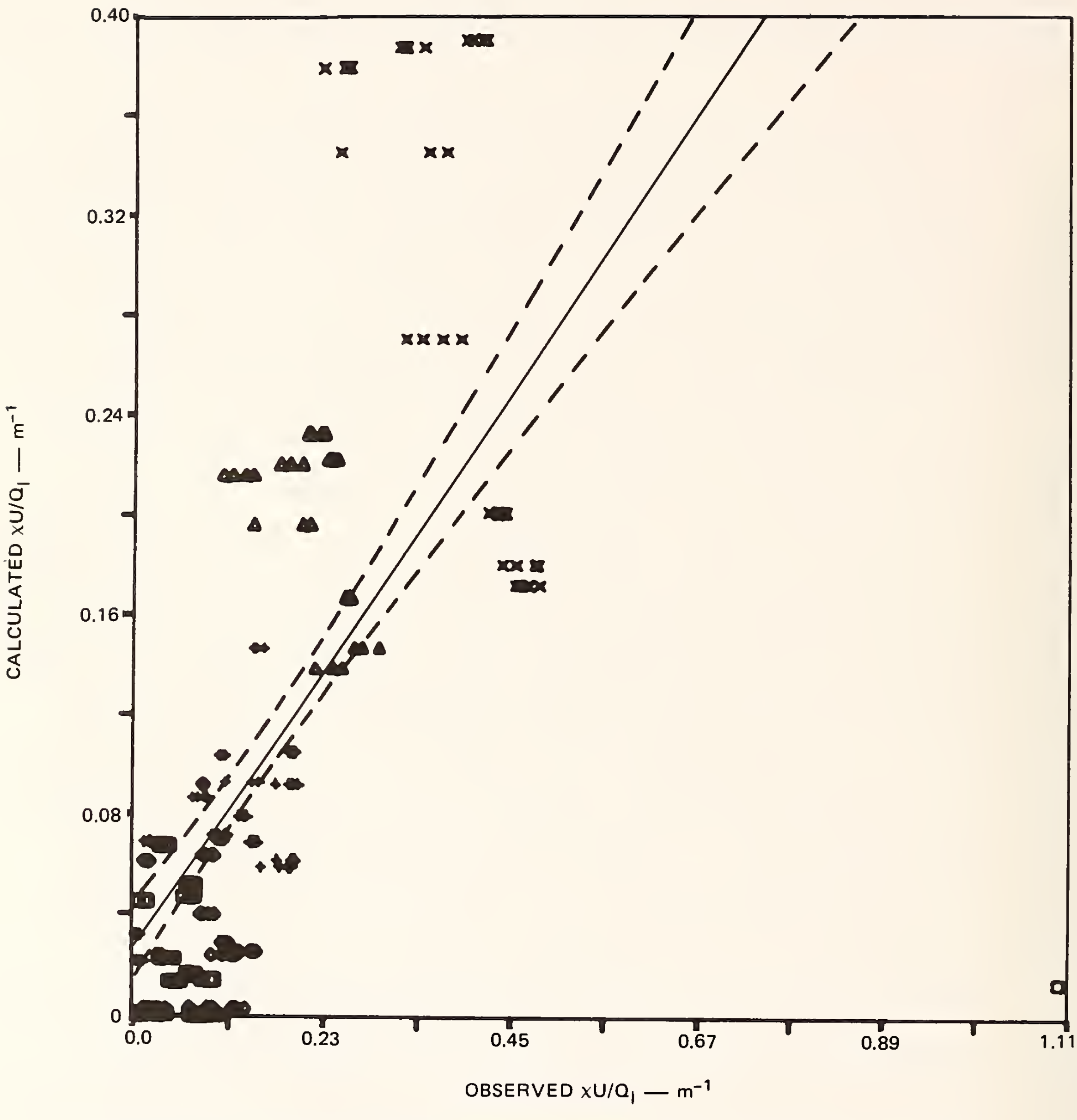

FIGURE 92 COMPARISON OF OBSERVED NORMALIZED CONCENTRATION WITH ROADMAP CALCULATION FOR WIND TUNNEL SERIES E, ALL WIND ANGLES

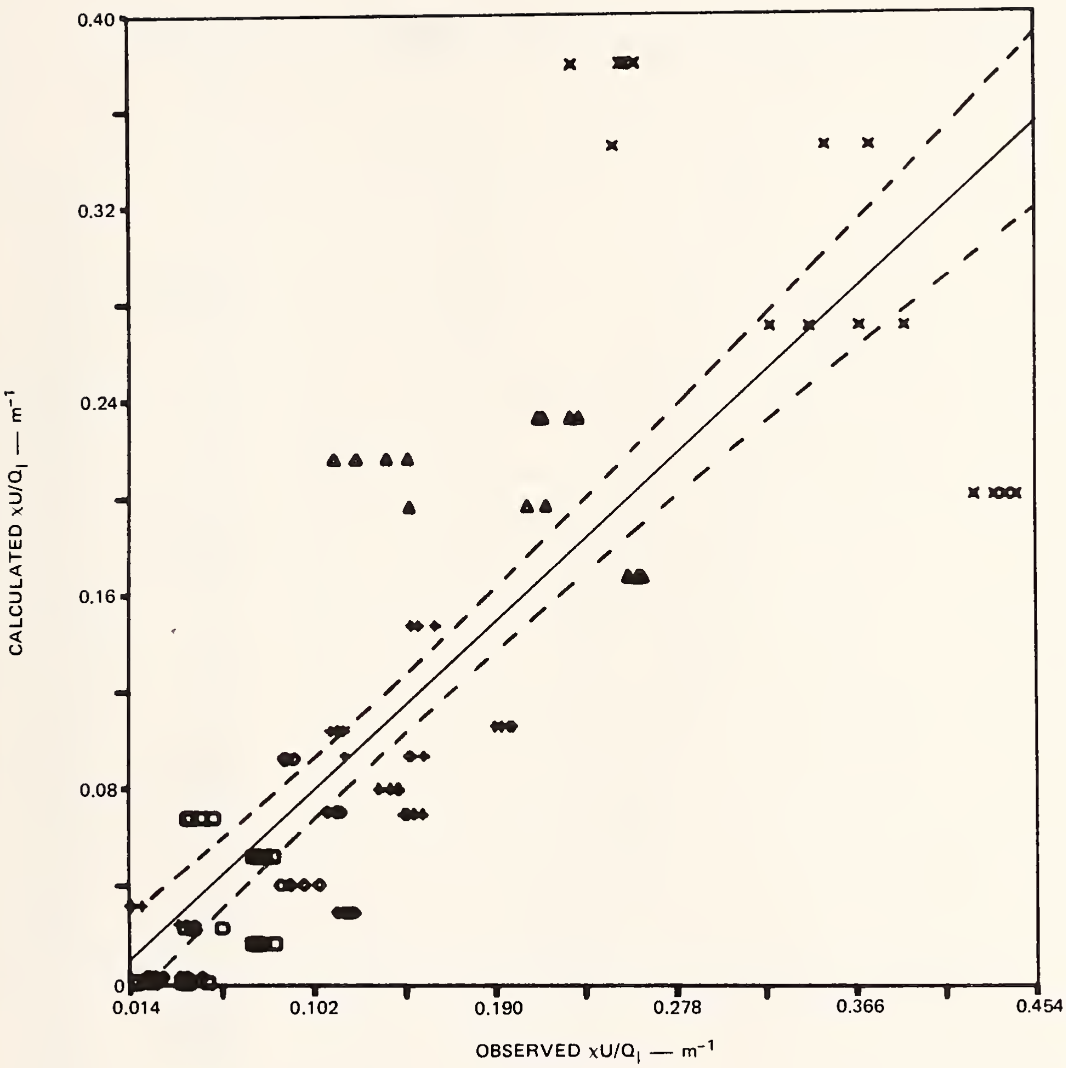

FIGURE 93 COMPARISON OF OBSERVED NORMALIZED CONCENTRATION WITH ROADMAP CALCULATION FOR WIND TUNNEL SERIES E, $\theta = 30^\circ$ AND 90°

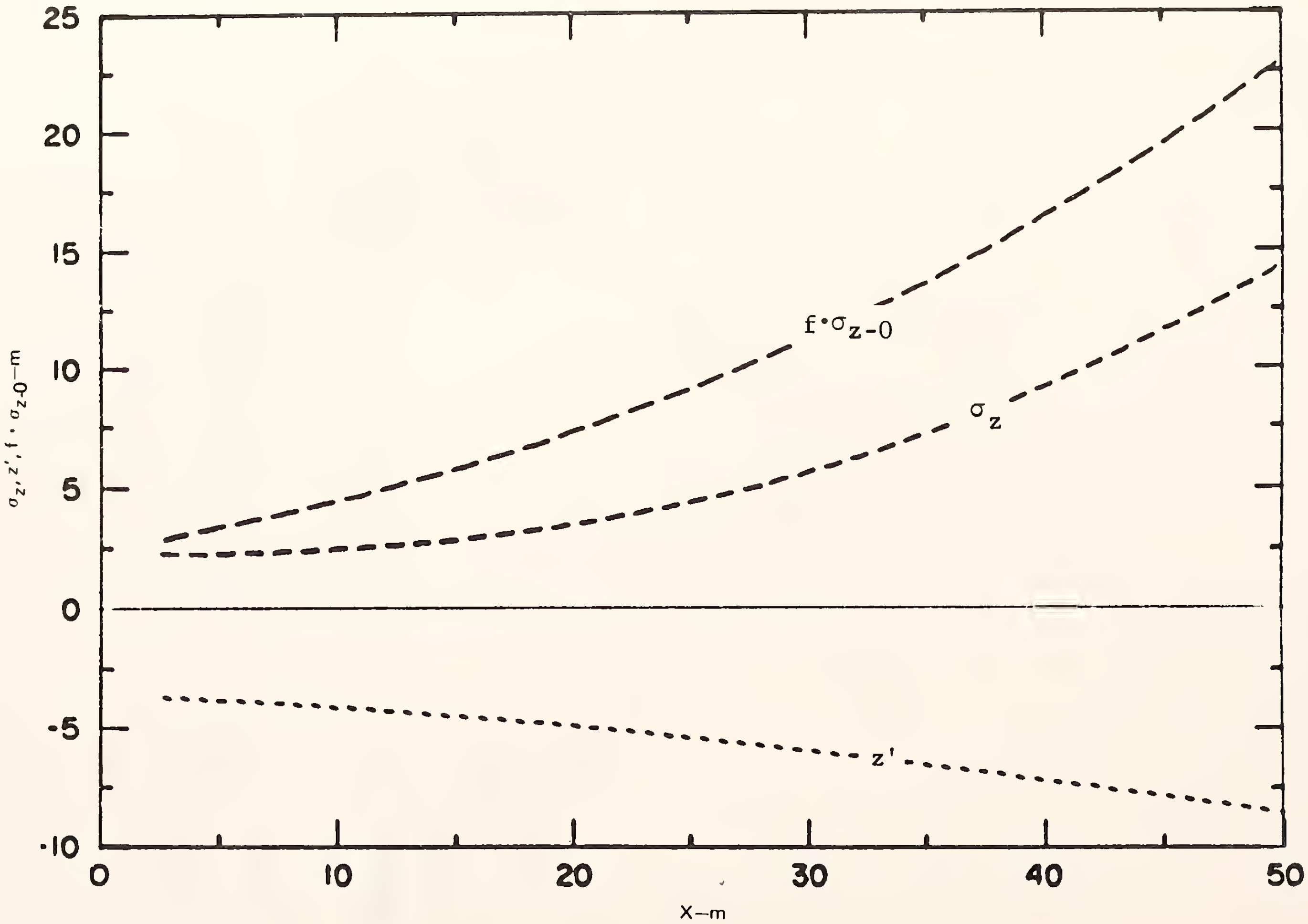

FIGURE 94 VARIATION OF ROADMAP DISPERSION PARAMETERS WITH CROSS-ROADWAY DISTANCE FOR WIND TUNNEL SERIES E

roadway edge, the normalized concentrations are significantly larger than they are for either the C- or Q-series configurations. With a near-parallel wind the peak concentration is about equal to the comparable Q-series peak, but with a perpendicular wind the peak is 3.6 times the Q peak and 4.2 times the C peak. As discussed in the C-series analysis, this is another example of the street canyon recirculation pattern. This region of very high concentrations is confined, however, to the upwind side of the cut and does not extend farther upwind.

Wind tunnel test series F with its sloping sides has concentration values and patterns quite dissimilar to the vertical-walled E series. The two-component ROADMAP is effective in simulating concentrations for all wind angles and locations. The sloping sides of the cut inhibit the street-canyon recirculation pattern; the accompanying upwind transport is minimal resulting in near-equal concentration peaks at both roadway edges. The perpendicular dispersion term yields $r^2 = 0.94$ ($r = 0.97$) for 90°-cases, while the parallel term yields $r^2 = 0.45$ ($r = 0.67$) for 0°-15°-cases. Figure 95 shows the σ_s, z', and $f \cdot \sigma_{z-o}$ values so derived. When these are used in the two-component model r^2 for all wind angle cases is 0.74 ($r = 0.86$), and $r^2 = 0.70$ ($r = 0.84$) for the 30°-cases; Figure 96 is a comparison of observations and ROADMAP predictions. Two particularly important results stand out for the F-series cut section analysis: (1) the excellent performance of ROADMAP indicates that the two-component dispersion concept is valid for the sloping cut where it was not for the vertical cut, and (2) the peak concentrations are comparable to those for the at-grade Q series for all wind/roadway angles, and are significantly less than for the vertical cut.

Figures 97 through 100 are scattergrams that compare data from the E and L Series for four different wind/roadway orientations. The L-configuration differs from E in one very important respect: a 90-m tall air-right building (53-m square) has been located directly over the cut section at a position 46 m from the E-series sampling probe array. In Figure 97, the wind direction (000°) is parallel to the roadway and the structure is directly downwind of the sampling array during the L-series. The slope of the E-versus-L linear regression line is 0.594

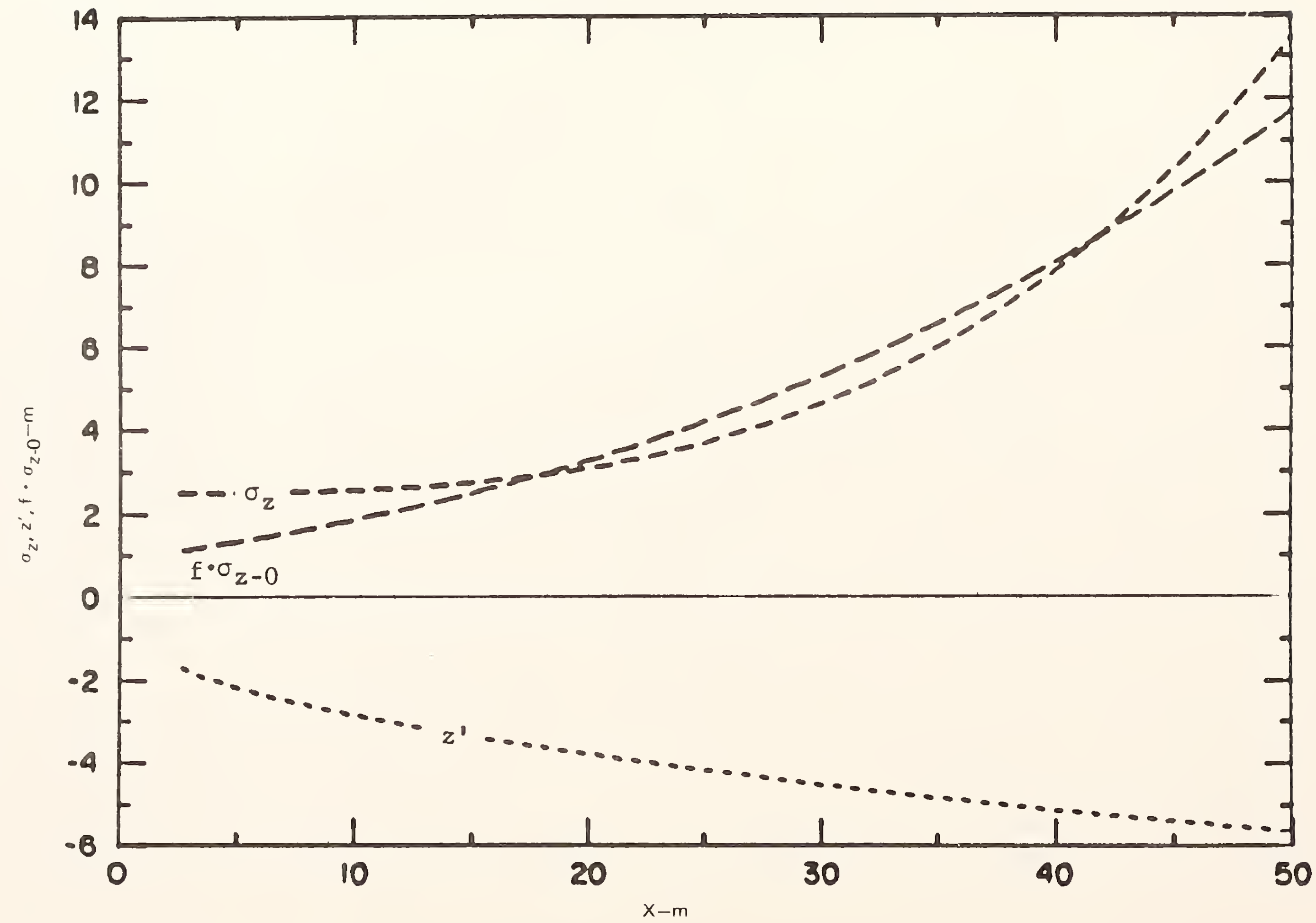

FIGURE 95 VARIATION OF ROADMAP DISPERSION PARAMETERS WITH CROSS-ROADWAY DISTANCE FOR WIND TUNNEL SERIES F

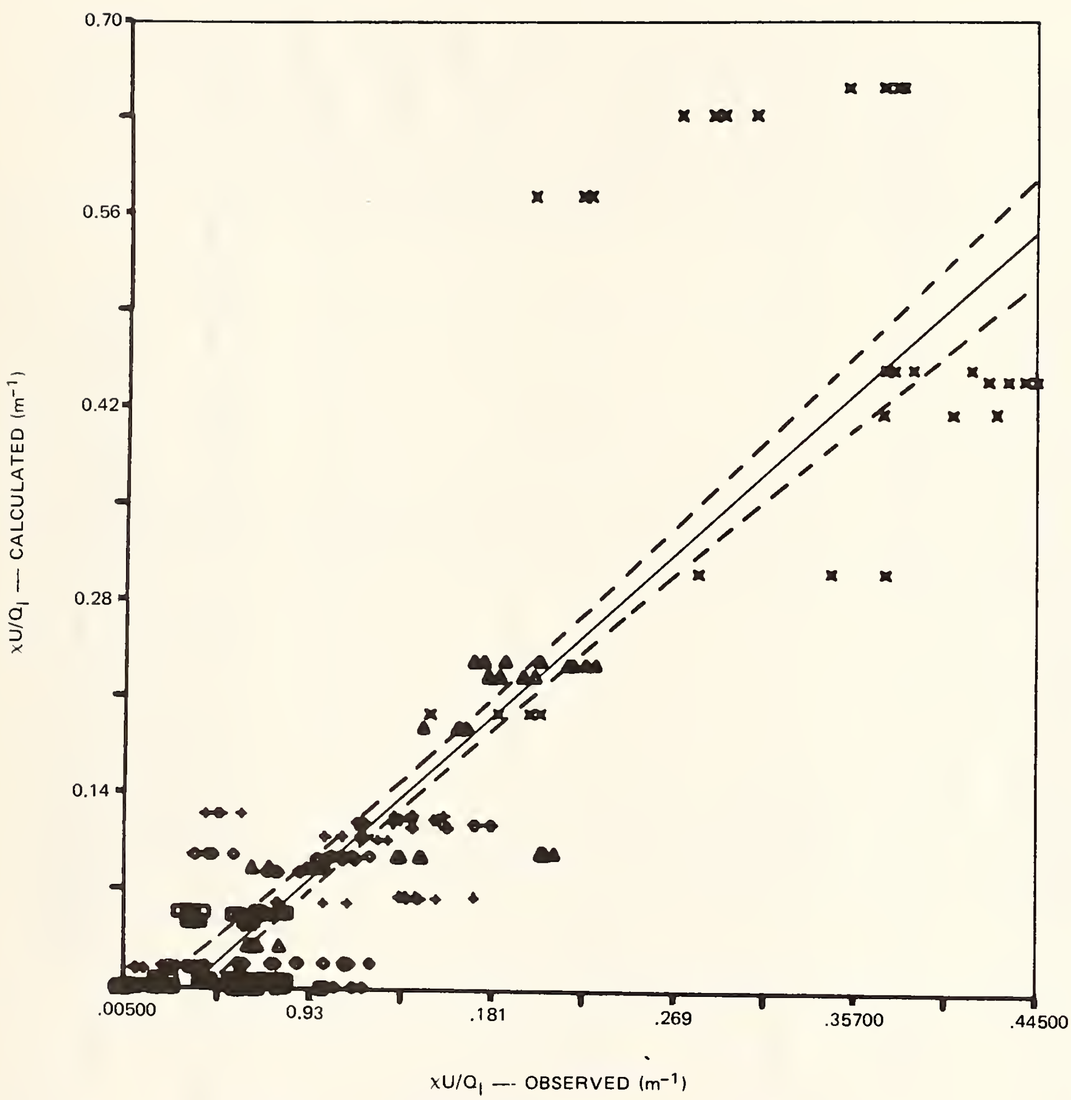

FIGURE 96 COMPARISON OF OBSERVED NORMALIZED CONCENTRATION WITH ROADMAP CALCULATION FOR WIND TUNNEL SERIES F, ALL WIND ANGLES

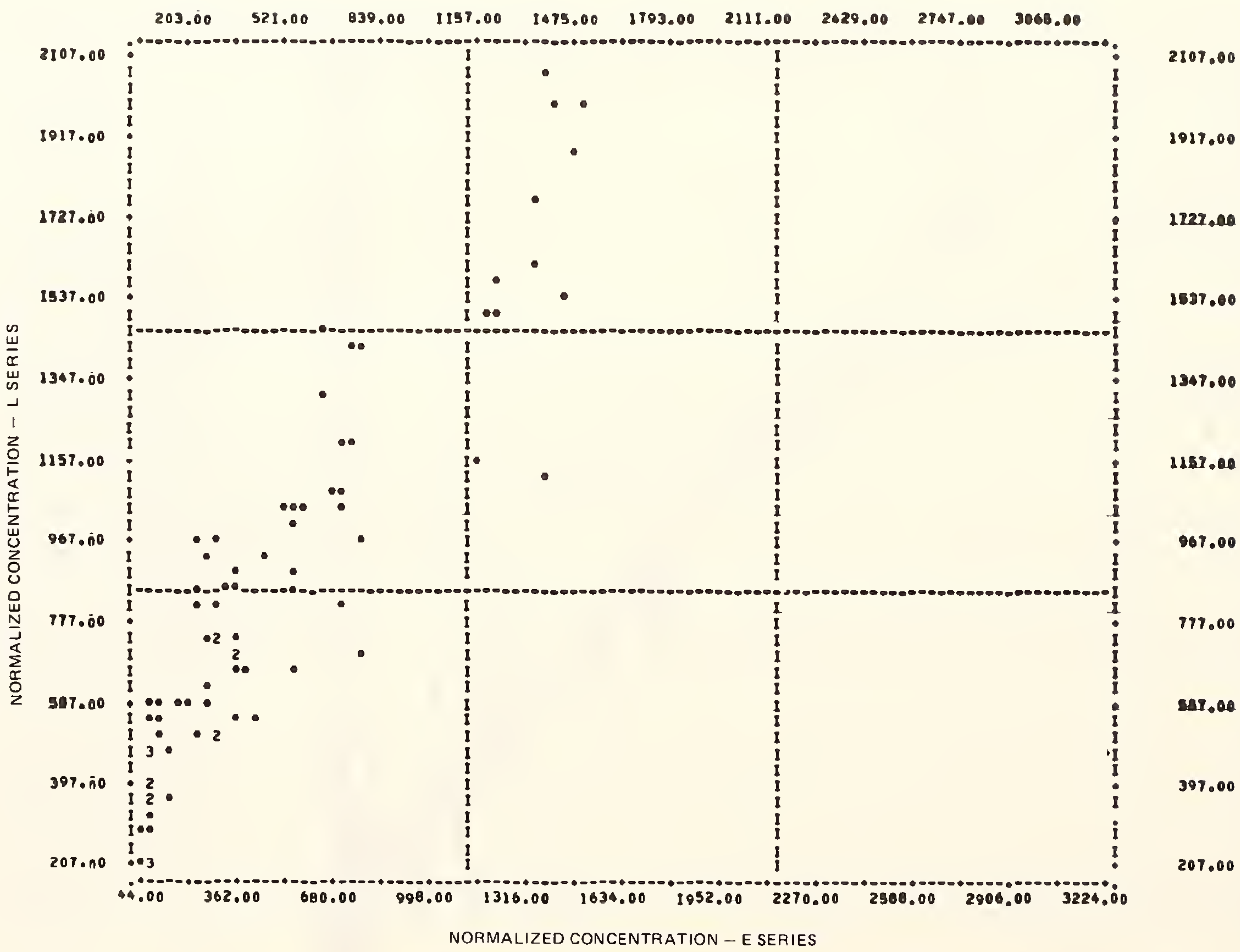

FIGURE 97 SCATTERGRAM OF E-VERSUS-L SERIES FOR ROADWAY-PARALLEL WIND AND SAMPLING ARRAY UPWIND OF AIR-RIGHT STRUCTURE (L SERIES)

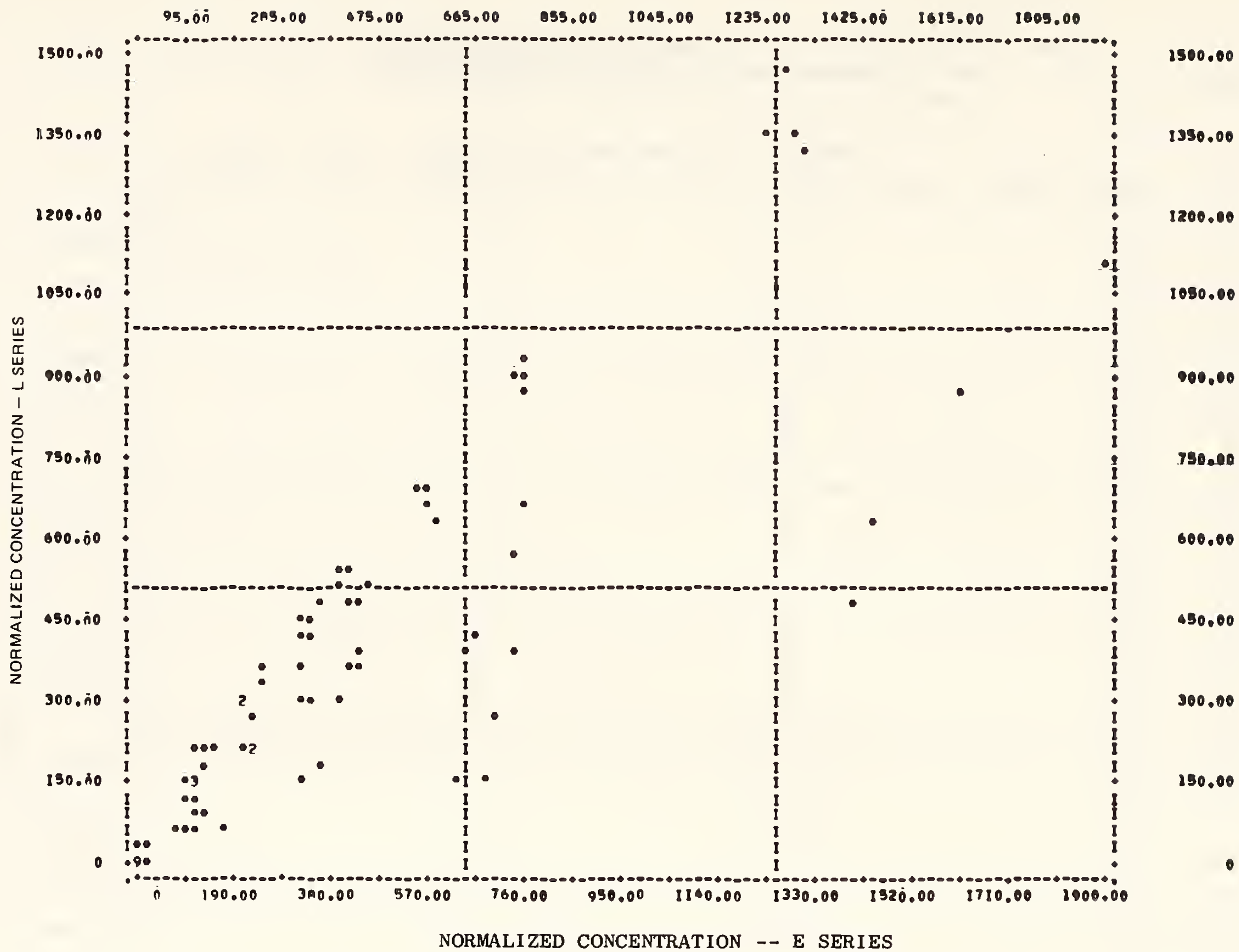

FIGURE 98 SCATTERGRAM OF E-VERSUS-L SERIES FOR ACUTE (30°) WIND-ROADWAY ANGLE AND SAMPLING ARRAY UPWIND OF THE AIR-RIGHT STRUCTURE (L SERIES)

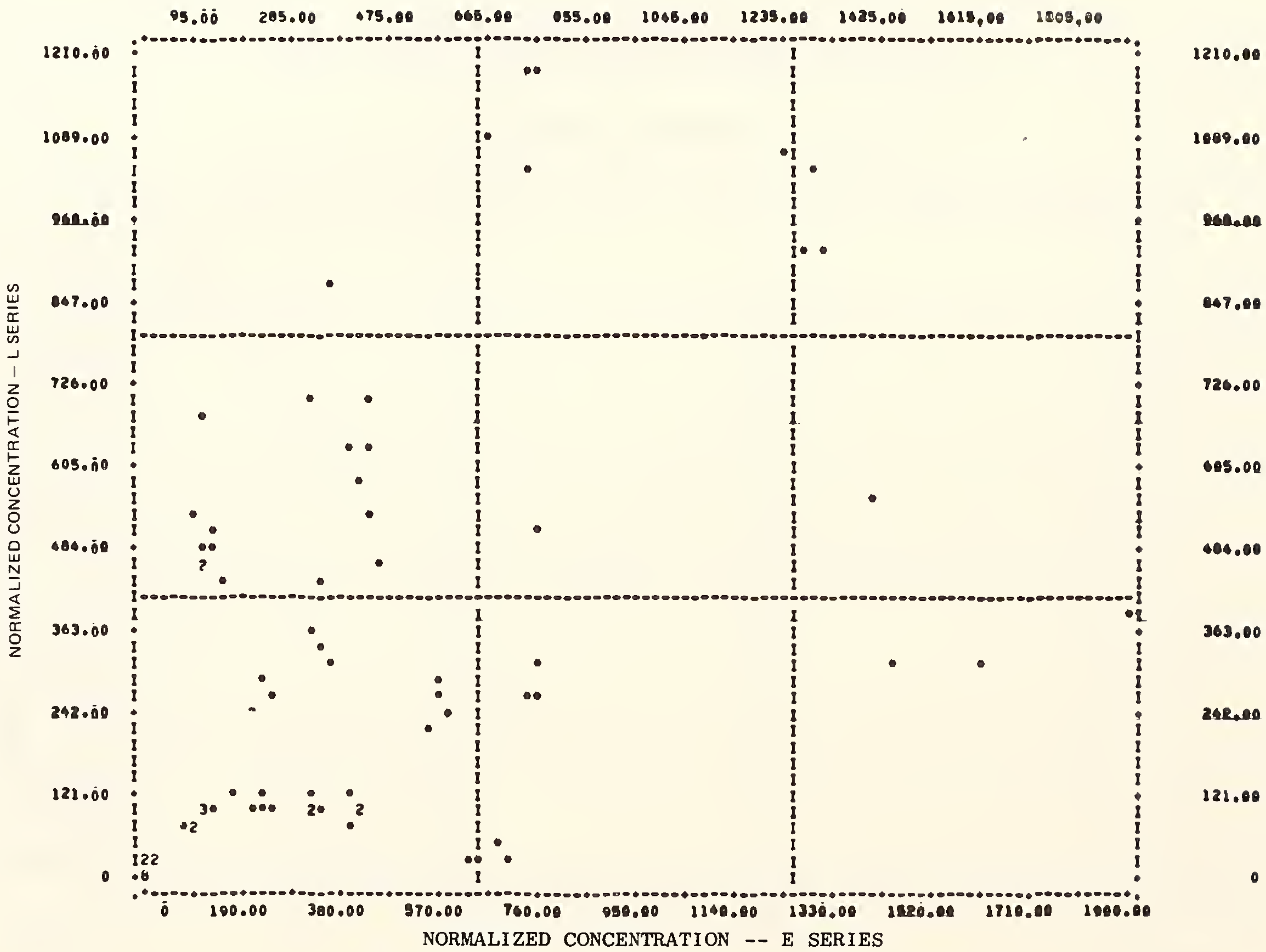

FIGURE 99 SCATTERGRAM OF E-VERSUS-L SERIES FOR ACUTE (30°) WIND-ROADWAY ANGLE AND SAMPLING ARRAY DOWNWIND OF THE AIR-RIGHT STRUCTURE (L SERIES)

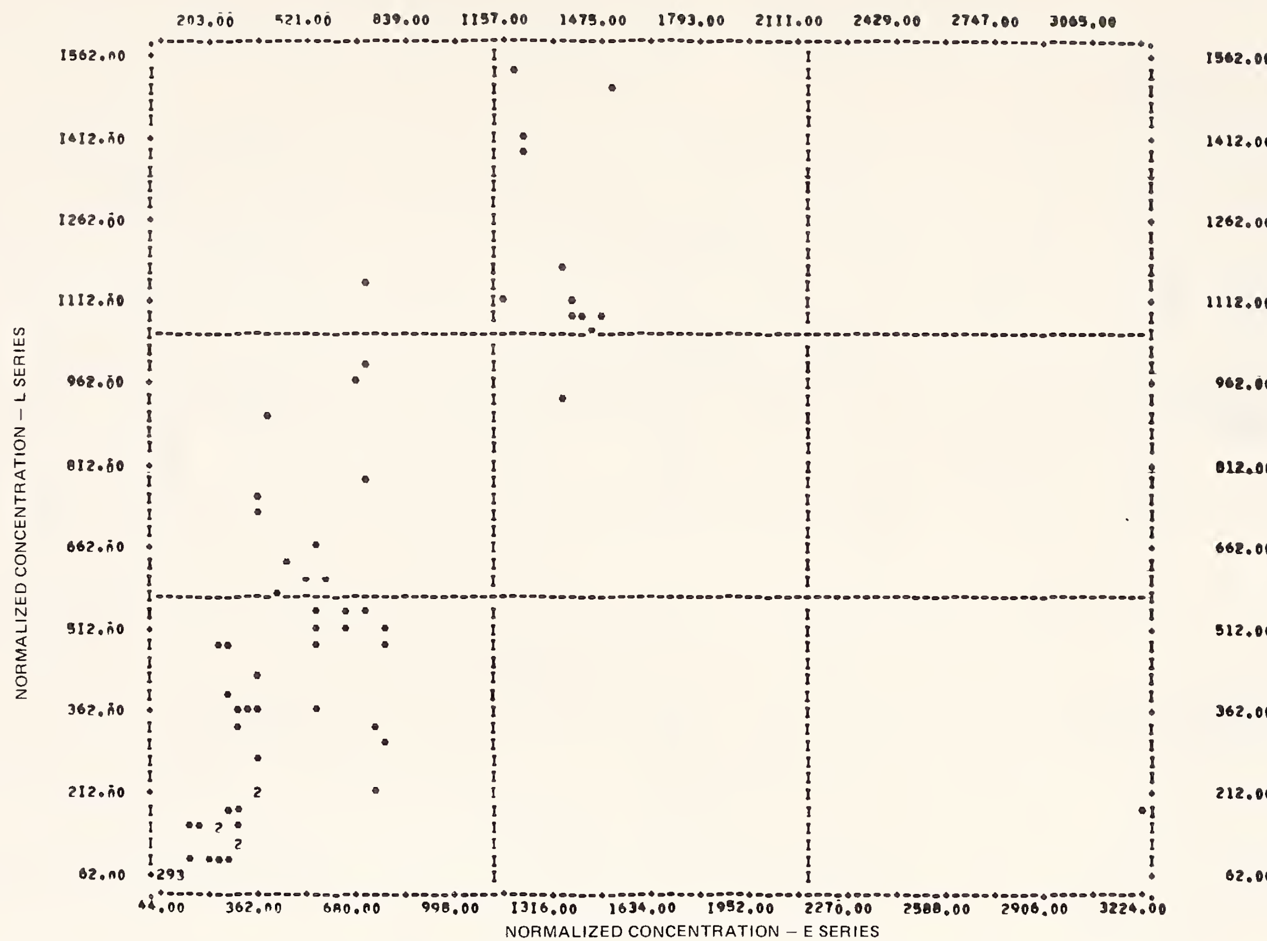

FIGURE 100 SCATTERGRAM OF E-VERSUS-L SERIES FOR ROADWAY-PARALLEL WIND-ANGLE AND SAMPLING ARRAY DOWNWIND OF THE AIR-RIGHT STRUCTURE (L SERIES)

indicating that the effect of the building is to increase the near-roadway concentrations by a factor of almost two (1.7). The variance explained by the linear regression is 46% ($r = 0.68$), thus implying a relatively uniform increase for all locations sampled. In Figure 98, the building is still downwind but the relative wind/roadway angle is 30°. There is less scatter in the data, and the similar slope of the regression line ($s = 0.706$) indicates that the effect of the building still is to increase concentrations (by about 42%). The variance explained by the linear regression is significantly greater than the previous comparison (Figure 97): $r^2 = 0.706$ ($r = 0.84$).

The same general pattern holds when the wind direction is reversed and the building is upwind of the sampling array. In Figure 99, the wind is parallel to the roadway ($\theta = 180°$). Again, the concentrations in the presence of the building are about double ($s = 0.54$) those without the building; the scatter about the regression line is moderate: $r^2 = 0.451$ ($r = 0.67$). The scatter increases markedly when the wind/roadway offset is 30° ($\theta = 150°$). The concentrations are still substantially increased overall with the building present ($s = 0.39$), but $r^2 = 0.244$ ($r = 0.49$). This may be the influence of turbulent eddies that are shed from the downwind corners of the building and which conceivably could have a more chaotic influence with the 30°-offset than with no offset (when the sampling array is in the center of the wake).

The effect of the air-right structure is more graphically depicted in Figures 101a and 101b which present concentration isopleths (on the plane of the sampling array) for parallel and acute wind-roadway angles, respectively, with and without the presence of the building. In Figure 101a ($\theta = 000°$ and $V = 4.6 \text{ m s}^{-1}$), the effect of the building on the vertical extent of the pollutant dispersion is seen; with the building downwind of the sampling array, the mixed layer is higher than it is either with no building or with the building upwind of the array. Close to the roadway in the cut, concentrations are highest with the building again downwind of the sampling array; the other two cases (i.e., no building and the building upwind of the array) are relatively similar.

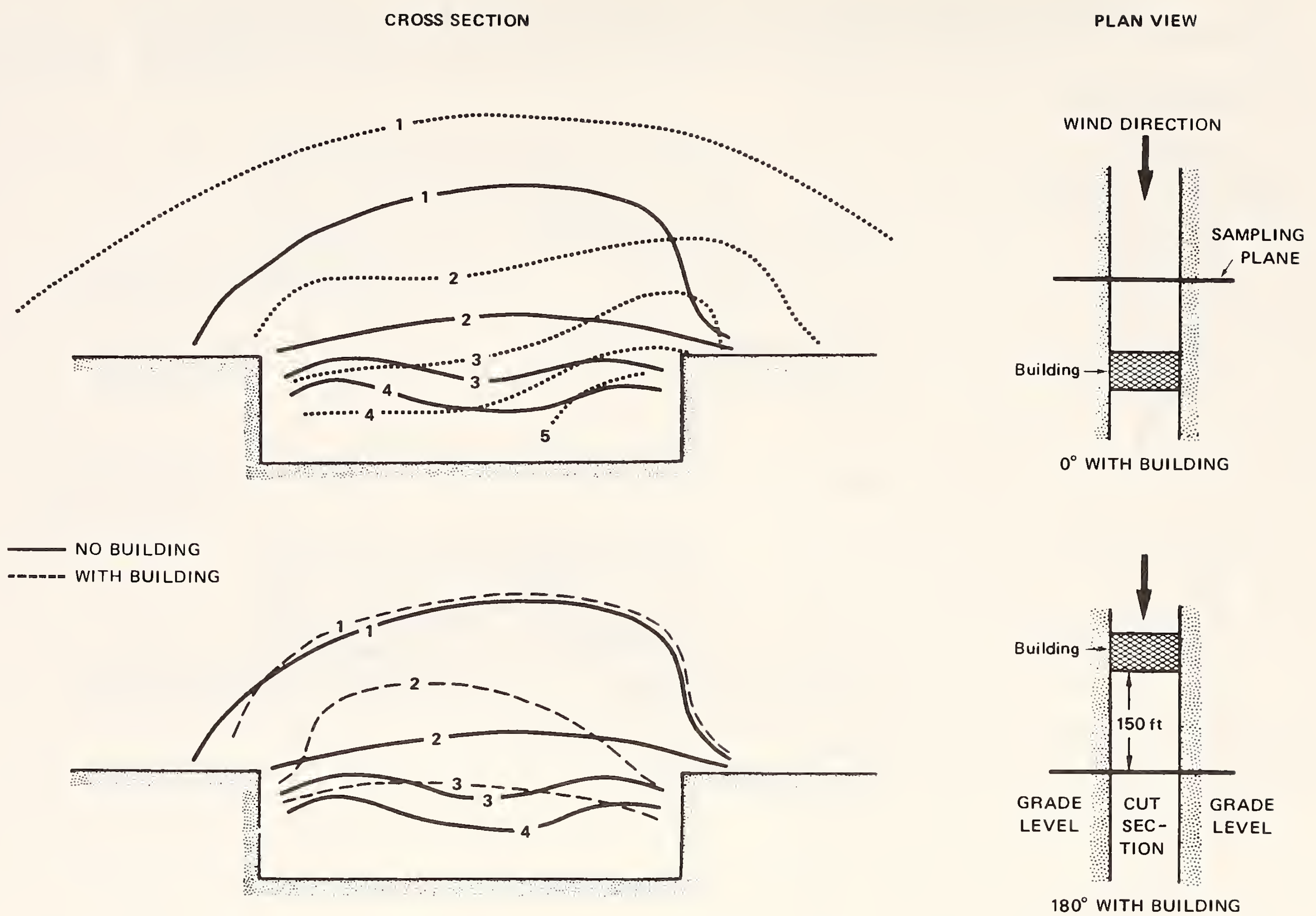

FIGURE 101a ISOPLETHS OF RELATIVE, EQUIVALENT CO CONCENTRATIONS FOR A ROADWAY-PARALLEL WIND AND A CUT SECTION (WITH AND WITHOUT THE PRESENCE OF AN AIR-RIGHT STRUCTURE NEARBY)

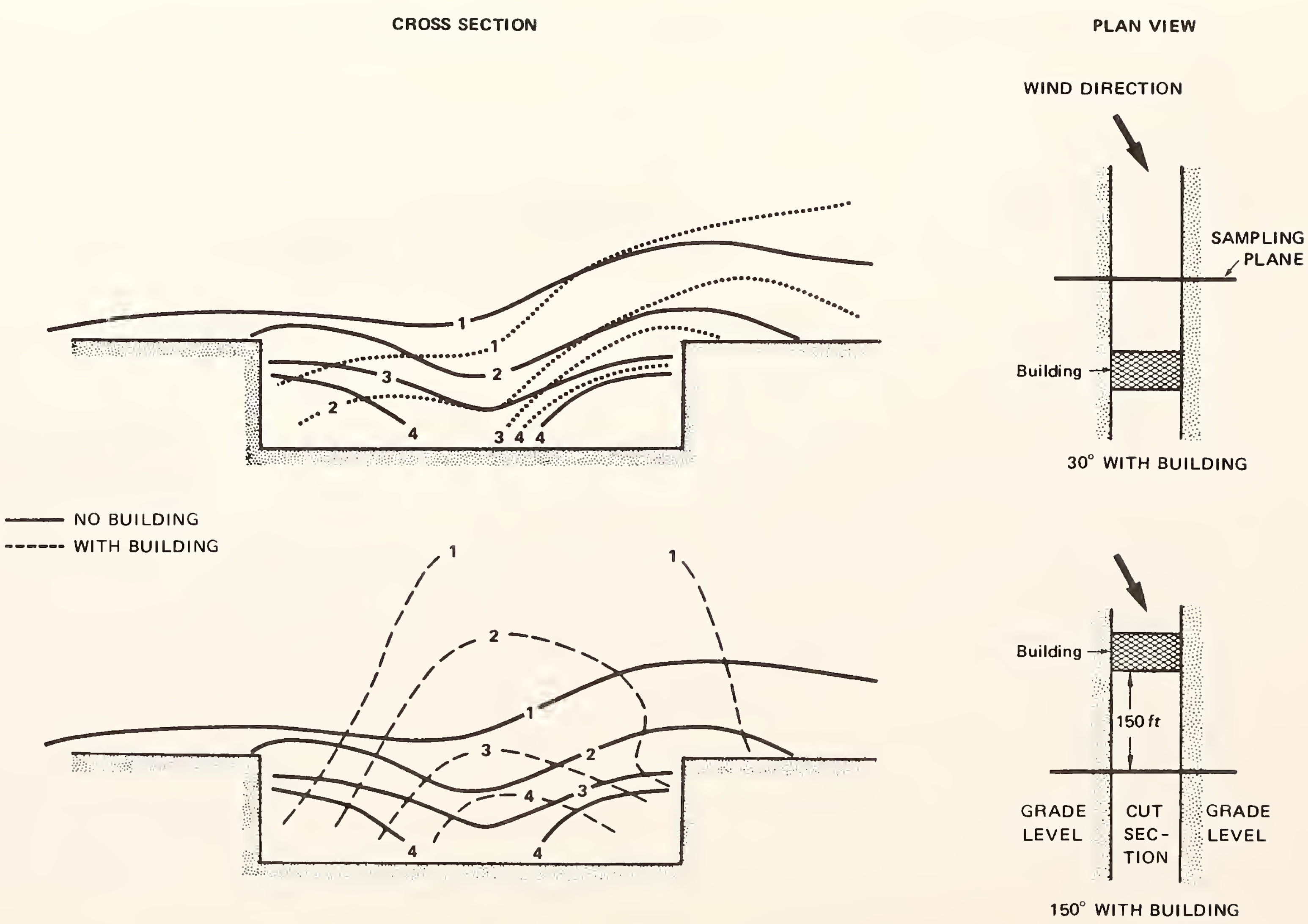

FIGURE 101b ISOPLETHS OF RELATIVE, EQUIVALENT CO CONCENTRATIONS FOR A ROADWAY-PERPENDICULAR WIND AND A CUT SECTION (WITH AND WITHOUT THE PRESENCE OF AN AIR-RIGHT STRUCTURE NEARBY)

With an acute roadway-wind angle (θ = 30° and V = 4.6 m s^{-1}), the differences among the three cases are more marked. In the cut itself, peak concentrations are about the same although their distribution differs. In the absence of the building, peaks are found in both corners of the cut with slightly lower concentrations in the center. With the sampling probe downwind of the building, the peak is centered nearly in the center of the cut with a tendency to extend further to the downwind half of the cut; the peak concentration region with the sampling array upwind of the building is located only in the downwind corner of the cut. Higher up, the concentration patterns are very similar for two of the three cases: one, without the building, and two, upwind of the building. However, downwind of the building the vertical extent of the mixed region is significantly greater while its lateral (crosswind) extent is suppressed.

2. <u>Atmospheric Test</u>

The hourly data periods from the cut-section experiment along I-280 were stratified into neutral and unstable categories in much the same way as was done with the 101 experiment data. The 19 neutral cases had the following ranges of meteorological parameters: (1) 16.1° $\leq \sigma_\theta \leq$ 22.7, (2) 9.1° $\leq \sigma_\phi \leq$ 18.8°, and (3) -0.97 $\leq$ Ri $\leq$ -0.03. The 19 unstable cases ranged as follows: (1) 22.6° $\leq \sigma_\theta \leq$ 38.4°, (2) 9.0° $\leq \sigma_\phi \leq$ 29.4°, and (3) -5.57 $\leq$ Ri $\leq$ -0.27.

Most wind directions recorded had θ values greater than 45° for both the neutral and unstable categories. None was small enough to estimate the f function from the parallel dispersion term. However, five neutral cases with $\theta \geq$ 70° were used to estimate σ_z and z' from the perpendicular dispersion term; five unstable cases with $\theta \geq$ 67° were similarly used. For the neutral cases, the perpendicular term had an r^2 = 0.34 (r = 0.58), while r^2 = 0.089 (r = 0.30) for the unstable cases. The corresponding σ_z and z' values are plotted in Figures 102 and 103 for the neutral and unstable cases, respectively. The initial σ_z values are similar in both cases, although the increase with x is larger for the unstable cases. The height-offset term z' is negative in both cases, although essentially independent of x for the unstable cases while decreasing rapidly with

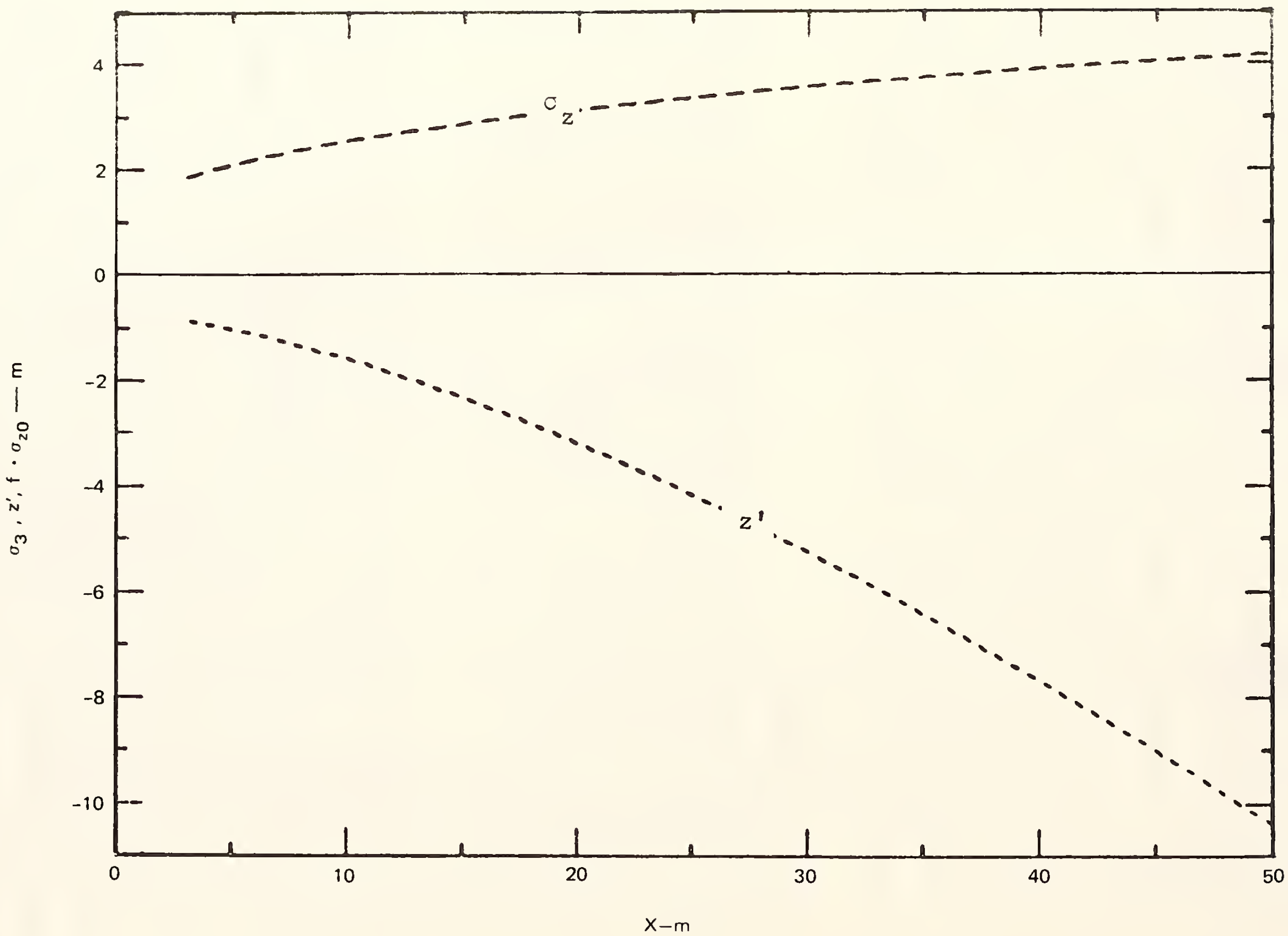

FIGURE 102 VARIATION OF ROADMAP DISPERSION PARAMETERS WITH CROSS-ROADWAY DISTANCE FOR HIGHWAY 280 CUT-SECTION TEST, NEUTRAL ATMOSPHERIC CONDITIONS

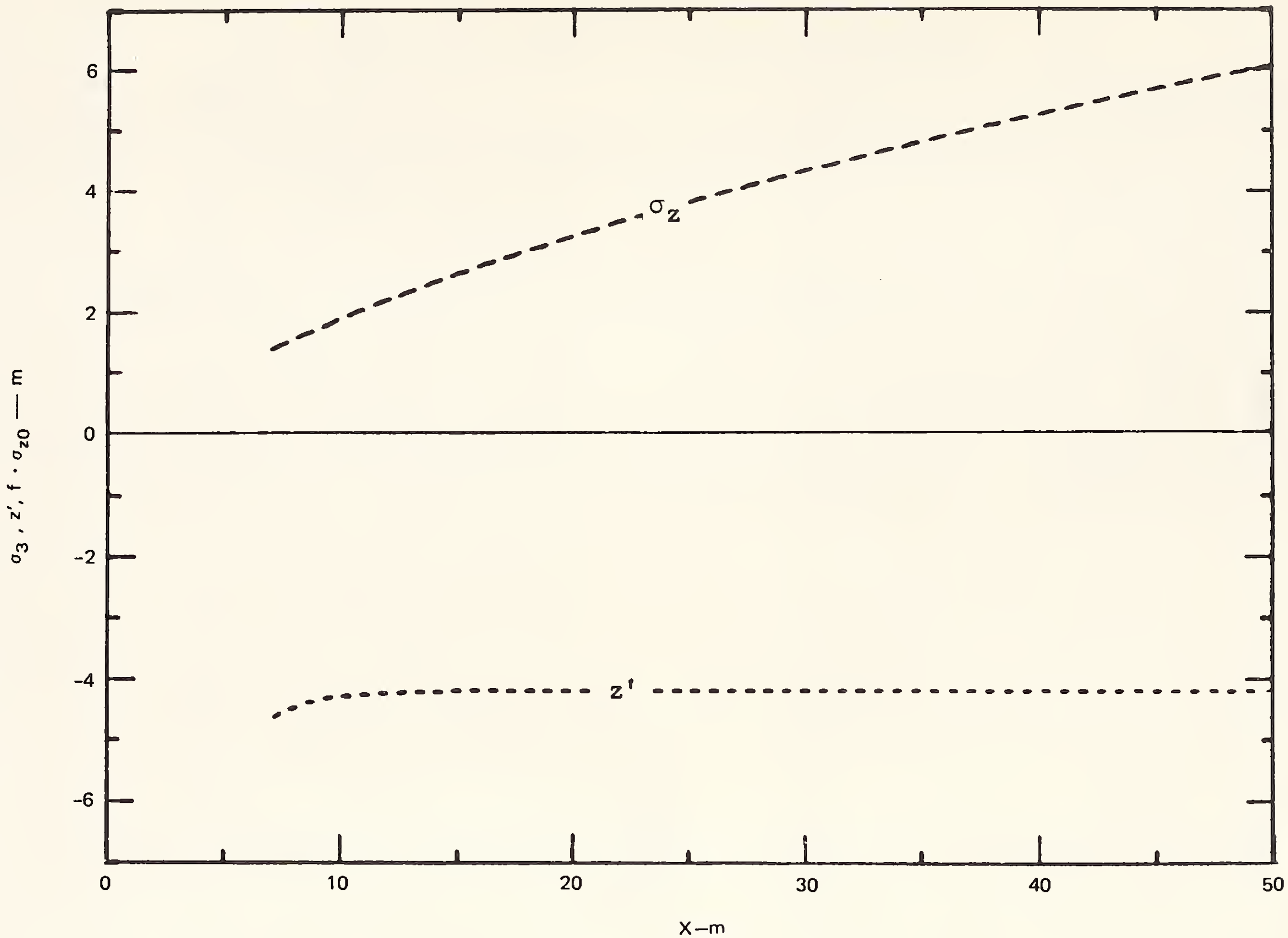

FIGURE 103 VARIATION OF ROADMAP DISPERSION PARAMETERS WITH CROSS-ROADWAY DISTANCE FOR HIGHWAY 280 CUT-SECTION TEST, UNSTABLE ATMOSPHERIC CONDITIONS

increasing x under neutral conditions. In view of the poor performance of the perpendicular term (even with nearly orthogonal winds), it would not be appropriate to attach much significance to the σ_z and z' functions.

Since no near-parallel winds were available to estimate f, we resorted to making a questionable approximation by selecting a_3, b_3, and c_3 from the wind tunnel analysis. The two-component model was then evaluated--with understandably poor results. For the neutral cases: (1) $r^2 = 0.172$ ($r = 0.41$) for $34° \leq \theta \leq 89°$, (2) $r^2 = 0.146$ ($r = 0.38$) for $70° \leq \theta \leq 89°$, and (3) $r^2 = 0.214$ ($r = 0.46$) for $45° \leq \theta \leq 89°$. For unstable cases: (1) $r^2 = 0.095$ ($r = 0.31$) for $22° \leq \theta \leq 84°$, (2) $r^2 = 0.445$ ($r = 0.67$) for $67° \leq \theta \leq 84°$, and (3) $r^2 = 0.190$ ($r = 0.44$) for $45° \leq \theta \leq 84°$. Further analysis would be desirable to evaluate the poor performance of the model (for example, evaluating possible bias in various grade-level sampling locations due to CO emissions from other sources).

C. Elevated Sections

1. Wind Tunnel Tests

Table 44 summarizes the results of the ROADMAP analyses for wind tunnel test series G and H. In both series, the roadway was 18.3 m above grade level; the surrounding terrain was smooth, while each of the two-lane traffic streams consisted of low-density flows at equal speeds. In the G series, the roadway rested on a fill section having 45° sloped sides (Figure 16), while the H series was a viaduct section open to the wind up to a height of 15 m above grade-level (Figure 17). Each series consisted of 16 tests comprising four different wind angles ($\theta = 0°$, 15°, 30° and 90°), two wind speeds, and three vehicle speeds.

In both series, the model properly represents the x- and z-variation of the concentration for a given wind/roadway angle; however, the model poorly represents the variability across different wind angles. For the fill section (G series), the explained variance (r^2) of the component model is: 0.90 ($r = 0.95$) at $\theta = 90°$, 0.87 ($r = 0.93$) at 30°, and 0.44 ($r = 0.67$) at 0° and 15°. Yet r^2 for all wind angles is only 0.23

Table 44

SUMMARY OF ROADMAP ANALYSES FOR ELEVATED-SECTION CONFIGURATIONS

Test Series	Perpendicular Dispersion Term									Parallel Dispersion Term						Two-Component Model				
	θ	N	a_1	b_1	c_1	a_2	b_2	c_2	R^2	θ	N	a_3	b_3	c_3	R^2	θ	N	R^2	m*	s†
G	90	4	0.390	0.810	0.185	0.127	1.07	-1.78	0.897	0,15	8	0.259	4.29	2.64	0.301	All	16	0.225	0.037	1.08
																0,15	8	0.443	0.002	4.66
																30	4	0.873	-0.011	2.42
																90	4	0.897	0.015	0.922
H	90	4	0.00005	3.14	3.07	-0.0018	2.20	1.44	0.898	0,15	8	0.0401	3.78	4.93	0.366	All	16	0.204	0.28	1.07
																0,15	8	0.388	0.020	5.29
																30	4	0.841	-0.010	2.57
																90	4	0.898	-0.014	0.982
280-CO Unstable	≥ 79	9	0.00169	1.62	2.15	-0.284	0.774	3.90	0.383	--‡	0‡	0.0401‡	3.78‡	4.93‡	--‡	All	25	0.246	0.082	0.708
																≥ 50	24	0.359	0.058	0.817
																≥ 79	9	0.378	0.055	0.838

*m - intercept

†s - slope

‡from H-Series

($r = 0.48$). A similar pattern holds for the viaduct section (H Series): $r^2 = 0.90$ ($r = 0.95$) for $\theta = 90°$, $r^2 = 0.84$ ($r = 0.92$) for 30°, $r^2 = 0.39$ ($r = 0.62$) for 0° and 15°, but $r^2 = 0.20$ ($r = 0.45$) for all wind angles. Figures 104 and 105 are comparisons of observed and predicted concentrations for all wind angles for the G and H series, respectively. Peak concentrations are virtually the same for both configurations and vary in the same way with the wind/roadway angle. For parallel winds, the peak is about 15% less than the smooth-ground, grade-level Q series and is located over the roadway. For perpendicular winds, the peak is less than half its Q-series counterpart.

A major difference between the fill and viaduct sections is seen if one compares Figures 106 and 107. In the fill section, the displacement term, z', displays a linear (positive) increase from its initially small negative value. This indicates a corresponding effective increase in the height of the plume centerline with a corresponding decrease in the magnitude of the ground-level concentrations. With the viaduct, z' decreases (from a small initial positive value) at an increasing rate with distance from the roadway. This suggests a corresponding decrease in the effective height of the plume centerline that results in an increase in ground-level concentrations, especially in comparison with the fill section. In both cases, however, the absolute values of the ground level concentration are greatly diminished from, say, the grade-level case because of the significant height of the roadway surface. This essentially provides a significantly larger reservoir or volume of air into which the pollutants can be mixed; in turn, the turbulence generated by the elevated roadway configurations enhances the mixing process.

2. Atmospheric Test

In stratifying the viaduct-section data there is a preponderance of moderately unstable cases, with relatively few neutral, stable, or very unstable cases. Of the 25 unstable cases that were analyzed, the following ranges in meteorological parameters were measured: (1) $19.0° \leq \sigma_\theta \leq 36.9°$, and (2) $15.7° \leq \sigma_\phi \leq 26.9°$; Richardson number data were

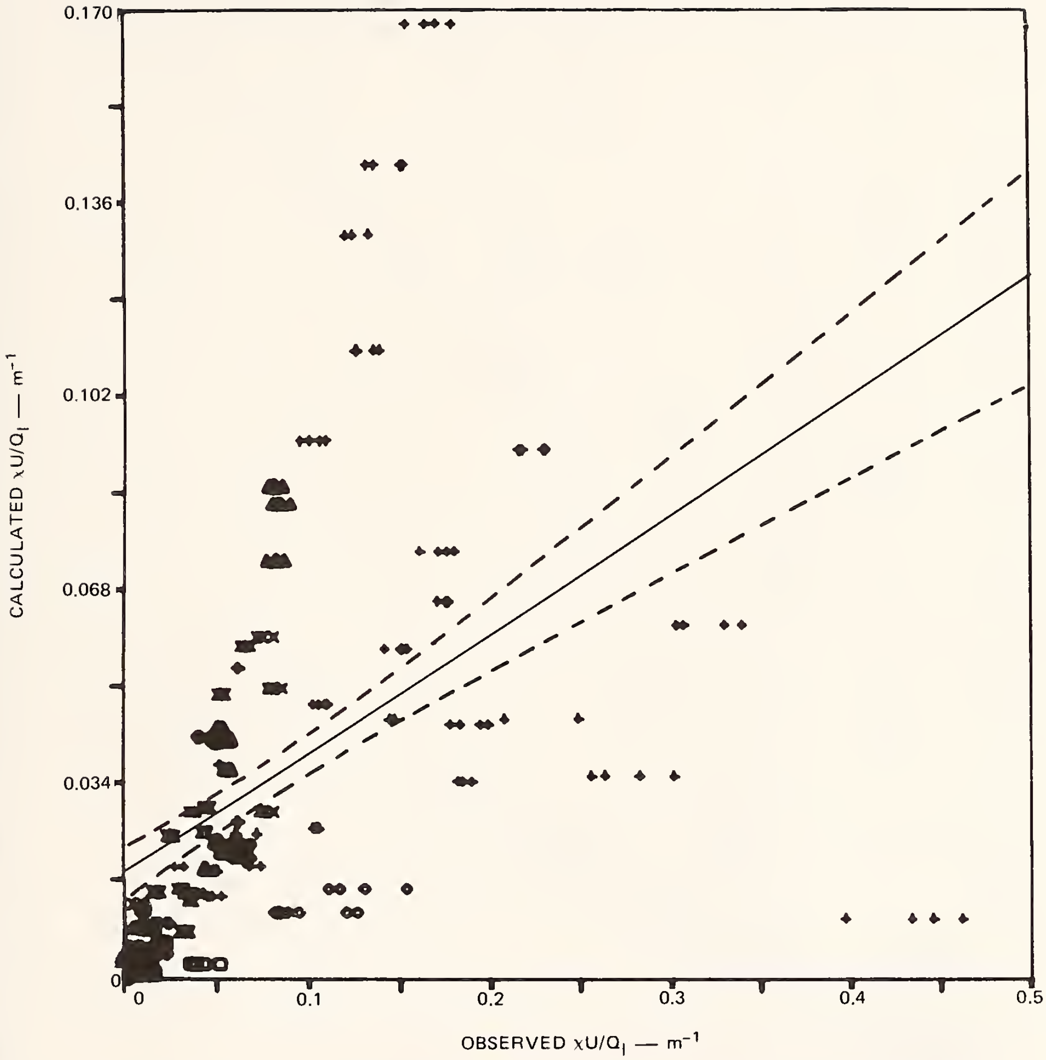

FIGURE 104 COMPARISON OF OBSERVED NORMALIZED CONCENTRATION WITH ROADMAP CALCULATION FOR WIND TUNNEL SERIES G, ALL WIND ANGLES

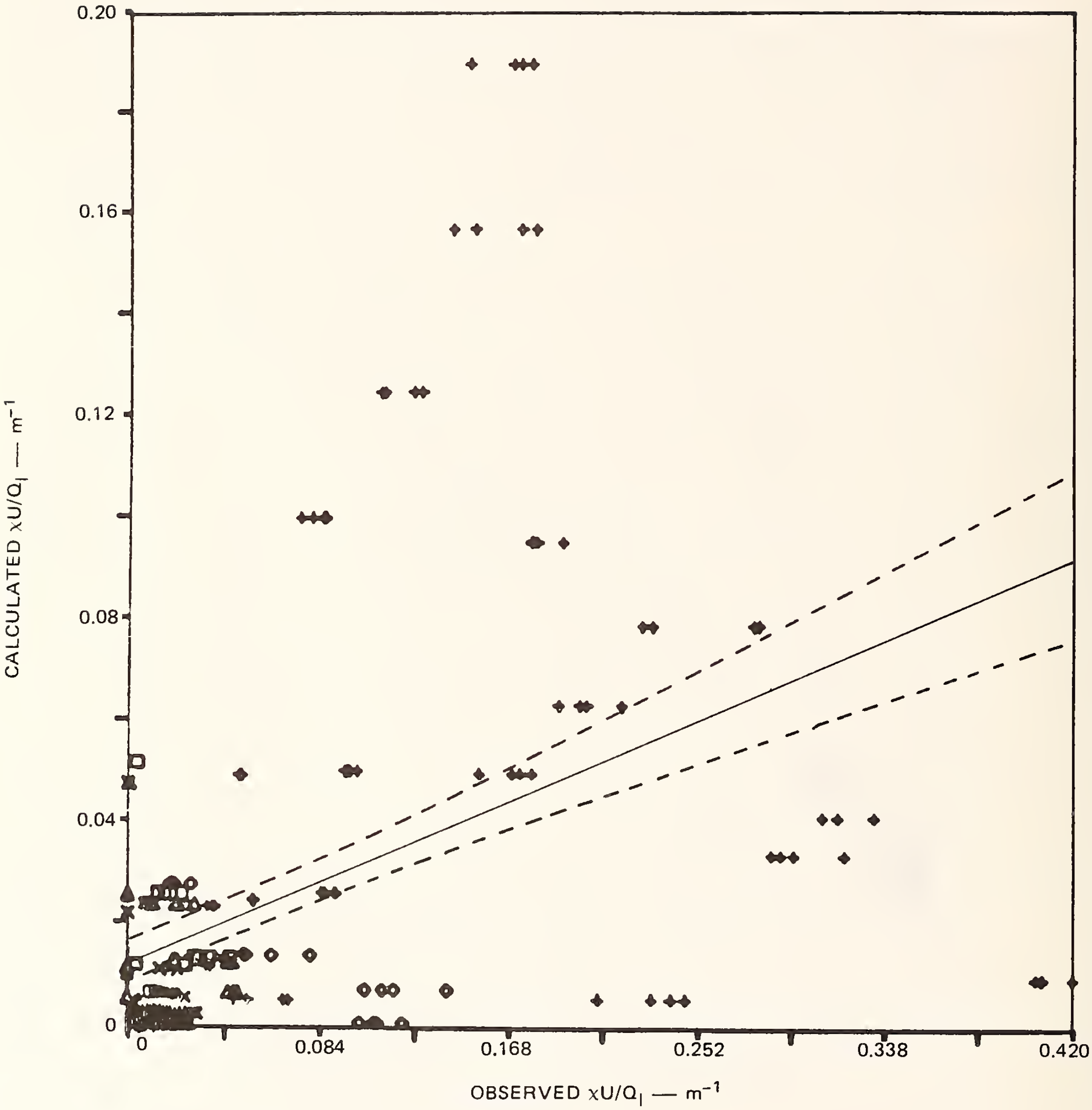

FIGURE 105 COMPARISON OF OBSERVED NORMALIZED CONCENTRATION WITH ROADMAP CALCULATION FOR WIND TUNNEL SERIES H, ALL WIND ANGLES

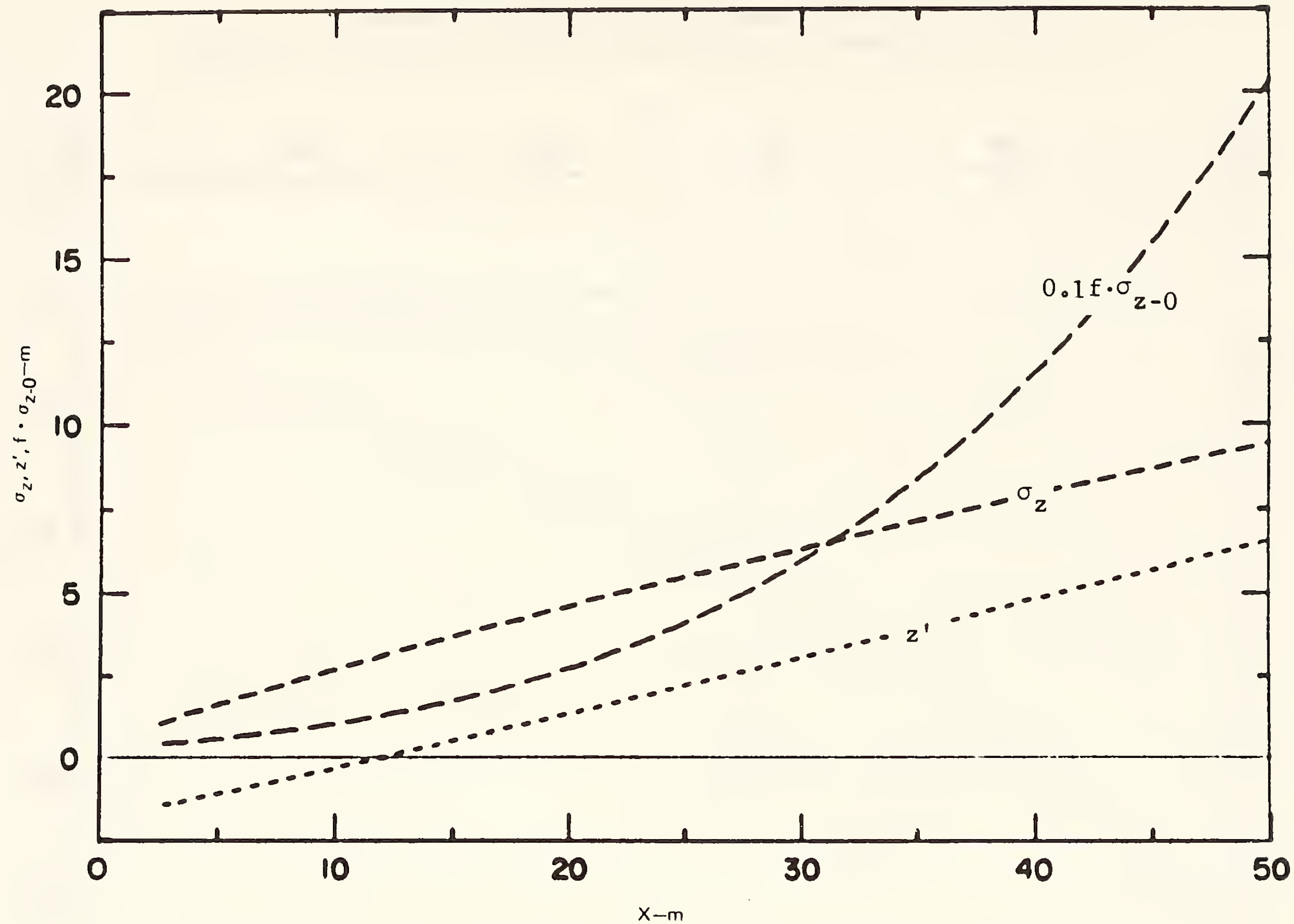

FIGURE 106 VARIATION OF ROADMAP DISPERSION PARAMETERS WITH CROSS-ROADWAY DISTANCE FOR WIND TUNNEL SERIES G

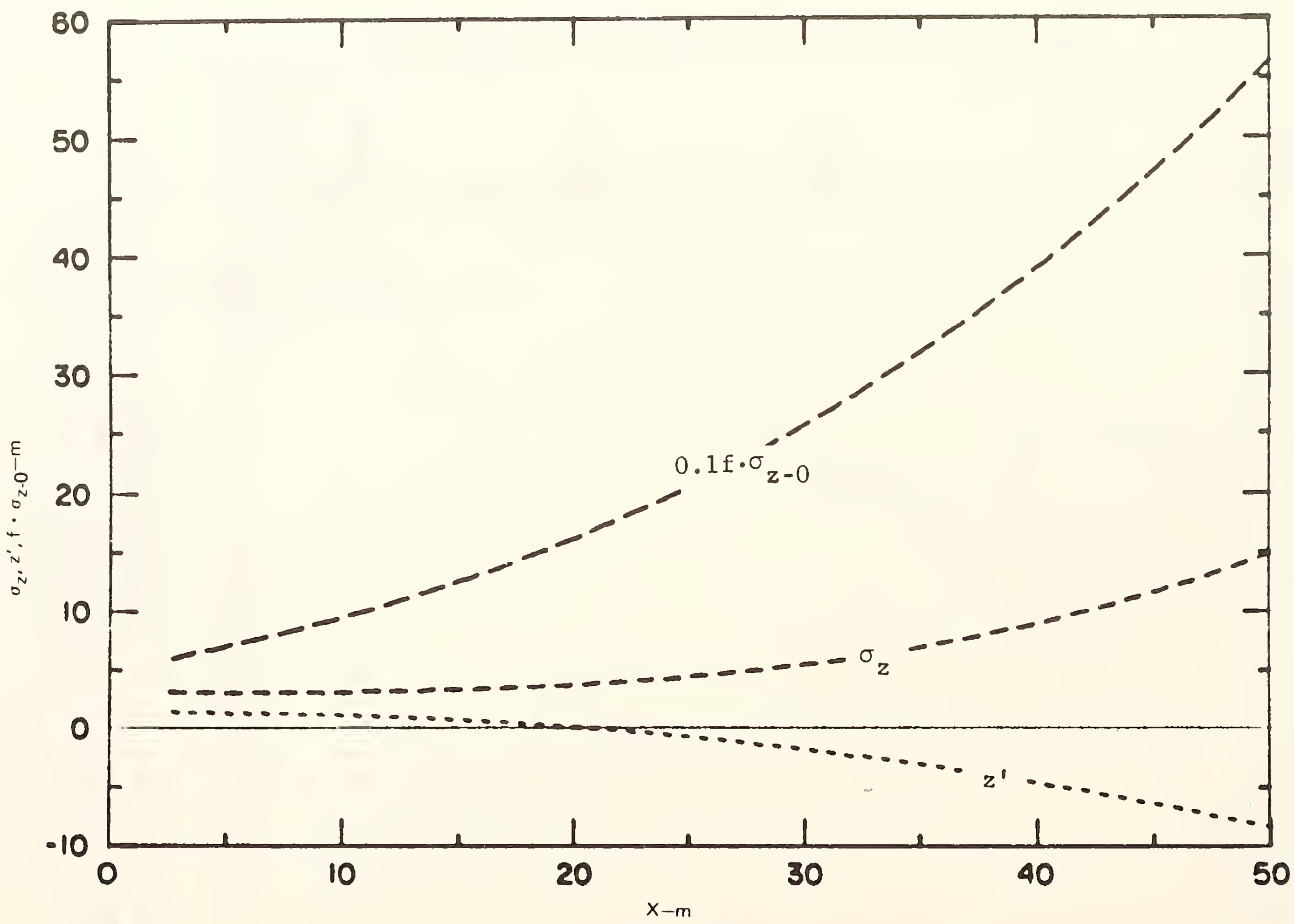

FIGURE 107 VARIATION OF ROADMAP DISPERSION PARAMETERS WITH CROSS-ROADWAY DISTANCE FOR WIND TUNNEL SERIES H

unreliable. Nine cases with $\theta \geq 79°$ were used to evaluate σ_z and z' (Figure 108). Considering the rough suburban nature of the surrounding terrain, it is a little surprising that σ_z is not larger than the 2-3 m computed for $x \leq 50$ m. The height-offset term decreases rapidly from $z' = 3$ m at $x = 10$ m to $z' = -2$ m at $x = 50$ m. This would indicate a tendency for downwind, near-ground concentrations to be increased, possibly due to considerable vertical mixing downwind [illegible] the roadway caused by the tall roughness elements (houses and trees). [illegible]hen σ_z and z' are used in the perpendicular term to predict the concentrations for the nine cases with θ values $\geq 79°$, the resulting $r^2 = 0.383$ ($r = 0.62$). As with the cut-section data, there are no small θ cases to evaluate f. Again, an estimate was made from the wind tunnel analyses (series H); in fact, the f term estimate is not particularly critical in the ROADMAP evaluation because of the dominance of the perpendicular term for the large θ values encountered. ROADMAP predictions were compared with the observed concentrations with the following results: (1) $r^2 = 0.246$ ($r = 0.$[illegible]) for $15° \leq \theta \leq 90°$, (2) $r^2 = 0.359$ ($r = 0.60$) for $50° \leq \theta \leq 90°$, and (3) $r^2 = 0.378$ ($r = 0.61$) for $79° \leq \theta \leq 90°$.

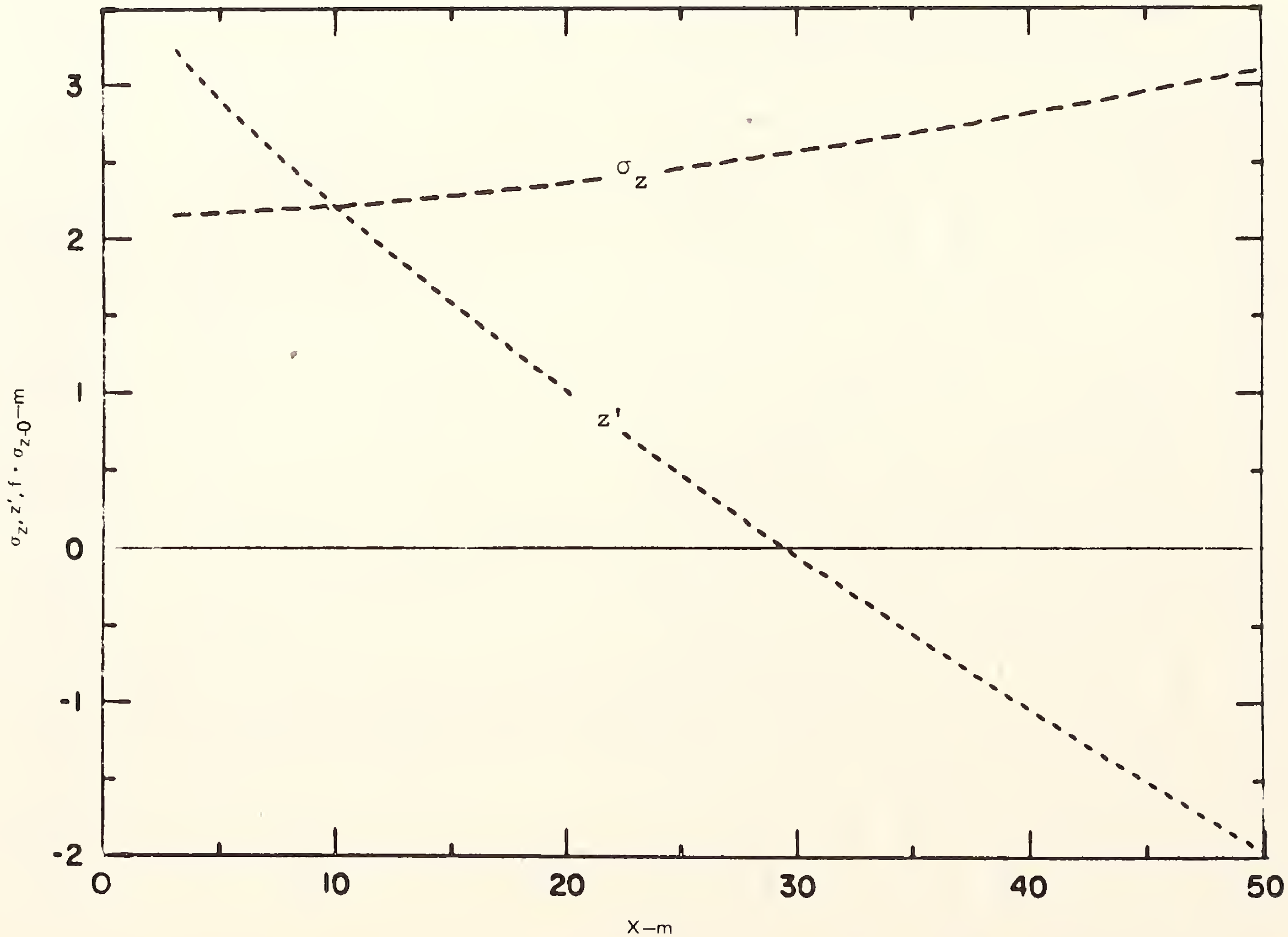

FIGURE 108 VARIATION OF ROADMAP DISPERSION PARAMETERS WITH CROSS-ROADWAY DISTANCE FOR HIGHWAY 280 VIADUCT-SECTION TEST, STABLE ATMOSPHERIC CONDITIONS

VII SUMMARY REMARKS

While not resolving all uncertainties in the understanding and definition of near-roadway pollution transport and dispersion problems and processes, this study has both resolved many of the uncertainties that existed at the time of its inception and provided the impetus and served as a model for other microscale highway dispersion programs.

The wind tunnel roadway model and simulation facility was in itself a technological advance, providing a device that could be used to study dispersion problems at a wide range of site configurations: cut and fill sections, hillsides, air-right structures, and so forth. With the roadway model, emissions were released in a manner that was physically consistent and analogous with actual conditions on the highway, and traffic density, speed and direction were systematically varied so as to provide the basis for understanding the impact and effects of each. As a result, the wind tunnel tests provided a range of reliable data that could not easily be acquired in the ambient environment.

The atmospheric tests provided data that shed new light into the dispersion process and permitted the identification of two mechanisms of initial pollution dispersion that were heretofore overlooked: one is the significance of waste heat emissions from highway vehicles which are sufficiently large to modify and dominate the thermal structure of the air over and immediately downwind of the roadway. The second mechanism identified is the shelterbelt-type influence exerted by the vehicles. As the ambient wind flow approaches and traverses the roadway, the vehicles act much as an agricultural shelterbelt or windbreak first to defelct the flow upward over the roadway, and then to enhance the turbulent mixing in an "entrainment" zone just downwind of the roadway. Both mechanisms are important in that they act to increase the near-roadway dispersion and thereby decrease concentration levels from what they would otherwise be in their absence.

Both the wind tunnel and atmospheric tests provided important insights into the significance of effect of vehicle speed on dispersion and the magnitude of near-roadway pollution concentrations. With a few exceptions, the data indicate vehicle speed is not an important determinant. The exceptions occur in cut-type sections where higher vehicle speeds result in nominal increases in dispersion and decreases in pollution level.

The development of the ROADMAP dispersion model is another important result of the study. The model is easy to apply, provides good-to-excellent agreement with observations, and is applicable to a wide range of roadway configurations. With the user's manual*, the model can easily be applied without the need for computers by highway engineers, research personnel, and others.

In addition to the results and findings generated in this program, the study has also served as a model for other experimental studies: both the General Motors (Chock, 1977) and New York State (Rao et al., 1979) atmospheric dispersion studies used the experimental design and tracer techniques employed in this program.

In summary, this program has provided a data base that will be useful for years to come; developed new insights into the process by which dispersion occurs on and near roadways; produced a simple, versatile, and representative model for calculating pollution concentrations at a wide range of site configurations; and made this knowledge available to the user community through the 16-mm film and the user's guide to the assessment methodology.

---

*Report No. FHWA-RD-78-180.

REFERENCES

Buckley, D. J., 1968: "A Semi-Poisson Model of Traffic Flow," Transportation Science, Vol. 2, No. 2, pp. 107-133.

Bureau of Mines, February 1975: "Crude Petroleum Products, and Natural Gas Liquids: 1973," Mineral Industry Surveys, Final Summary, Washington, D.C.

Chock, D. P., 1977: "A Simple Line-Source Model for Dispersion Near Roadways," General Motors Research Publication, GMR-2407.

Cope, E. M., October 1973: "The Effect of Speed on Automobile Gasoline Consumption Rates," U.S. Department of Transportation, Washington, D.C.

Dabberdt, W. F., 1968: "Wind Disturbance by a Vertical Cylinder in the Atmospheric Surface Layer," J. Appl. Meteor., Vol. 7, June.

Dabberdt, W. F. et al., 1974: "Studies of Air Quality On and Near Highways, "First Interim Report, FHWA Contract No. DOT-FM-11-8125, Stanford Research Institute, Menlo Park, California 94025. *

Dabberdt, W. F., 1975: "Studies of Air Quality On and Near Highways," Second Interim Report, FHWA Contract No. DOT-FH-11-8125, Stanford Research Institute, Menlo Park, California 94025. *

Dabberdt, W. F. et al., 1976: "Rationale and Evaluation of Technical Guidelines for the Review of Indirect Sources," SRI Project 4429, EPA Contract No. 69-02-2073, SRI International, Menlo Park, California (October).

Dabberdt, W. F. and R. C. Sandys, 1976: "Guidelines for Evaluating Indirect Sources," SRI Project 4429, EPA Contract No. 68-02-2073, SRI International, Menlo Park, California (September).

EPA, Office of Air and Water Programs, March 1975: "A Study of Emissions from Light-Duty Vehicles in Six Cities" (APTD-1497).

EPA, Office of Air and Waste Management, April 1975: "Supplement No. 5 to Compilation of Air Pollutant Emission Factors (AP-42)."

Fay, J. A., 1973: "Buoyant Plumes and Wakes," Annual Review of Fluid Mechanics, Vol. 5, pp. 151-160, Annual Reviews, Inc., Palo Alto, California.

* Available from NTIS

Harman, Harry H., 1967: Modern Factor Analysis, The University of Chicago Press, Chicago, Illinois.

Johnson, W. B. et al., 1971: "Field Study for Initial Evaluation of an Urban Diffusion Model for Carbon Monoxide," Final Report to Coordinating Research Council and Environmental Protection Agency, Contract CAPA-3-68(1-69), Stanford Research Institute, Menlo Park, California, NTIS No. PB-203469.

Ludwig, F. L. and W. F. Dabberdt, 1976: "Comparison of Two Practical Atmospheric Stability Schemes in an Urban Application," J. Appl. Meteor., Vol. 15, p. 11.

Ludwig, G. R., T. R. Sundaram, and G. T. Skinner, 1971: "Laboratory Modeling of the Atmospheric Surface Layer with Emphasis on Diffusion," Calspan Report No. VC-2740-S-2, July.

Ludwig, G. R., and T. R. Sundaram, 1969: "On the Laboratory Simulation of Small-Scale Atmospheric Turbulence," Calspan Report No. VC-2740-S-1, December.

McVehil, G. E., G. R. Ludwig, and T. R. Sundaram, 1967: "On the Feasibility of Modeling Small Scale Atmospheric Motions," Calspan Report No. ZB-2328-P-1, April.

Morse, S., 1974: Tables of Yearly Emission Factors for California, Personal Communication.

Nägeli, W., 1941: "Untersuchungen über die Windverhältnisse im Bereich von Windschutzstreifen," Mitt. Schweiz. Anst. Forstl. Versuchsw. 23:221-276.

Nie, N. H. et al., 1975: Statistical Package for the Social Sciences, 2nd Ed., ISBN 0-07-046531-2, McGraw-Hill Book Company, New York, 675 pp.

Panofsky, H. A., and G. W. Brier, 1965: "Some Applications of Statistics to Meteorology," College of Mineral Industries, Penn. State University Park, Pennsylvania.

Peterson, J. T., 1970: "Distribution of Sulfur Dioxide Over Metropolitan St. Louis, As Described by Empirical Eigenvectors, and Its Relation to Meteorological Parameters," Atmospheric Environment, Vol. 4, pp. 501-518.

Plate, E. J., and C. Y. Lin, 1965: "The Velocity Field Downstream from a Two-Dimensional Model Hill," Final Report, Part I, to U.S. Army Material Agency.

Plate, E. J., 1971: "Aerodynamic Characteristics of Atmospheric Boundary Layers," AEC Critical Review Series (TID-25465) NTIS, Springfield Virginia, 190 pp.

Rao, S. T., M. Keenan, G. Sistala, and P. Samson, 1979: "Dispersion of Pollutants Near Highways--Data Analysis and Model Evaluation," EPA 600/4-79-011, February.

Rummel, R. J., 1967: "Understanding Factor Analysis," Conflict Resolution, Vol. 11, pp. 44-480.

Rozeboom, W. F., 1966: Foundations of the Theory of Prediction, Dorsey Press, Homewood, Illinois.

Sundaram, T. R., G. R. Ludwig, and G. T. Skinner, 1972: "Modeling of the Turbulence Structure of the Atmospheric Surface Layer," AIAA Journal, Vol. 10, No. 6, June. (Originally presented as AIAA Paper No. 71-136 at the AIAA 9th Aerospace Sciences Meeting, New York City, January 1971.)

Turner, D. B., 1967: "Workbook of Atmospheric Dispersion Estimates," PHS Publ. No. 999-AP-26, 84 pp.

Zimmerman, J. R. and R. S. Thompson, 1975: "User's Guide for HIWAY, A Highway Air Pollution Model," EPA Report No. 650/4-74-008, Research Triangle Park, North Carolina 27711.

APPENDIX A

SUMMARY OF STATISTICAL ANALYSIS OF
CROSS-ROADWAY TURBULENCE VARIATIONS*

WIND DIR. CATEGORY	N	DEPENDENT VARIABLE	X MEAN	STANDARD DEVIATION	INDEPENDENT VARIABLE	Y MEAN	STANDARD DEVIATION	CORRELATION COEFFICIENT
1	20	HDNTT11	.02	.44	A	-.07	.86	-.05
					B	1.78	.92	.06
					C	.22	.24	.20
					D	.13	.41	.37
					E	19.52	12.22	.09
					F	54914.30	27064.77	-.01
					G	1027.75	565.78	.05
		HDTT11	-.02	.26	A	-.07	.86	.02
					B	1.78	.92	-.22
					C	.22	.24	.14
					D	.13	.41	.38
					E	19.52	12.22	.08
					F	54914.30	27064.77	-.06
					G	1027.75	565.78	.01
		HDNTT15	-.83	.60	A	-.07	.86	-.51
					B	1.78	.92	.67
					C	.22	.24	.48
					D	.13	.41	-.10
					O	7.54	5.67	.25
					P	23283.10	13413.77	.26
					Q	-3.68	3.59	-.41
					R	416.45	268.77	.26
					S	3.22	2.08	.26
					T	4.20	2.99	.47
		HDTT15	-.45	.24	A	-.07	.86	-.57
					B	1.78	.92	.59
					C	.22	.24	.50
					D	.13	.41	-.07
					O	7.54	5.67	-.01
					P	23283.10	13413.77	-.07
					Q	-3.68	3.59	-.19
					R	416.45	268.77	-.04
					S	3.22	2.08	-.04
					T	4.20	2.99	.32
2	27	HDNTT11	-.13	.24	A	-.03	.83	-.22
					B	2.14	1.19	.36
					C	.76	.74	.40
					D	.48	.52	.27
					E	24.46	13.33	.12
					F	63515.89	18502.71	-.00
					G	1194.37	375.63	.06
		HDTT11	-.04	.20	A	-.03	.83	-.28
					B	2.14	1.19	.21
					C	.76	.74	.34
					D	.48	.52	.41
					E	24.46	13.33	.12
					F	63515.89	18502.71	.13
					G	1194.37	375.63	.15
		HDNTT15	-.76	.47	A	-.03	.83	-.22
					B	2.14	1.19	.57
					C	.76	.74	.49
					D	.48	.52	-.02
					O	13.23	11.22	-.05
					P	29762.41	11195.02	.14
					Q	-5.38	3.42	-.20
					R	579.74	211.92	.05
					S	4.48	1.64	.05
					T	5.68	3.08	.23
		HDTT15	-.50	.24	A	-.03	.83	-.34
					B	2.14	1.19	.53
					C	.76	.74	.47
					D	.48	.52	.09
					O	13.23	11.22	-.03
					P	29762.41	11195.02	.05
					Q	-5.38	3.42	-.17
					R	579.74	211.92	.01
					S	4.48	1.64	.01
					T	5.68	3.08	.25

*Definitions of the various terms and abbreviations are given in Chapter III.

APPENDIX A (Continued)

WIND DIR. CATEGORY	N	DEPENDENT VARIABLE	X MEAN	STANDARD DEVIATION	INDEPENDENT VARIABLE	Y MEAN	STANDARD DEVIATION	CORRELATION COEFFICIENT
3	42	HDNTTI1	-.24	1.08	A	.38	.68	.15
					B	1.72	.99	.23
					C	.89	.83	.24
					D	.45	.57	.10
					E	23.97	12.65	.07
					F	61510.90	14634.93	.00
					G	1178.07	372.57	.05
		HDTTI1	.02	.27	A	.38	.68	-.38
					B	1.72	.99	-.11
					C	.89	.83	.18
					D	.45	.57	.73
					E	23.97	12.65	.03
					F	61510.90	14634.93	-.22
					G	1178.07	372.57	-.07
		HDNTTI5	-1.35	1.42	A	.38	.68	.21
					B	1.72	.99	.57
					C	.89	.83	.47
					D	.45	.57	-.26
					O	10.10	8.12	.02
					P	26201.60	8812.12	-.04
					Q	-3.21	2.54	.17
					R	492.45	194.90	-.02
					S	3.81	1.51	-.02
					T	3.73	2.06	-.09
		HDTTI5	-.61	.27	A	.38	.68	.05
					B	1.72	.99	.65
					C	.89	.83	.68
					D	.45	.57	.30
					O	10.10	8.12	-.02
					P	26201.60	8812.12	-.25
					Q	-3.21	2.54	.22
					R	492.45	194.90	-.16
					S	3.81	1.51	-.16
					T	3.73	2.06	-.11
4	35	HDNTTI1	-.05	.73	A	.26	.88	.11
					B	2.10	1.07	-.32
					C	1.55	.93	-.15
					D	.76	.74	.70
					E	34.83	16.67	-.23
					F	67651.94	12649.80	-.14
					G	1433.91	366.14	-.21
		HDTTI1	.06	.26	A	.26	.88	-.36
					B	2.10	1.07	-.32
					C	1.55	.93	-.19
					D	.76	.74	.31
					E	34.83	16.67	.29
					F	67651.94	12649.80	-.11
					G	1433.91	366.14	.18
		HDNTTI5	-1.04	.92	A	.26	.88	.25
					B	2.10	1.07	.58
					C	1.55	.93	.61
					D	.76	.74	.05
					O	17.94	13.55	-.12
					P	29227.37	9863.74	.24
					Q	-4.94	2.49	.14
					R	655.00	210.34	.03
					S	5.06	1.63	.03
					T	5.31	2.39	-.05
		HDTTI5	-.52	.25	A	.26	.88	.48
					B	2.10	1.07	.41
					C	1.55	.93	.47
					D	.76	.74	.07
					O	17.94	13.55	-.16
					P	29227.37	9863.74	.18
					Q	-4.94	2.49	.27
					R	655.00	210.34	-.05
					S	5.06	1.63	-.05
					T	5.31	2.39	-.20

APPENDIX A (Continued)

WIND DIR. CATEGORY	N	DEPENDENT VARIABLE	X MEAN	STANDARD DEVIATION	INDEPENDENT VARIABLE	Y MEAN	STANDARD DEVIATION	CORRELATION COEFFICIENT
5	31	HDNTT11	.29	.60	A	.51	.62	-.02
					B	2.00	1.22	-.12
					C	1.57	1.51	.21
					D	1.00	.84	.59
					E	31.54	17.86	.17
					F	63826.32	20696.23	.02
					G	1327.16	477.34	.16
		HDTT11	.14	.25	A	.51	.62	-.06
					B	2.00	1.22	.19
					C	1.57	1.51	.56
					D	1.00	.84	.76
					E	31.54	17.86	.37
					F	63826.32	20696.23	.05
					G	1327.16	477.34	.27
		HDNTT15	-1.00	.72	A	.51	.62	.24
					B	2.00	1.22	.42
					C	1.57	1.51	.31
					D	1.00	.84	-.08
					O	16.85	15.34	.19
					P	26899.90	11224.76	-.17
					Q	-4.11	1.83	-.03
					R	600.32	256.29	.08
					S	4.64	1.98	.08
					T	4.64	1.87	.16
		HDTT15	-.55	.21	A	.51	.62	.17
					B	2.00	1.22	.14
					C	1.57	1.51	.12
					D	1.00	.84	.04
					O	16.85	15.34	-.05
					P	26899.90	11224.76	-.47
					Q	-4.11	1.83	.37
					R	600.32	256.29	-.31
					S	4.64	1.98	-.31
					T	4.64	1.87	-.27
6	12	HDNTT11	-.09	.54	A	.81	.47	.09
					B	1.45	.58	-.17
					C	-.60	1.42	.54
					D	.07	.93	.83
					E	29.14	14.59	.60
					F	67939.17	13332.57	.66
					G	1354.00	416.58	.70
		HDTT11	-.05	.32	A	.81	.47	-.01
					B	1.45	.58	-.20
					C	-.60	1.42	.34
					D	.07	.93	.72
					E	29.14	14.59	.59
					F	67939.17	13332.57	.64
					G	1354.00	416.58	.68
		HDNTT15	-.78	.45	A	.81	.47	.78
					B	1.45	.58	.56
					C	-.60	1.42	.08
					D	.07	.93	-.11
					O	11.96	8.76	-.06
					P	30036.92	8468.03	-.13
					Q	-4.40	1.48	.19
					R	567.17	166.39	-.14
					S	4.38	1.29	-.14
					T	4.68	1.42	-.09
		HDTT15	-.47	.23	A	.81	.47	.55
					B	1.45	.58	.52
					C	-.60	1.42	.20
					D	.07	.93	-.04
					O	11.96	8.76	-.04
					P	30036.92	8468.03	-.09
					Q	-4.40	1.48	.13
					R	567.17	166.39	-.10
					S	4.38	1.29	-.10
					T	4.68	1.42	-.04

FEDERALLY COORDINATED PROGRAM (FCP) OF HIGHWAY RESEARCH AND DEVELOPMENT

The Offices of Research and Development (R&D) of the Federal Highway Administration (FHWA) are responsible for a broad program of staff and contract research and development and a Federal-aid program, conducted by or through the State highway transportation agencies, that includes the Highway Planning and Research (HP&R) program and the National Cooperative Highway Research Program (NCHRP) managed by the Transportation Research Board. The FCP is a carefully selected group of projects that uses research and development resources to obtain timely solutions to urgent national highway engineering problems.*

The diagonal double stripe on the cover of this report represents a highway and is color-coded to identify the FCP category that the report falls under. A red stripe is used for category 1, dark blue for category 2, light blue for category 3, brown for category 4, gray for category 5, green for categories 6 and 7, and an orange stripe identifies category 0.

FCP Category Descriptions

1. Improved Highway Design and Operation for Safety

Safety R&D addresses problems associated with the responsibilities of the FHWA under the Highway Safety Act and includes investigation of appropriate design standards, roadside hardware, signing, and physical and scientific data for the formulation of improved safety regulations.

2. Reduction of Traffic Congestion, and Improved Operational Efficiency

Traffic R&D is concerned with increasing the operational efficiency of existing highways by advancing technology, by improving designs for existing as well as new facilities, and by balancing the demand-capacity relationship through traffic management techniques such as bus and carpool preferential treatment, motorist information, and rerouting of traffic.

3. Environmental Considerations in Highway Design, Location, Construction, and Operation

Environmental R&D is directed toward identifying and evaluating highway elements that affect the quality of the human environment. The goals are reduction of adverse highway and traffic impacts, and protection and enhancement of the environment.

4. Improved Materials Utilization and Durability

Materials R&D is concerned with expanding the knowledge and technology of materials properties, using available natural materials, improving structural foundation materials, recycling highway materials, converting industrial wastes into useful highway products, developing extender or substitute materials for those in short supply, and developing more rapid and reliable testing procedures. The goals are lower highway construction costs and extended maintenance-free operation.

5. Improved Design to Reduce Costs, Extend Life Expectancy, and Insure Structural Safety

Structural R&D is concerned with furthering the latest technological advances in structural and hydraulic designs, fabrication processes, and construction techniques to provide safe, efficient highways at reasonable costs.

6. Improved Technology for Highway Construction

This category is concerned with the research, development, and implementation of highway construction technology to increase productivity, reduce energy consumption, conserve dwindling resources, and reduce costs while improving the quality and methods of construction.

7. Improved Technology for Highway Maintenance

This category addresses problems in preserving the Nation's highways and includes activities in physical maintenance, traffic services, management, and equipment. The goal is to maximize operational efficiency and safety to the traveling public while conserving resources.

0. Other New Studies

This category, not included in the seven-volume official statement of the FCP, is concerned with HP&R and NCHRP studies not specifically related to FCP projects. These studies involve R&D support of other FHWA program office research.

* The complete seven-volume official statement of the FCP is available from the National Technical Information Service, Springfield, Va. 22161. Single copies of the introductory volume are available without charge from Program Analysis (HRD-3), Offices of Research and Development, Federal Highway Administration, Washington, D.C. 20590.